# UNDERSTANDING LARGE-SCALE HUMAN-WATER INTERACTIONS FOR SUSTAINABLE HYDROPOWER DEVELOPMENT

By

Suyog Chaudhari

A DISSERTATION

Submitted to
Michigan State University
in partial fulfillment of the requirements
for the degree of

Civil Engineering – Doctor of Philosophy

2021

## ABSTRACT

## UNDERSTANDING LARGE-SCALE HUMAN-WATER INTERACTIONS FOR SUSTAINABLE HYDROPOWER DEVELOPMENT

By

Suyog Chaudhari

Hydropower dams have received increased global attention due to their detrimental socioenvironmental ramifications, resulting in increased concerns as to whether their energy benefits can outweigh the detrimental consequences. To fulfill rising energy demands driven by rapid population growth, especially in the developing world, hydropower has often been developed with a primary focus on energy generation. The re-emergence of large dams could very well bring large energy and economic incentives especially to the developing economies; however, these incentives may come at the expense of altering the natural flow regime of rivers with additional repercussions on the biodiversity and ecological productivity within the basins. With the continued interest in hydropower development, it is imperative to examine and understand the intricate changes to the basin's hydrology due to dam operations and further rethink hydropower design to avoid potentially catastrophic consequences. To date, several studies have simulated and examined the impacts of reservoir operation on the hydrological characteristics of global rivers. Although, these studies have made great strides in examining the impact of dams on river flow, the observation-based studies alone are not sufficient to disentangle the major drivers of change and there are major deficiencies in simulation-based studies in providing a comprehensive picture of the large-scale and cumulative impacts of dams. Hence, the actual impacts of the existing dams and the potential effects of new dams remain poorly understood. The overarching goal of this dissertation is to address this important research gap by employing a mechanistic approach to develop a holistic understanding of the hydrology

of global river basins under the effects of climate change and human interventions, such as LULC change and dam operations. The study is conducted over the Amazon River basin that is increasingly dammed with hundreds of dams planned for the near future. The historical interannual and interdecadal hydrological changes in the Amazon River basin and its sub-basins are first investigated by implementing a high-resolution, physically based, continental-scale hydrological model, LEAF-Hydro-Flood (LHF), to determine the dominant mechanisms that modulate terrestrial water storage (TWS). The historical impacts of existing dams and the potential impacts from collective operation of existing and planned dams on a basin-wide scale in the Amazon are then quantified under the historical climate using a new dam operation scheme in a high-resolution hydrodynamic model, CaMa-Flood-Dam (CMFD). Using this new dam operation scheme, the potential future changes to the hydrology of the Amazon River basin are then quantified under cumulative operation of existing and planned dams and multiple climate change scenarios for the entire twenty first century. Lastly, this dissertation explores viable alternatives for hydropower generation, by assessing the feasibility—with respect to energy potential and cost—of implementing in-stream turbines to harness a large portion of the power that is expected to be generated by building large dams. The results from the aforementioned analysis provide major advances and crucial insights on the understanding of the integrated river-floodplain-reservoir dynamics in a flood and hydropower dominant river system, such as the Amazon, with further implications for sustainable hydropower development. Over the long run, this assessment could prove beneficial in investigating the future of hydropower in the Amazon and other regions worldwide (for example, the Mekong and Congo River basins) where a boom in construction of mega-scale hydropower dams is underway.

## ACKNOWLEDGEMENTS

I wish to express my deepest gratitude to my advisor, Dr. Yadu Pokhrel, for his invaluable support, guidance, encouragement, and mentoring throughout my graduate studies. His inspiring and invaluable guidance is something I would cherish forever. This dissertation would have been impossible without his help, and I am grateful that I had the opportunity to work with him. Dr. Pokhrel, thank you for bearing with me and pushing me to perform beyond my recognized capabilities.

I would also like to express my great appreciation to my committee members, Dr. Shu-Guang Li, Dr. Phanikumar Mantha and Dr. David Hyndman for serving on my dissertation committee and for their meticulous comments, suggestions, and advice to improve this research work. I also thankfully acknowledge all my co-authors and peers for being critical to my research and providing helpful comments.

I would not be where I am today and would not have been able to complete my research without the unconditional trust, timely encouragement and unparalleled support of my parents, Narendra and Chetana Chaudhari, and my sister and brother-in-law, Samruddhi and Rohan Bhanushali. Although we are oceans apart, they have always been my unwavering pillar of motivation and support. Completing this dissertation is a success for all of us.

Special thanks must go to my dear friends and colleagues Sanghoon Shin, Farshid Felfelani, Mateo Burbano, and Tamanna Kabir for their endless hours of help, steadfast support, and fruitful advice.

I gratefully acknowledge the financial support provided by the National Science Foundation (INFEWS, award no. 1639115 and CAREER, award no. 1752729), and Environmental Science and Policy Program and College of Engineering at Michigan State University. Model simulations

were conducted at Cheyenne (https://doi.org/10.5065/D6RX99HX) provided by NCAR's Computational and Information Systems Laboratory sponsored by the National Science Foundation.

## TABLE OF CONTENTS

## LIST OF TABLES

## LIST OF FIGURES

# Chapter 1. Introduction

## 1.1. Research Motivation

### 1.1.1. Global Hydrological Cycle and the Amazon River Basin

Water is fundamental to Earth System functioning and human society. Due to the central role of water for maintaining global biosphere integrity, regulating climate, and mediating carbon and nutrient cycling, changes to the water cycle can propagate through the Earth System and disrupt processes interacting across numerous scales. For millennia, rivers have provided food, contributed water for domestic use and agriculture, sustained transportation corridors and, more recently, enabled power generation and industrial production (Zarfl et al., 2015). These goods and services generally require built infrastructure, and societies have addressed this demand by constructing an estimated >2.8 million dams (Lehner et al., 2011), regulating and creating over 500,000 km of rivers and canals for navigation and transport and building irrigation and water-diversion schemes (Grill et al., 2019) globally. As a result, rivers are exposed to sustained pressure from fragmentation and loss of river connectivity (Nilsson et al., 2005), constraining their capacity to flow unimpeded, affecting many fundamental processes and functions characteristic of healthy rivers and leading to the rapid decline of biodiversity and essential ecosystem services (Cardinale et al., 2012; Zarfl et al., 2019).

The global growth in food and energy demand is placing unprecedented pressure on the land and water resources of our planet, by encouraging countless human activities coughed up to cope with this increasing demand (Best, 2019). Activities such as land use change in one setting can alter evapotranspiration from land and lead to widespread precipitation alteration in the downwind regions (Wei and Dirmeyer, 2019). Intensified land-water interactions due to human interference are already well-known to incur catastrophic changes to the Earth system, from

large-scale deforestation (Hansen et al., 2013) that may lead to regional forest dieback in areas such as the Amazon (Malhi et al., 2009; Nepstad et al., 2008; Zemp et al., 2017), reduction in sediment delivery by large dams causing mega deltas to sink at an alarming rate in the Mekong (Schmidt, 2015; Syvitski et al., 2009), disappearance of the Aral Sea in central Asia (Pokhrel et al., 2017), and many more impacting its stability as a whole (Rockström et al., 2009; Steffen et al., 2018). Moreover, socioeconomic factors driven by a global food, energy and water demand can impact local hydrological conditions, which is the current state in most global river basins with cattle ranching in the Amazon (Castello and Macedo, 2016), logging in the Congo (Kleinschroth et al., 2019) and agriculture in the Mekong (Pokhrel et al., 2018a).

This emerging understanding of interconnections between local and global water systems is mainly uprooted from world's most biodiverse river basin—the Amazon. Being the largest river system in the world, it contributes to ~20-30% of the world's total river discharge into the oceans (Clark et al., 2015; Muller-Karger et al., 1988; Nepstad et al., 2008), while playing a major role in global atmospheric circulation system (Malhi et al., 2008; Soares-Filho et al., 2010). The vast latitudinal extent causes diverse climatic systems in every corner of the basin, making the Amazon River basin a focal point for many hydrological and meteorological studies in the past century (Coe et al., 2002; Costa and Foley, 1999; Eltahir and Bras, 1994; Hirabayashi et al., 2013; Lesack, 1993; Marengo, 2006, 1995, 1992; Marengo et al., 1998; Matsuyama, 1992; Muller-Karger et al., 1988; Rodrigo Cauduro Dias Paiva et al., 2013; Salati and Vose, 1984; Stehman, 1996; Timpe and Kaplan, 2017; Winemiller et al., 2016; Woodroffe, 1914; Zeng, 1999). Realizing the basin's importance, most of the global studies have considered Amazon region as one of the benchmarks (Felfelani et al., 2017; Haddeland et al., 2014, 2006; Hanasaki et al., 2018; Scanlon et al., 2019), while studying the potential impact on the Amazonian

rainforests and hydrology under the influence of climate change (Coe et al., 2009; Cook and Vizy, 2008; Cox et al., 2004; Guimberteau et al., 2017; Malhi et al., 2008; Nepstad et al., 2008; Pokhrel et al., 2014).

The Amazon River system holds the most diverse fish assemblages and one of the most productive inland fisheries on Earth (Castello and Macedo, 2016). Andean origin rivers contribute roughly half of the Amazon mainstem's annual flow and export massive quantities of sediment, organic matter, and nutrients to the lowlands (Anderson et al., 2018; Finer and Jenkins, 2012; Forsberg et al., 2017) while largely controlling geomorphological processes like river meandering, sediment deposition, and floodplain formation for thousands of kilometers downstream. This annual flood pulse, which inundates over 750,000 $km^2$ of area annually in the Amazon Basin (Resende et al., 2019), in turn supports the largely endemic Amazonian rainforests and the habitats for many vertebrate and invertebrate species, with an estimated 2,411 described and 1,089 endemic species (Arantes et al., 2019), both terrestrial and aquatic, hence maintaining the biodiversity of the entire basin. Some of the fish species are known to migrate thousands of kilometers from Andes to Amazonian lowlands recording the longest freshwater migration in the world (Barthem et al., 2017). Local livelihoods and diets of riverine populations depend heavily on these fisheries that provide the main source of animal protein (Castello et al., 2015). Such an important global region is under-going a hydrological and ecological change at a very large scale mainly due to anthropogenic activities driven by ever increasing food and power demand in the South American continent (Fearnside, 2015, 2014; Finer and Jenkins, 2012; Forsberg et al., 2017; Kahn et al., 2014; Kalamandeen et al., 2018; Latrubesse et al., 2017; Timpe and Kaplan, 2017). Dam constructions, being one of such anthropogenic activities, have been causing unprecedented alterations in the natural hydrological regime of the Amazon, hence

complicating the naturally complex food-energy-water system into a food-energy-water-human system, which has not yet been adequately studied.

### 1.1.2. Climate Change, Hydropower, and Land Use Change in the Amazon

Even though the Amazon receives plentiful rainfall during normal years, it periodically experiences extreme droughts which has been widely observed across the basin (Malhi et al., 2009; Marengo and Espinoza, 2016). These catastrophic droughts had major implications on the hydrology of the Amazon River basin; for example, the 2005 hydrological drought led to reduction in streamflow by 32% from the long-term mean, (Zeng et al., 2008), and in 2010 moisture stress induced persistent declines in vegetation greenness affecting an area of ~2.4 million $km^2$ (Xu et al., 2011). Moreover, forest fires being a direct consequence of the extreme droughts showed an increase of ~3 standard deviations in fire anomalies during the 2005 and 2010 mega-droughts (Aragão et al., 2018, 2007; Brando et al., 2014; Davidson et al., 2012; Malhi et al., 2008; Rammig et al., 2010), generating huge smoke plumes and negatively impacting the health of local populations. The basin has also experienced anomalous wet events causing massive flooding, such as that in 2012 (Satyamurty et al., 2013). Often, these extreme weather events are caused by climatological changes occurring over the Pacific and Atlantic oceans; for example, majority of the historical droughts in Amazon River basin were caused due to the direct consequence of the El Nino events (Marengo, 2004; Marengo and Espinoza, 2016; Satyamurty et al., 2013). However, some of the most severe droughts (e.g., the 2005 and 2010 mega droughts), were not stirred by the El Nino Southern Oscillation and have been suggested to be a result of ongoing human-induced changes such as deforestation, intensive agricultural development, and dam construction (Cook et al., 2012; Cook and Vizy, 2008; Espinoza et al., 2011; Lee et al., 2011; Lewis et al., 2011; Malhi et al., 2008; Marengo, 2004; Marengo et al.,

2008; Marengo and Espinoza, 2016; Phillips et al., 2009; Xu et al., 2011; Zeng et al., 2008). With on-going climate change and potential intensification of human activities, such as the plans for hydropower development of the Amazonian countries' energy sector, these extreme events are expected to increase further in the future (Wanders et al., 2015; Wanders and Van Lanen, 2015; Wanders and Wada, 2015).

Several hundreds of large dams are planned to be built globally, with a major portion of it situated in tropical river basins such as the Amazon. Although, with the growing recognition of the hydrological, ecological, and social impacts of storage-based dams, dam removal due to aging and increased failures is on an upward trend in developed countries such as United States, the developing countries, such as the Amazonian countries, are ramping up dam constructions even though existing ones have been surrounded by controversies due to environmental concerns and complaints from downstream riparian communities (Moran et al., 2018; Winemiller et al., 2016). Currently, 147 dams are under construction and hundreds more are planned in the Andes and the Amazonian lowlands. These dams are continued to be built in a way that disrupts river ecology, causes large-scale deforestation, and negatively affects both the food systems nearby and downstream communities. Further, with the well-known and already felt impacts of climate change, the existing and under construction dams in the Amazon are predicted to generate only a fraction of their originally intended power generation capacity. The recently completed, Belo Monte dam in the Xingu River will produce only 4.46 GW of the 11.23 GW installed capacity in many months of the year due to low river levels, whereas the Jirau and Santo Antonio dams on the Madeira River are predicted to produce only 3 GW each (Moran et al., 2018).

Large dams that impound water forming large reservoirs are one of the main causes of deforestation in the Amazon, with further stimulation from road network expansion that

accompanies dam construction (Hansen et al., 2013). Tree clearing for the purpose of agriculture, dam constructions and cattle ranching has already shrunk the forest by ~15% from its 1970s extent of more than 6 million square kilometers (Amigo, 2020); in Brazil which encompass more than half of the Amazonian forest, 20% has been reported to be disappeared (Nobre et al., 2016; Zemp et al., 2017). Given consensus on the value of natural forests to the Earth system, slowing deforestation in the Amazon rainforest has been a central agenda of Brazil's intervention policy. These efforts played an important role in lowering deforestation rates since their peak in 2004, but the rate has since risen as a result of political turmoil and an economic recession, reaching a decadal high in 2018 (Amigo, 2020). Deforestation at a continental scale, especially in the Amazonian continent, could cause reduced regional precipitation, feeding to the already upscaled climate change processes, eventually reaching a "tipping point" when a permanent shift to a drier ecosystem will be observed (Lovejoy and Nobre, 2018). Compounding the adverse climate impacts caused due to dam construction with ample evidence suggesting a characteristically irreversible (Latrubesse et al., 2017), large-scale degradation of the environment by greenhouse emissions from reservoirs (Fearnside and Pueyo, 2012), loss of suspended solids in rivers (Latrubesse et al., 2017), and erosion of food security (Stone, 2011), there is an urgent need to rethink hydropower technology in order to avoid the future catastrophic impacts of large dams. Therefore, it is imperative to better understand the changing dynamics of the Amazonian floodplains and thereby predict its future evolution under projected water resource development (especially dam construction) and climate change.

### 1.1.3. Implications of Hydropower Development on Hydrology, Ecology, and Societies

Hydropower, being the primary renewable energy resource, is expected to remain a promising source of energy for the foreseeable future, both globally and for the Amazonian countries

(Moran et al., 2018; Winemiller et al., 2016). Therefore, it is critical to develop a better understanding of the hydrological and ecological impacts of the dams along with their performance efficiency and suitability under climate change. Large-scale, storage-based dams are known to cause significant changes in the downstream regions such as impediments to fish migration (Stone, 2016), alterations in freshwater discharge to oceans (Pokhrel et al., 2012b), reductions in sediment movement (Latrubesse et al., 2017) and nutrient transport (Eiriksdottir et al., 2017), river fragmentation (Anderson et al., 2018), disruption of flood pulse dynamics (Pokhrel et al., 2018b), and delta erosion (Yang et al., 2017). There are evidences that even the run-of-the-river hydropower plants incur profound influence on riverine habitat(Anderson et al., 2015) even though the impacts are less severe compared to that of large dam projects.

Past literature has widely reported the impacts of the existing dams on the Amazon River basin and has improved our understanding of their complex interactions with the environment based on the historical changes in hydrology (Anderson et al., 2018; Arantes et al., 2019; Cochrane et al., 2017; Finer and Jenkins, 2012; Kemenes et al., 2011, 2007; Pokhrel et al., 2012a; Resende et al., 2019; Timpe and Kaplan, 2017). Based on these understandings, an index-based framework was developed to quantify their overall impact on the basin with respect to new roads, deforestation and the ever-advancing agricultural frontier, along with the changes to hydrology and sediment transport, which are crucial for downstream floodplains, the estuary and coastal ecosystems (Latrubesse et al., 2017). The critical role of the Andes-to-Amazon connectivity was also highlighted by a regional analysis of river fragmentation by existing and planned hydropower dams in the Andean headwaters of the Amazon (Anderson et al., 2018; Finer and Jenkins, 2012). While such many pieces of knowledge have been accrued, a holistic view of the entire Amazon River basin under the influence of climate change and hydropower dams has not been presented.

Further, several of these studies collectively quantify the changes in the hydrological variables caused by both climate variations and human activities, hence failing to isolate the impacts caused by them individually. These studies provide a spatially and hydrologically fragmented outlook of the dam impacts in the Amazon, which is barely sufficient to comprehensively understand the impact of dams and their dependency on climate change with the entire basin perspective. Moreover, the impact from cumulative operations of existing dams and the potential additional stress caused by introducing the numerous planned dams on the entire basin still remains largely unexplored.

To address this knowledge gap, this dissertation begins by investigating the natural hydrology of the entire Amazon River basin, focusing on the interdecadal and interannual variations in hydrological variables and the dominant factors driving their evolution. Impacts of dams on the entire Amazon River basin as whole are quantified by taking an integrated approach which utilizes a river-floodplain-reservoir hydrodynamic model enabling a mechanistic investigation of natural and human-induced changes in surface water dynamics at high-resolution over a large domain. Further, the role of the existing and planned dams in shaping the hydrology of the Amazon in the future under various climate change scenarios is investigated using a set of multi-model hydrological simulations (20 ensemble members) from the selected five terrestrial hydrology models driven by atmospheric forcing from four global climate models (GCMs) as defined in the Inter-Sectoral Impact Model Intercomparison Project, phase 2b (ISIMIP2b; https://www.isimip.org/). Lastly, the dissertation explores viable alternatives for hydropower generation, by assessing the feasibility of implementing in-stream turbines to harness a large portion of the power that is expected to be generated by building large dams. The aforementioned analysis framework is indispensable for the Amazon—where the flow is

characterized by a highly pronounced seasonal dynamics and an unprecedent boom in the construction of hydropower dams is underway—to understand the impacts of dam construction in order to plan a sustainable hydropower future for the basin.

### 1.2. Research Goal, Objectives, and Science Questions

As referenced above, our current knowledge of the rapidly changing hydro-climatology and the complex human-climate interactions provides both gaps/challenges and opportunities to improve the understanding of the role of human interventions such as dam operations, in shaping the hydrological future of global river basins. The necessity of using realistic hydrological modelling schemes to quantify the holistic impact of dam operations on the hydrological characteristics of a river basin and exploring alternative sustainable technology for hydropower generation to address the increasing issues related to the sustainability of food, energy, and water systems under changing earth environment led me to pursue this dissertation. The overarching goal of this dissertation is to advance our understanding of the complex interactions of human activities, such as LULC change and dam operations, with the hydrology of large river basins and quantify their long-term impacts on hydrological characteristics. The insights from this dissertation are expected to be useful to the broader scientific community in addressing the ever-increasing concerns related to sustainable development of hydropower along with the management of food, water, and energy systems in the Amazon and other parts of the world. The overarching goal is achieved by addressing a set of key science questions, which are posed for each chapter of the dissertation.

**Chapter 2:**

Question 1. How do interannual and interdecadal changes in drought conditions manifest as long-term variations in TWS at varying spatial and temporal scales in the Amazon River basin?

Question 2. What are the impacts of TWS variations on dry-season water deficit and release? Is the Amazonian dry season getting stronger or more severe?

Question 3. What are the dominant factors driving the evolution of TWS and drought conditions at varying spatial and temporal scales?

Question 4. How does the sub-surface water storage regulate the water deficiency caused by the surface drought conditions?

**Chapter 3:**

Question 5. What are the impacts of flow regulations induced by large-scale storage-based hydropower dams on downstream river flow and flood dynamics in the Amazon River basin?

Question 6. What is the role of hydropower dam operations in modulating the flood pulse along the mainstem of the Amazon?

Question 7. What will be the potential impacts of the combined operation of existing and planned hydropower dams in the Amazon?

**Chapter 4:**

Question 8. What are the future implications of the on-going hydropower development combined with climate change on the downstream flood dynamics in the Amazon?

Question 9. What will be the role of planned hydropower dams in controlling the floodplain dynamics in the Amazon mainstream?

**Chapter 5:**

Question 10. Are in-stream turbines feasible alternative to building large dams?

### 1.3. Dissertation Outline

The following provides a summary of the remainder of the dissertation.

**Chapter 2.** Multi-decadal hydrologic change and variability in the Amazon River basin: Understanding terrestrial water storage variations and drought characteristics.

- Basin-wide spatiotemporal TWS variations are investigated in comparison with GRACE satellite data.
- Major historical droughts in the Amazon River basin are characterized with respect to their type, propagation, and hydrological impact on the river basin.

**Chapter 3.** Alteration of River Flow and Flood Dynamics by Existing and Planned Hydropower Dams in the Amazon River Basin.

- Impacts of the existing and planned large-scale hydropower dams in the Amazon are investigated using individually optimized dam operation schemes in a high-resolution river-floodplain routing model, the CaMa-Flood-Dam.

**Chapter 4.** Hydrological future of the dammed Amazon under climate change.

— Impacts of existing and planned large-scale hydropower dams in the Amazon are investigated under multiple climate change scenarios using a multi-model ensemble of 20 simulations

**Chapter 5.** In-stream turbines for rethinking hydropower development in the Amazon basin.

— Suitability of in-stream turbines for future hydropower generation in the Amazon is investigated with respect to its power potential and cost.

**Chapter 6.** Summary

# Chapter 2. Multi-Decadal Hydrologic Change and Variability in The Amazon River Basin: Understanding Terrestrial Water Storage Variations and Drought Characteristics

*Based on*: **S. Chaudhari**, Y. Pokhrel, E. F. Moran, and G. Miguez-Macho, 2019. Multi-decadal Hydrologic Change and Variability in the Amazon River Basin: Understanding Terrestrial Water Storage Variations and Drought Characteristics. ***Hydrology and Earth System Sciences (HESS).*** DOI: https://doi.org/10.5194/hess-23-2841-2019

## 2.1. Introduction

The Amazon River basin is one of the most hydrologically and ecologically diverse regions in the world (Fan and Miguez-Macho, 2010; Latrubesse et al., 2017; Lenton et al., 2009; Lesack, 1993; Malhi et al., 2008; Moran et al., 2018; Timpe and Kaplan, 2017; Tófoli et al., 2017). It is home to the world's largest tropical rainforest and hosts ~25% of all terrestrial species on Earth (Malhi et al., 2008). Hydrologically, it contributes to 20-30% of the world's total river discharge into the oceans (Clark et al., 2015; Muller-Karger et al., 1988; Nepstad et al., 2008) and accounts for ~15% of global terrestrial evapotranspiration (Field et al., 1998; Malhi et al., 2008). Thus, the Amazon is an important component of global terrestrial ecosystems and the hydrologic cycle (Cox et al., 2004; Nobre et al., 1991); it also plays a major role in global atmospheric circulation through precipitation recycling and atmospheric moisture transport (Malhi et al., 2008; Soares-Filho et al., 2010).

The hydro-ecological systems of the Amazon are dependent on plentiful rainfall (Cook et al., 2012; Espinoza et al., 2016, 2015; Espinoza Villar et al., 2009; Nepstad et al., 2008) and the vast amount of water that flows down through extensive river networks and massive floodplains (Bonnet et al., 2008; Coe et al., 2002; Frappart et al., 2011; Miguez-Macho and Fan, 2012a; Yamazaki et al., 2011; Zulkafli et al., 2016). The spatiotemporal patterns of precipitation are,

however, changing due to climate change and variability (Brando et al., 2014; Cook et al., 2012; Lima et al., 2014; Malhi et al., 2009, 2008; Nepstad et al., 2008), large-scale alterations in land use (e.g., deforestation) (Chen et al., 2015; Coe et al., 2009; Davidson et al., 2012; Kalamandeen et al., 2018; Lima et al., 2014; Panday et al., 2015; Tollefson, 2016), and more recently the construction of mega-dams (Finer and Jenkins, 2012; Latrubesse et al., 2017; Moran et al., 2018; Soito and Freitas, 2011; Timpe and Kaplan, 2017; Winemiller et al., 2016), among others. Such changes in precipitation patterns typically manifest themselves in terms of altered magnitude, duration, and timing of streamflow (Marengo, 2005). A prominent streamflow alteration pattern that has been widely observed across the Amazon is the extended dry-season length (Espinoza et al., 2016; Marengo et al., 2011) and an increase in the number of dry events (i.e., droughts) over the longer term (Malhi et al., 2009; Marengo and Espinoza, 2016), which has been suggested to be a result of ongoing climatic and human-induced changes (Cook et al., 2012; Cook and Vizy, 2008; Lee et al., 2011; Malhi et al., 2008; Shukla et al., 1990). However, the cross-scale interactions and feedbacks in the human-water relationship make it difficult to explicitly quantify the causes. These changes have resulted in decreases in runoff (Espinoza et al., 2009; Haddeland et al., 2014; Lima et al., 2014), and loss of terrestrial biodiversity (Barletta et al., 2010; Newbold et al., 2016; Tófoli et al., 2017; Toomey et al., 2011; Winemiller et al., 2016). Increased variability in streamflow has also resulted in the disruption of the food pulse and fishery yields, which the Amazon region thrives upon (Castello et al., 2015, 2013; Forsberg et al., 2017). Moreover, persistent dry events create social negative externalities, such as deterioration of respiratory health due to drought induced fires (Smith et al., 2014), exhaustion of family savings (Brondizio and Moran, 2008), isolation of communities that are affected by navigation and drinking water scarcity (Sena et al., 2012), hence affecting the overall livelihood of the local

communities. Thus, it is critical to understand the characteristics of the historical droughts to better understand the dominant mechanisms that modulate droughts and their evolution over time.

As often is the case, droughts in the Amazon are driven by El Niño events, however, some droughts are suggested to be caused by climate change and variability (Espinoza et al., 2011; Lewis et al., 2011; Marengo et al., 2008; Marengo and Espinoza, 2016; Phillips et al., 2009; Xu et al., 2011; Zeng et al., 2008) and due to accelerating activities causing rapid changes in land use/water cycle (Lima et al., 2014; Malhi et al., 2008). Numerous studies have quantified the impacts and spatial extent of these periodic droughts on the hydrological and ecological systems in the Amazon (Alho et al., 2015; Brando et al., 2014; Castello et al., 2015, 2013; Chen et al., 2010, 2009; da Costa et al., 2010; Davidson et al., 2012; Fernandes et al., 2011; Lewis et al., 2011; Phillips et al., 2009; Saleska et al., 2016, 2007; Satyamurty et al., 2013; Schöngart and Junk, 2007; Xu et al., 2011; Zeng et al., 2008). For example, Lewis et al., (2011) found that the 2010 drought was spatially more extensive than the 2005 drought; the spatial extent was over 3.0 million $km^2$ in 2010 and 1.9 million $km^2$ in 2005. These catastrophic droughts had major implications on the hydrology of the Amazon River basin; for example, the 2005 hydrological drought led to reduction in streamflow by 32% from the long-term mean, as reported in Zeng et al., (2008), and in 2010 moisture stress induced persistent declines in vegetation greenness affecting an area of ~2.4 million $km^2$ which was 4 times greater than the area impacted in 2005 (Xu et al., 2011). Moreover, these extreme drought events, coupled with forest fragmentation have caused widespread fire-induced tree mortality and forest degradation across Amazonian forests (Aragão et al., 2007; Brando et al., 2014; Davidson et al., 2012; Malhi et al., 2008; Rammig et al., 2010).

Due to the limited availability of observed data (e.g., precipitation, streamflow) for the entire basin, hydrologic characteristics of droughts in the Amazon has been studied primarily by using hydrological models and satellite remote sensing. For example, early studies (Coe et al., 2002; Costa and Foley, 1999; Lesack, 1993; Vorosmarty et al., 1996; Zeng, 1999) examined different components of the Amazon water budget and their trends through relatively simpler models. More recent literature (Dias et al., 2015; Fan et al., 2019; Getirana et al., 2012; Miguez-Macho and Fan, 2012a, 2012b; Rodrigo C D Paiva et al., 2013; Rodrigo Cauduro Dias Paiva et al., 2013; Pokhrel et al., 2012b, 2012a, 2013; Shin et al., 2019; Siqueira et al., 2018; Wang et al., 2019; Yamazaki et al., 2012a, 2011) provided further advances in modeling the hydrological dynamics connected with anthropogenic activities in the Amazon and other parts of the world. Methods with varying complexities were used in similar studies, ranging from simple water budget analyses, (Betts et al., 2005; Costa and Foley, 1999; Fernandes et al., 2008; Lesack, 1993; Sahoo et al., 2011; Vorosmarty et al., 1996; Zeng, 1999) to state-of-the-art land surface models (Getirana et al., 2012; Miguez-Macho and Fan, 2012a, 2012b; Rodrigo C D Paiva et al., 2013; Rodrigo Cauduro Dias Paiva et al., 2013; Pokhrel et al., 2013; Siqueira et al., 2018; Wongchuig Correa et al., 2017; Yamazaki et al., 2012a, 2011), with some targeting the overall development of parameterization and process representation in the model (Coe et al., 2009, 2008; Dias et al., 2015; Getirana et al., 2012, 2010; Miguez-Macho and Fan, 2012a, 2012b; Rodrigo Cauduro Dias Paiva et al., 2013; Pokhrel et al., 2013; Yamazaki et al., 2011), and others on the hydrological changes occurring in the basin due to weather variability (Coe et al., 2002; Lima et al., 2014; Wongchuig Correa et al., 2017).

The major droughts events in the Amazon, particularly those in recent years, have been detected by satellite remote sensing and their impacts on terrestrial hydrology have been examined (Chen

et al., 2010; Filizola et al., 2014; Xu et al., 2011). In particular, the hydrologic impact of droughts has been revealed by examining the anomalies in terrestrial water storage (TWS) inferred from the Gravity Recovery and Climate Experiment (GRACE) satellites. A significant decrease in TWS over Central Amazon in the summer of 2005, relative to the average of the five other summer months during 2003-2007 period, was reported by Chen et al., 2009. However, due to the vast latitudinal extent of the Amazon basin, these severe dry conditions were observed only in some regions of the basin. Xavier et al., (2010) and Frappart et al., (2013) used GRACE TWS estimates to identify the signature of these drought events and suggested that the 2005 drought only affected the western and central parts of the basin, whereas very wet conditions peaking in mid-2006 were observed in the eastern, northern and southern regions of the basin. Although the ramifications of these extreme droughts have been widely studied using remote sensing datasets (e.g., GRACE), the understanding of their time-evolution is limited due to data gaps and short study periods, hence hindering their comprehensive categorization. Further, GRACE provides the changes in vertically integrated TWS variations, thus variations in the individual TWS components cannot be estimated solely by GRACE. This shortcoming is overcome by using hydrological models that separate TWS into its individual components and provide simulations for an extended timescale. However, discrepancy between models and GRACE observations has also become a major topic of discussion, as most of the global models show an opposite trend in TWS compared to GRACE in Amazon and other global river basins (Scanlon et al., 2018); yet, no clear explanation or quantification exist in the published literature, apart from the attribution of the discrepancy to model shortcomings (see Section 2.3.3 for details).

As referenced above, the changing hydro-climatology of the Amazon basin, along with specific drought related analysis (e.g., 2005, 2010) has been widely reported in a large body of literature published over recent decades. Several studies have used statistical measures to quantify drought severity (Espinoza et al., 2016; Gloor et al., 2013; Joetzjer et al., 2013; Marengo, 2006; Marengo et al., 2011, 2008; Wongchuig Correa et al., 2017; Zeng et al., 2008; M. Zhao et al., 2017a), concerning common variables, such as streamflow and precipitation, thus limiting the quantification of drought impact on water stores viz. flood, groundwater and TWS. Further, even though these studies encompass different aspects of hydrological and climatic changes, most span over only a few years to a decade, except for some precipitation related studies (Marengo, 2004; Marengo et al., 1998). Other studies have used a relatively longer study period (Costa et al., 2003; Espinoza et al., 2016; Zeng, 1999), but the spatial extent is limited. Thus, a comprehensive understanding of the interdecadal hydrologic change and variability across the entire basin and that of changes in drought characteristics is still lacking. Given the number of droughts that have occurred and their widespread impact in the Amazon, it is imperative to have a better understanding of these past events so as to anticipate future hydrological conditions (Phipps et al., 2013). Many aspects of the droughts are yet to be studied, such as, the inter-dependence between TWS and meteorological (precipitation-related) and hydrological (streamflow-related) droughts. A complete categorization of the drought events with respect to their causes and impacts and the resulting basin response is still coming up short.

In this chapter, we investigate the interannual and interdecadal variability in TWS and drought events in the Amazon River basin over 1980-2015 period. Our study is driven by the following key science questions: (1) how do interannual and interdecadal changes in drought conditions manifest as long-term variations in TWS at varying spatial and temporal scales in the Amazon

River basin? (2) What are the impacts of TWS variations on dry season water deficit and release? Is the Amazonian dry season getting stronger/severe? (3) what are the dominant factors driving the evolution of TWS and drought conditions at varying spatial and temporal scales? And (4) how does the sub-surface water storage regulate the water deficiency caused by the surface drought conditions? These questions are answered by using hydrological simulations from a continental-scale hydrological model and the TWS data from GRACE satellites; the goal is to provide a comprehensive picture of characteristics and evolution of droughts in the Amazon with respect to their types and spatial impact. Specifically, this chapter aims to: i) examine the impacts of drought conditions on TWS and other hydrological variables; ii) understand the hydrological variability and drought evolution in the Amazon at an annual and decadal scale over the past four decades; iii) quantify the role of sub-surface water storage in alleviating the surface drought conditions; and iv) summarize each drought year by providing a comprehensive characterization for the major drought events in the Amazon and its sub-basins.

## 2.2. Model and Data

### 2.2.1. The Leaf-Hydro-Flood (LHF) Model

The model used in this chapter is LHF (Fan et al., 2013; Miguez-Macho and Fan, 2012b, 2012a; Pokhrel et al., 2014, 2013), a continental-scale land hydrology model that resolves various land surface hydrologic and groundwater processes on a full physical basis. It is derived from the model Land-Ecosystem-Atmosphere Feedback (LEAF) (Walko et al., 2000), the land surface component of the Regional Atmosphere Modeling System (RAMS) (Pielke et al., 1992). The original LEAF was extensively improved and enhanced to develop LEAF-Hydro for North America (Fan et al., 2007; Miguez-Macho et al., 2007) by adding a prognostic groundwater storage and allowing (1) the water table to rise and fall or the vadose zone to shrink or grow, (2)

the water table, recharged by soil drainage, to relax through streamflow into rivers, and lateral groundwater flow, leading to convergence to low valleys, (3) two-way exchange between groundwater and rivers, representing both losing and gaining streams, (4) river routing to the ocean as kinematic waves, and (5) setting sea level as the groundwater head boundary condition. Miguez-Macho and Fan, (2012a) further enhanced the LEAF-Hydro framework by incorporating the river-floodplain routing scheme which solves the full momentum equation of open channel flow, giving more realistic streamflow estimates by considering the prominent backwater effect observed in the Amazon (Bates et al., 2010; Yamazaki et al., 2011). LHF model has been extensively validated in the North and South American continents at 5km and 2km grids, respectively (Fan et al., 2013; Miguez-Macho et al., 2008; Miguez-Macho and Fan, 2012a, 2012b; Pokhrel et al., 2013; Shin et al., 2019) and used to examine the impacts of climate change on groundwater system in the Amazon (Pokhrel et al., 2014). A complete description of the parameterization of LHF can be found in Miguez-Macho and Fan (2012a) and its key elements are summarized below.

The sub-surface water store in LHF is partitioned by the water table into two components: soil water in the vadose zone above and groundwater in the saturated zone (GW) below. Soil column in LHF follows a configuration of 14 layers extending to a depth of 4 m and a bottom layer of variable thickness that extends to the water table. The downward drainage due to gravity and capillary flux (C) are obtained from solving the Richard's equation.

$$q = K_\eta \left(\frac{\partial \psi}{\partial z} - 1\right), \qquad K_\eta = K_f \left(\frac{\eta}{\eta_f}\right)^{2b+3}, \qquad \psi = \psi_f \left(\frac{\eta_f}{\eta}\right)^b \tag{2-1}$$

where q is water flux between two adjacent layers, $K_\eta$ is hydraulic conductivity at given volumetric water content $\eta$, $\psi$ is soil capillary potential, b is soil pore size index, and subscript $f$

denotes the quantity at saturation. Soil data is obtained from UNESCO's Food and Agriculture Organization (FAO) digital soil map of the world at 5 arc-minute grids (http://www.fao.org/nr/land/ soils/digital-soil-map-of-the-world/en/). Fractions of silt, clay, and sand are mapped into 12 texture classes as defined by the U.S. Department of Agriculture (http://soils.usda.gov/ education/resources/lessons/texture/). For each texture class, the soil parameters are assigned based on the method of Clapp and Hornberger (1978). If the water table is within 4.0 m, saturation boundary condition occurs at this depth, above which soil water flux is calculated as described above. If the water table is below 4.0 m, a variable thickness layer is added to extend the soil column to the water table. The flux across the water table is converted to water table rise or fall according to the saturation level above the water table. Further, the mass balance in the groundwater store in each grid cell is explicitly tracked as follows,

$$\frac{dS_G}{dx} = \Delta x \Delta y(-R - FG) - RG + \sum_1^8 Q_g \quad (2\text{-}2)$$

where $S_G$ is the groundwater store, R is recharge flux across the water table, FG is groundwater-floodplain exchange, RG is river-groundwater exchange, and $Q_g$ is the lateral groundwater flow from or to the eight neighboring cells calculated from Darcy's law. In case, the water table is at the surface, R = 0, and the groundwater directly interacts with the floodplain through FG which is groundwater seepage as a result of lateral groundwater convergence from neighboring cells.

The exchanges between river and floodplain in LHF are governed by the following mass balance equation,

$$\frac{dS_S}{dx} = SR + RG + \Delta x \Delta y FG + \sum_1^7 Q_i - Q_o - \Delta x \Delta y(I + E) + \sum_1^8 Q_f \quad (2\text{-}3)$$

where, SR is surface runoff from within the cell, $Q_i$ is the inflow from the upstream river cells, $Q_o$ is the river outflow to the downstream cell, E evaporation from flood water, I, is the infiltration to the unsaturated soil below, and $Q_f$ is the floodwater movement among adjacent cells. The river-floodplain store ($S_S$) comprises of the water in the river channel and floodplain within each grid cell. At a given timestep, if the water level in the river exceeds its bank height, the excess water is spread uniformly over the cell containing the channel, and the flood height is calculated with a surface elevation equal to that of the water in the river channel, now above bank height. Flood water spreads to neighbor cells in eight directions, as determined by water surface elevation difference, or converges towards the river as it recedes. The exchanges between river and groundwater (RG) are calculated with Darcy's law following the widely used groundwater model, MODFLOW. The following equation governs the RG flux,

$$RG = RC \cdot \left(h_g - h_r\right) \tag{2-4}$$

where RC is the river hydraulic conductance and, $h_g$ and $h_r$ represents the water table head in the cell and river elevation, respectively. Since, RC a dynamic parameter and our objective is to reflect the long-term ground- water drainage efficiency in terms of the mean river conductance, we define RC as the product of an equilibrium part and a dynamic part.

$$ERC = \frac{\Delta x \Delta y R + \sum_1^8 Q_g}{h_{ge} - h_r}, DRE = \exp\left[a(h_g - h_{ge}\right] \tag{2-5}$$

where ERC and DRC are the equilibrium and dynamic part of the river conductance respectively, $h_{ge}$ is the equilibrium water table head obtained from the high-resolution equilibrium results (Fan et al., 2013). The long-term groundwater recharge plus lateral convergence from upland cells (numerator) balances long-term river base flow (denominator x ERC), and ERC represents

this long-term mean groundwater-river hydraulic connection. Whereas, as water table rises, stream channels widen and extend, increasing drainage density and accelerating groundwater discharge and vice versa; these fluctuations are represented by the DRC component of the river conductance.

Finally, the surface water fluxes, namely, $Q_f$, $Q_o$ and $Q_i$, are solved from the river and floodplain mass balances and the momentum equation of open channel flow.

$$\frac{\partial v}{\partial t} + v\frac{\partial v}{\partial x} + g\left(\frac{\partial d}{\partial x} + S_f + S_b\right) = 0 \quad (2\text{-}6)$$

where $v$ is mean flow velocity in the cross-section, $d$ is the flow depth, and $S_f$ and $S_b$ are the friction and riverbed slope, respectively. The first , second and third term in the 1d momentum equation represent the inertia force from local acceleration and advection, and the pressure force, respectively. Neglecting the first three terms gives the kinematic wave method, which is commonly applied for continental-scale river routing. It follows the simplest approach and velocity is estimated by equating the friction and riverbed slope. However, the kinematic wave method is sufficient for regions with bed slope is steep and the flow is shallow and neglects the flood movement is uninhibited by rising waters below, which is especially true in the Amazon. Another form of the 1D momentum is the diffusion equation which is obtained by summing the third and the last term ($S_b$) giving the water surface slope and equating it to the friction slope ($S_f$). Although, the backwater effects can be accounted using the diffusion equation, its explicit finite difference solutions are unstable at finer grids (Bates et al., 2010; Miguez-Macho and Fan, 2012a), unless they are run at a smaller timesteps or solved implicitly, which makes the solution computationally expensive at decadal scales. Hence, in this study we implement the quasi-explicit method to solve the full momentum equation with both inertia terms. Approximating the

hydraulic radius and flow depth using common means, we implement the finite difference equation to solve for velocity as follows,

$$\frac{v_i^{t+\Delta t}-v_i^t}{\Delta t}+v_i^{t+\Delta t}\frac{v_{i+1}^t-v_i^t}{\Delta x}+g\frac{h_{i+1}^{t+\Delta t}-h_i^{t+\Delta t}}{\Delta x}+\frac{gn^2v_i^t}{(a_i^{t+\Delta t})^{\frac{4}{3}}}v_i^{t+\Delta t}=0 \quad (2\text{-}7)$$

where, $d$ is the water depth and $h$ is the water surface elevation. The water height at the next time step is obtained from the mass continuity equation with known the flow velocity from the previous timestep.

***Table 2-1. River, Floodplain, and groundwater parameterization in LHF model.***

| Variable | Equation | Description |
|---|---|---|
| River Width | $W = aA^b$ | $a$ = 0.421, $b$ = 0.592, $A$ = drainage area (Coe et al., 2008) |
| Channel Depth | $D = \overline{d} + H$ | H = riverbank height |
| Long-term mean flow depth | $\overline{d} = \left(\frac{\overline{v}n}{\sqrt{S}}\right)^{\frac{3}{2}}$ | $S$ = longitudinal channel slope (Miguez-Macho and Fan, 2012a) |
| Long-term mean flow velocity | $\overline{v} = \frac{\overline{Q}}{W\overline{d}}$ | $\overline{Q}$ = long-term mean flow, $W$ = river width (Miguez-Macho and Fan, 2012a) |
| Manning's constant | $n$ = 0.03 | |
| Hydraulic Conductivity | $K = K_o e^{\left(-\frac{z}{f}\right)}$ | $K_o$= hydraulic conductivity of the top layer, $z$ = depth, $f$ = decay factor (Miguez-Macho and Fan, 2012a) |
| Hydraulic Conductivity of the top layer | $K_o$ | Obtained from the UNESCO's FAO soil map (Miguez-Macho and Fan, 2012a) |

### 2.2.2. Atmospheric Forcing

Atmospheric forcing data are taken from WATCH Forcing Data methodology applied to ERA-Interim reanalysis data (WFDEI) (Weedon et al., 2014), available for the 1979-2016 period at 0.5° spatial resolution and 3-hr timesteps. WFDEI dataset is widely used in for both global and regional scales studies (Beck et al., 2016; Felfelani et al., 2017; Hanasaki et al., 2018; Schmied et al., 2014), and has been suggested to well represent the observations in the Amazon region (Monteiro et al., 2016). The original WFDEI data at 0.5° resolution are spatially interpolated using a bilinear interpolation method to model grid resolution (~2km), following our previous studies (Miguez-Macho and Fan, 2012a, 2012b; Pokhrel et al., 2014, 2013; Shin et al., 2019). The more recent European Centre for Medium-Range Weather Forecasts Reanalysis 5$^{th}$ (ERA5) dataset, which provides atmospheric forcing data from 1979 to present day at a spatial resolution of 0.25°, show promise by outperforming its predecessors (Towner et al., 2019). However, as no studies existed in the past literature which comprehensively validated the ERA5 dataset over the Amazon region until recently, WFDEI forcing remains a better alternative as a model input.

### 2.2.3. Land Use Land Cover and Leaf Area Index

The land cover data used in this chapter are obtained from the European Space Agency Climate Change Initiative's Land Cover project (ESA-CCI; http://maps.elie.ucl.ac.be/CCI/). The data comprise of an annual timeseries of high-resolution land cover maps for 1992-2015 period at a 300m spatial resolution, generated by combining the baseline map from the Medium-spectral Resolution Imaging Spectrometer (MERIS) instrument and the land use land cover (LULC) changes detected from AVHRR (1992 - 1999), SPOT-Vegetation (1999 - 2012) and PROBA-V (2013 - 2015) instruments. The classification follows the LULC classes defined by the UN Land Cover Classification System (LCCS). Spatiotemporal coverage and resolution of these LULC

maps are consistent with the specific LHF model requirements; hence we use annual land cover input, spatially aggregated to 2km LHF model grids, following the general practice in hydrologic impact studies (Arantes et al., 2016; Panday et al., 2015). Land cover maps for the last years of each decade are shown Figure 2-1).

Because the ESA-CCI data did not cover the simulation period prior to year 1992, we derive the time-series products for 1980-1991 period by using the trend in leaf area index (LAI) and the ESA-CCI landcover map for year 1992 as a baseline. A pixel-by-pixel analysis is conducted and the pixels with mean annual LAI higher than 5 are transitioned into forest canopy, whereas for other pixels LULC type is retained from the previous year's LULC map. The threshold of LAI equal to 5 for facilitating the land cover transition into forest is determined based on the LAI classifications provided in past literature (Asner et al., 2003; Myneni et al., 2007; Xu et al., 2018). Reverse prediction of LULC changes was constrained to forest canopy only, as it is difficult to predict the LULC type based on LAI values less than 5. Also, forest cover is known to be the most prominent land cover in the Amazon, hence it is reasonable to assume that most of the LULC changes occurring in the basin are transitioned from forest cover.

Monthly LAI data are derived by temporally aggregating the 8-day composites from Global Land Surface Satellite (GLASS) LAI product (Liang and Xiao, 2012; Xiao et al., 2014) to monthly values for the entire model domain. GLASS LAI values for the period of 1982-1999 are derived from AVHRR reflectance, whereas MODIS reflectance values are used for period 2000-2012. Because of the data constraint, LAI data for years before 1982 and after 2012 are assumed to be the same as that of years 1982 and 2012, respectively.

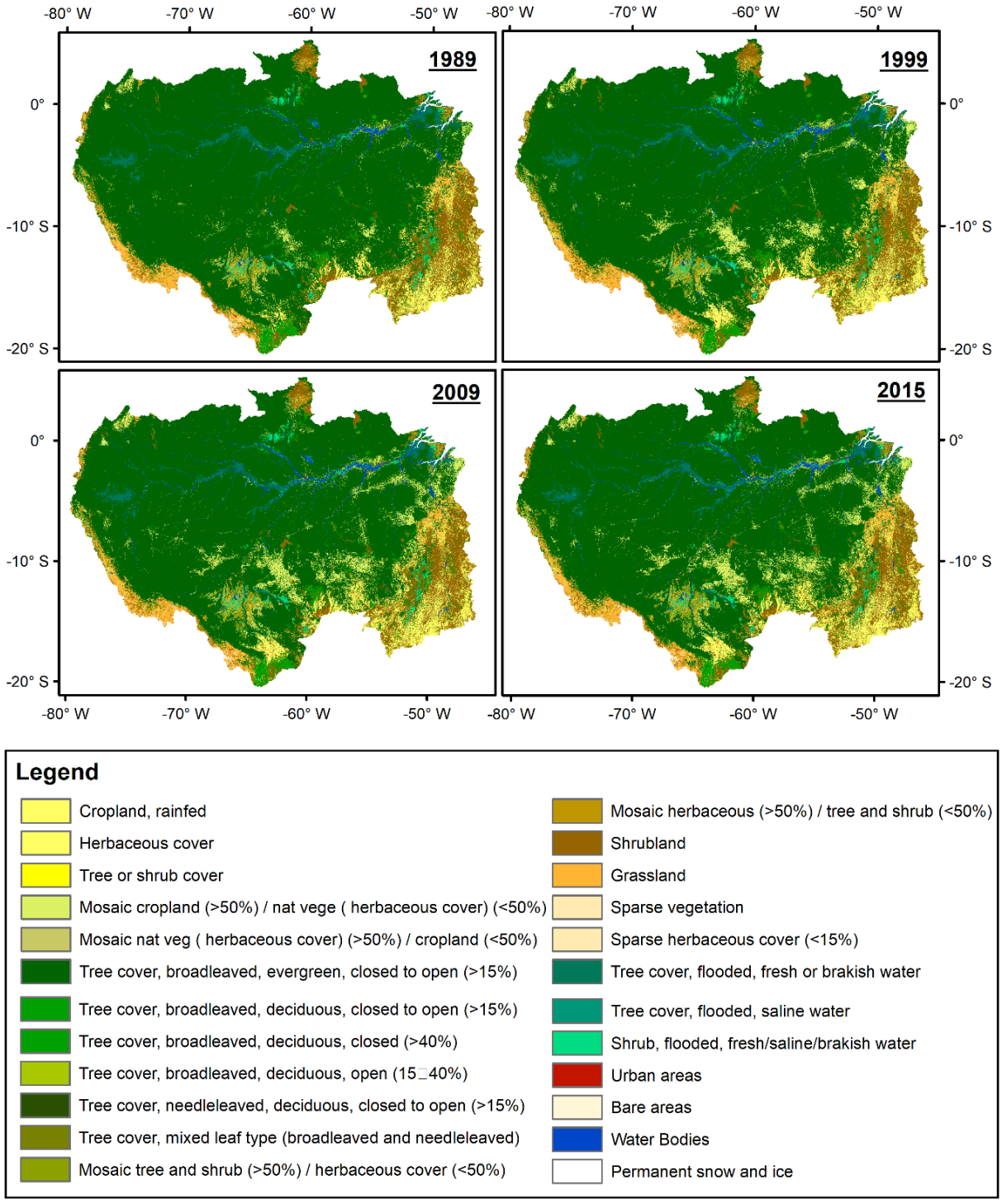


***Figure 2-1. LULC maps obtained from ESA-CCI Land Cover product.*** *LULC maps at the end of each decade from 1980-2010 and 2015 representing the on-going decade at ~2km resolution. Original data is available as annual maps from 1992-2015 at 300m resolution. The 1989 LULC map is derived using a pixel-by-pixel analysis explained in Section 2.2.3. Original data is aggregated to ~2km for model runs.*

### 2.2.4. Validation Data

#### 2.2.4.1. Observed Streamflow

We use monthly averaged streamflow data obtained from the Agência Nacional de Águas (ANA) in Brazil (http://hidroweb.ana.gov.br). Fifty-five stream gauge stations are selected considering a wide coverage over the Amazonian sub-basins, and a good balance between low and high flow values (Figure 2-2). The major selection criterion is the data length, i.e., we only include gauges with at least 30 years coverage. In a few cases, such as for Japura sub-basin, the threshold was overlooked because this criterion resulted in a small number of gauging stations. All the selected stations have observational data for varying time frames with minimal data gaps; the months with missing data are skipped in the statistical analysis.

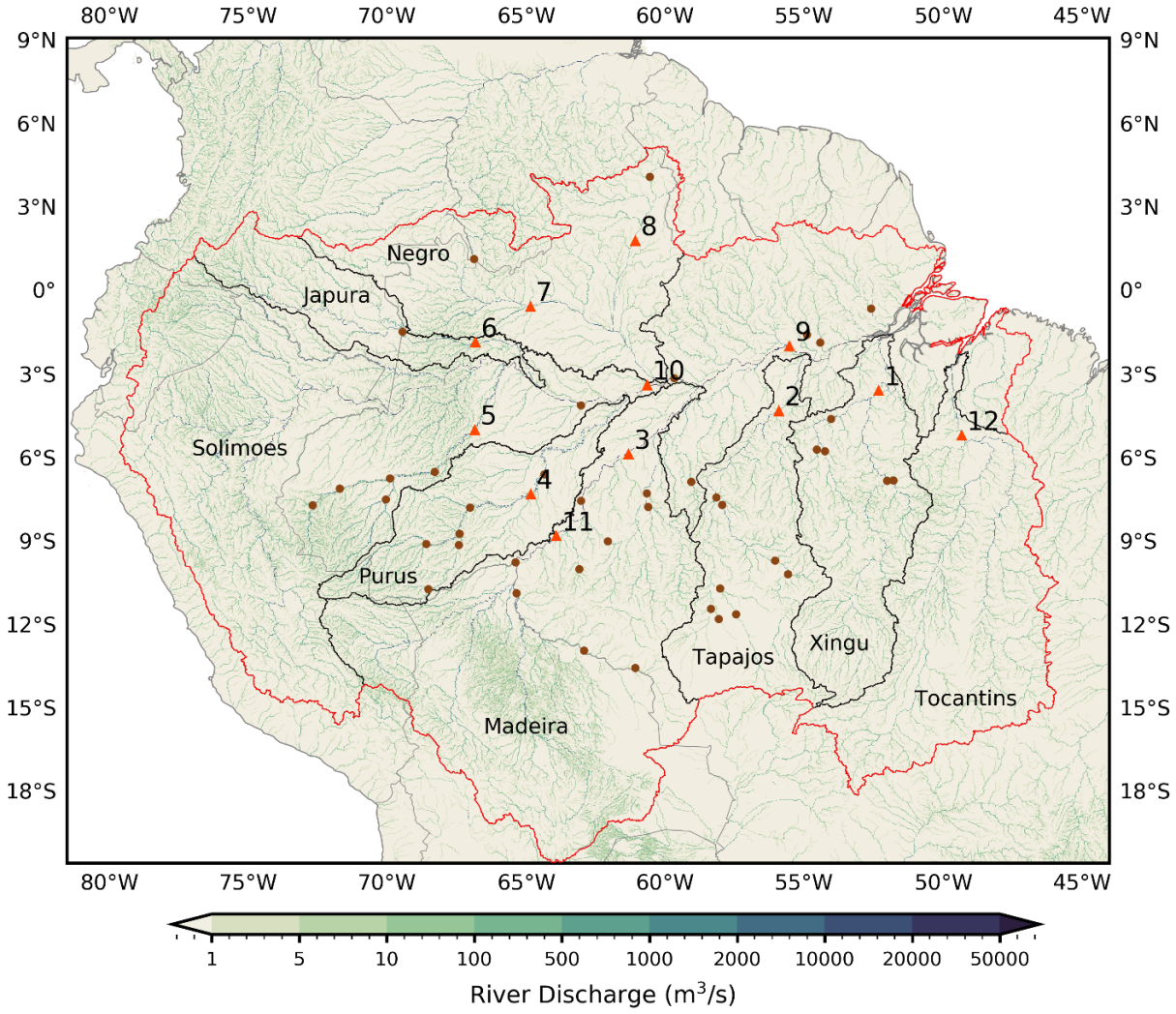


***Figure 2-2. Spatial distribution of simulated streamflow from LHF at the original ~2 km model grids.*** *Markers indicate the locations of the stream gauge stations we use to validate the simulated streamflow from LHF. Highlighted and indexed markers are the gauge stations for which a timeseries comparisons are shown in Figure 2-5.. Red line shows the extend of Amazon River basin including the Tocantins region.*

#### 2.2.4.2. GRACE Data

The TWS products from the GRACE satellite mission are used to validate the TWS simulated by LHF for 2002-2015 period. Equivalent water height from three processing centers, namely: (i) Jet Propulsion Laboratory (JPL) , (ii) the Center for Space Research (CSR), and (iii) the German Research Center for Geoscience (GFZ) (http://grace.jpl.nasa.gov/data/ get-data/) (Landerer and Swenson, 2012) are used along with two mascon products from CSR and JPL; mascon products have been suggested to better capture TWS signals in many regions (Scanlon et al., 2016). Basin-averaged data of variation in TWS anomalies are calculated from GRACE by taking an area-weighted arithmetic mean with varying cell area (Felfelani et al., 2017).

### 2.2.5. TWS Drought Severity Index

To examine the occurrence and severity of hydrological droughts over the past decades, we employ the drought severity index derived from time-varying TWS change from GRACE, known as the GRACE Drought Severity Index (GRACE-DSI) (M. Zhao et al., 2017b). We apply GRACE-DSI framework to the 36-year simulated TWS (referred hereafter to as TWS-DSI) to examine the interannual and interdecadal drought evolution over the entire basin. This index is solely based on the TWS anomalies and has been shown to capture the past droughts with favorable agreement with other drought indices derived from precipitation (e.g., PDSI and SPEI) (M. Zhao et al., 2017b, 2017a). TWS-DSI is calculated for each grid cell in the model domain as follows,

$$TWS_{DSI\,i,j} = \frac{TWS_{i,j} - \overline{TWS}_j}{\sigma_j} \tag{2-8}$$

where, $TWS_{i,j}$ is the TWS anomaly from LHF for year $i$ and month $j$; and $\overline{TWS}_j$ and $\sigma_j$ are the temporal mean and standard deviation of TWS anomalies for month $j$, respectively.

### 2.2.6. Occurrence and Duration of Drought

The characteristics of hydrological droughts are identified from the simulated streamflow using the widely used threshold level approach. Different thresholds have been proposed in previous studies: mean flow, minimum and maximum flows (Marengo and Espinoza, 2016; Wongchuig Correa et al., 2017), 80$^{th}$ percentile ($Q_{80}$) flow (Van Loon et al., 2012; Van Loon and Laaha, 2015; Wanders and Van Lanen, 2015), and 90$^{th}$ percentile ($Q_{90}$) flow (Wanders et al., 2015; Wanders and Wada, 2015). In this analysis, we use $Q_{90}$ which is derived from the flow duration curve where $Q_{90}$ is the streamflow that is equaled or exceeded for 90% of the time. $Q_{90}$ is used to isolate severe drought events over the simulation period. Monthly threshold values are derived using the 36-year simulated streamflow and are smoothed by a 30-day moving average. Drought condition is identified by determining whether the variable is below the threshold, expressed mathematically as,

$$Ds(t,x) = \begin{cases} 1 & for\ Q(t,x) < Q_{90}(t,x) \\ 0 & for\ Q(t,x) \geq Q_{90}(t,x) \end{cases} \quad (2\text{-}9)$$

where $Ds(t,x)$ indicates whether the grid $(x)$ is in a drought state at time $(t)$, $Q(t,x)$ is the streamflow and $Q_{90}(t,x)$ is the threshold for grid $(x)$ at time $(t)$. Consecutive drought states are added to get the drought duration. Events with duration less than 3 days are not considered as droughts. The number of drought days per year is calculated by aggregating the duration of all the drought events in a year.

### 2.2.7. Dry Season Total Water Deficit

We define the dry season total water deficit (TWD) as the cumulative difference between monthly potential evapotranspiration (PET) and precipitation (P) for the period during which P<PET. The corresponding drop in the simulated TWS, during the same period as of TWD, is

defined as the TWS release (TWS-R). TWD and TWS-R can be conceptualized as the annual water demand and supply as described in Guan et al., (2015). PET estimated at the daily interval using the Penman Monteith approach (Monteith, 1965) as in Pokhrel et al., (2014) is aggregated to the monthly scale to calculate TWD; for consistency, we use the WFDEI forcing data that is used for LHF simulations (section 2.2). TWS anomalies required for the estimation of storage release are obtained from the LHF model.

### 2.2.8. Simulation Setup

LHF is setup for the entire Amazon basin (~7.1 million $km^2$) including the Tocantins River Basin. Simulations are conducted for the 1979-2015 period at a spatial resolution of 1 arc minute (~2 km). Model time step is 4 minutes as in previous studies (Miguez-Macho and Fan, 2012b, 2012a; Pokhrel et al., 2014, 2013), however, model output is saved at daily timesteps. To stabilize water table depth, the model is spun up for ~150 years starting with the equilibrium water table (Fan et al., 2013) for 1979 and results for 1980-2015 period (36 years) are analyzed. As this study aims to analyze the hydrological changes in Amazon on a decadal scale, simulations for 1979 are considered as additional spin-up and hence not used. Dynamic monthly LAI and annual LULC maps are used to account for LULC changes (see Sections 2.2.3). Moreover, as the model simulates land surface, hydrologic and groundwater processes on a complete physical basis, no calibration was performed on the model output. Original novelty of the LHF model framework, combined with the incorporated dynamic human role through land cover change creates a “state-of-the-art” framework for assessing long-term hydrological changes. Complete LHF framework along with the input data employed in this study is presented in Figure 2-3.

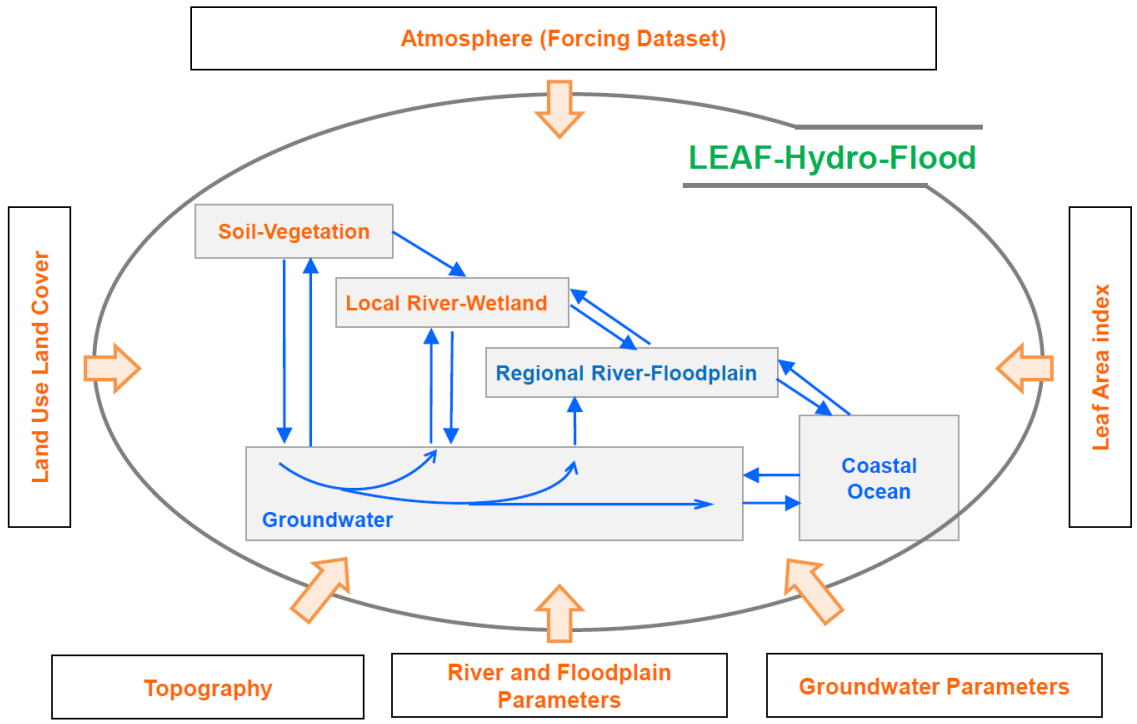


***Figure 2-3. LEAF-Hydro-Flood (LHF) framework.*** *Stores and fluxes included in LHF model along with its overall structure and inputs. This flowchart is modified after Miguez-Macho and Fan, (2012a).*

## 2.3. Results and Discussion

### 2.3.1. Evaluation of Simulated Streamflow

Figure 2-4 presents the Taylor diagram (Taylor, 2001) illustrating the statistics of the simulated streamflow against observations at 55 gauging locations (see Section 2.2.4.1 and Figure 2-2) across the entire Amazon basin. The Taylor diagram provides a synthetic view of error in the simulations in terms of the ratio of standard deviation (SD) of the simulated streamflow to the observed as a radial distance and their correlation as an angle in the polar axis. Most of the stations show a high correlation (> 0.8) and a SD ratio close to unity, indicating a good model performance overall for varying geographical locations and stream sizes over the Amazon. Low correlation (~0.6) is seen for some gauging stations situated on streams with smaller annual mean flow and steep slope profile; for example, the smaller streams across the Andes in Japura

and Negro sub-basins, along with the streams in northeastern parts of Amazon. In these streams with high topographic gradients, precipitated water quickly flows away causing slightly erratic patterns of seasonal streamflow, which is apparent in both simulated and observed timeseries (Figures 2-5). However, due to the difficulty in resolving hillslopes processes for low-order streams using 2km grids, the model is unable to fully capture the flow seasonality in the streams with high topographic gradient.

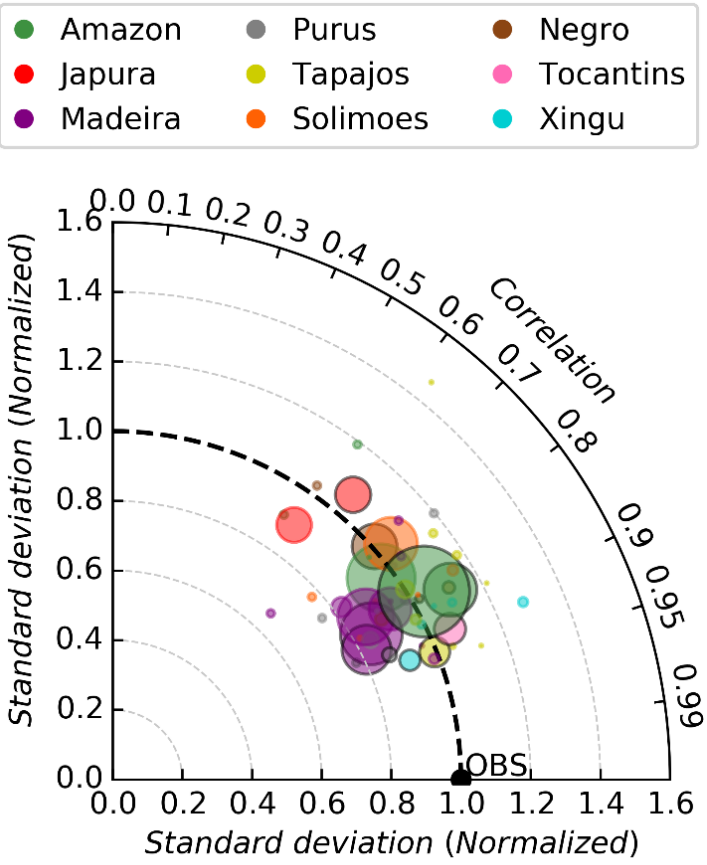


***Figure 2-4. Validation of LHF simulated streamflow.*** *Taylor diagram showing the correlation and standard deviation ratio between the simulated and observed streamflow at 55-gauge stations across the Amazon. The locations of the 55-gauge stations are shown in Figure 2-2. Highlighted points with a black border are the gauge stations for which time series comparisons are shown in Figure 2-5. The size of the markers indicates the annual mean simulated streamflow at that station, whereas the color indicates the Amazon sub-basin in which the station is located. The linear distance between each marker and the observed data (i.e., OBS; the black dot) is proportional to the root mean square error (RMSE).*

The spatial distribution of the simulated streamflow across the entire model domain and the timeseries comparison of simulated vs. observed streamflow at 12 selected stations are presented in Figure 2-5. The simulated seasonal cycle compares well with the observed one for the entire basin (i.e., Obidos station) as well as for most sub-basins; however, discrepancies in the seasonal peaks can be seen in some basins (e.g., Xingu, Tocantins, and Tapajos). Man-made reservoirs generally attenuate streamflow peaks and seasonal variability, reducing the SD, which is reflected in the observed data but not yet accounted for in the model; this could have exaggerated the SD ratio in some cases. For example, the streamflow in the Tocantins River shows higher SD compared to observed streamflow, likely due to the operation of the Tucurui I and II dams. Conversely, the SD ratio is lower than unity at some stations, including those in the Madeira River (Figure 2-4) due to the dry bias found in the input precipitation (see Figure 2-8 and Section 2.3.2). For sub-basins with higher groundwater contribution to streamflow, such as Xingu, Tapajos, Tocantins and Madeira, the dry-season flow is overestimated (Figure 2-5), which results from possibly exaggerated groundwater buffer in the model for these regions (Miguez-Macho and Fan, 2012a). Given that LHF is a continental-scale model, simulates streamflow on a full physical basis, and is not calibrated with observed streamflow, we consider these results to be satisfactory to study the hydrologic changes and variability.

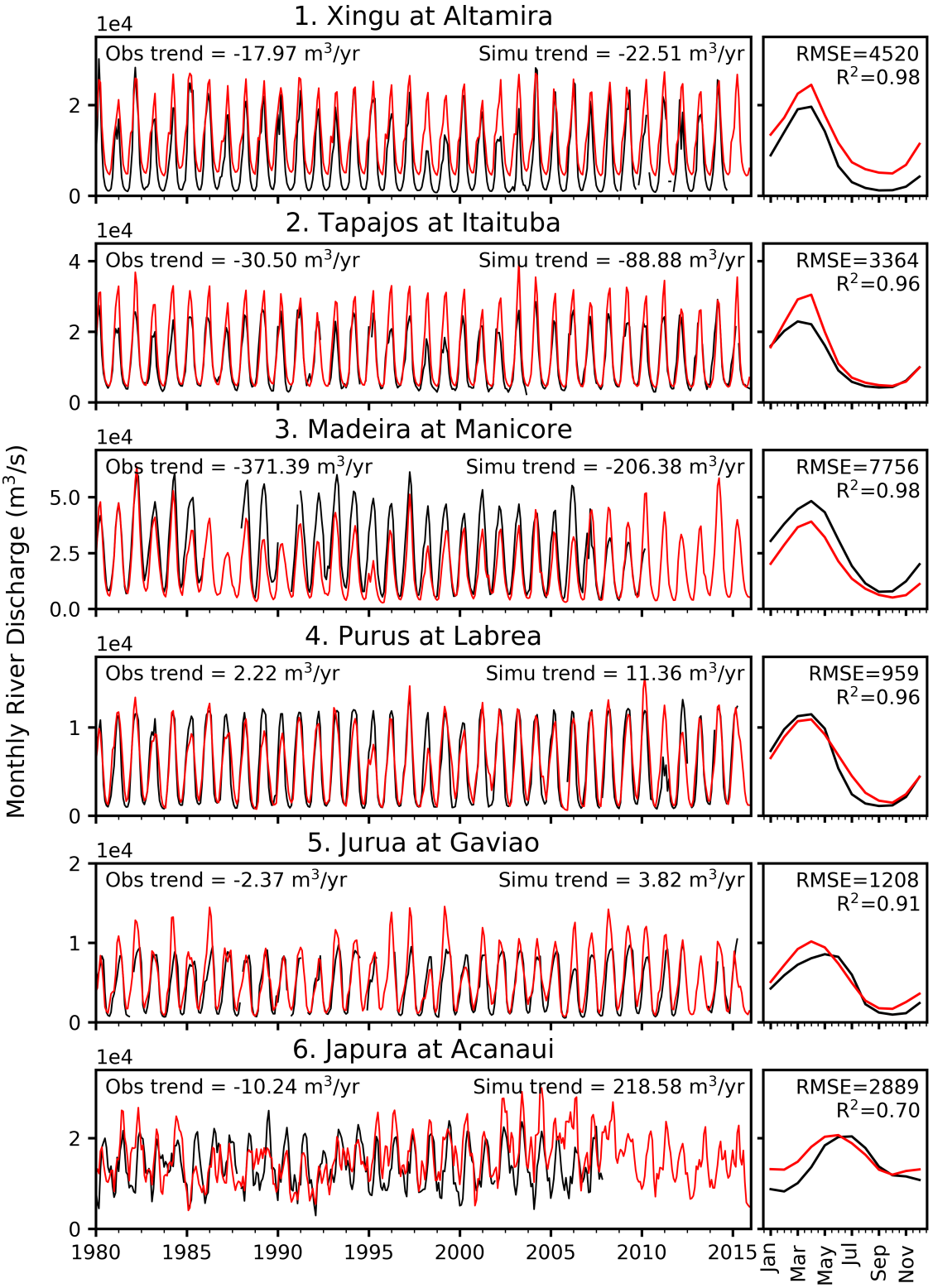


***Figure 2-5. Comparison of observed streamflow (black) obtained from ANA Brazil and simulated streamflow (red) from LHF at 12 main gauge stations.*** *Seasonal cycle for each station is also shown in the right panel of each subplot. The locations of the streamflow gauge stations are indicated in Figure 2-2.*

***Figure 2-5 (cont'd)***

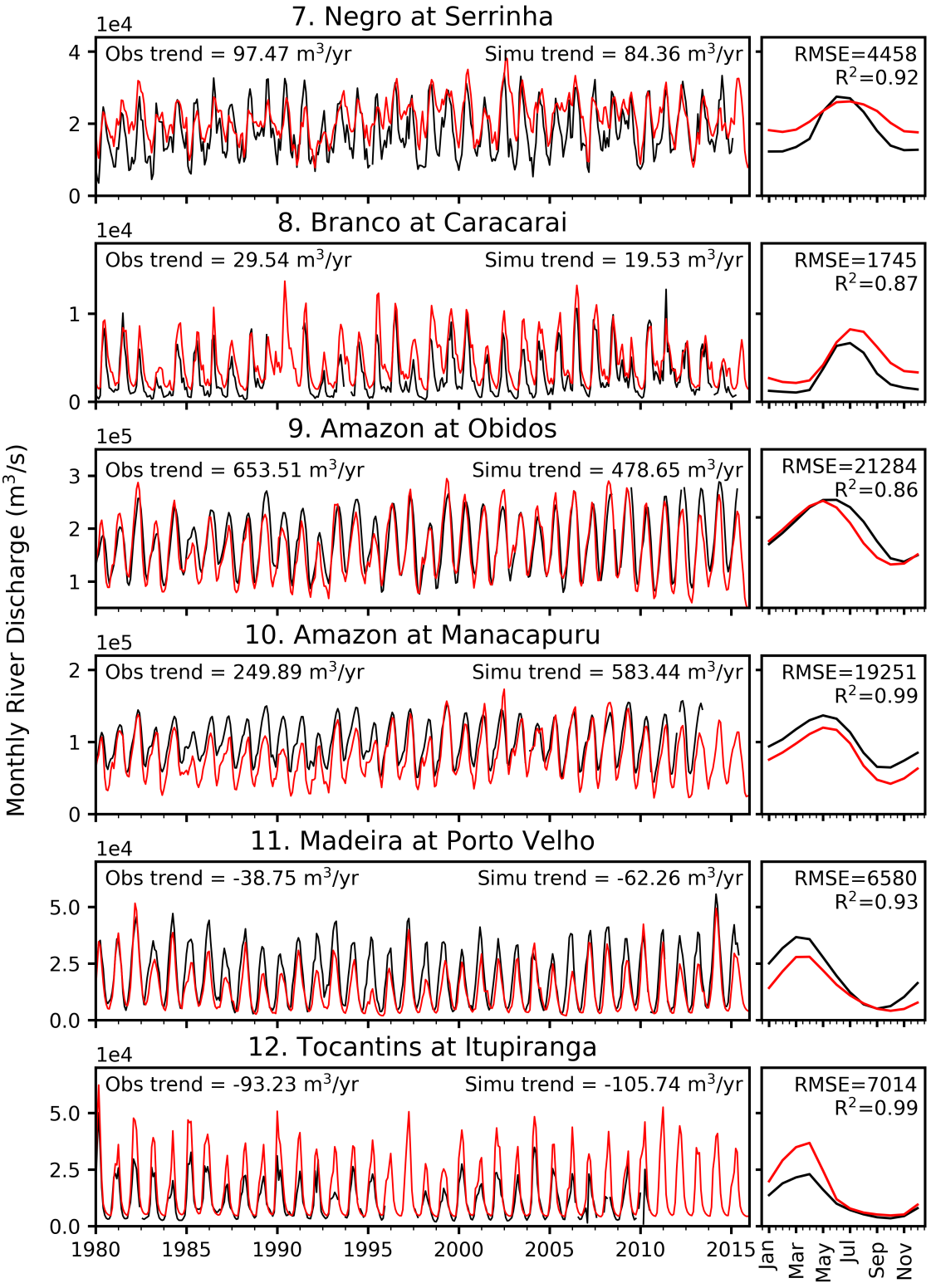

### 2.3.2. Evaluation of Simulated TWS Anomalies with GRACE

Figure 2-5 presents the comparison of simulated TWS anomalies and GRACE data for the entire Amazon basin and its eight sub-basins; for model results, the individual TWS components are also provided. The model performs very well in simulating the basin averaged TWS anomalies for the entire Amazon basin and most sub-basins. However, some difference between the simulated and GRACE-based TWS anomaly are evident, especially in sub-basins with relatively smaller area and elongated shape (e.g., Purus and Japura). Note that accuracy of GRACE-model agreement is generally low in such small basins due to high bias and leakage correction errors (Chaudhari et al., 2018; Felfelani et al., 2017; Longuevergne et al., 2010), reflected by higher RMSE values in Figure 2-5. Simulated TWS evidently follows precipitation anomalies (shown in grey bars in Figure 2-6), implying that any uncertainties in the precipitation forcing could have directly impacted TWS. For example, the simulated TWS peak in 2002 in the Solimoes River basin results from the anomalous high precipitation, however this could not be validated due to a data gap in GRACE. Overall, the model performance is better in the first half of the simulation period (i.e., 2002-2008) compared to the second half, especially in the western sub-basins including the Solimoes and Japura, which could be partially attributed to the decreasing trend in the precipitation forcing noted in Figure 2-8.

Figure 2-5 also shows the seasonal cycle including the contribution of different storage components to TWS. In all the basins, simulated seasonal cycle matches extremely well with GRACE, adding more confidence to the model results. TWS signal is sturdily modulated by the sub-surface water storage, demonstrating the importance of groundwater in the Amazon, especially in the southwestern sub-basins. The inverse relationship in the seasonal cycle of two sub-surface water stores, viz. soil moisture and groundwater, is readily discernable in Figure 2-5,

which is caused by the competing use of the sub-surface compartment by the two terms (Felfelani et al., 2017; Pokhrel et al., 2013). However, in some sub-basins, such as the Purus, Solimoes and Negro, the low-lying area with large floodplains causes flood water storage to be equally prominent.

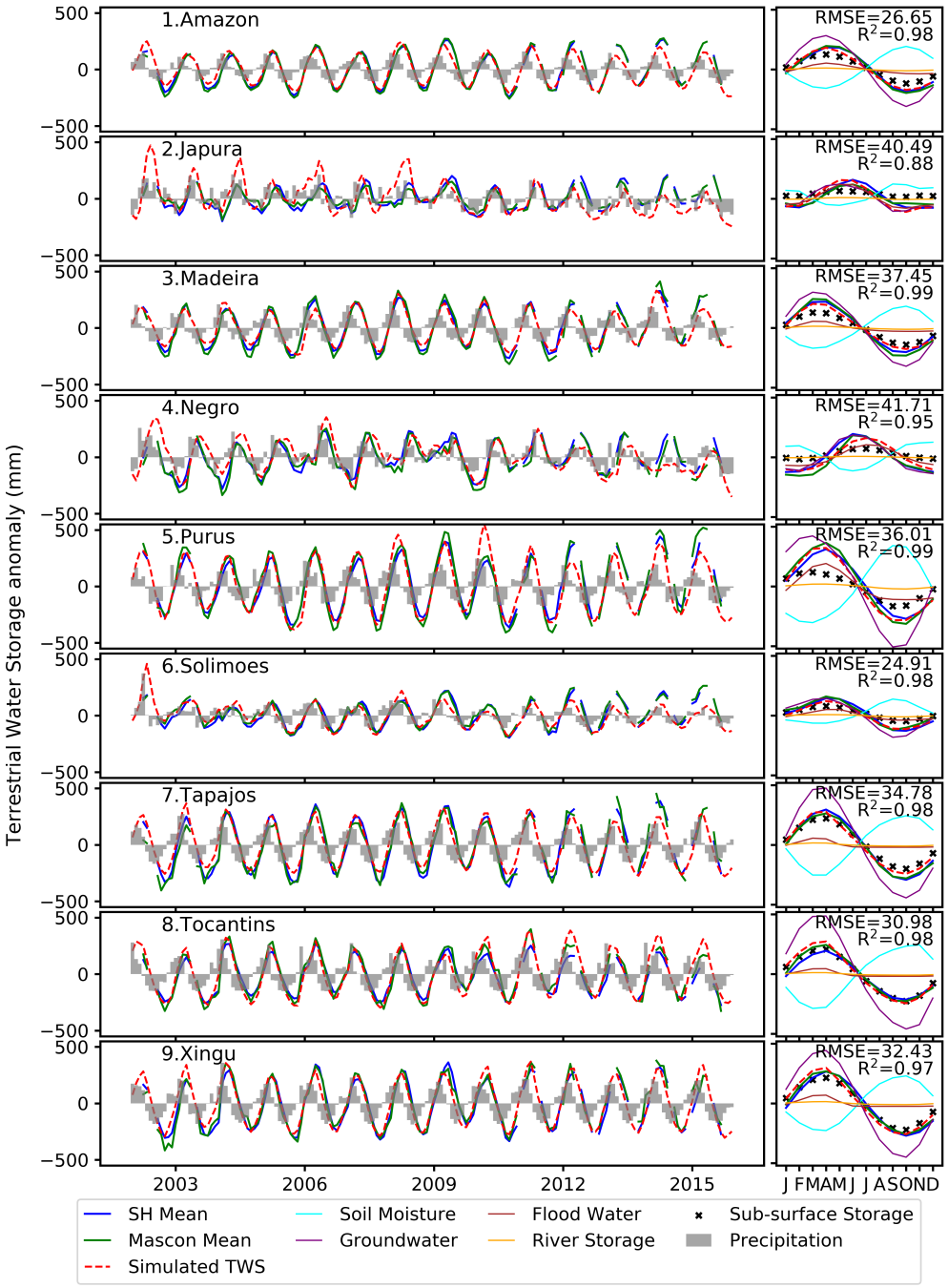


***Figure 2-6. Comparison of simulated TWS anomalies from LHF and TWS anomalies obtained from GRACE.*** *Comparison is shown for the entire Amazon and its eight sub-basins for the 2002–2015 period. Basin-averaged precipitation anomalies obtained from the WFDEI forcing dataset are also shown as grey bars. Seasonal cycles of GRACE and simulated TWS are shown in the right panel of each basin along with the simulated individual TWS components. GRACE results are shown as the mean of the spherical harmonics (SH) solutions from three different processing centers (i.e., CSR, JPL, and GFZ) and mascon solutions from CSR and JPL. Simulated TWS anomalies are calculated with respect to the GRACE anomaly window of 2004–2009 for consistency.*

### 2.3.3. Trends in Simulated TWS and Comparison with GRACE

Here, we present a more detailed examination of the simulated TWS by comparing its spatial variability and trend with GRACE data. Because a shift in agreement between model and GRACE was detected in Figure 2-6, we conduct a trend analysis for two different time windows: 2002-2008 and 2009-2015 (Figure 2-7). It is evident from Figure 2-7 that the model captures the general spatial pattern of TWS trend in GRACE and its north-south and east-west gradients especially for the first half of the analysis period; however, notable differences are evident in the second half (2009-2015), particularly over the Madeira River basin. This is a noteworthy observation given that the basin averaged TWS variability matches extremely well with GRACE data (Figure 2-6), and thus warrants further investigation. There could be a number of factors contributing to the disagreement, some of which could be model-specific (e.g., wet bias in simulated discharge; Figure 2-5); however, this is a general pattern observed in many hydrological models as reported in a recent study (Scanlon et al., 2018).

Scanlon et al., (2018) indicated a low correlation between GRACE and models, which they attributed to the i) lack of surface water and groundwater storage components in most of the models, ii) uncertainty in climate forcing and iii) poor representation of human intervention in the models (Scanlon et al., 2018; Sun et al., 2019). Here, we shed more light on the disagreement issue by investigating the contributions from the explicitly simulated surface and sub-surface storage components and their latitudinal patterns, addressing the first concern noted above which is the most critical among the three in the Amazon because of varying contribution of different stores across scales (Pokhrel et al., 2013). Figure 2-10Figure 2-10 shows trends in TWS anomalies from GRACE products and the LHF simulation for the complete model-GRACE overlap period (i.e., 2002-2015) with climatology and with climatology removed; for LHF

results, the surface and sub-surface component contributions to the TWS are shown. Also shown in the figure are the zonal means.

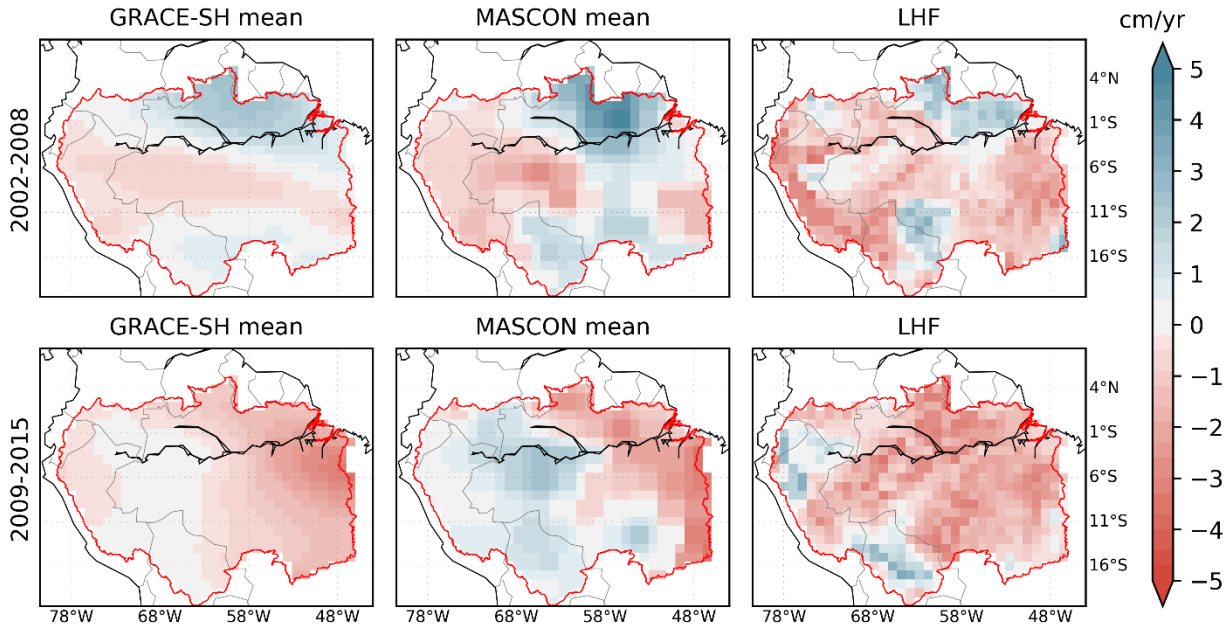


***Figure 2-7. Temporal trend of GRACE solutions compared to the trend in simulated TWS from LHF.*** *Comparison is shown for the entire Amazon River basin for two different time periods. GRACE-SH trends displayed are mean trends computed from water thickness anomalies obtained from CSR, GFZ, and JPL processing centers, whereas the mascon mean trend is computed from anomalies obtained from CSR and JPL centers.*

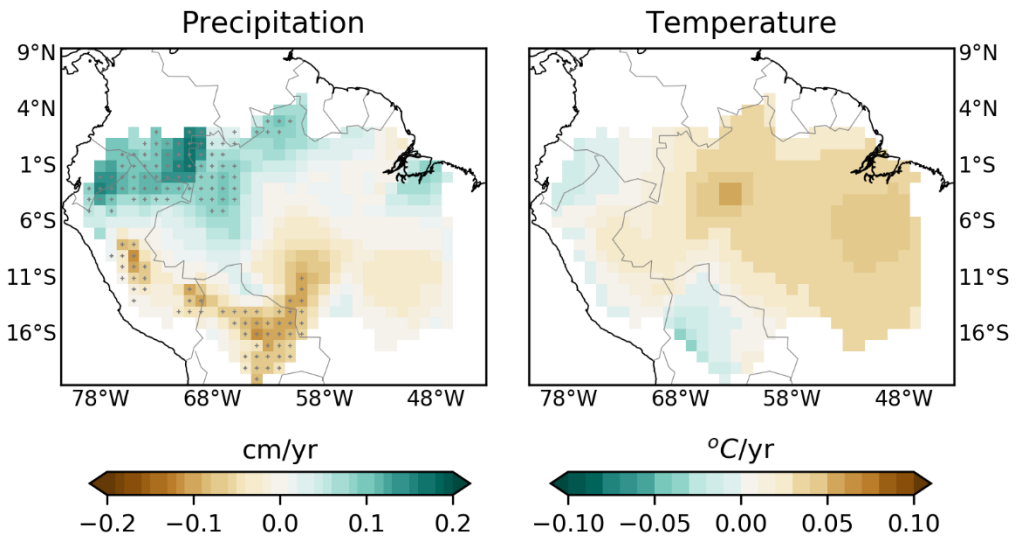


***Figure 2-8. Temporal trend in precipitation and temperature obtained from WFDEI forcing dataset for the simulation period (i.e., 1980-2015).*** *Markers indicate significant trends at 99% level.*

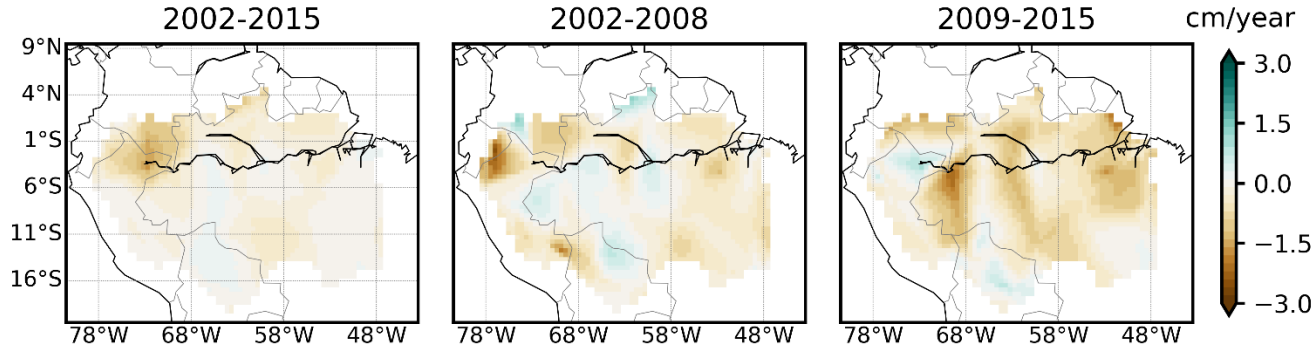


***Figure 2-9. Temporal trend in precipitation obtained from WFDEI forcing dataset for the model-GRACE overlap period (i.e., 2002-2015).*** *Note that the entire model-GRACE overlap period was split in two timeframes for further analysis.*

Simulated TWS from LHF model displays a higher correlation with GRACE trends compared to most of the global models discussed in Scanlon et al., (2018). Due to the incorporation of a groundwater scheme and other surface water dynamics, trend in basin-averaged TWS with climatology removed for the Amazon River basin is found to be -1.64 mm/yr, much less negative than most of the simulated TWS trends reported in Scanlon et al., (2018). The difference in the sign of trend can partly be explained by the negative trend observed in the WFDEI precipitation

(Figure 2-9), concentrated over the Andes region which eventually drains into the mainstem of the Amazon through the Solimoes River. Due to steep topography, the impact of decreased precipitation over the Andes range is carried over to its foothills in terms of runoff, hence corresponding well with the negative trends in simulated surface water storage over the Central Amazon (Figure 2-10). Lower recharge rates in the region with decreasing precipitation trend (Figure 2-9) are also very likely, which is supported by the negative trend visible in the sub-surface water storage in Figure 2-10, over the northwest region of Amazon. Hence, it can be concluded that, even though the model shows some bias in TWS compared to GRACE data, the model accurately represents the key hydrologic processes in the Amazon basin; yet these results should be interpreted with some caution while acknowledging the uncertainty in the forcing dataset. We also emphasize that it is important to evaluate models using spatiotemporal trends, especially with GRACE, instead of just using the basin averaged timeseries, a commonly used approach in most previous studies.

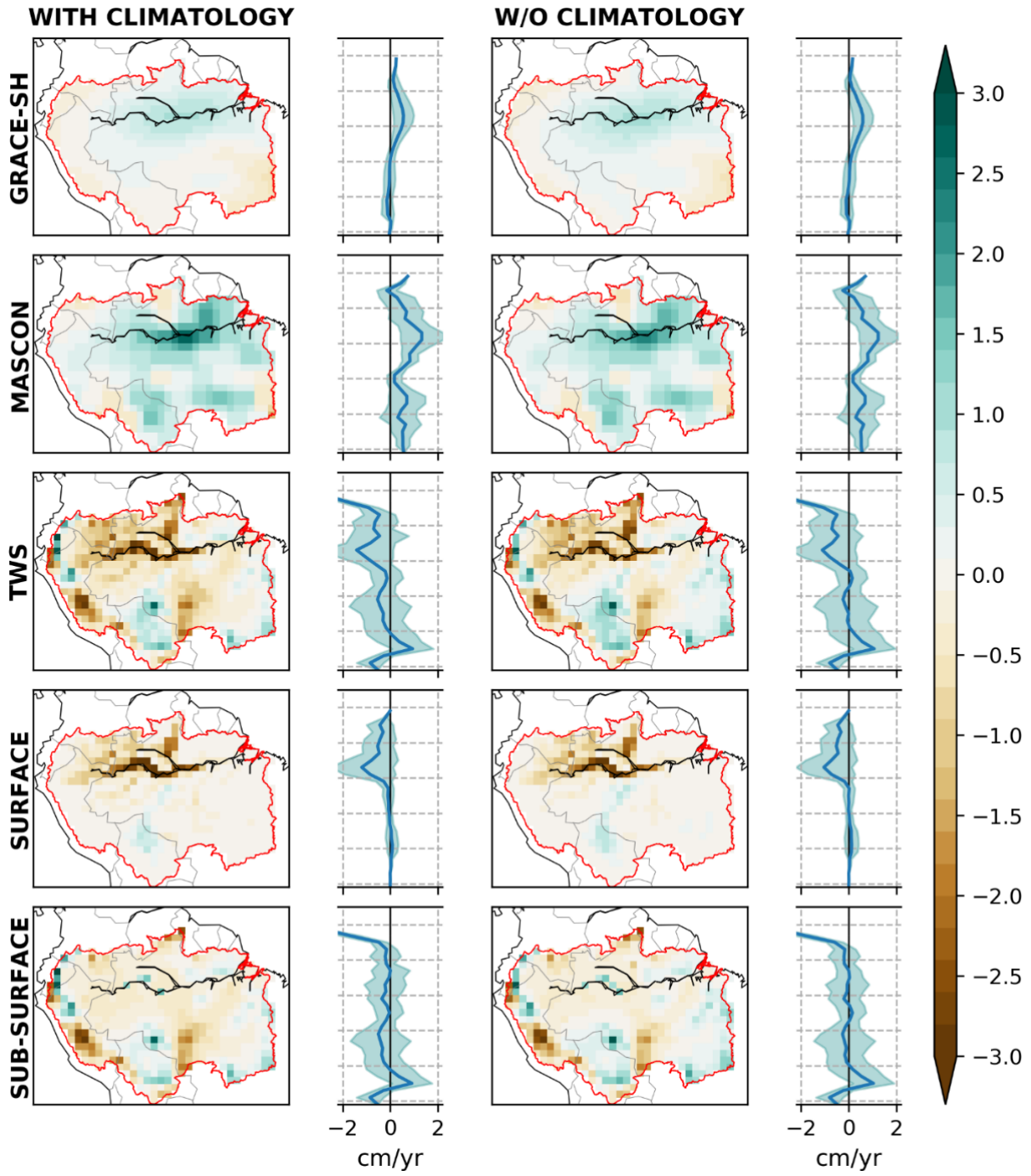


***Figure 2-10. Comparison of temporal trend of GRACE solutions with simulated TWS from LHF for the complete model–GRACE overlap period (i.e., 2002–2015).*** *The latitudinal mean is shown on the right side of each panel.*

### 2.3.4. Interannual and Interdecadal TWS Change and Variability

Figure 2-11 show the interdecadal shifts in mean simulated TWS (total and its components) for the simulation period. Several observations can be made from this figure. First, the change between 2010s-2000s suggests high negative anomalies in all the water stores especially over Central Amazon. This is likely a result of increasing drought occurrence and severity in the region (e.g., the 2010 (Lewis et al., 2011; Marengo et al., 2011) and 2015 (Jiménez-Muñoz et al., 2016) Amazonian droughts). Second, although, the 2000s encompassed one of the severe Amazonian droughts viz. 2005 (Marengo et al., 2008; Zeng et al., 2008), its impact was not pronounced in terms of the decadal mean, which could be due to the offset caused by anomalous wet years including 2006 and 2009 (Chen et al., 2010; Filizola et al., 2014). Third, we find an increase in river water storage in the northwestern region and decrease in the southwest of the Amazon on a decadal scale (Figure 2-11, column 1, row 2), which is in line with the findings reported in previous studies based on the observed streamflow in 18 sub-basins for the 1974-2004 period (Espinoza et al., 2009; Wongchuig Correa et al., 2017).

The most remarkable feature we observe in Figure 2-11 is the exceptional interdecadal shifts between the 2000s and 2010s. Central and northwestern part of the Amazon region, encompassing the Negro and Solimoes, along with some parts of the Madeira in southwest, experienced a major decadal dry spell compared to the previous decades. Although a major part of this decadal dry condition could be attributed to the decreasing trend in input precipitation discussed in section 2.3.3 (Figure 2-8), the regional hydrologic changes in terms of TWS are also prominent. Another peculiar phenomenon observed at the decadal scale is the start of the negative anomaly in groundwater storage over the Central Amazon. A small but spatially well distributed below-decadal-average water table (dictated by groundwater storage) is evident in the

Central Amazon region and the upper stretches of the Madeira basin during the 2010s (Figure 2-11, column 3, row 4). Since the water table is shallow and groundwater is the major contributor of streamflow in this region (Miguez-Macho and Fan, 2012a), some part of the negative anomaly in surface water stores can be attributed to the below-decadal-average groundwater table.

Significant long-term trends in simulated TWS and its components are evident in sizeable portions of the basin (Figure 2-12). While a negative trend is found in the southern and southeastern regions (e.g., Madeira, Tapajos, Xingu, and Tocantins), the trend is positive in the northern and western regions (Solimoes and Negro). Being the major contributor, sub-surface water storage, mimics the trend patterns in TWS (see Section 2.3.2). On the contrary, surface water storage trends are mainly dominated by floodwater and are concentrated along the main stem of Amazon and the upper reaches of the Negro. The positive trends in floodwater can be explained by the corresponding trends in input precipitation (Figure 2-8). Excess precipitation in sub-basins, such as the Solimoes and Negro, which are characterized by a high topographic gradient, is directly translated in the surface water storage, in this case floodwater. Although a corresponding increment in river water storage is also expected, its smaller storage makes the trend magnitudes negligible. Nominal negative trends, but significant, in floodwater storage are found in the upper reaches of Madeira as well, corresponding to the negative trends in input precipitation over that region.

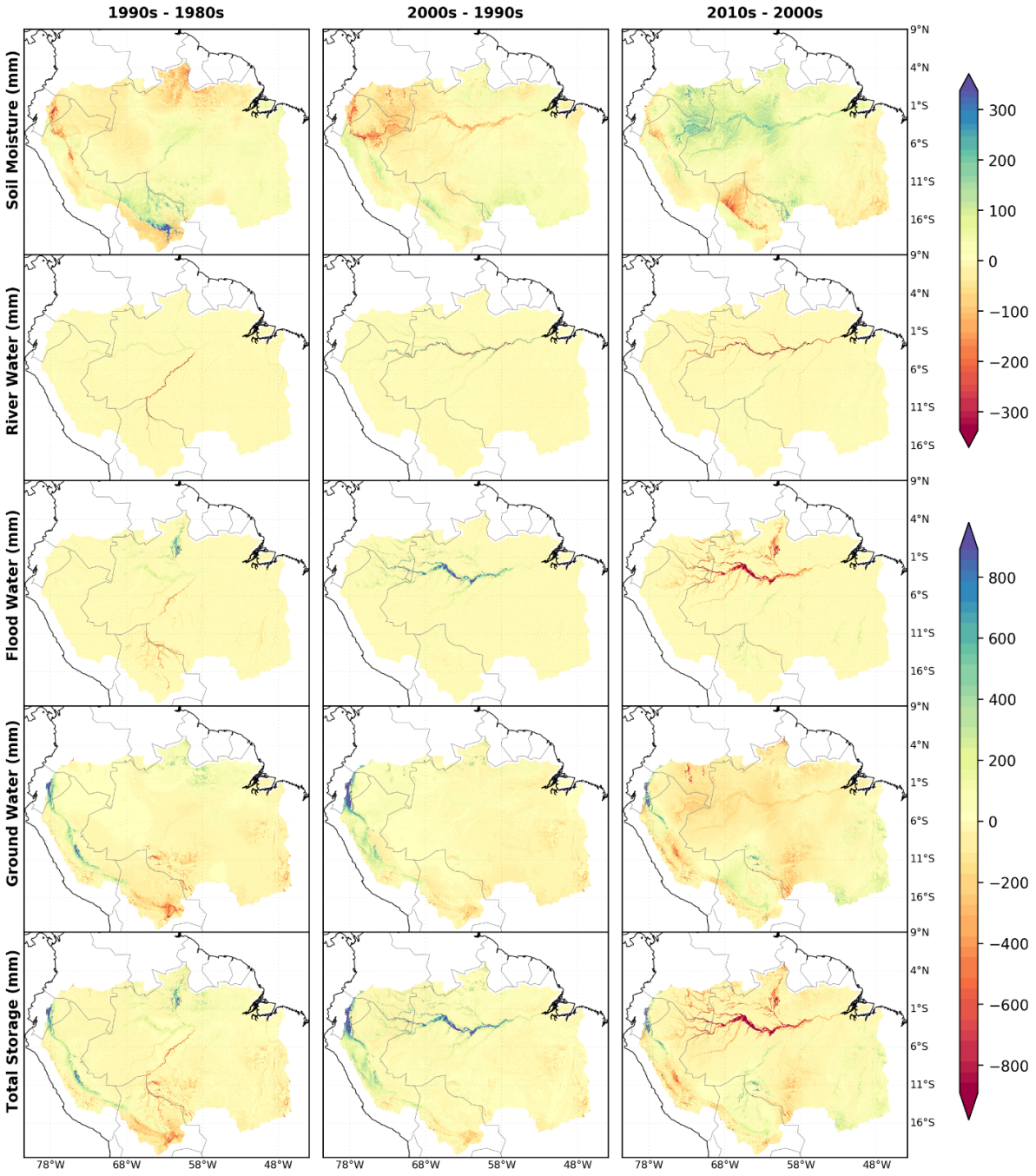


***Figure 2-11. Interdecadal difference between individual water store and TWS storage for the period of 1980–2015 at the original ~2km model grids.*** *The changes are displayed as the difference between consecutive decadal means for TWS and its components. Decadal windows are 1980–1989 as 1980s, 1990–1999 as 1990s, 2000–2009 as 2000s, and 2010–2015 as 2010s. Note that the 2010s period consists of only six years.*

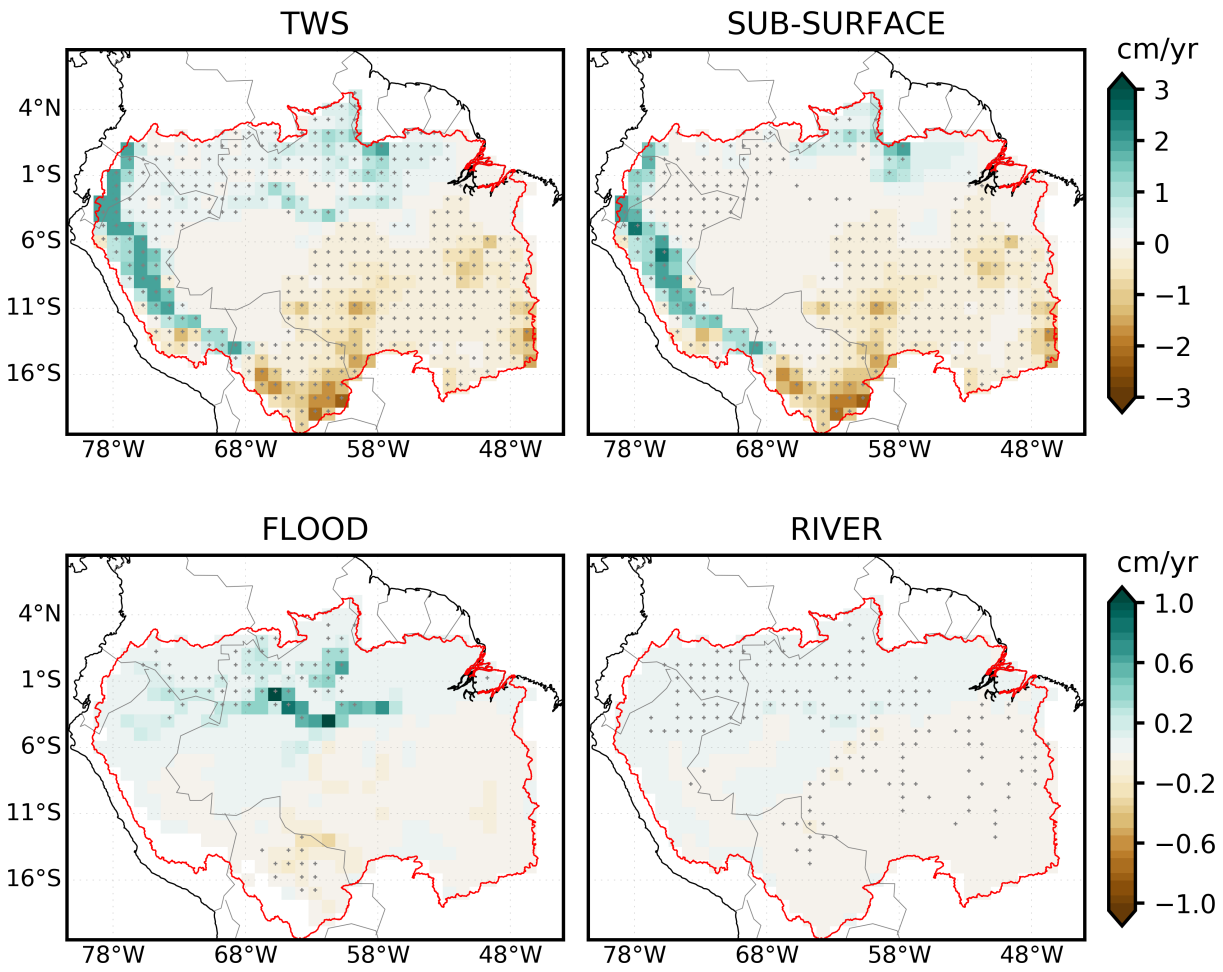


***Figure 2-12. Temporal trend in simulated TWS and its components for the period of 1980 to 2015.*** *Values are expressed in centimeters per year (cm yr−1). Markers indicate significant trends at the 99% level. Note that the ranges of color bars differ among the plots.*

To provide an in-depth understanding of the interdecadal changes occurring in the Amazon region and to determine whether the changes observed in Figure 2-11 are significant, we applied a t-test methodology to the long term TWS anomalies at basin and sub-basin levels. The spatial changes observed in Figure 2-11 are summarized with their interdecadal significance in Table 2-2, along with the decadal means and standard deviations. Significant change at 99% level is found in Negro River basin throughout the study period, followed by the Solimoes River basin exhibiting significant change in the last three decades. These changes can be attributed to the corresponding changes in precipitation (Figure 2-8), which follow a similar change in respective

basins. However, the significant hydrologic changes in the Tocantins and Madeira can be primarily attributed to LULC changes, as the corresponding changes in precipitation were relatively negligible. For example, the Tocantins River basin underwent major LULC changes in response to heavy deforestation caused by dam construction and cattle farming (Costa et al., 2003) until policies were imposed in 2004 by the Brazilian government (captured in the ESA dataset, Figure 2-1). Similarly, the Madeira River basin also endured major LULC changes in the late 1990s which were dominated by agricultural expansion (Dórea and Barbosa, 2007).

***Table 2-2. Significance of Interdecadal TWS differences in Amazon basin and its sub-basins.*** *Mean and standard deviations (STD) of monthly TWS timeseries of individual decades are also shown. The significance is calculated using a t-test methodology.*

| Basin | Period | Mean | STD | Statistical Significance | Basin | Period | Mean | STD | Statistical Significance |
|---|---|---|---|---|---|---|---|---|---|
| **Amazon** | 1980s | -12.1 | 108.0 | No | **Solimoes** | 1980s | -5.6 | 76.6 | No |
| | 1990s | -14.4 | 111.4 | Significant | | 1990s | -20.7 | 86.6 | Significant |
| | 2000s | 24.7 | 123.2 | No | | 2000s | 56.8 | 118.9 | Significant |
| | 2010s | 3.1 | 129.7 | | | 2010s | -50.9 | 82.7 | |
| **Japura** | 1980s | -33.3 | 100.4 | No | **Tapajos** | 1980s | 24.1 | 169.2 | No |
| | 1990s | -43.0 | 110.3 | Significant | | 1990s | 9.4 | 171.5 | No |
| | 2000s | 84.1 | 147.2 | Significant | | 2000s | -10.9 | 180.2 | No |
| | 2010s | -7.7 | 90.1 | | | 2010s | -43.7 | 184.5 | |
| **Madeira** | 1980s | -4.9 | 138.9 | No | **Tocantins** | 1980s | 53.8 | 185.1 | Significant |
| | 1990s | -5.8 | 122.9 | Significant | | 1990s | -11.9 | 179.9 | No |
| | 2000s | -37.6 | 131.7 | No | | 2000s | -53.0 | 176.4 | No |
| | 2010s | -40.3 | 144.6 | | | 2010s | -0.4 | 200.5 | |
| **Negro** | 1980s | -59.9 | 107.6 | Significant | **Xingu** | 1980s | 25.5 | 183.6 | No |
| | 1990s | 16.5 | 139.3 | Significant | | 1990s | 4.7 | 186.1 | No |
| | 2000s | 61.0 | 140.8 | Significant | | 2000s | -28.2 | 184.7 | No |
| | 2010s | -15.6 | 116.7 | | | 2010s | -18.7 | 203.5 | |
| **Purus** | 1980s | -5.6 | 200.6 | No | | | | | |
| | 1990s | -13.2 | 201.7 | No | | | | | |
| | 2000s | 18.0 | 216.6 | No | | | | | |
| | 2010s | 6.2 | 235.1 | | | | | | |

### 2.3.5. Interannual and Interdecadal Drought Evolutions

#### 2.3.5.1. Severity of TWS-Drought

In this section, we examine the time-evolution of droughts and quantify their impacts on TWS variability by using TWS-DSI. The use of TWS-DSI enables the depiction of a "bigger picture" encompassing all water stores that represent the vertically integrated total water availability during droughts and dictate the streamflow. Figure 2-13 shows the TWS-DSI for individual Amazonian sub-basins, and the 12-month standard precipitation index (SPI) (Mckee et al., 1993) calculated from the basin-averaged precipitation timeseries. As expected TWS-DSI follows a

similar pattern of the SPI but differences in the index peaks can be noted for the drought years. For example, the 2005 drought was prominent in terms of TWS in the southwest region, comprising of Purus and Madeira rivers, with TWS-DSI going as high as -3, whereas the corresponding SPI were -1.78 and -2.2, respectively. Similarly, severe TWS drought (e.g., 2001) is detected in the southeastern basins of Amazon (Madeira, Xingu and Tocantins), however, the corresponding SPIs are negligible; the sub-surface storage (major contributor of TWS in these sub-basins) characteristic can be noted in these cases which has a delayed response from the preceding series of low precipitation events due to slow residence time.

The impact of drought conditions on TWS is quantified by examining the seasonal dynamics in the simulated sub-surface water storage for the four most extreme historical drought years during the simulation period (Figure 2-14). Although no clear trend can be seen in terms of the evolution of the drought impact on sub-surface water storage, the spatial variability between different drought years is readily discernible. For example, the 1995 and 2010 droughts more or less had a similar magnitude and spatial impact on the sub-surface storage, however, the 2005 drought was more intense and dramatic in the Solimoes River basin; findings also noted in previous studies (Marengo et al., 2008; Phillips et al., 2009; Zeng et al., 2008). Similarly, the more recent drought in 2015 had a more pronounced impact in the eastern and northeastern region and average impact on the other parts of the basin. Due to the shallow water table in the Amazonian lowlands, sub-surface storage acts as a buffer during the low precipitation events, hence facing higher anomalies during drought conditions compared to the long-term mean. As the Negro River (i.e., Northern region of Amazon) basin experiences an opposite seasonal phase compared to rest of the Amazon region, the drought conditions in this basin are observed during the period of December to March. The opposite seasonal cycle of precipitation and flooding in

the north and south banks of the Amazon mitigates the amount of flood and droughts in the basin as a whole, while resulting in more dramatic flood or drought in particular sub-basins (e.g. Tocantins, Tapajos and Madeira).

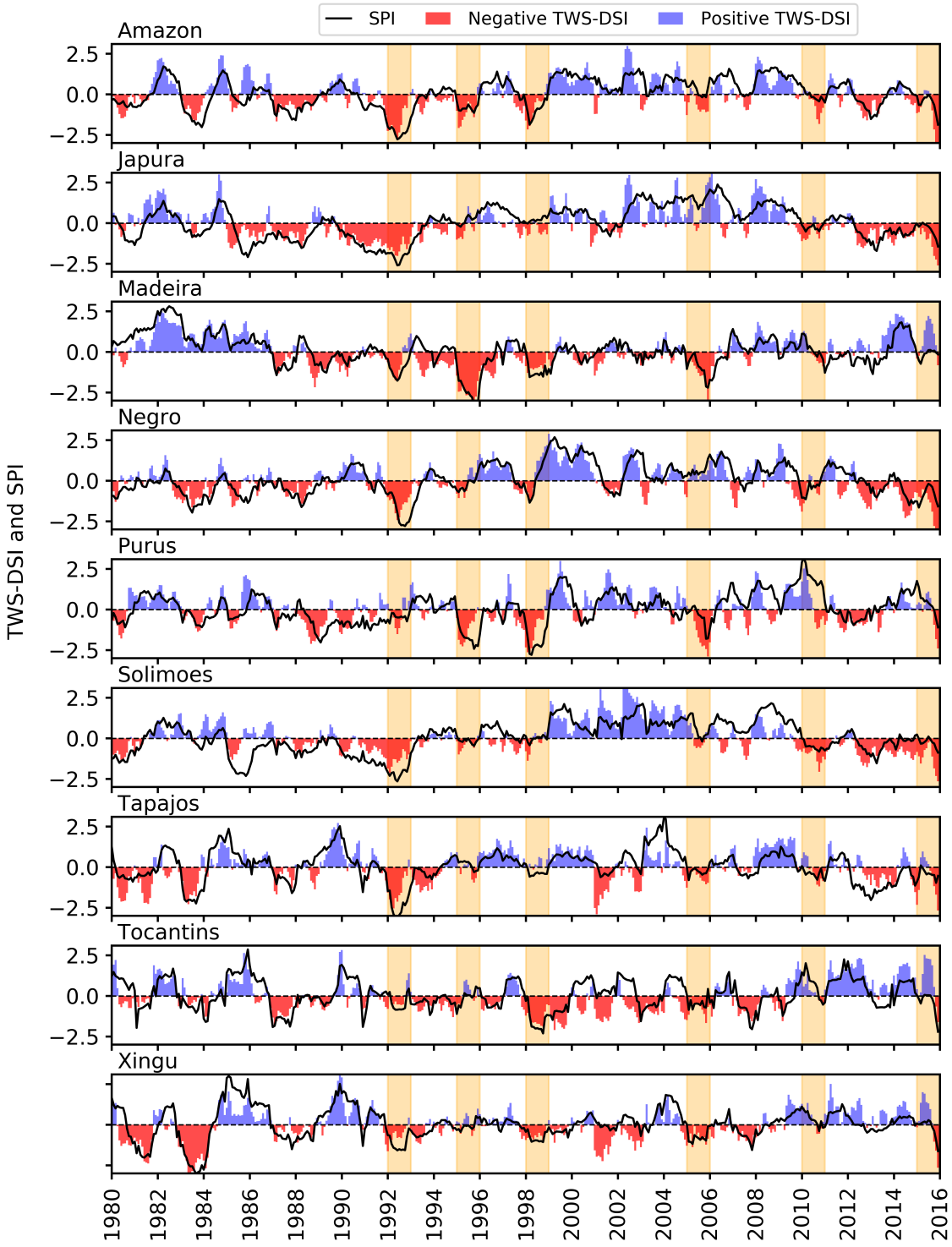


***Figure 2-13. TWS drought severity index (TWS-DSI).*** *TWS-DSI is calculated using basin-averaged TWS anomalies on a monthly scale simulated using LHF for Amazon and its sub-basins. Shaded areas indicate the severe drought years reported in the past literature. The black line is the 12-month Standardized Precipitation Index (SPI) calculated by using basin-averaged precipitation data from the WFDEI forcing dataset.*

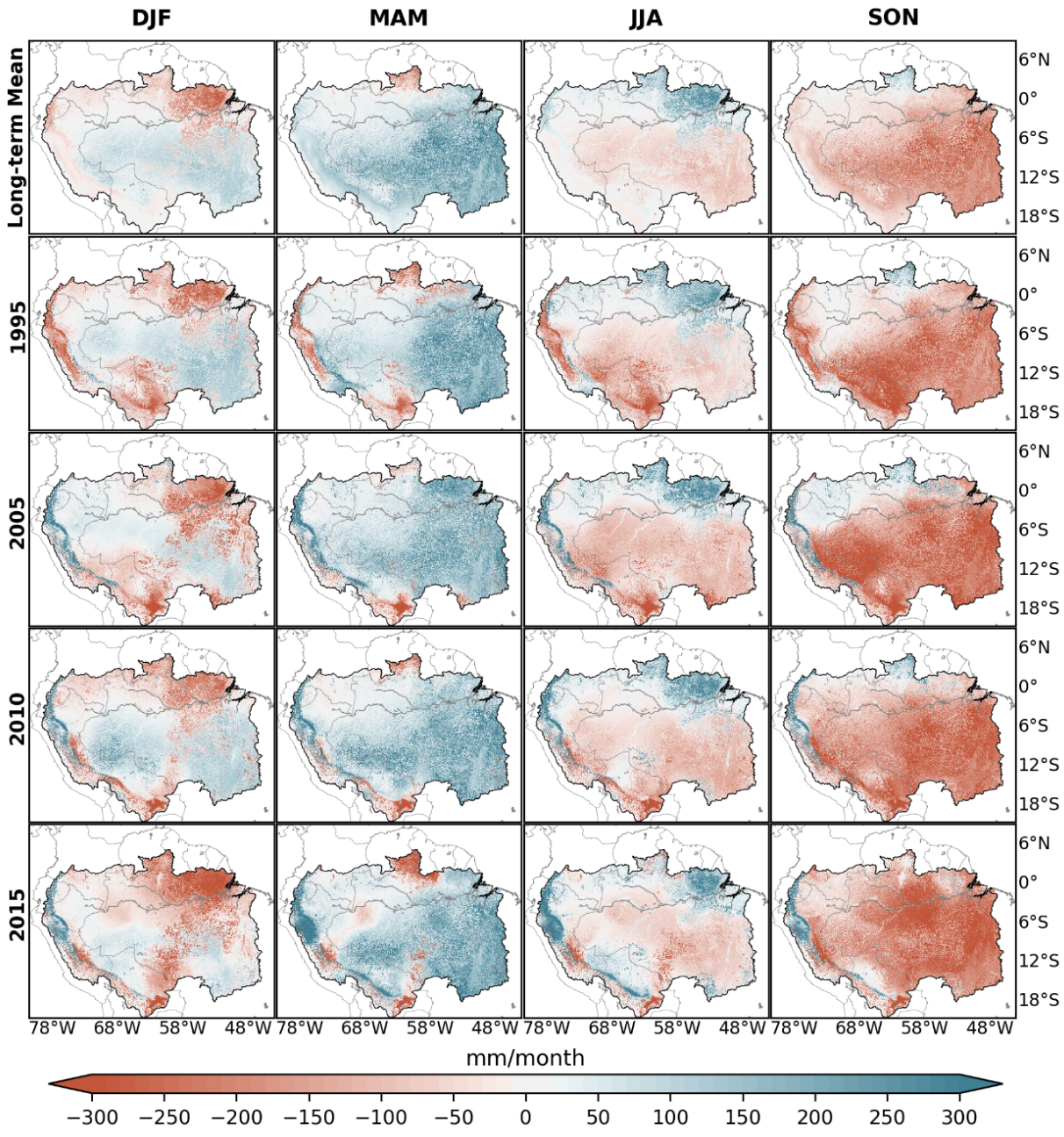


***Figure 2-14. Seasonal dynamics of simulated sub-surface water storage from LHF.*** *Results are shown for the Amazon River basin for extreme droughts during the simulation period. Long term mean is the mean seasonal anomaly for the 1980–2015 period, where DJF is December to February, MAM is March to May, JJA is June to August, and SON is September to November.*

#### 2.3.5.2. Time Evolution of Dry Season Total Deficit and TWS Release

The dry season TWS variability is examined by using the cumulative difference between PET and P, termed as the TWD (see Section 2.2.7). Further, to examine the response from TWS against TWD, we quantify the TWS-R, hence creating a supply-demand relationship between them. Results indicate TWD, the corresponding TWS-R, and the total contribution of the surface water storage to TWS-R for the extreme drought years during 1980-2015 compared to their respective long-term means. Spatial patterns in TWD and TWS-R are analogous to the patterns in the simulated sub-surface storage during the months of September to November (SON) as seen in Figure 2-14. We find that TWS-R receives a fairly equal contribution from surface (along the rivers) and sub-surface (soil moisture and groundwater) water stores (rest of the region); however, the latter is more dominant during drought years. A clear positive trend in drought years is found, indicating an increase in TWS-R, with significant sub-surface contribution, especially in the southeastern part of Amazon. This change can be directly attributed to the major LULC changes occurring in the basin, causing loss of TWS to evapotranspiration through agricultural expansion, especially in the Tocantins, Xingu, Tapajos and Madeira river basins (Chen et al., 2015; Costa et al., 2003; Dórea and Barbosa, 2007).

#### 2.3.5.3. Hydrological drought trends in Amazonian sub-catchments

The hydrological drought behavior of each sub-basin is characterized by quantifying the drought days per year at the Level-5 Hydro-Basins scale (Lehner and Grill, 2013), referred here to as ‘sub-catchments’. Based on the streamflow simulated at the most downstream grid in the sub-catchments, temporal trends for the 1980-2015 period are calculated and presented in Figure 2-15. Significant trends in drought durations are discernible in the Tapajos and Madeira sub-basin along with the southeastern portions of the Amazon, congruent to the heavy deforestation

activities found in these sub-basins (Chen et al., 2015; Costa et al., 2003; Dórea and Barbosa, 2007). Although, LULC changes, such as deforestation activities, generally increase streamflow and are also known to offset the impact on streamflow caused by decrease in precipitation over the Amazon (Panday et al., 2015), this mechanism is dominant mostly during the wet season. In the dry season, however, the streams in the Amazon are fed primarily by the sub-surface water storage (see Section 2.3.2), which is negatively impacted by deforestation activities (e.g., increased regional evapotranspiration).

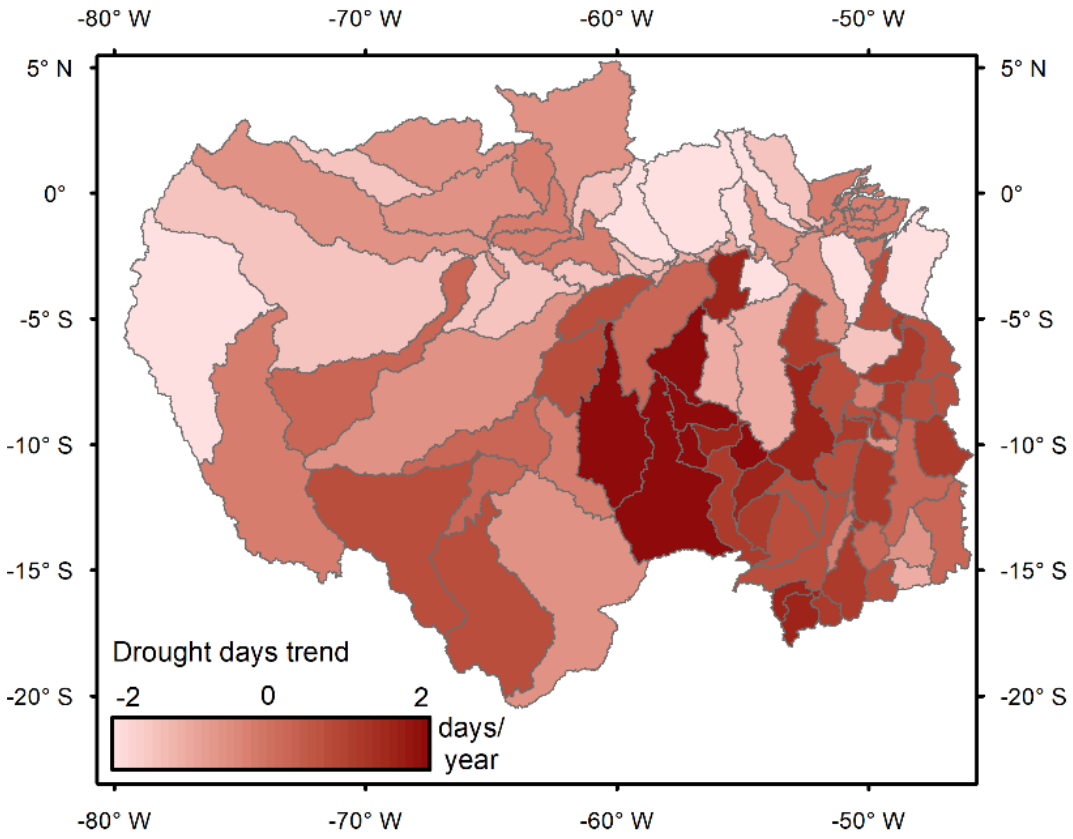


***Figure 2-15. Trends in drought duration per year in the Amazon River basin.*** *Results are shown at a Level-5 HydroBASINS scale as defined in Lehner and Grill, (2013), derived by using the Q90 threshold from the simulated streamflow by the LHF model. Darker colors indicate the higher positive trend magnitudes.*

### 2.3.6. Comprehensive Characterization of Amazonian Droughts

As a first attempt to comprehensively characterize the Amazonian droughts, we present a summary of all the drought characteristics discussed in the previous sections on a spider plot (Figure 2-16). Each spider plot is a representation of a drought year with respect to the i) causes of drought and their type in terms of common indices, ii) response of different water stores, such as TWS, to the drought event, iii) role of groundwater storage in alleviating the dry conditions on surface, and iv) the spatial impact of the drought in different sub-basins of the Amazon. Although no significant trend in the combined drought characteristic is apparent, Figure 2-16 provides important insights on the variability of Amazon droughts. It is evident from the figure that the drought variability over the years was significant in terms of both magnitude and spatial impact. The most notable feature in Figure 2-16 is the distinct relationship between SPI and drought duration. For example, during the 1995 drought, most of the river basins (e.g., Tocantins, Tapajos, Xingu, and Negro) experienced significant meteorological and TWS droughts, however, the severity of hydrological droughts was relatively negligible in those basins. Groundwater-surface water exchange is the key mechanism behind this unique behavior, causing groundwater to fulfill the drought deficit in streamflow over the basin. Due to shallow water tables at the downstream end of these basins, significant quantity of groundwater is fed to the rivers, which manifests as high peaks in total groundwater release evident in Figure 2-16. Similarly, high number of drought days are found corresponding to less groundwater release, such as during the 1995 drought in Madeira. On the contrary, TWS-DSI, generally follows the same pattern as that of SPI but with a lesser magnitude, which can be attributed to the delayed response from groundwater.

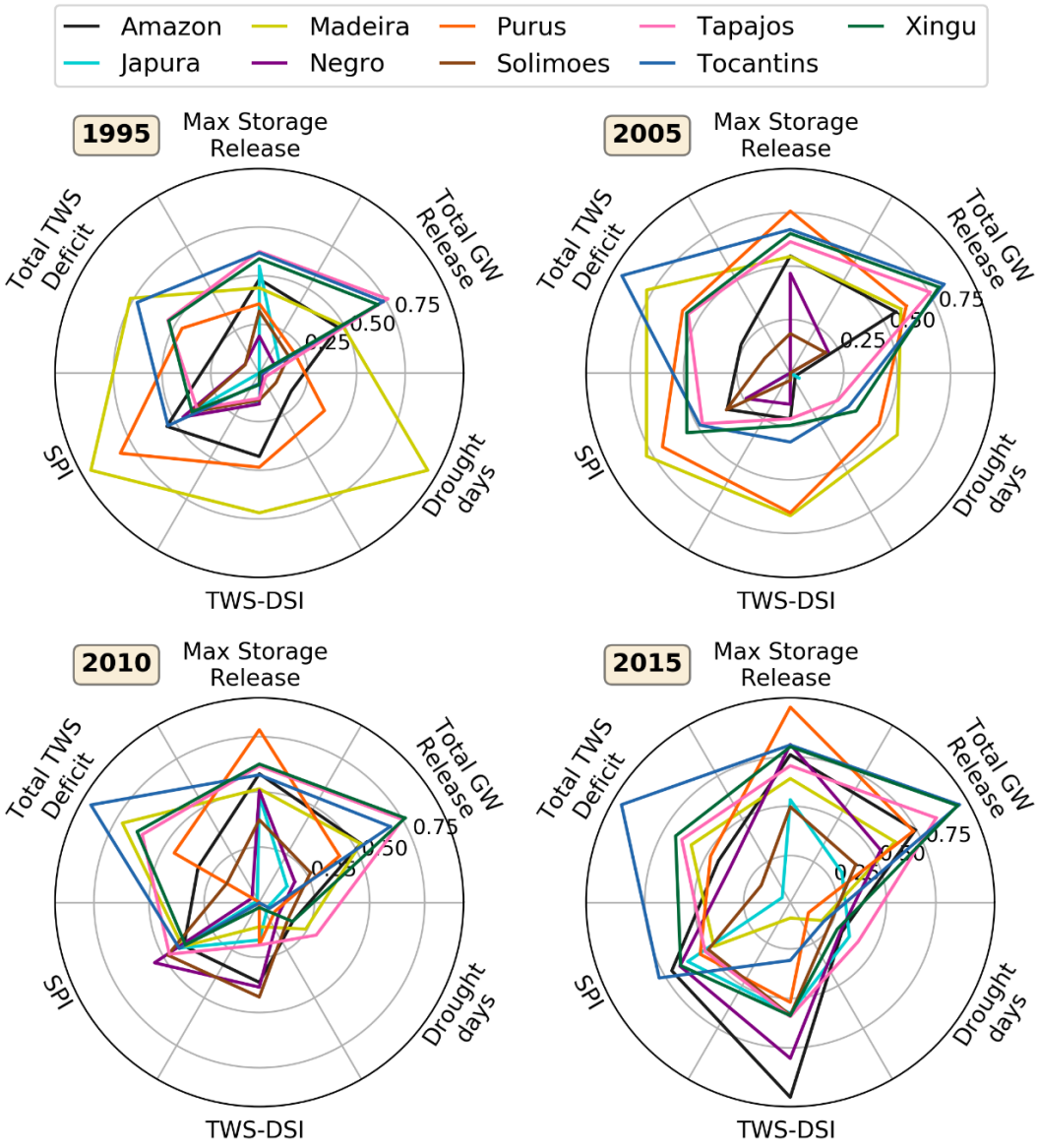


***Figure 2-16. Intercomparison and comprehensive characterization of the severe drought events during the study period in the Amazon River basin and its sub-basins.*** *Color coding in each subplot represents individual river basins. Note that all variables are basin averages normalized (0–1) for each variable over all drought years. The bottom half of the variables in the figure are drought in- dices representing different types of droughts: TWS-DSI denotes TWS drought severity index (Sect. 2.7), SPI (Standardized Precipitation Index) represents meteorological drought severity, and "drought days" represents hydrological drought severity in the basin (Sect. 2.6). The top half of the variables quantify the water deficit in terms of total TWS deficit (cumulative PET-P), water supply as the TWS release (max storage release), and the groundwater contribution of TWS release (total GW release).*

Further, the behavior of the Amazonian sub-basins can be characterized by the shape of the polygon formed by the comparison of different aspects of past droughts. The convex and concave characteristic in the plots mainly depends on the interrelation between meteorological and hydrological drought indices, which is further controlled by the sub-surface water storage. A convex polygon indicates lower groundwater contribution to streamflow in the sub-basin, such as in Purus during 1995 and 2005, whereas a concave polygon suggests higher groundwater release to streamflow in that particular year.

### 2.3.7. Intensification of the Amazonian Dry Season

Results suggest an increasing trend in TWD with significant decadal variability over the Amazon and its sub-basins, indicating an increase in dry season length over the past 36 years (Figure 2-17). Further, the increasing gap between TWD and TWS-R suggest an intensified terrestrial hydrologic system over the dry season during the study period. As the LULC impact is partly accounted for in the PET calculations (i.e., through changing surface albedo), the river basins with substantial LULC change, such as Madeira, Tapajos, Tocantins and Xingu, portray higher TWD trend magnitudes (significance > 95%). The peaks in the TWD corresponds well with drought years, for example, the peaks in the TWD for Madeira are analogous to the drought years (e.g., 1988, 1995, 2005 and 2010). Due to this definitive response to drought conditions, TWD is also used to characterize historical drought events in the earlier sections. We note that the trends in the total deficit should be interpreted with caution as the uncertainty in the forcing could have affected TWD and TWS-R trend estimates.

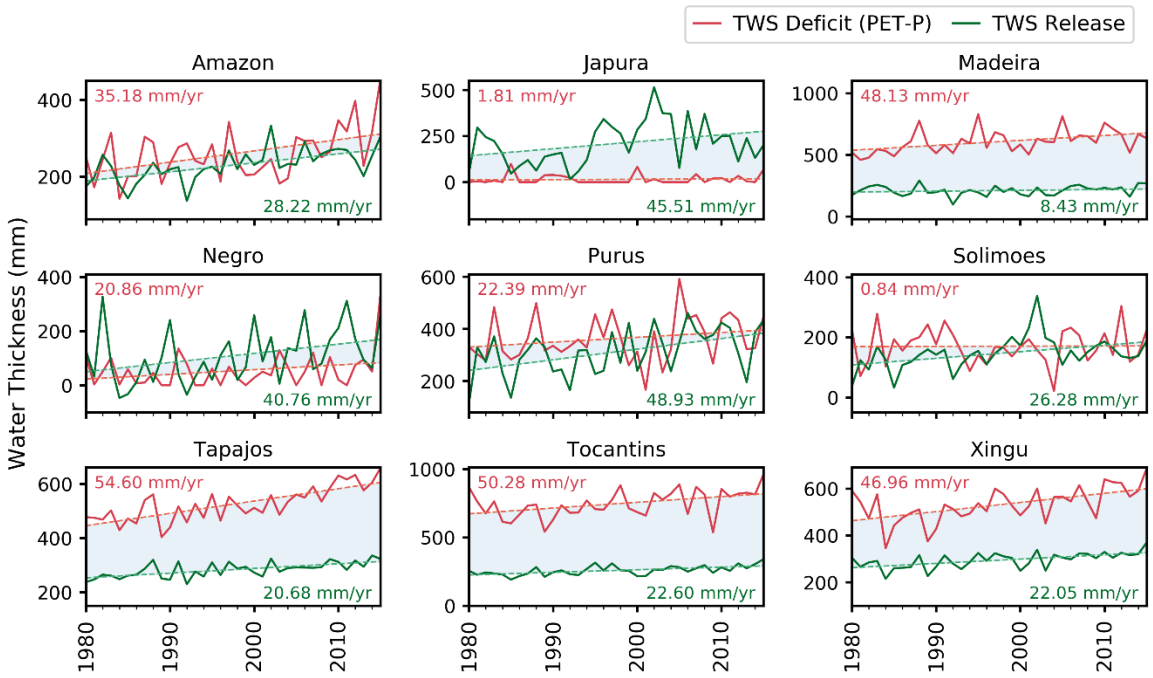


***Figure 2-17. Trends in dry-season total deficit (TWD) and corresponding simulated TWS release (TWS-R) from LHF for Amazon and its sub-basins.*** *TWD is quantified as the cumulative difference between potential evapotranspiration and precipitation (PET-P).*

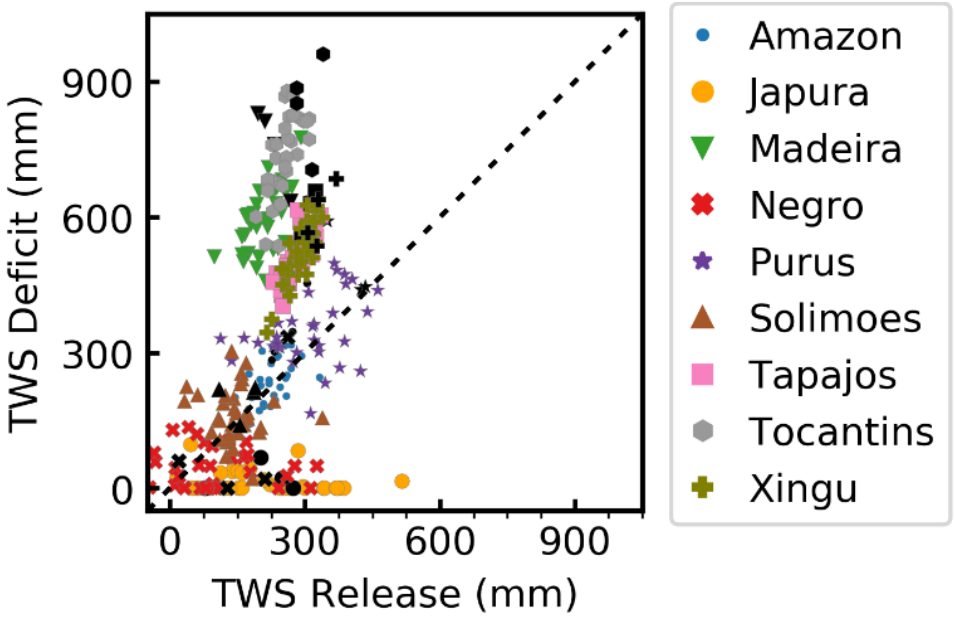


***Figure 2-18. Relationship between annual TWD and TWS-R for the period of 1980-2015, color coded by Amazonian sub-basins.*** *Points for extreme drought events are highlighted in black. Each marker type represents different river basins, totaling 36 markers for each river basin for the period of 1980-2015. Black dashed line indicates 1:1 relationship between TWD and TWS-R.*

We find that the river basins housing high altitudinal areas (Purus, Solimoes and Negro) have a fairly balanced relationship between TWD and TWS-R, but southern and southeastern sub-basins exhibit a higher water deficiency (Figure 2-18) with approximately 2 to 3-fold differences between TWD and TWS-R during regular years. For drought years, however, the difference between TWD and TWS-R is even higher, creating highly anomalous dry conditions in the sub-basins. Consistent higher values of TWD in southern and southeastern sub-basins of Amazon further highlights the intensification of the dry season with increasing water deficiency corresponding to an almost constant water supply from TWS-R. This phenomenon is also highlighted in Espinoza et al., (2016), which showed an significant increase in dry day frequency in the central and southern parts of Amazon. Results from this study combined with the reported increasing trend in wet season (Gloor et al., 2013), implies an overall intensification of the Amazonian hydrological cycle.

## 2.4. Conclusion

In this chapter, we examine the interannual and interdecadal trends and variability in the terrestrial hydrological system in the Amazon basin and its sub-basins, with a focus on droughts and their time evolution during the 1980-2015 period by using a continental-scale hydrological model Leaf-Hydro-Flood (LHF) and terrestrial water storage (TWS) data from GRACE satellite mission. For the first time, we provide a comprehensive characterization of extreme drought events in the Amazon basin during the past four decades, while categorizing them with respect to their i) cause, ii) type, iii) spatial extent, and iv) impacts on different water stores. We also provide an in-depth understanding of the interrelation between different drought types and the corresponding response of the sub-surface storage to surface drought conditions. Our key findings are summarized below.

First, the LHF model simulates the basin averaged TWS variations and seasonal cycle remarkably well for most of the sub-basins compared to GRACE data, however, some differences are observed in the spatial distribution of temporal trends for post-2008 period. We find that this discrepancy is caused primarily by the uncertainty in surface water storage simulations along the mainstem of the Negro and Amazon, whereas uncertainty in sub-surface storage prevails over the Andes. Second, the 2010-2015 period was found to be the driest in the past four decades due to an increase in frequency and severity of droughts. A t-test conducted on the TWS timeseries also indicated significant changes at the 99% level in the decadal mean TWS in the Negro and Solimoes sub-basins. Third, high negative long-term trends in TWS and increasing divergence between dry season total water deficit (TWD) and corresponding TWS release (TWS-R) indicate significant drying in sub-basins such as Madeira, Tapajos, Xingu, and Tocantins. Basin-averaged trends indicate that the Amazon is getting wetter (1.13 mm/yr), however, its southern and southeastern portions are getting drier. TWD is also found to be higher than TWS-R in these sub-basins, with approximately a three-fold difference between the two during some drought years, indicating a strengthening dry season in the region. Fourth, most of the extreme meteorological droughts do not propagate to hydrological droughts significantly, as the deficit is absorbed by the subsurface water storage and further reducing TWS drought severity compared to that of a meteorological drought in the Amazonian sub-basins.

Altogether, these results provide important insights on the interannual and interdecadal hydrological changes and the key mechanisms that govern drought events in the Amazon, along with a novel way of categorizing basin behavior during drought occurrence (Figure 2-16). This framework can be applied to better predict the future hydrological conditions and their corresponding socio-economic impacts toward taking measures to mitigate the drought impacts

and facilitate a relatively facile transition of the local population through a future drought event. Basin drying trends reported in this study can also provide key leverage by applying them toward anticipation of the future hydrological conditions for sustainable management of water resources. We also highlight the importance of using spatiotemporal trend estimates for model validation, especially with GRACE, instead of the commonly employed approach of timeseries comparison. Improvement in the correlation between the temporal trends in simulated TWS and GRACE anomaly through the inclusion of a prognostic groundwater scheme which allows dynamic groundwater-surface water interactions in the model framework is also highlighted. Further, the need to investigate the effects of uncertainties in model forcing to TWS simulations is noted because we find that the trends in precipitation are strongly propagated to TWS simulations.

A limitation of the present study is that the effects of irrigation and manmade reservoirs are not yet incorporated in the model. The basin-wide effects of the existing dams in the Amazon are small (Pokhrel et al., 2012a); however, as more dams are added across the basin, it will become critical to account for such effects. Model improvement is underway (Pokhrel et al., 2018b; Shin et al., 2019), and these issues will be addressed in our forthcoming publications. Despite some limitations, this study significantly advances the understanding of changing Amazonian hydrology, and our results have important implications for predicting and monitoring extreme droughts in the region; the research framework can also be applied to other global regions undergoing similar hydrological changes.

# Chapter 3. Alteration of River Flow and Flood Dynamics by Existing and Planned Hydropower Dams in the Amazon River Basin

*Based on:* **S. Chaudhari**, and Y. Pokhrel, 2021. Alteration of river flow and flood dynamics by existing and planned hydropower dams in the amazon river basin. ***Water Resources Research*** (*In review*)

## 3.1. Introduction

Hydropower is currently the largest renewable energy resource (IRENA, 2019) and is likely to remain a dominant source of energy for the near future (Moran et al., 2018; Winemiller et al., 2016). The future growth in hydropower production is expected to rely on the construction of large dams, such as those planned across the tropics (Winemiller et al., 2016). If built, the planned dams—together with many existing ones—are feared to interrupt the planet's last free-flowing rivers, including the Amazon, Mekong and Congo (Barbarossa et al., 2020; Davidson et al., 2012; Latrubesse et al., 2017; Winemiller et al., 2016). Although the expected surge in hydropower development may fulfill the much needed energy requirements in those regions, they are often advocated based on overestimated economic benefits and underestimated social and environmental impacts (Barbarossa et al., 2020; Latrubesse et al., 2017; Moran et al., 2018; Stone, 2016; Waldman et al., 2019). While the positive versus negative effects of dams have been and can be debated (Fearnside, 2006; Stone, 2011; Tófoli et al., 2017), unprecedented losses in biodiversity (Forsberg et al., 2017; Latrubesse et al., 2017; Moran et al., 2018; Timpe and Kaplan, 2017; Winemiller et al., 2016) and disruptions in river connectivity (Anderson et al., 2018; Finer and Jenkins, 2012) are inevitable.

Large-scale, storage-based dams and even run-of-the-river hydropower plants are known to cause profound alterations in the downstream regions, accruing many hydrological, ecological and social losses—including those caused by water impoundment (Aragão et al., 2018; Fearnside and Pueyo, 2012; Kemenes et al., 2011), impediment to sediment and nutrient transport (Eiriksdottir et al., 2017; Latrubesse et al., 2017), resettlement of populations (Berkun, 2010), reduced fish productivity and migration (Alho et al., 2015; Castello et al., 2015; Stone, 2016), alterations in freshwater discharge to oceans (Pokhrel et al., 2012b), and disruption of flood pulse dynamics (Pokhrel et al., 2018b). Further, given that river flows around the world are changing in response to climate change and variability (Gernaat et al., 2021; Gudmundsson et al., 2021), there are heightened concerns regarding the reliability of hydropower generation from existing and planned dam projects (Moran et al., 2018). Yet, countries are undertaking ambitious plans to expand hydropower development even in extremely biodiverse regions such as the Amazon River basin (ARB). Therefore, it has become increasingly imperative to better understand the changes in hydrological dynamics caused by existing dams as well as the potential effects of future dams in these regions.

Numerous studies have examined the impacts of reservoir operation in large river systems, such as the Amazon and Mekong. For example, observation-based studies—using pre- and post-dam analyses—have shown that dams have incurred a shift in flow patterns in many global river basins (Cochrane et al., 2017, 2014; Latrubesse et al., 2017; Räsänen et al., 2017). These studies have provided important advances in understanding the role of dams, but the observed data alone cannot justify these impacts as the hydrological changes are also subjected to climate change and variability. Further, most studies have focused only on river flow alterations downstream of dams; the impact of dams on inundation dynamics both upstream and downstream remains little

studied over large scales. Hydrological models are indispensable for such a mechanistic quantification. These models enable a holistic investigation of the impact of dams and their potential future role under climate change. Shin et al., (2020) introduced one of such models and demonstrated its application over the Mekong River basin, however, no such study has been conducted over other large river systems such as the Amazon that are being increasingly dammed.

Specifically for the Amazon, our present understanding of the cumulative impact of existing hydropower dams over the entire basin is extremely limited. Some previous studies have presented critical insights on the changing hydrology due to dams with their overall impact on the basin with respect to new roads, deforestation (Lovejoy and Nobre, 2018; Zemp et al., 2017) and the ever-advancing agricultural frontier (Davidson et al., 2012; Freitas et al., 2018; Nobre et al., 2016), along with the changes in hydrology and sediment transport, which are crucial for downstream floodplains, estuary and coastal ecosystems (Latrubesse et al., 2017). The critical role of the Andes-to-Amazon connectivity was also highlighted by a regional analysis of river fragmentation by existing and planned hydropower dams in the Andean headwaters of the Amazon (Anderson et al., 2018; Finer and Jenkins, 2012). While these studies have provided crucial information on various aspects of dam impacts, the insights gained have been rather disparate. Crucially, a mechanistic understanding of the effects of hydropower dams and climate change across the entire basin is critically lacking. Further, since most previous studies are based on observational streamflow data, there is a lack of direct attribution of the observed changes to dams and climate change and variability.

Here, we address the aforementioned issues by using an improved version of a recently developed integrated river-floodplain-reservoir hydrodynamics model, the CaMa-Flood-Dam

(CMFD; Shin et al., 2020). The model enables a mechanistic investigation of the basin-wide climate- and human-induced changes in the hydrological system through simulation of river-floodplain-reservoir hydrodynamics with and without dams. In this study, we improved the existing modeling framework by implementing an optimized reservoir operation scheme to realistically represent dam-induced changes and maximize total energy production while also following the common practice of water management through different seasons (Figure 3-1). Specifically, this study aims to (i) quantify the impacts of flow regulations by existing large-scale hydropower dams on downstream river flow and flood dynamics in the Amazon, (ii) examine the cumulative potential impacts of existing and planned hydropower dam operations on the downstream hydrology of the Amazon and its sub-basins, and (iii) understand the role of hydropower dam operations in modulating the flood pulse along the mainstem of the Amazon.

## 3.2. Materials and Methods

### 3.2.1. Model and Data

CaMa-Flood-Dam (Catchment-based Macro-scale Floodplain with Dam scheme; CMFD) model (Pokhrel et al., 2018b; Shin et al., 2020; Yamazaki et al., 2013, 2012a, 2011) is global-scale distributed river model which simulates river and floodplain hydrodynamics by solving shallow water equations of open channel flow, explicitly accounting for backwater effects and reservoir operations. The CMFD model discretizes the study domain into unit catchments in which the water level and inundation area are diagnosed based on the water storage at every time step. The temporal variation of water storage in each unit catchment is calculated using mass conversation between upstream and downstream river flow, and total runoff input from the forcing data. Flow in natural rivers is represented by the 1-D St. Venant equation for momentum conservation and the continuity equation:

$$\frac{\partial Q}{\partial t} + \frac{\partial}{\partial x}\left(\frac{Q^2}{A}\right) + gA\frac{\partial}{\partial x}(h+z) + \frac{gn^2Q^2}{R^{\frac{4}{3}}A} = 0 \quad (3\text{-}1)$$

$$\frac{\partial Q}{\partial x} + \frac{\partial A}{\partial t} = \mathrm{q} \quad (3\text{-}2)$$

where Q is the river discharge ($m^3/s$), A is the flow cross- section area ($m^2$), h is the flow depth (m), z is the bed elevation (m), R is the hydraulic radius (m), g is acceleration due to gravity ($m/s^2$), q is the lateral flow ($m/s^2$), and n is the Manning's friction coefficient ($m^{-1/3}$ s). The parameters x and t are the flow distance and time, respectively. The first, second, third, and fourth terms represent the local acceleration, advection, water slope (i.e., pressure and bed gradients), and friction slope, respectively. In the earlier versions of CaMa-Flood model (Yamazaki et al., 2011), diffusion wave equation has been used, which is obtained by neglecting the first and second terms of the 1-D St. Venant equation. However, the more recent version (Yamazaki et al., 2013) employs the local inertial equation which is derived by neglecting only the advection term in the 1-D St. Venant equation. Discretizing the local inertial equation for the time step Δt using a forward in time finite difference approximation, Q at the next timestep can be calculated explicitly as:

$$Q_{t+\Delta t} = (Q_t + \Delta t g A S) \Big/ \left(1 + \frac{\Delta t g n^2 Q_t}{R^{\frac{4}{3}}A}\right) \quad (3\text{-}3)$$

The local inertial equation is computationally more efficient than the diffusion wave equation used in the CaMa-Flood model for previous studies (Yamazaki et al., 2013, 2011) because it can be solved stably at a much higher time step in areas with a small water surface slope and a large water depth. To accurately represent the process of floodplain inundation, the river channel and floodplain topography are represented by sub-grid scale topographic parameters such as the

ground elevation ($Z$), unit-catchment area ($A_c$), channel length ($L$), and floodplain elevation profile, are explicitly derived from fine-resolution flow direction maps and digital elevation models. The model is parameterization and initial conditions are similar to Yamazaki et al., (2013).

More recent development in the CaMa-Flood model framework was the incorporation of reservoir operation schemes yielding CaMa-Flood-Dam model (Shin et al., 2020). The update includes a reservoir release scheme which utilizes a demand-driven approach for irrigation dams and an optimization approach to maximize power generation for hydropower and multipurpose dams. A complete description of CaMa-Flood-Dam can be found in Shin et al., (2020).

Existing and planned dam locations and their attributes such as dam height, reservoir capacity, and power generation capacity in the Brazilian Amazon are compiled from Agência Nacional de Energia Elétrica (ANEEL; http://www.aneel.gov.br/), Global Georeferenced Database of Dams (GOOD; Mulligan et al., 2009), and Future Hydropower Reservoirs and Dams (FHReD; Zarfl et al., 2015), database. A total of 33 existing dams and 25 planned dams were selected based on their power generation capacity (≥30 Mega Watts; MW), storage capacity (≥1 million $m^3$; $Mm^3$) and attribute availability; selected planned dams are limited to the Brazilian Amazon due to lack of data availability in other regions of the Amazon.

### 3.2.2. Reservoir Operation Scheme for the Amazon

In this study, we utilize an optimization scheme from Shin et al., (2020) for simulating reservoir operations of hydropower dams in the Amazon. Reservoir operation for hydropower can be formulated as an optimization problem that maximizes power benefits, F [$] as

$$E = \sum_{t=1}^{365} \eta \cdot \gamma \cdot \min(Q_t, Q_{turbine}) \cdot H_t \cdot \Delta t \quad (3\text{-}4)$$

where E is the energy generated [Watts-hour], during the time span of Δt [hr], η is efficiency [−], γ is specific weight of water [kg/m$^3$], $Q_t$ is the reservoir release (m$^3$/s), $Q_{turbine}$ is turbine design flow(m$^3$/s), and $H_t$ is turbine head [m]. Further, we allow a common practice in hydropower management of storing excess water during low-demand and releasing during wet periods by formulating it in terms of minimizing reservoir storage variation ($\sigma_{STOR}$) within a year. The time-varying inflow to the reservoir is estimated using the river discharge simulated without considering dams as,

$$In(t) = \sum_{k=1}^{K} Out_{k,t} + \left(1 - \frac{\sum_{t=1}^{T}\sum_{k=1}^{K} Out_{k,t}}{\sum_{t=1}^{T} Q_{NAT,t}}\right) \cdot Q_{NAT,t} \quad (3\text{-}5)$$

where $Out_{k,t}$ is monthly outflow of the k$^{th}$ immediate upstream reservoir at time t, $Q_{NAT,t}$ is river discharge from the no-dam simulation at the reservoir location and time t, K is the number of immediate upstream reservoirs, and T is the total simulation period.

We implement only the reservoir release for the purpose of hydropower in this study, since the data on irrigation in the Amazon are not available, and it is expected that irrigation water use is relatively minimal compared to the flow volume in the ARB. Building on the original reservoir release scheme based on the optimization approach for hydropower in the CMFD model, dam outflow at each of the dam location ($Q_{turbine}$) is optimized to maximize annual energy production using the upper and lower flow thresholds. The upper threshold for reservoir release is set to the flow with 30% exceedance probability ($Q_{30}$; the flow equaled or exceeded 30% of the time in a year), which is a widely accepted flow threshold for hydropower operation (Gernaat et al., 2017; Hoes et al., 2017; Shin et al., 2020). Whereas the lower threshold for reservoir release (dam outflow during the dry season) is optimized using the reservoir capacity and inflow to the reservoir, such that the water stored in the reservoir during the wet season will sustain constant

energy production during the dry season. The dam storage is simulated based on the available data on reservoir capacity. In order to reduce the computational cost required for the optimization of dam outflow which needs iterative hydrodynamic modeling to sequentially determine the river flows for each reservoir from upstream to downstream, we implement the scheme outside of CMFD model. We utilize the simulated river flow under natural condition (NAT simulation) to sequentially optimize the reservoir release starting from the most upstream to the downstream reservoir (Shin et al., 2020). A schematic representation of reservoir operation is provided in Figure 3-1.

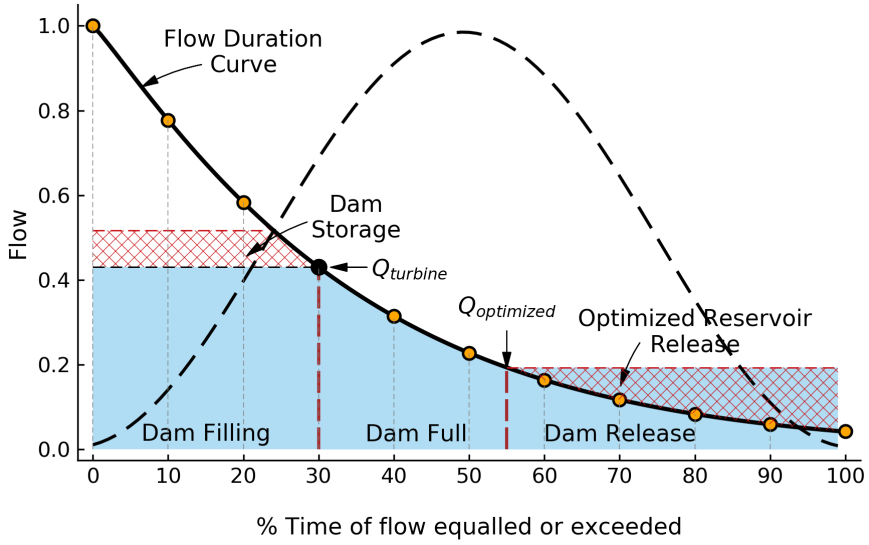


***Figure 3-1. Schematic representation of the dam operation scheme.*** *The approach utilizes daily variations in the streamflow simulated in CaMa-Flood-Dam (CMFD) model. Black solid and dashed line indicate a standard flow duration curve and a seasonal flow cycle, respectively. Black filled circle indicates the upper discharge threshold (i.e., $Q_{30}$) used for reservoir release during the wet period. Reservoir release in the dry period is optimized ($Q_{optimized}$) using the available dam storage. Shaded blue area indicates the total hydropower energy generated. Red hatches indicate dam storage in the wet period and dam release in the dry period.*

Dams are accurately located on the model grids, by first determining their upstream drainage from a high-resolution (3-arcsec) digital elevation model (DEM) (Yamazaki et al., 2017) and their location attributes. The estimated upstream drainage areas are then used as a reference to determine the respective dam locations on the 3-arcmin model grid. Further, the DEM indicates water surface levels over inundated areas, hence the DEM indicates a flat topography at some existing reservoir locations, especially if the reservoir is created before the DEM is produced. These uncertainties are also carried over to the downscaled flood, however they do not reservoir operation scheme as the scheme is based on the volumetric flow. Moreover, to overcome this issue, we estimate the water depth required to achieve the dam storage capacity using upstream reservoir tracking from respective dam locations and consider them as dam heights in the model environment.

### 3.2.3. Simulation Settings

In this study, the CMFD model is setup for the entire ARB and is driven by daily runoff obtained from ERA-5 dataset with spatial resolution of 0.1° × 0.1° (~10 × ~10 km) for the 1981–2019 period. The spatial resolution of the CMFD model is set to 3-arcmin (5 km) and the simulated flood dynamics are further downscaled to 3-arcsec (~90 m) resolution using high-resolution digital elevation model (DEM). All model parameters are identical to those used in Yamazaki et al., (2011). Specifically, we conduct four simulations: i) without dams as in natural setting (NAT), ii) with all existing dams introduced year-by-year following their commission year (YBY_E), iii) all existing dams introduced in 1981 (start of simulation; ALL_E) and iv) all existing and planned dams introduced in 1981 (ALL_EP). All these model scenarios are designed to quantify the historical and potential future impact of existing and planned dam operations, either individually or cumulatively, on an annual and long-term averaged time

periods. Although, these model setups may not fully capture the effects of future dams, they represent a credible outline of the probable impact from the combined operation of existing and planned dams in the future under the effects of historical climate change/variability.

***Table 3-1. CaMa-Flood-Dam Model Simulation settings***

| Simulation Name | Year of Dam Introduction | Hydropower operation scheme | $Q_{turbine}$ |
|---|---|---|---|
| NAT | No dams | - | - |
| DamBCY-opt-$Q_{30}$ | By commission year | Optimized Level | $Q_{30}$ |
| DamBCY-opt-$Q_{40}$ | | Optimized Level | $Q_{40}$ |
| DamBCY-Full | | Full Level | - |
| DamALL-opt-$Q_{30}$ | Start of the simulation | Optimized Level | $Q_{30}$ |
| DamALL-opt-$Q_{40}$ | | Optimized Level | $Q_{40}$ |
| DamALL-Full | | Full Level | - |

## 3.3. Results

### 3.3.1. Evaluation of simulated river flow, water level, and flood occurrence

Simulated river flow and water level from CMFD model compare well with the observations obtained from Agência Nacional de Águas (ANA), Brazil (Figure 3-2, Figure 3-3 and Figure 3-4). Building on our recent studies (Chaudhari et al., 2021, 2019), we present the evaluation of simulated river flow and water level from CMFD model at selected locations across the Amazon in a Taylor diagram (Figure 3-2a), which provides a statistical summary of the comparison between observations and model results. The evaluation is expressed in terms of the ratio of standard deviation (SD) of simulated estimates to the observed as a radial distance and their correlation as an angle on the polar axis. At most of the eighty observation stations located across the Amazon and at varying stream sizes (Figure 3-2b), a high correlation (> 0.9) and a

standard deviation ratio close to unity for both simulated river flow and water level is found, demonstrating a good model performance overall. Evidently, the model exhibits a wet bias, especially in the Tocantins River basin. A part of such discrepancies could be attributed to uncertainties in forcing, input parameters, and model parameterizations. These have been discussed in detail in previous studies (Chaudhari et al., 2019; Miguez-Macho and Fan, 2012a; Yamazaki et al., 2012b).

When compared with the satellite-based flood occurrence from Global Surface Water (GSW) dataset (Pekel et al., 2016), the model well captures the broad spatial patterns of flood occurrence during the 39-year simulation period, especially at the Amazon mainstem and major existing dam locations (Figure 3-5 and Figure 3-6). In many locations, especially in the Amazon mainstem, the model shows larger flood occurrence, which could partly be due to under-representation of flooding in these areas in the GSW dataset, as also discussed in previous studies (Aires et al., 2017; Pekel et al., 2016; Pokhrel et al., 2018b; Shin et al., 2020), likely due to the underestimated flooded areas owing to cloud contamination and dense forest cover. Additionally, certain discrepancies could be attributed to the different observational period of GSW data (1984-2018) as opposed to the model period (1981-2019), uncertainties in the topographical data used in the model and errors arising from downscaling of flood occurrence (see Methods). Overall, given that the model is implemented over the entire basin without any parameter tuning, we find the results to be reasonable for assessing the hydrological alterations caused by dams and the role of historical climate change with the current limitations on model resolution and data availability.

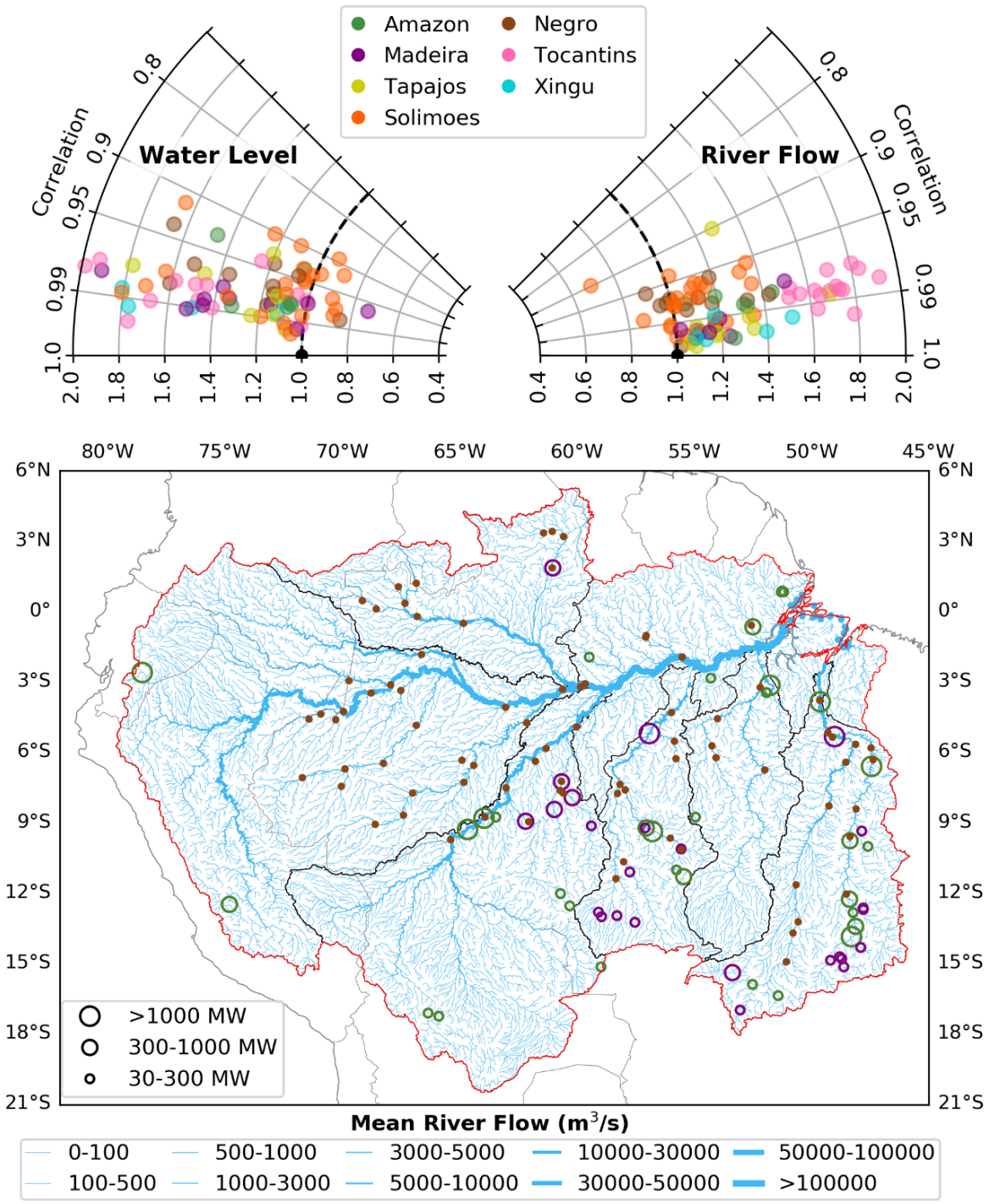


***Figure 3-2. Evaluation of simulated river flow and water level. a****, Taylor diagrams showing correlation and standard deviation ratio between the simulated and observed river flow and water level at 80-gage stations across the Amazon.* ***b****, Location of the 80 gaging stations (brown dots) and spatial distribution of long-term (1981-2019) averaged river flow from the CaMa-Flood-Dam model at 5-km spatial resolution. Green and purple circles mark the existing and planned dam sites, respectively. Red and black lines indicate the boundaries of the ARB and its major sub-basins.*

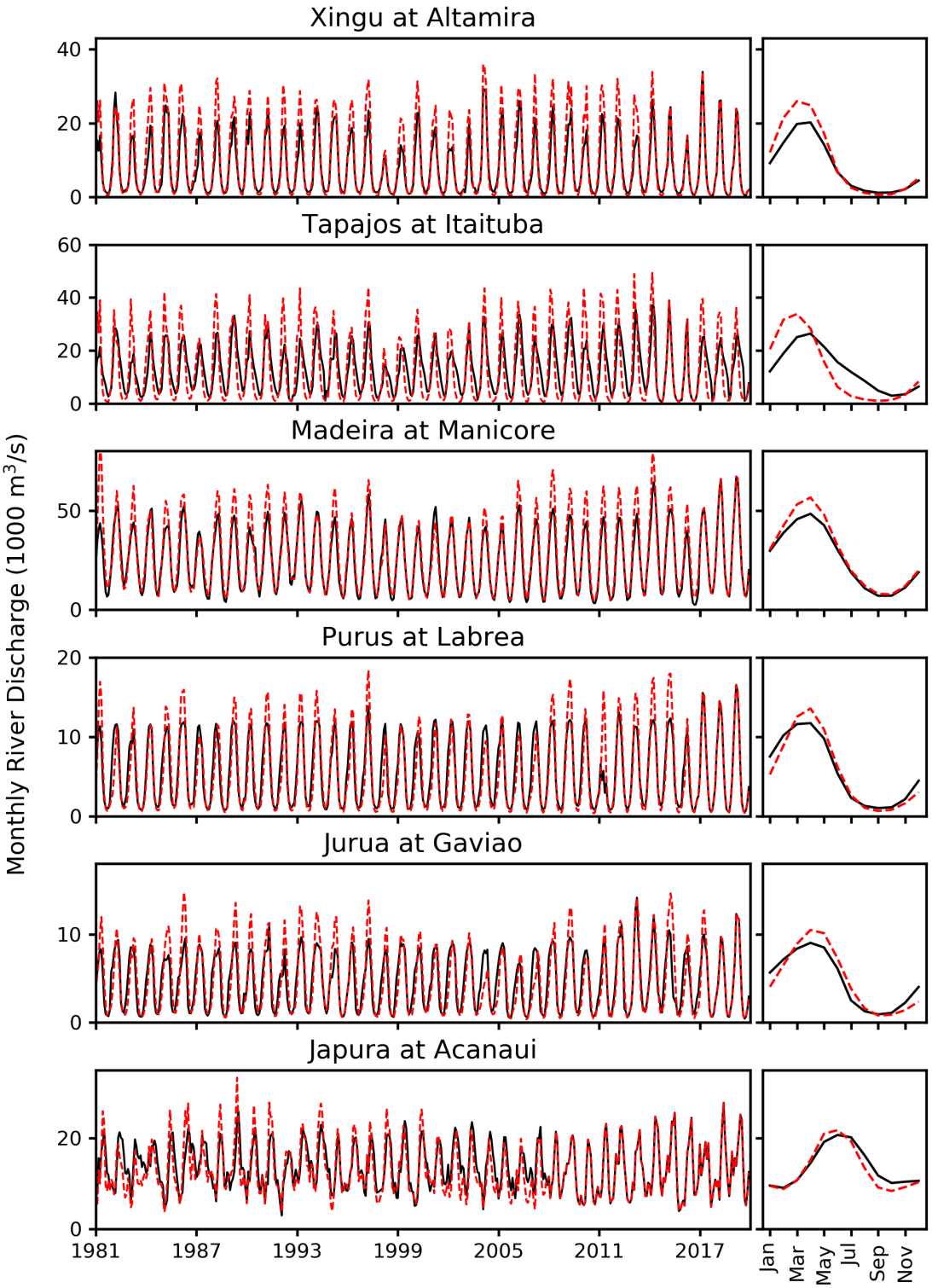


***Figure 3-3. Comparison of observed and simulated river flow in the Amazon.*** *Observed river flow (black) is obtained from ANA Brazil and simulated river flow (red) is obtained for CMFD model with a YBY_E setup. Results are shown for 12 main gauge stations. Seasonal cycle for each station is also shown in the right panel of each subplot.*

***Figure 3-3 (cont'd)***

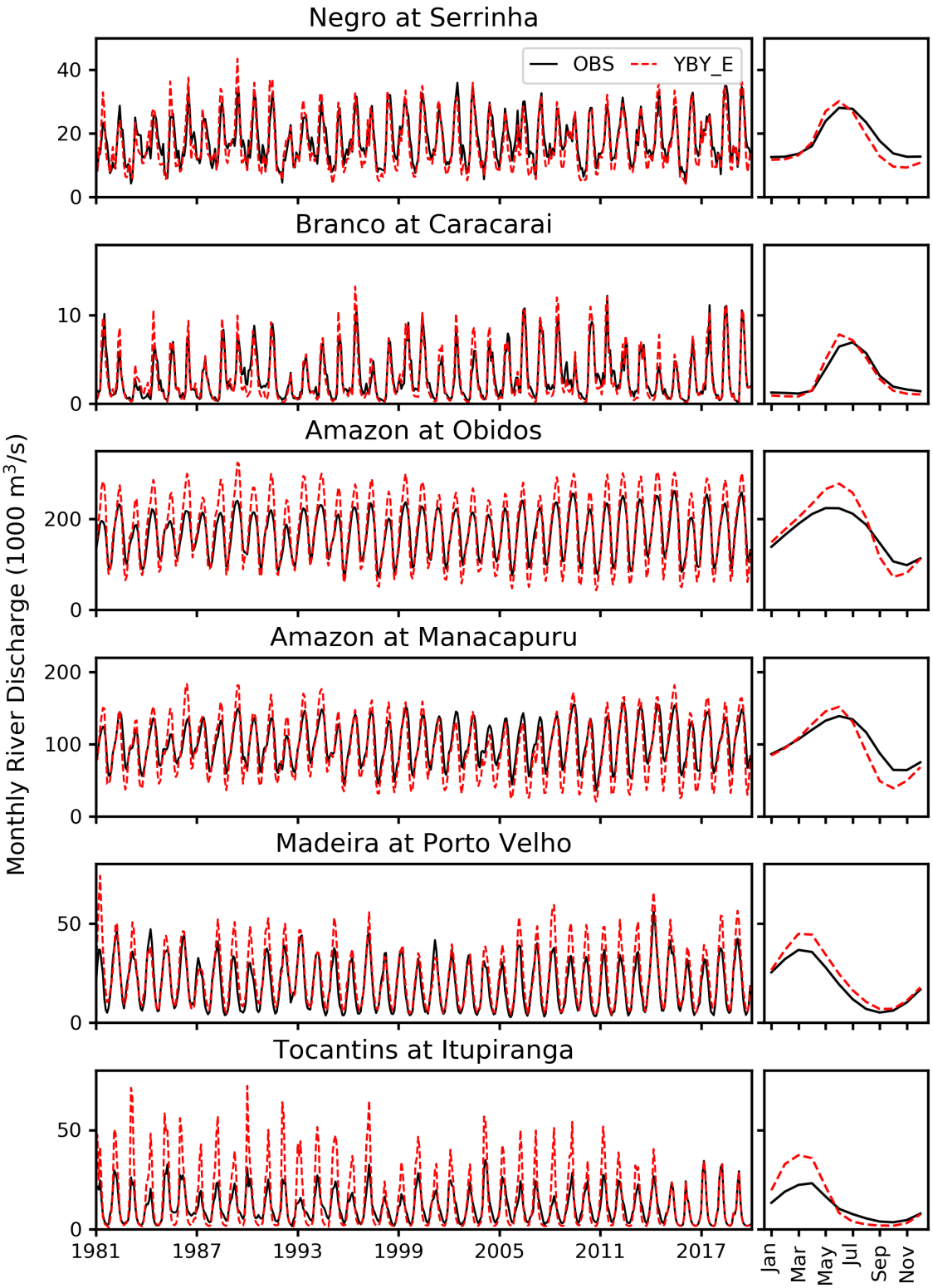

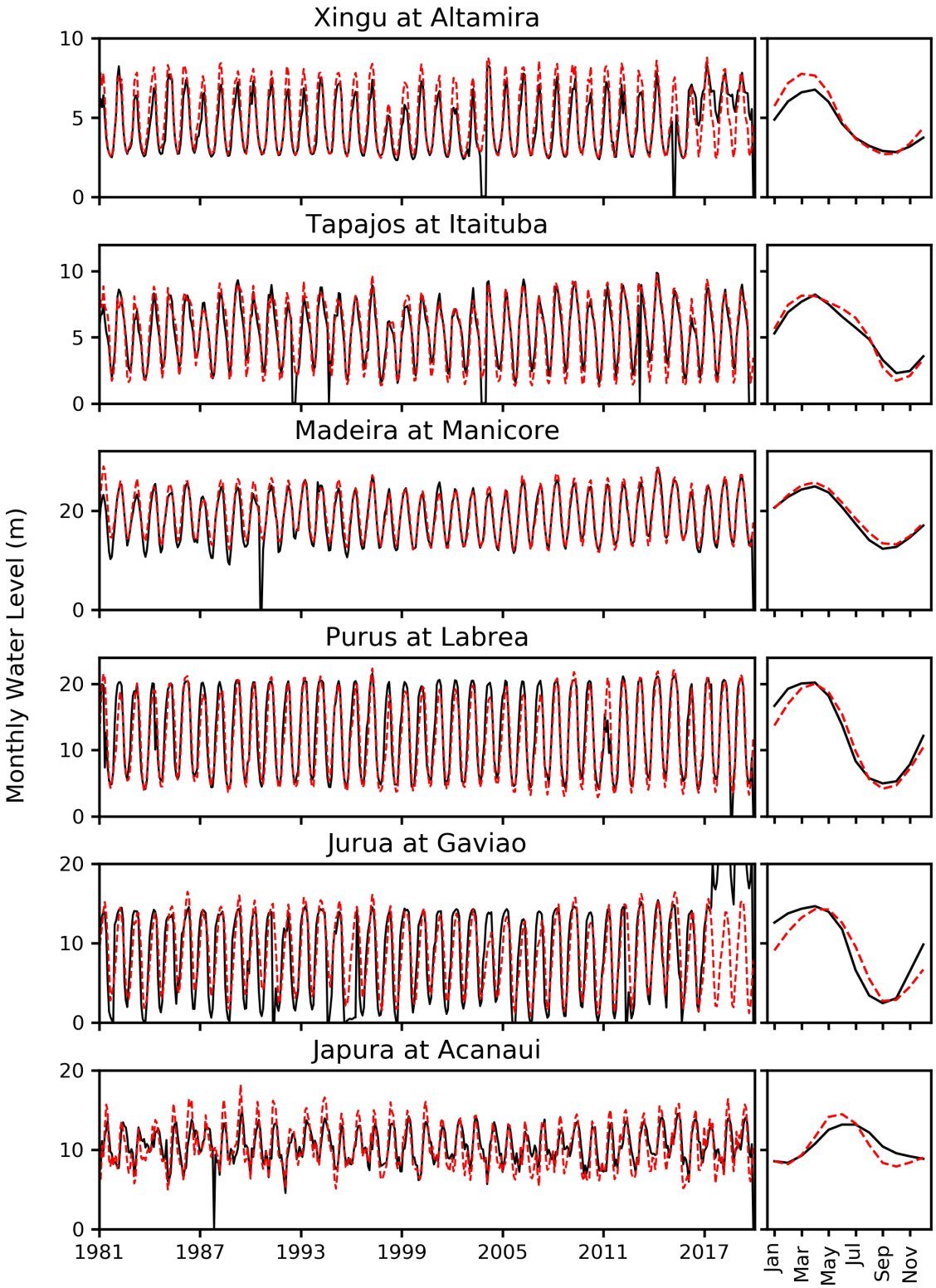


***Figure 3-4. Comparison of observed and simulated water level in the Amazon.*** *Same as in Figure 3-3 but for water level.*

***Figure 3-4 (cont'd)***

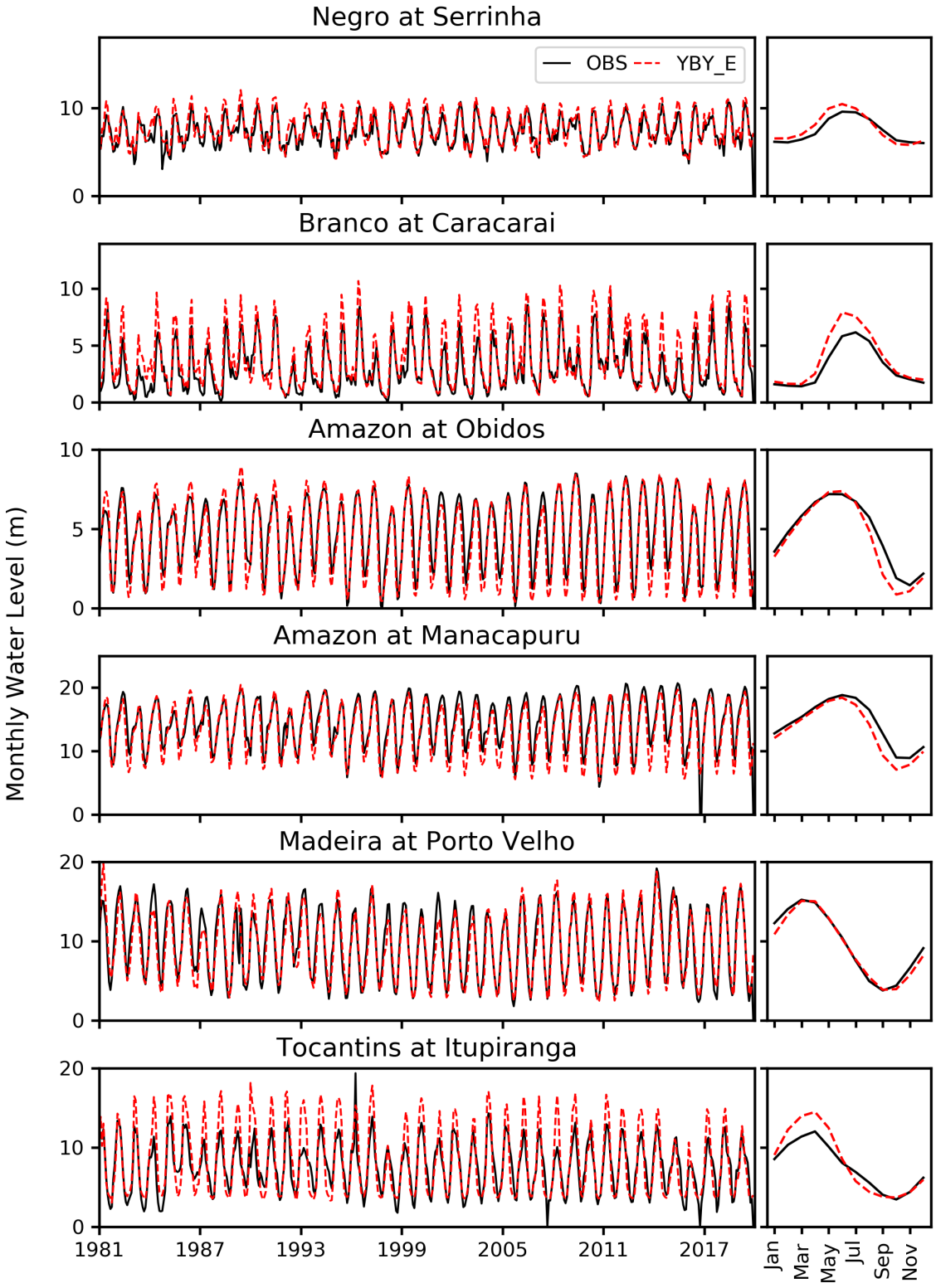

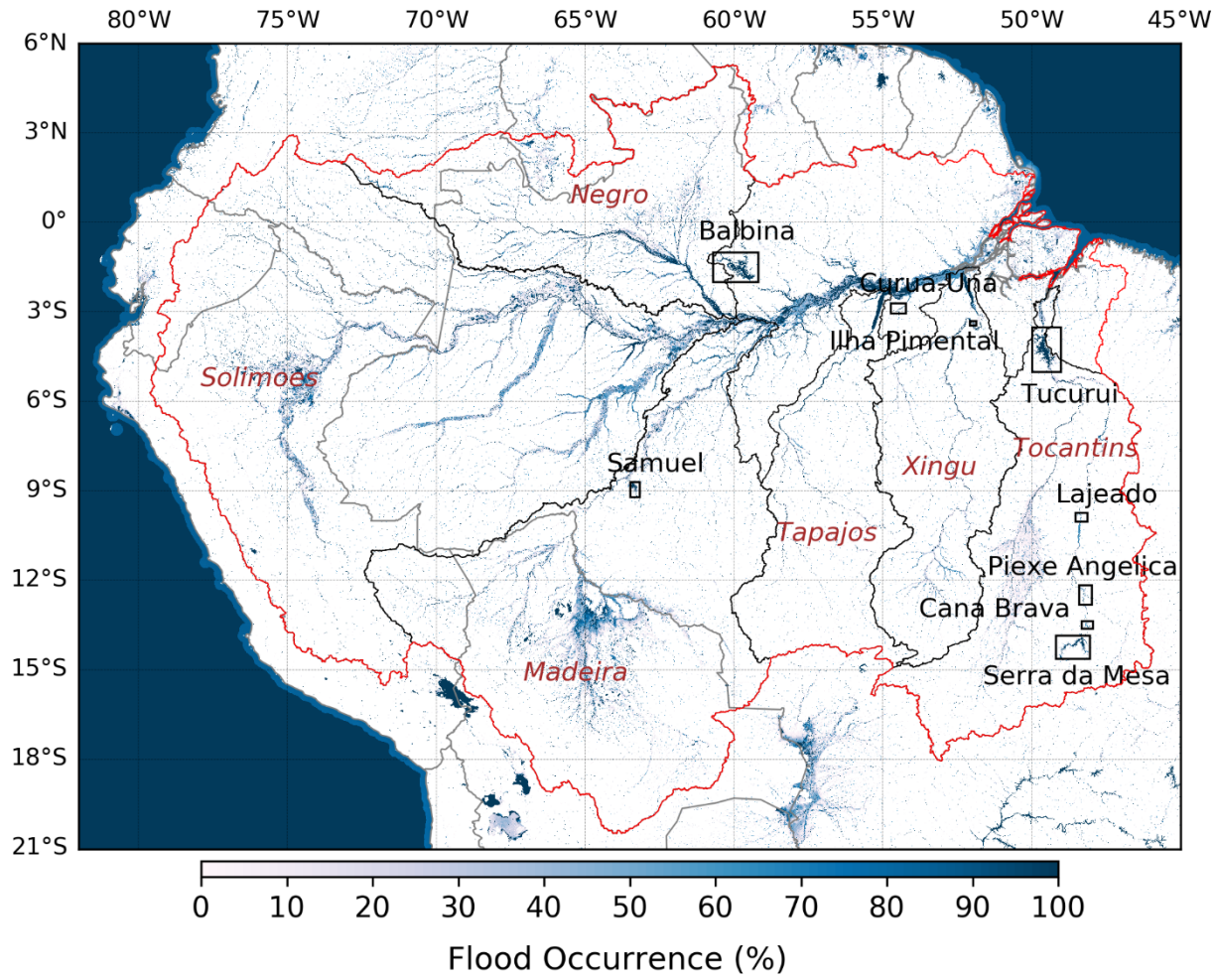


***Figure 3-5. Simulated flood occurrence from YBY_E simulation downscaled at 3 arcsec (~90m) spatial resolution.*** *Boxes indicate the locations of major existing dams shown in Figure 3-6 of the main text. Red and black boundaries indicate the Amazon River basin and its sub-basins, respectively. Brown italic texts indicate the names of the Amazonian sub-basins.*

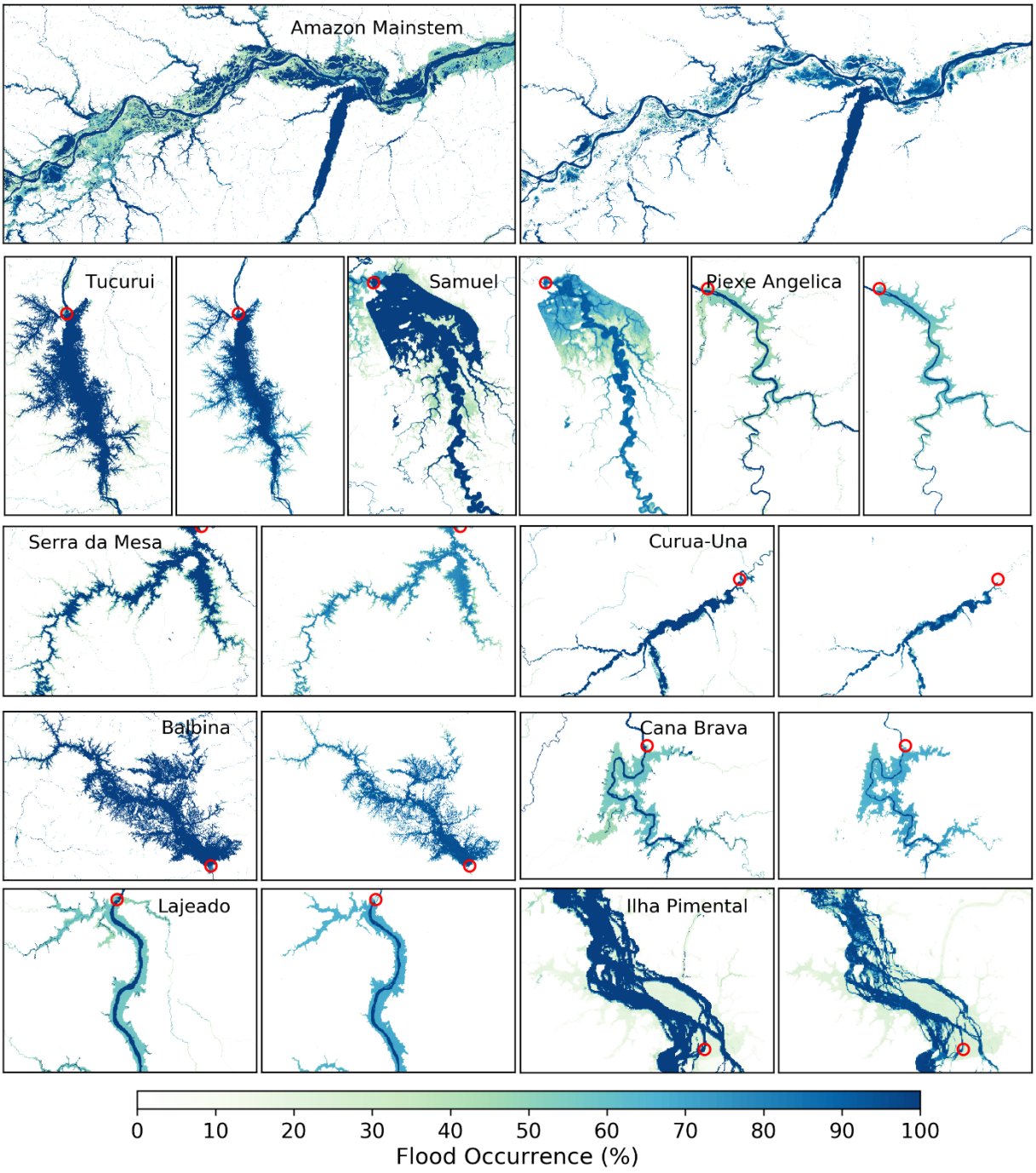


***Figure 3-6. Modeled (YBY_E simulation) and observed flood occurrence in the Amazon mainstem and selected existing dam locations.*** *For each site, the left and right panel shows the simulated flood occurrence (~90m spatial resolution) for the 1981-2019 period and the satellite derived flood occurrence from Global Surface Water (GSW) dataset (1984-2018), respectively. Red circles mark dam locations and label within the panel indicates the location or dam name. Locations of dams marked in the ARB are shown in Figure 3-5.*

### 3.3.2. Hydrologic alterations by existing dams

Results indicate that some of the large existing dams including Tucurui (8,370 MW), Estreito (1,087 MW) and Serra da Mesa (1,275 MW) in the Tocantins, and Samuel (216 MW) in the Madeira River basin have caused substantial alteration to river flow in the Amazonian sub-basins throughout the study period (Figure 3-7, locations shown in Figure 3-5). We make the following key observations. First, major shifts in river flow coincide well with the commission years of the existing dams (Figure 3-7a). Second, existing reservoir operations have considerably altered the dry season flow (i.e., low flow) as well as the 39-year median flow in the Amazonian sub-basins. Third, substantial impacts on the river flow due to the operation of existing dams are evident even on the multidecadal averages of the hydrological signatures.

Change in river flow by up to three orders of magnitude is observed following the introduction of Belo Monte dam cascade in the Xingu River basin and Colider, Sinop, Teles Pires and Sao Manoel dams in the Tapajos River basin. Similarly, a two orders of magnitude alteration in river flow is observed after the commissioning of Samuel dam in the Madeira River basin. Santo Antonio and Jirau dams, operated as run-of-river dams, are found to have caused relatively less impact with respect to the alterations in river flow. In the rest of the Amazonian sub-basins, such as Solimoes, the impact on river flow due to reservoir operation is found to be minimal (Figure 3-7a).

Existing dam operation has caused the median monthly river flow to increase by ~29% over the study period in the Tocantins River basin (Figure 3-7b). Further, results indicate a maximum change of ~208% increase, 37% decrease and ~40% decrease in the low flow, peak flow, and river flow seasonal amplitude in the Tocantins River basin over the study period, due to the operation of the existing dams (Table 3-2). Other Amazonian sub-basins also indicate a similar

change pattern in low flow and river flow seasonal amplitude from existing dam operations with 114% increase and 1% decrease in the Xingu, and 37% increase and 3% decrease in the Tapajos sub-basins.

Moreover, a ~7% reduction in the climatological mean peak flow and ~84% increase in the climatological mean low flow (Figure 3-7c) during 1981-2019 period are observed in the Tocantins River basin. In rest of the Amazonian sub-basins, namely Madeira, Xingu and Tapajos, the impact of existing dams on the river flow climatology are comparatively less prominent as most of the operational dams in these basins are relatively new (commissioned after 2000). The climatological changes in low flows are +5%, +3% and +2% in the Xingu, Madeira, and Tapajos River basins, respectively.

***Table 3-2. Alterations of the river flow signatures from the YBY_E simulation with respect to the NAT simulation.***

| River Basin | Simulation | %Change in Median from NAT | %Max Change in Seasonal Amplitude from NAT | % Max Change in Peak flow from NAT | % Max Change in Low flow from NAT |
|---|---|---|---|---|---|
| Amazon | YBY_E | 0.0% | -1.5% | -0.4% | 4.0% |
| Madeira | YBY_E | -0.5% | -1.8% | -0.8% | 14.5% |
| Negro | YBY_E | 0.1% | -0.3% | -0.2% | 0.2% |
| Solimoes | YBY_E | -0.1% | -0.1% | -0.1% | 0.2% |
| Tapajos | YBY_E | -0.1% | -3.3% | -2.2% | 36.5% |
| Tocantins | YBY_E | 28.5% | -40.2% | -36.8% | 207.9% |
| Xingu | YBY_E | -0.7% | -1.2% | -0.2% | 113.9% |

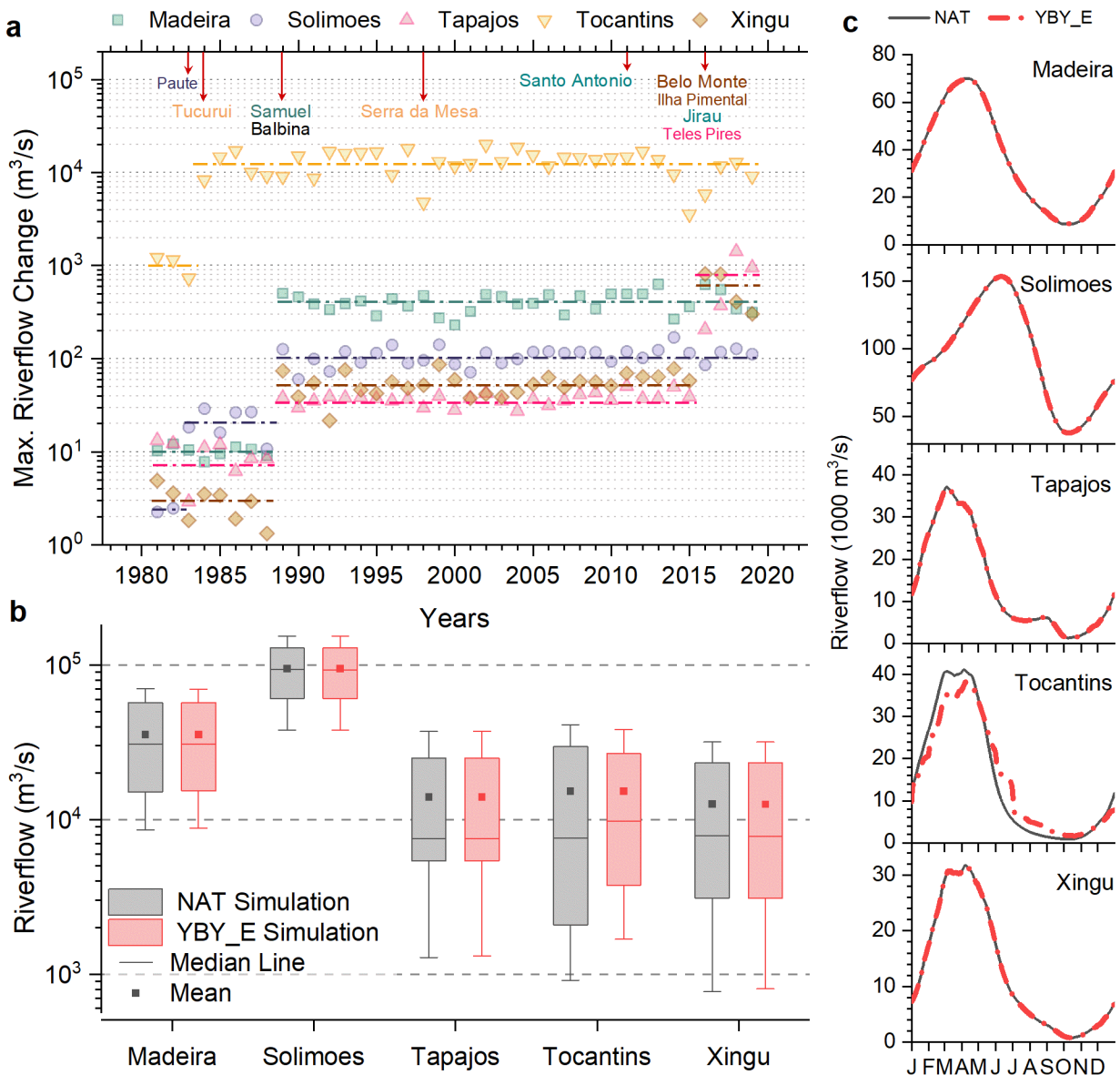


***Figure 3-7. River flow alterations caused by the operation of existing dams. a,*** *Difference in the seasonal amplitude between NAT and YBY_E simulations at the mouth of the major sub-basins of the ARB (color coding). Red arrows indicate the year of dam commissioning.* ***b****, Box plot of the simulated monthly river flow at the mouth of the major sub-basins of the Amazon.* ***c****, Simulated daily long-term (1981-2019) averaged river flow at the mouth of the major Amazonian sub-basins.*

### 3.3.3. Hydrological change expected from the collective operation of existing and planned dams

Profound changes in the 39-year flood occurrence would occur in the Amazon mainstem if all the planned dams in the basin were to be operated (Figure 3-8). Different areas on the Amazon mainstem indicate a >10% decrease in the long-term flood occurrence, which could be a direct result of the reduced peaks from reservoir operation in the wet season. Additionally, increase in flood occurrence is observed in some parts of the Amazon mainstem (Box. 1, downstream of existing Balbina Dam), which corresponds with dry season water release from reservoirs.

Dams included in the Brazil's 10-year energy expansion plan namely, Bem-Querer, Tabajara and Castanheira, contribute toward ~171 square kilometers of additional inundation upstream from their dam sites. Overall, our estimate suggests that the planned dams in the Brazilian Amazon could inundate ~1,550 square kilometers of land in addition to that inundated by the existing dams. Impacts from the individual operation of existing and planned dams on the 39-year flood occurrence along the Amazon mainstem is shown in Figure 3-10.

Potential future dam impacts in the Amazon River basin could be considerably larger than that caused by the existing dams (Figure 3-9, Table 3-3). Specifically, in the Tocantins River basin, the collective operation of existing and planned dams could cause a ~37% increase and ~12% decrease in the 39-year averaged median of daily river flow and seasonal amplitude, respectively. Substantial alterations to the 39-year averaged peak flow (-8.3%) and low flow (149%) could occur in the Tocantins River basin. Similar level of alterations to the river flow signatures could also occur in the other Amazonian sub-basins. For example, ~61%, ~39% and ~14% change in the 39-year averaged low flow could occur in the Tapajos, Xingu, and Madeira River basins, respectively, due to the operation of existing and planned dams. Our estimate

suggests that the collective operation of existing and planned dams in the Amazon could alter the median, amplitude, peak flow and low flow of the 39-year averaged daily seasonal cycle at the mouth of the ARB by -0.4%, -1.6%, -0.4% and 3.4%, respectively. Although, the percentage change estimates of the river flow signatures in the ARB seem to be fairly low, their magnitudes are substantially larger due to the large flow volume.

***Table 3-3. Alterations of the 39-year averaged river flow signatures from the ALL_E and ALL_EP simulations with respect to the NAT simulation.***

| River Basin | Simulation | %Change in Median from NAT | %Change in Seasonal Amplitude from NAT | %Change in Peak flow from NAT | %Change in Low flow from NAT |
|---|---|---|---|---|---|
| Amazon | ALL_E | -0.2% | -1.1% | -0.3% | 2.4% |
| | ALL_EP | -0.4% | -1.6% | -0.4% | 3.4% |
| Madeira | ALL_E | -1.0% | -1.6% | -0.4% | 8.9% |
| | ALL_EP | -1.4% | -2.5% | -0.5% | 14.1% |
| Negro | ALL_E | 0.1% | 0.1% | -0.1% | -0.5% |
| | ALL_EP | 0.1% | -0.4% | -0.1% | 0.6% |
| Solimoes | ALL_E | -0.1% | 0.0% | 0.0% | 0.0% |
| | ALL_EP | -0.1% | 0.0% | 0.0% | 0.1% |
| Tapajos | ALL_E | 0.0% | -1.5% | -0.6% | 25.5% |
| | ALL_EP | -1.7% | -3.3% | -1.1% | 61.0% |
| Tocantins | ALL_E | 30.0% | -10.2% | -7.6% | 106.6% |
| | ALL_EP | 37.4% | -11.8% | -8.3% | 149.0% |
| Xingu | ALL_E | -0.7% | -1.0% | 0.0% | 39.3% |
| | ALL_EP | -0.6% | -1.0% | 0.0% | 39.4% |

*NAT – Natural simulation setup.

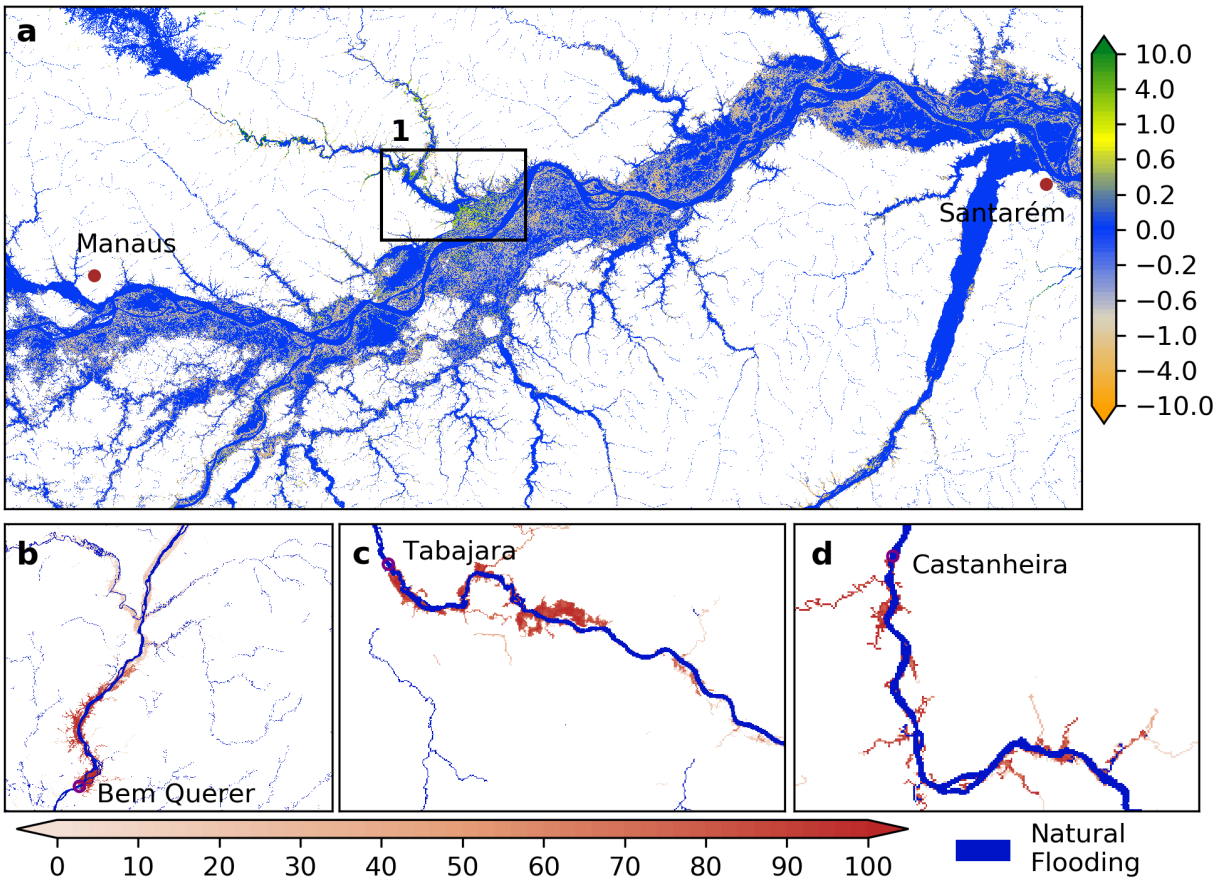


***Figure 3-8. Comparison of simulated flood occurrence from ALL_EP and NAT simulations.*** *a, Difference between the 39-year flood occurrence (%, ~90m spatial resolution) obtained from ALL_EP and NAT simulations. b, c, d, Additional inundation caused by the planned dams included in the Brazil's 10-year energy expansion plan(Ministry of mines and energy, 2019) expressed as flood occurrence (%, ~90m spatial resolution) from ALL_EP simulation. Brown filled markers indicate major cities. Purple circles indicate planned dam location.*

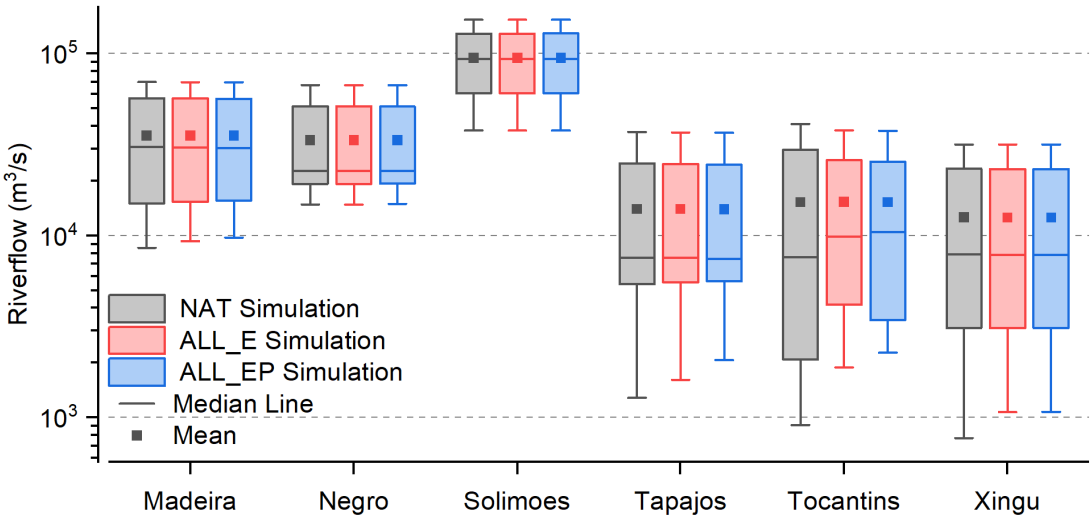


***Figure 3-9. River flow alterations caused by existing and planned dams.*** *Box plot of the simulated daily climatological (1981-2019 average) river flow at the mouth of the major Amazonian sub-basins.*

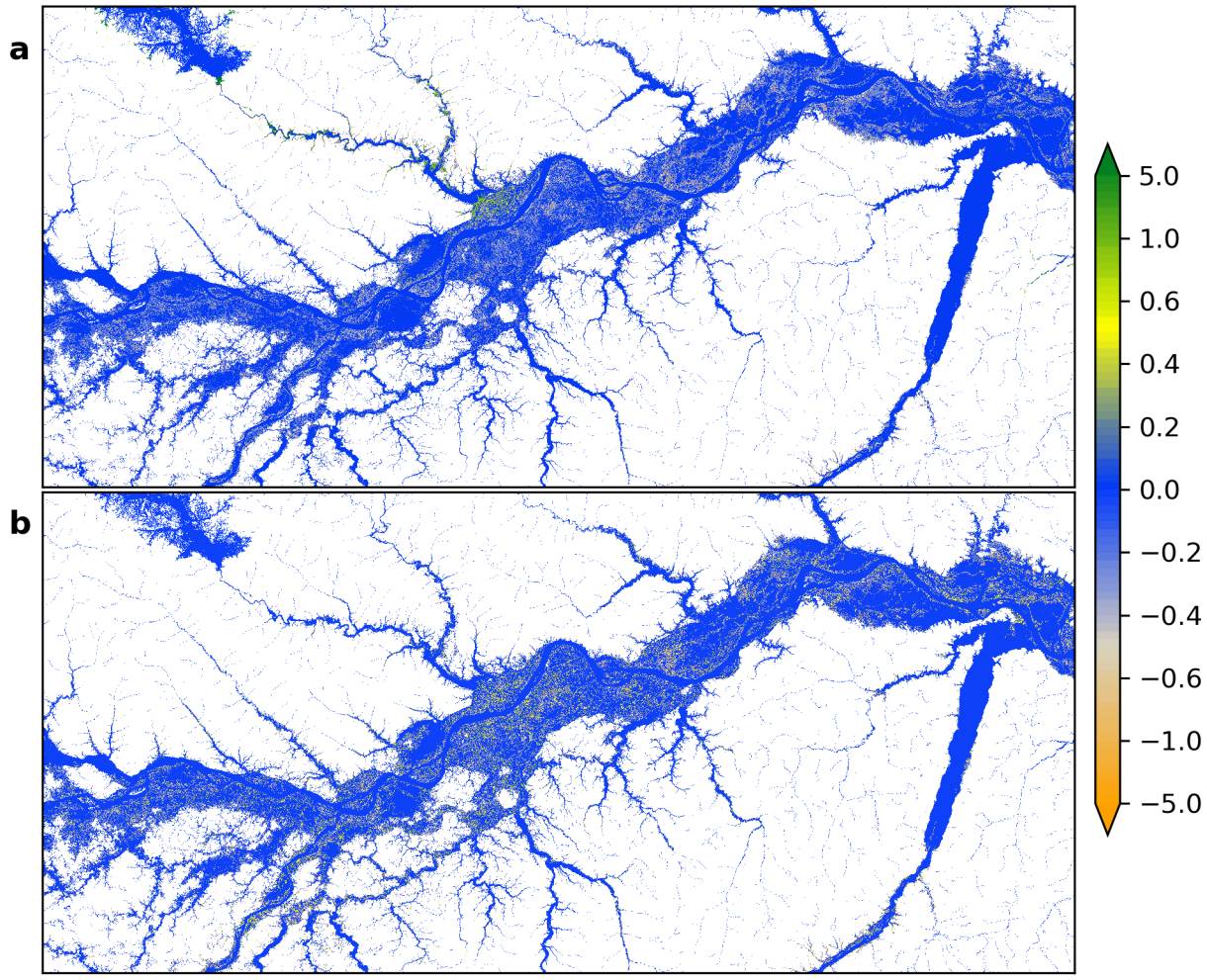


***Figure 3-10. Comparison of simulated flood occurrence from NAT, ALL_E, and ALL_EP simulations.*** ***a****, Difference between the 39-year flood occurrence (%, 3 arcsec or ~90m spatial resolution) obtained from ALL_E and NAT simulations.* ***b****, Difference between the 39-year flood occurrence (%, 3 arcsec or ~90m spatial resolution) obtained from ALL_EP and ALL_E simulations.*

## 3.4. Discussion

Our results suggest that the collective impact from the operation of existing and planned dams in the Amazon could be substantial, causing a pronounced alteration of the hydrological dynamics not only in the sub-basins but also in the mainstem of the Amazon River. Sub-basin wise analysis indicates that the impact from the existing dams and the potential impact from the collective operation of existing and planned dams will be most prominent in the Tocantins River basin. Historical alterations induced by the existing dams are found to be marginal in other Amazonian sub-basins, such as the Madeira, Tapajos, Solimoes and Xingu, due to the relatively smaller number of operational dams compared to the large annual river flow volume in these river basins. However, the cumulative impact from existing and planned dams in these sub-basins could be equally prominent as that in the Tocantins River basin.

Several large dams, such as Tucurui, Estreito and Serra da Mesa, are operational in the Tocantins River basin for more than three decades. The impacts from these dams on the downstream river flow are massive and have caused alterations to river flow by orders of magnitude. These impacts, further extend well beyond the direct alterations to the river including the population resettlement, loss of fertile land and deforestation. Moreover, evidence shows that these existing dams have also altered the river ecology with respect to reduction of fish population and alterations to the sediment movement (Moran et al., 2018). The newly operational dams in the Madeira and Xingu River basins have already incurred substantial environmental impacts concerning upstream inundation (Cochrane et al., 2017), sediment dredging (Fearnside, 2014), biodiversity loss (Ritter et al., 2017; Tófoli et al., 2017), and others, hence dwarfing their original impact assessment quantifications with a considerable margin. As of now, the impact of dams in the Amazonian sub-basins such as Madeira, Negro, Tapajos, and Xingu, are not as severe as that

in Tocantins. However, with the collective operation of the existing and planned dams—if constructed—these sub-basins are also expected to experience dramatic hydrologic alterations following the similar footprints of the Tocantins.

With the ongoing deforestation and potential reduction in power generation (Moran et al., 2018) from the existing dams due to climate change and variability, the reliability of these dams in the future is increasingly questioned. Following these concerns, alternative technologies for hydropower generation such as in-stream turbines (Chaudhari et al., 2021), as well as alternative renewable energy sources such as wind (Veers et al., 2019) and solar (Waldman et al., 2019) are gaining considerable traction in the last decade. However, hydropower is expected to remain the major source of base renewable energy in the near future as the diversification of the energy sector with the combination of wind, solar, hydro and biomass is estimated to be couple decades away (Santos et al., 2017). Hence, moving forward, a sustainable transformation of hydropower is urgently needed that follows environmentally less invasive energy generation techniques, in order to keep hydropower a part of the sustainable future.

Our assessment is based on the best datasets currently available, combined with a state-of-the-art, extensively validated hydrodynamic model and dam operation scheme. However, the results should be interpreted with caution as there are certain limitations to our approach. First, it is expected that the impact estimates in this study would differ, as our approach assumes a generic dam operation scheme which optimizes energy generation based on the simulated dam storage and long-term (39-year) historical averaged river flows (see Methods). Second, since the reservoir bathymetry is parameterized from the digital elevation model (DEM), discrepancy between the simulated spatial patterns is evident especially in the reservoirs that existed before the time DEM was derived. Additionally, the spatial inundation patterns of reservoirs formed

from large diversions, such as the Belo Monte reservoir, differ from the observed patterns. Since, the actual diversion channel characteristics at such sites are not publicly available, implementing flow diversions in the model environment becomes difficult, leading to discrepancies in geolocation of reservoirs in the model. Yet, the model realistically simulates the dam effect on the downstream as its operation depends on the controlled reservoir release.

### 3.5. Conclusion

In this chapter, we investigate the changes in the river flow and fine scale (~90m, downscaled from ~5km CMFD model output) inundation dynamics caused by individual and cumulative operation of the existing and planned dams. We find that dam operations have been consistently altering the river flow in the Amazonian sub-basins even in the absence of climate change. Further, results indicate that the potential impact of the collective operation of existing and planned dams could be considerably larger than the alterations caused by the existing dam operation.

Despite some inevitable uncertainties, this study provides major advances and insights on the understanding of the integrated river-floodplain-reservoir dynamics in a flood and hydropower dominant river system, such as the Amazon. This study is the first to simulate and mechanistically quantify the impacts of existing dams and the potential impact from the collective operation of existing and planned dams on a basin-wide scale in the Amazon. Given the on-going hydropower boom in the Amazon and other regions worldwide (for example, the Mekong and Congo River basins), this assessment could prove beneficial in investigating the future of hydropower in these regions. Further, our framework could be useful for future studies on the optimization of dam operation to reduce downstream dam impacts, globally.

# Chapter 4. Hydrological future of the dammed Amazon under climate change

*Based on:* **S. Chaudhari** and Y. Pokhrel, 2021. Hydrological future of the dammed Amazon under climate change. ***Earth's Future*** (*Manuscript in preparation*).

## 4.1. Introduction

Expansion of renewable energy resources is gaining traction and becoming important in the global energy mix. With the fastest year-on-year growth since the 1970s, renewables are on track to set new records in 2021, with an expected surge of more than 8% in the electricity generation (IEA, 2021). This expanding generation from renewables is expected to provide just over half of the increase in electricity supply in 2021. Hydropower being the largest source of global renewable energy and electricity, along with its predicted upsurge from a combination of economic recovery and new capacity additions from large projects, it is expected to remain a prominent source of renewable energy in the foreseeable future.

Since hydropower reservoirs can be used to store energy in the form of potential energy and convert it when required, the increase in hydropower capacity can, at the same time, support the expansion of other renewable energy technologies (Chaudhari et al., 2021; Schmidt et al., 2016; Waldman et al., 2019) when installed in combination with hydropower. Hence, hydropower increases the security of energy supply in an integrated electricity market in which solar and wind technologies are being expanded (Berga, 2016). In addition, hydropower plants are often not only used to generate electricity, but impounded reservoirs serve the human population as recreational areas, flood protection, for aquaculture, drinking water or for irrigation purposes (Berga, 2016). Hence, the expansion of hydropower is considered a potential solution to multiple challenges.

The re-emergence of large dams could bring large energy, economic and climate change mitigation incentives especially to the developing economies which house the major tropical river basins such as the Amazon River basin. Increased demand for electric energy in South America has led to ambitious plans for building as many as 282 new hydroelectric dams in the Amazon River Basin, in addition to the 238 currently operational dams as reported in the Agência Nacional de Energia Elétrica (ANEEL) database (http://www.aneel.gov.br/). These plans include the construction of as many as 102 dams with capacities larger than 30 MW, categorized as large dams by the Brazilian government, in the western Amazon during the next two decades. However, these will come at the expense of altering the natural flow regime of these tropical rivers which are responsible for biodiversity, ecological and agricultural productivity, as well as the cultural value of the local communities residing on their banks and extensive floodplains. While dams provide direct economic benefits by contributing to water security (Rodell et al., 2018), flood protection (Boulange et al., 2021), and renewable energy (Gernaat et al., 2021), they affect freshwater ecosystems by upstream inundation, downstream hydrologic alteration (Timpe and Kaplan, 2017), river fragmentation (Anderson et al., 2018), and impediments to fish migration (Moran et al., 2018; Stone, 2016) and sediment flow (Latrubesse et al., 2017). For example, under future dam development scenarios the river network connectivity from Andes to Amazon is expected to suffer >50% losses (Anderson et al., 2018), which can directly translate to drastic alteration to downstream river channel and floodplain geomorphology and associated ecosystem along the mainstem of the Amazon. The seasonal flood-pulse of the Amazon River, created by the dynamic interplay between floodplain topography and river flood cycle (Castello et al., 2015; Forsberg et al., 2017), plays a fundamental role in maintaining the diversity and productivity of lowland floodplain

environments (Forsberg et al., 2017; Resende et al., 2019). The operational norm of the planned hydropower dams in the Amazon can have a large impact on the flood-pulse below the dam, reducing maximum stage heights and flooded areas, increasing minimum stage heights and flooded areas and altering the spatial pattern of inundation across the floodplain, which remains largely unexplored.

Climate change is also of particular concern in the Amazon River basin due to the sensitivity of the snow accumulation processes that dominate runoff generation within the basin, and the basin's high-water demand to maintain its ecological productivity (Christensen et al., 2004). General Circulation Models (GCMs) of the atmosphere predict increases in mean annual air temperature between 1.2-3.5$^{o}$C over the next century across the Amazon River basin (Gudmundsson et al., 2021; Pokhrel et al., 2021; Prudhomme et al., 2014; Wanders et al., 2015). Further, the terrestrial water storage of the Amazon River basin is projected to experience a decline across all seasons, which may translate into more frequent and extended drought conditions in the basin (Pokhrel et al., 2021).

Several recent attempts have been made to evaluate the potential impacts of hydropower development on the Amazon (Arias et al., 2020; Barbarossa et al., 2020; Castello and Macedo, 2016; Forsberg et al., 2017; Latrubesse et al., 2017; Syvitski et al., 2009; Winemiller et al., 2016; Zarfl et al., 2019). These analyses have focused on aquatic and terrestrial biodiversity (Barbarossa et al., 2020; Winemiller et al., 2016; Zarfl et al., 2019), sediment dynamics (Latrubesse et al., 2017; Syvitski et al., 2009) or integrated multiple impacts (Castello and Macedo, 2016). All of the aforementioned studies have generally been qualitative analyses, with the exception of Latrubesse et al., (2017), which devised spatial indices to evaluate vulnerability of the Amazonian sub-basins to hydropower development, however, the exact nature and

magnitude of the dam impacts were not examined. Several efforts have quantified trade-offs among hydropower generation, hydrological alterations, and ecosystem services in the Amazon River basin at local to regional scales (Anderson et al., 2018; Finer and Jenkins, 2012; Strand et al., 2018), making it possible to identify regions and particular locations where improvements could be made to increase the overall sustainability of hydropower projects. However, a holistic view of the entire Amazon River basin under the influence of climate change, based on mechanistic and process-based models that include reservoir operation, is largely missing.

In this study, we focus on future changes to the hydrology of the Amazon River basin under existing and planned dam operations and climate change. For the first time, we apply an improved version of a recently developed, integrated river-floodplain-reservoir hydrodynamics model, the CaMa-Flood-Dam and runoff estimated by five terrestrial hydrology models driven by forcing data derived from four general circulation models (GCM) output. This methodology allows us to simulate and quantify the potential hydrological changes due to the operation of existing and planned dams, and climate change in the Amazon River basin and its sub-basins. Specifically, we discuss the relative contribution of uncertainties from GCMs and LSMs in future projections of river flow, with a special focus on the more vulnerable southern Amazon catchments. Further, the future implications of the on-going hydropower development combined with climate change on the downstream flood dynamics along the Amazon mainstem are also discussed. With the perspective of sustainable hydropower development, we additionally examine the potential reliability of the existing and planned hydropower dams to generate energy under future climate change scenarios.

## 4.2. Model, Data and Methods

### 4.2.1. Input Runoff Forcing Datasets

The climate of the Amazon Basin is notoriously difficult to model, hence introducing multiple levels of uncertainty in its simulations. First, there is wide variation between GCMs in the estimated precipitation and its changes (Boisier et al., 2015). Similarly, several LSMs exist, and to a greater extent, they all incorporate existing process knowledge into their parameterizations (Gash et al., 2004; Keller et al., 2009). However, because of their different structures and the values of the parameters used, LSMs also simulate a range of changes in the water and energy balances even when forced by the same input climate data. The differences between models' results relate in a complex way to simulated vegetation structure, phenology and physiology as well as to soil hydrological processes, hence introducing another level of uncertainty in the hydrological estimates. Moreover, additional uncertainty stems from the land use land cover (LULC) change scenarios used in the models.

***Table 4-1. Multi-model ensemble simulation summary.***

| **Radiative Forcing →** | | **Historical** | **RCP 2.6** | **RCP 6.0** |
|---|---|---|---|---|
| Period → | | 1981-2005 | 2006-2099 | |
| Hydrological Models ↓ | Socio-economic scenarios → | histsoc | 2005soc | 2005soc |
| CLM4.5 | | GFDL-ESM2M, HADGEM2-ES, IPSL-CM5A-LR, MIROC5 | | |
| H08 | | | | |
| LPJ-mL | | | | |
| PCR-GLOBWB | | | | |
| WaterGAP2 | | | | |

To overcome these uncertainties to a certain extent, we implement multi-model hydrological simulations (20 ensemble members) from five terrestrial hydrology models (LSMs and GHMs) driven by atmospheric forcing from four GCMs (models participating in the Coupled Model Intercomparison Project Phase 5; CMIP5). Three cases of radiative forcing are considered for each GCM: historical climate (HIST), and low (Representative Concentration Pathway (RCP) 2.6) and medium– high (RCP6.0) emission scenarios available from the Inter-Sectoral Impact Model Intercomparison Project (ISIMIP2b) (Frieler et al., 2017; Warszawski et al., 2014). We use output from 20 ensemble members for the surface runoff (qtot; kg m−2 s−1) for the historical period (1981–2005), mid-21$^{st}$ century (2030-2059) and late-21$^{st}$ century (2070-2099) at a daily interval and spatial resolution of 0.5$^{o}$ × 0.5$^{o}$ (~50km × 50km).

### 4.2.2. CaMa-Flood-Dam Model and Simulation Setup

CaMa-Flood-Dam (CMFD) is a new generation, recently improved global river routing model that simulates floodplain dynamics and backwater effects by explicitly solving the local inertia equation (Shin et al., 2020; Yamazaki et al., 2013). The model was reported to outperform other GHMs for reproducing historical discharge (F. Zhao et al., 2017) and was further found to well simulate the hydrological changes due to dam operations, historically (Shin et al., 2020) and in the future (Boulange et al., 2021). The CMFD model requires only daily runoff as an input, and by computing the inflow from upstream cells and outflow to downstream, the evolution of water storage can be predicted. CMFD model has also been extensively used in multiple tropical basins (Getirana et al., 2012; Shin et al., 2020; Yamazaki et al., 2012b, 2011) and globally (Boulange et al., 2021; Pokhrel et al., 2018b; Yamazaki et al., 2013; F. Zhao et al., 2017), and validated. It is capable of faithfully reproducing historical flood patterns and daily measurements at river

gauging stations across the globe (F. Zhao et al., 2017), partly owing to the integration of satellite- based topography data (Yamazaki et al., 2012a).

In this study, the CMFD model is setup for the entire ARB and is driven by daily runoff obtained from 20 ensemble members described in Section 4.2.1. The spatial resolution of the CMFD model is set to 3-arcmin (5 km), with its output such as flood depth, further downscaled to 3-arcsec (~90 m) resolution using high-resolution digital elevation model (DEM). All model parameters are identical to those used in Yamazaki et al., (2011). Dams are accurately located on the model grids and the reservoir operation for each dam is optimized similar to our previous study as described in Section 3.2.2. With each ensemble member's runoff forcing, we conduct seven simulations as described in Table 4-2.

***Table 4-2. Simulation Setup.***

| Simulation | Period | Description |
|---|---|---|
| Hist-Nat | 1981-2005 | Historical simulation with no dams |
| Hist-DamBCY | 1981-2005 | Historical simulation with dams introduced as per their commission year |
| RCP2.6-DamBCY | 2006-2020 | Historical simulation with dams introduced as per their commission year with RCP2.6 runoff forcing; used only for extended period validation |
| RCP2.6-Nat | 2021-2099 | Future simulation with no dams and RCP2.6 runoff forcing |
| RCP2.6-Dam | 2021-2099 | Future simulation with dams all introduced in 2021 and RCP2.6 runoff forcing |
| RCP6.0-Nat | 2021-2099 | Future simulation with no dams and RCP6.0 runoff forcing |
| RCP6.0-Dam | 2021-2099 | Future simulation with dams all introduced in 2021 and RCP6.0 runoff forcing |

### 4.2.3. Model Evaluation and Validation

We combine the model results from Hist-DamBCY (1981-2005) simulations with results from RCP2.6-DamYBY (2006–2020) to extend the model validation period. The river flow simulation results from each ensemble runoff forcing are validated against observations obtained from the Agência Nacional de Águas (ANA) in Brazil (http://hidroweb.ana.gov.br). We selected river flow gage stations located along the mainstems of the Amazon River and its major tributaries. The selected gage stations include at least 30 years of observational coverage with minimal data gaps; the days with missing data are skipped in the statistical analysis.

## 4.3. Results and Discussion

### 4.3.1. Validation of Simulated River Flow

The combined evaluation of river flow simulated by the CMFD model from each ensemble member's runoff forcing is shown in Figure 4-1. As the evaluation period (1981-2020) is not entirely covered by the Hist simulations, we combine the results from Hist-DamBCY (1981-2005) and the RCP2.6-DamYBY (2006–2020) for an in-depth comparison of observed and simulated river flows for the entire historical period. Most of the ensemble members indicate a high correlation (> 0.8) and a standard deviation ratio close to unity, hence indicating a good prediction performance overall for varying geographical locations and stream sizes over the Amazon. Low correlation is seen for the gaging stations located on high topographical gradients, especially for the forcing obtained from the GFDL-ESM2M model, which could be the direct result of the uncertainties arising from climate forcing (driven by GCMs). Further, these low correlations could also be a result of uncertainties from GHM/LSM parameterizations, and its variability is dependent on their respective runoff generation schemes. Evidently, some of the GCM-GHM/LSM combination exhibits a wet bias, resulting into a standard deviation ratio

higher than one. This wet bias in the simulated river flow is in alignment with the findings of previous studies (Chaudhari et al., 2019; Miguez-Macho and Fan, 2012a; Yamazaki et al., 2012b). However, the simulated river flow averaged over all ensembles indicate a good agreement with observation (Figure 4-2), indicating high confidence in the projections.

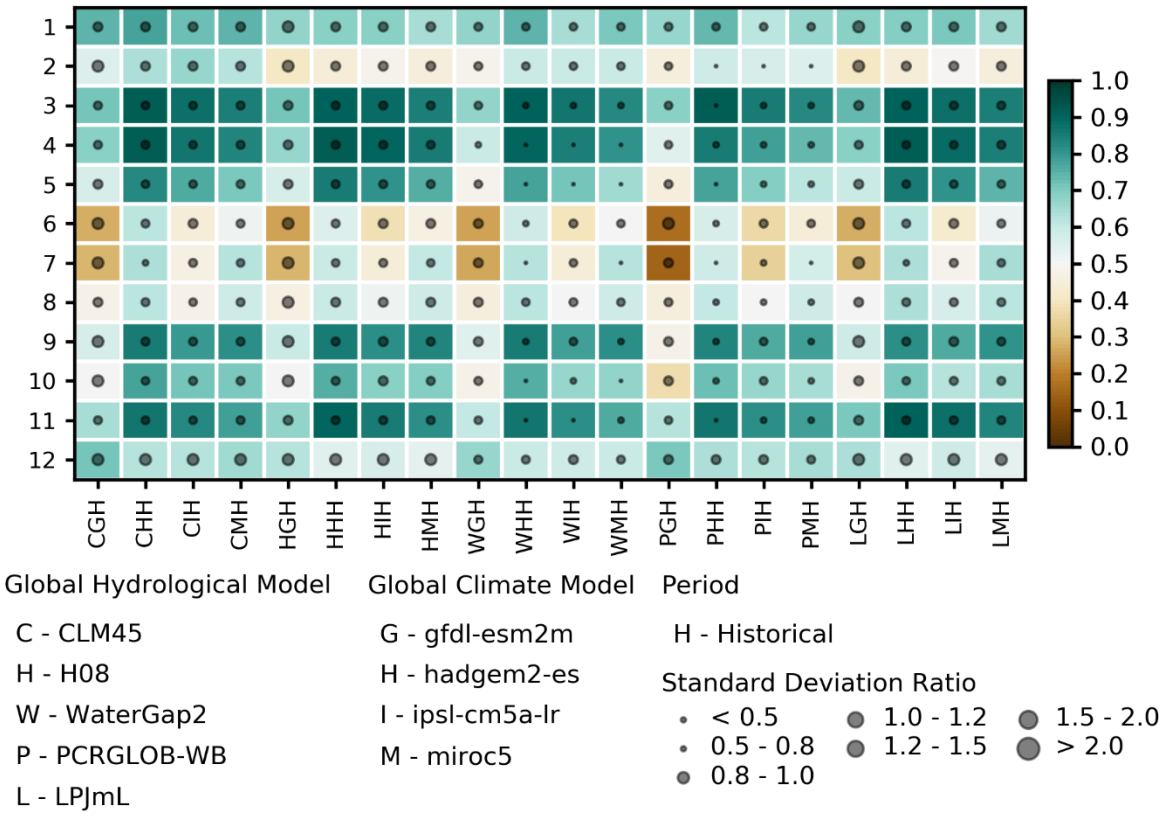


***Figure 4-1. Evaluation of simulated river flow.*** *Statistical comparison of river flow simulated by CMFD model forced by each ensemble member (Table 4-1) at 12 main gage stations (locations shown in Figure 2-2) for the 1981-2020 period. Results are combined from the Hist-DamBCY (1981-2005) simulations and the RCP2.6-DamYBY (2006–2020). Colors indicate the correlation and scatter points indicate the standard deviation ratio between the simulated and observed river flows.*

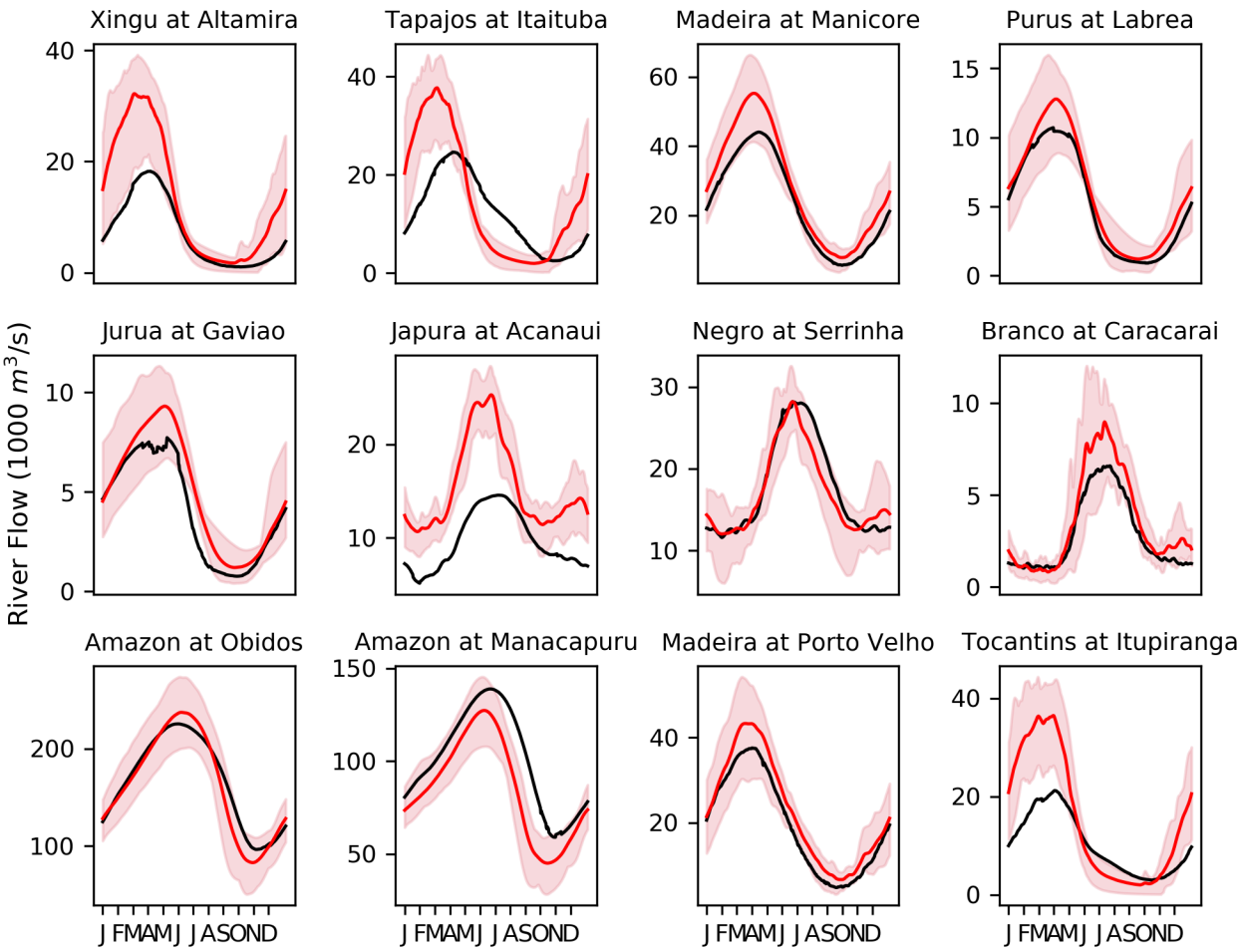


***Figure 4-2. Comparison of seasonal cycles of simulated and observed river flow.*** *Red line indicates the average simulated river flow and shaded region shows the distribution across all ensemble members. Black line indicates the observed river flow obtained from gage stations.*

### 4.3.2. Surface Runoff and River Flow in the Amazon under Climate Change

Figure 4-3 portrays the future changes in river flow during mid- (2030-2059) and late-21st century (2070-2099) with respect to the historical period (1981-2005) under the impacts of projected climate change based on RCP2.6 and RCP6.0 scenarios. Similar spatial map is shown for projected runoff used to drive the CMFD model (Figure 4-4) for the same periods, climate scenarios and ensembles. The projected changes in river flow under the effect of climate change solely, vary spatially among the Amazonian sub-basins. While south-western region of Amazon, containing the upstream areas of the Solimoes and Madeira rivers, is projected to experience a

decline in mean river flow, the northern and eastern regions could experience an increase in mean river flow. These changes in mean river flow are the direct translation of the corresponding projected change observed in surface runoff (Figure 4-4). As expected, the changes in mean river flow are more drastic and widespread in RCP6.0 compared to RCP2.6 in all regions, except for the Negro River basin. During mid-twenty-first century, the Negro River basin is projected to experience a major increase in mean river flow under RCP2.6, which further continues in the late-twenty-first century but with a lesser magnitude. Overall, we find a southwestern (dry)–northeastern (wet) contrast pattern in the mean river flow of the Amazon River basin.

On visualizing the simulated long-term averaged low flow ($Q_{95}$) in the Amazon as projected by the multi model ensembles, a substantial drying of the entire basin is found in both the mid- and late-twenty-first century, further implying that the regions with historical drying trends are expected to become even drier under climate change. Under both RCP2.6 and RCP6.0 the long-term averaged low flow is expected to experience ~20% decrease compared historical average with the latter being more drastic. This decline is especially greater in magnitude in the upper reaches of the Madeira, Solimoes and Negro rivers. The eastern sub-basins of the Amazon, such as the Tocantins, is also expected to experience a decline in the low flow, with a notable increase in magnitude at the end of the 21$^{st}$ century.

A contrasting wetting pattern is expected in the central and northern parts of the Amazon with notable increase in the long-term averaged low flow. However, this wetting pattern in mostly prominent in the mid-21$^{st}$ century and is expected to decrease in magnitude and spatial extent close to the end of the 21$^{st}$ century. Similarly, the increase in long-term average low flow in the northeastern smaller sub-basins of Amazon is expected to last only till the end of mid-21$^{st}$ century under RCP2.6, before following the basin-wide spatial pattern of decline in low flow.

On the contrary to the basin-wide decline in low flow, the Amazon is expected to encounter a rise in the long-term averaged peak flow under both RCP2.6 and RCP6.0. This rise in peak flow suggests a higher number of flood events in the future. There are few exceptions to this rising trend, such as the middle reaches of the Madeira River basin, where a decrease in peak is expected, especially in the late-21$^{st}$ century under RCP2.6. This decrease in peak flow in the Madeira River basin could be attributed to undergoing heavy LULC changes in the region. Under RCP6.0, the middle reaches of the Madeira River basin indicate a same trend, but with a smaller spatial extent.

Overall, with the decrease in low flow and increase in peak flow in the Amazon River basin, it is evident that the basin may experience a higher frequency of extreme events in the 21$^{st}$ century under both RCP2.6 and RCP6.0. With the considerable decrease in the long-term averaged low flow, a major part of the Amazon is expected to suffer from the lengthening dry-season, further prolonging the forest fire season, leading to an increase of fire counts during October and November. Moreover, the projections also indicate a strengthening of the monsoon seasonal cycle of the Amazon, resulting into higher number of flood events in many parts of the basin. These results agree with the current hydrologic trends (Chaudhari et al., 2019; Jiménez-Muñoz et al., 2016; Marengo and Espinoza, 2016; Zeng et al., 2008), and also corroborate the widely discussed drying and lengthening of the Amazonian dry season (Aragão et al., 2018; Boisier et al., 2015; Pokhrel et al., 2021; Wanders et al., 2015; Wanders and Wada, 2015), suggesting that the findings are robust and further contributing to the long-standing debate on the fate of the Amazon under climate change.

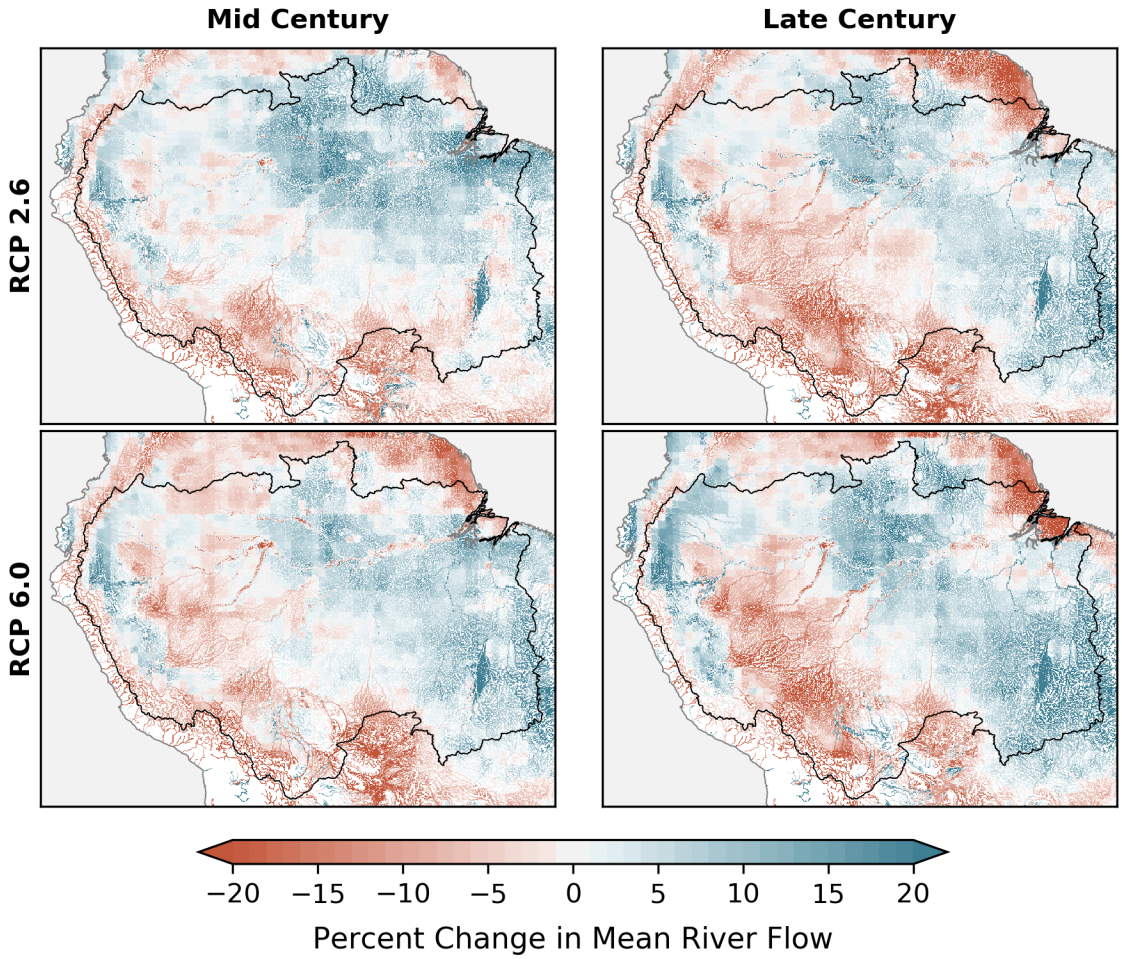


***Figure 4-3. Simulated change in mean river flow solely under climate change.*** *Results are shown as multi-model spatiotemporal averages for 30-year periods, namely mid (2030-2059) and late (2070-2099) 21st century.*

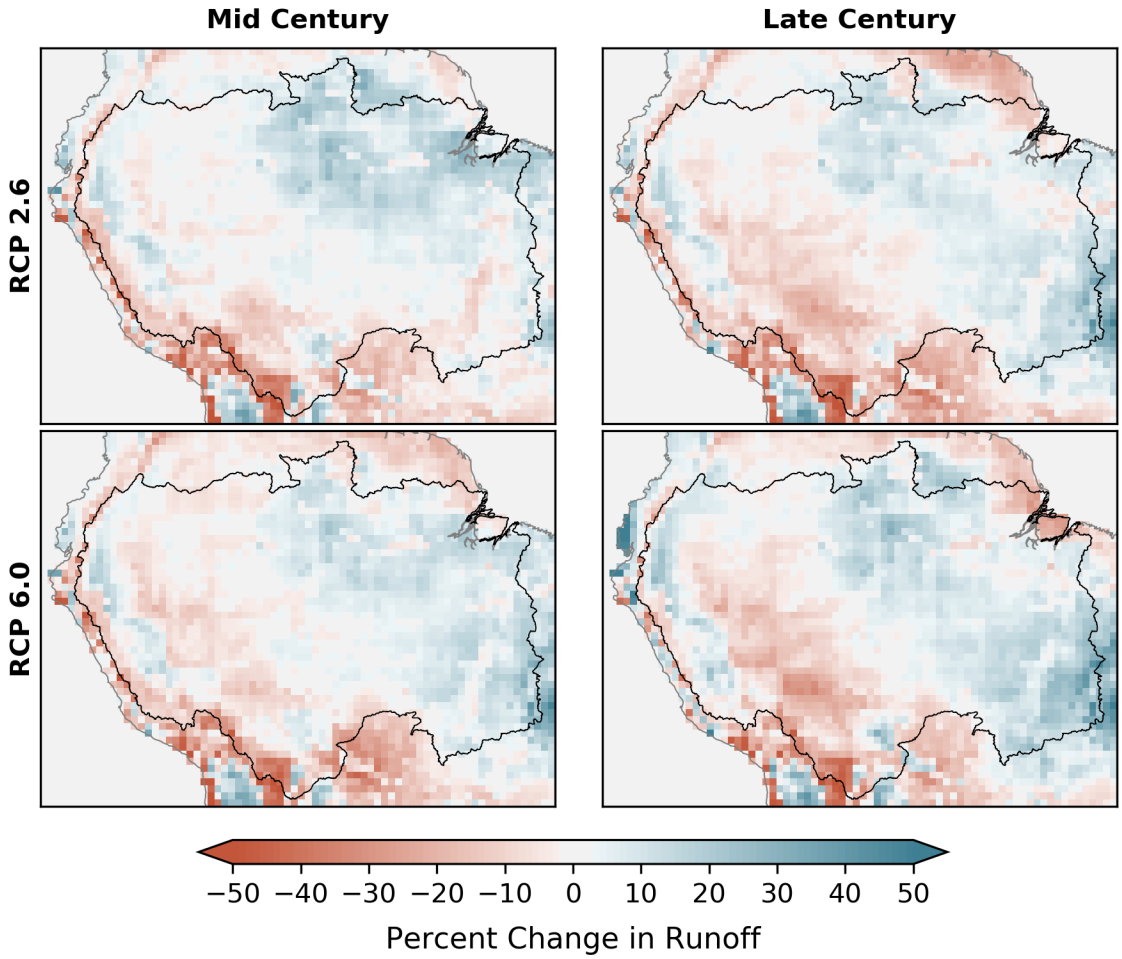


*Figure 4-4. Same as Figure 4-3 but for surface runoff averaged over all ensemble members.*

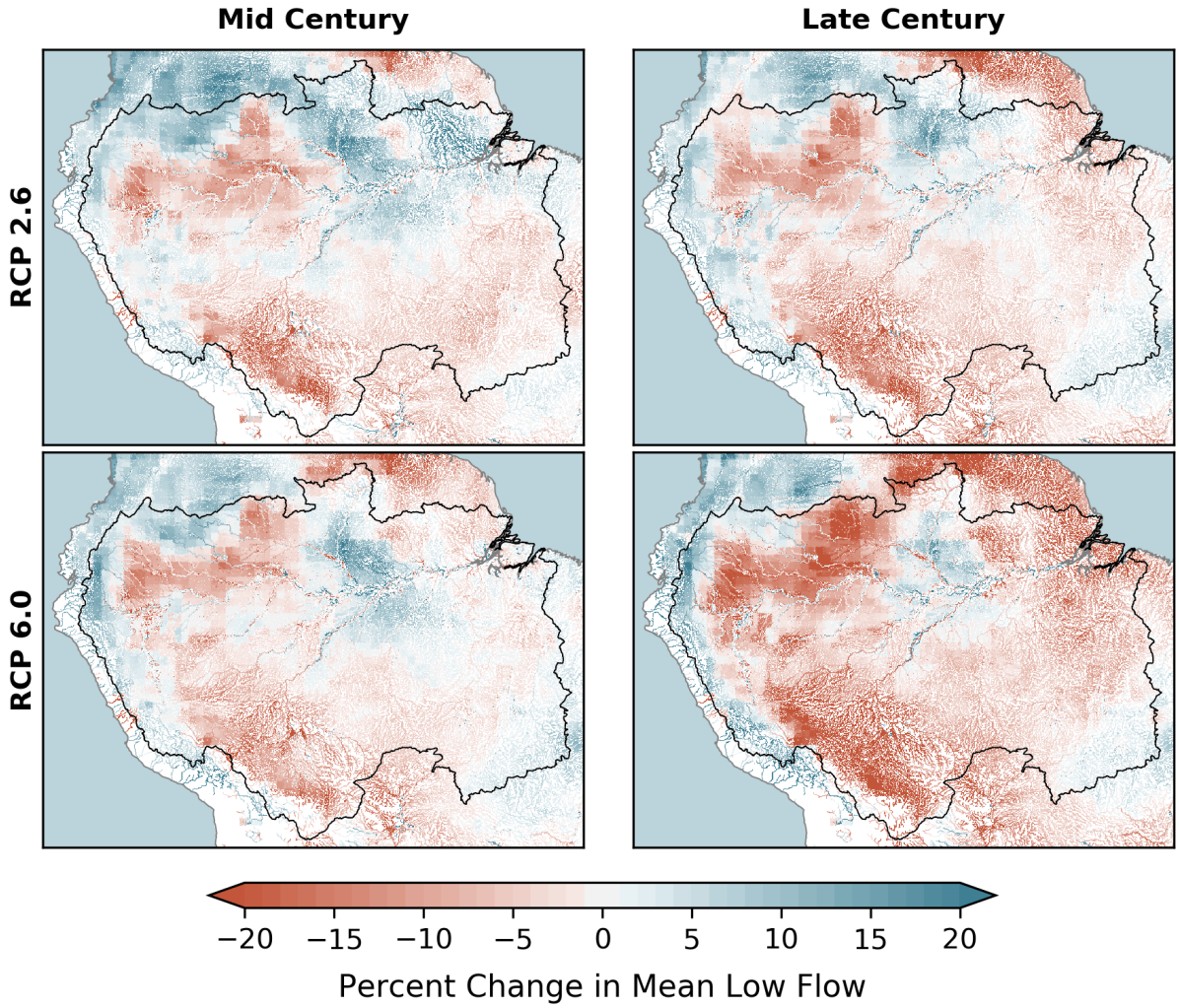


***Figure 4-5. Same as Figure 4-3 but for dry season flow ($Q_{95}$).***

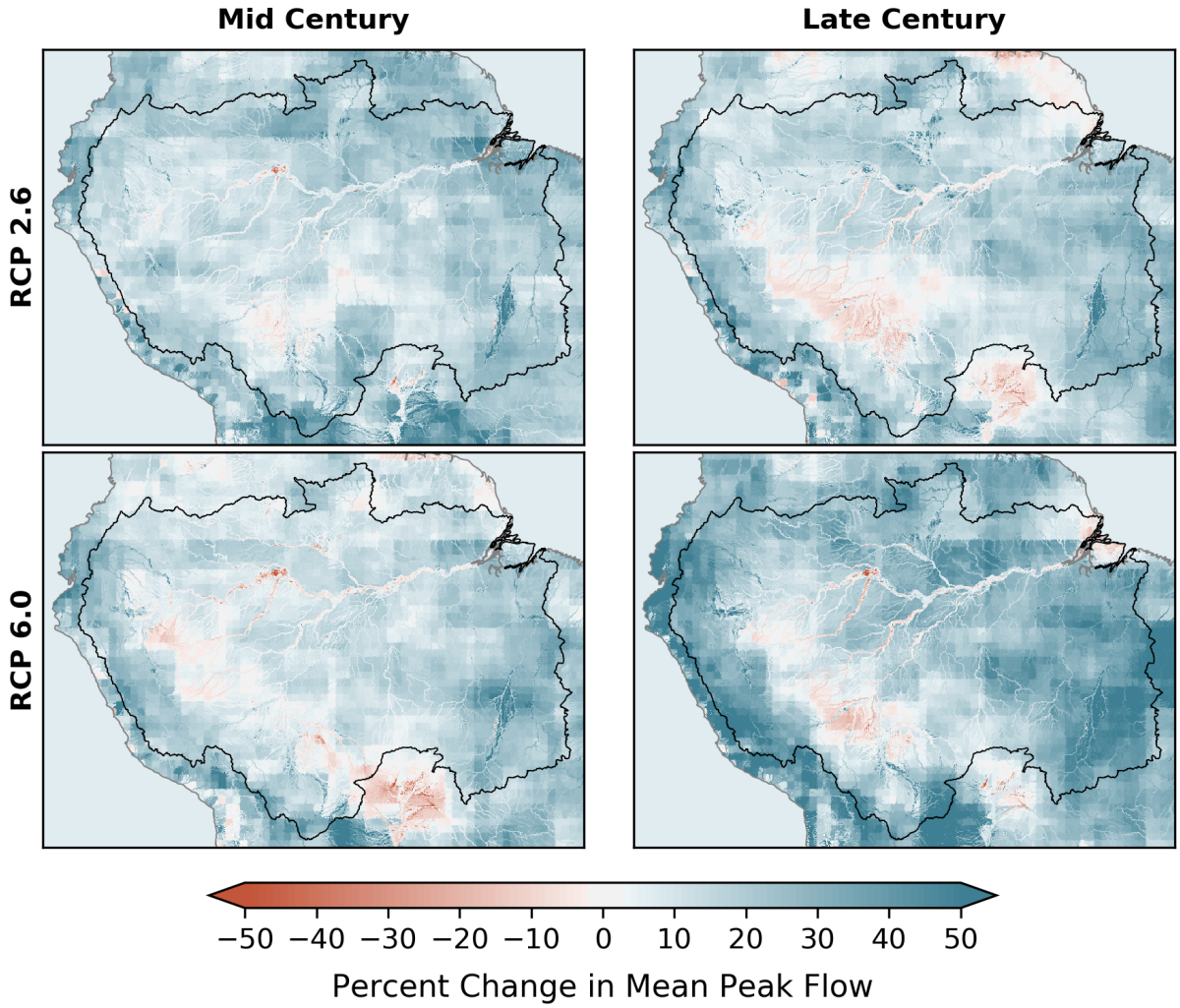


***Figure 4-6. Same as Figure 4-3 but for wet season flow ($Q_5$).***

### 4.3.3. Potential River Flow Alterations Caused by Dam Operations

We compare the river flow signatures obtained from Nat (without dams) and Dam (with dams) simulations to study the impact of dam operations on the river flow regime in the Amazon and its sub-basins (Figure 4-7). As expected, the cumulative operation of existing and planned dams in the Amazon, bring forth a noticeable dampening effect on the annual cycle of the river flow. In general, a decrease in peak flows and an increase in low flows are observed as a result of the reservoir's buffering capacity. The projected impacts vary slightly for different RCPs; however, the trend directions are similar. The Amazonian sub-basin with the largest potential impact from dam operations is found to be the Tocantins, followed by Xingu, Madeira, and Tapajos. In the Tocantins River basin, the cumulative impact from the operation of existing and planned dams is expected to cause a change of ~15.2% and 15.4% in the median of the daily river flow during the mid- and late-twenty-first century under RCP2.6. Correspondingly, a ~68% and ~78% increase in low flow and ~13% and ~9% decrease in peak flow are expected in the Tocantins River basin during the mid- and late-twenty-first century, respectively, under RCP2.6. Similar level of alterations to the river flow signatures are expected in the Maderia, Xingu and Tapajos River basins.

The alterations to river flow signatures in the Amazonian sub-basins under RCP6.0 follows an unanalogous pattern compared to the alterations under RCP2.6. For example, the alterations to the low flow in the Madeira, Tocantins and Xingu River basins are found be greater under RCP6.0 compared to that under RCP2.6; whereas the alterations to low flow in Negro and Tapajos River basin and along the Amazon mainstem follow an opposite trend, with higher magnitudes under RCP2.6.

Overall, the largest impact of dam operations in the Amazon is expectedly found on the dry season flows. Due to the buffering effect of the dam reservoir, a substantial increase in the river flow during the dry season in expected in the 21st century at the mouths of the major Amazonian tributaries. Wet season flows are expected to suffer comparatively less alterations, mainly due to the small cumulative storage capacity of the existing and planned dams with respect to the total flow volume generated during the Amazonian wet season.

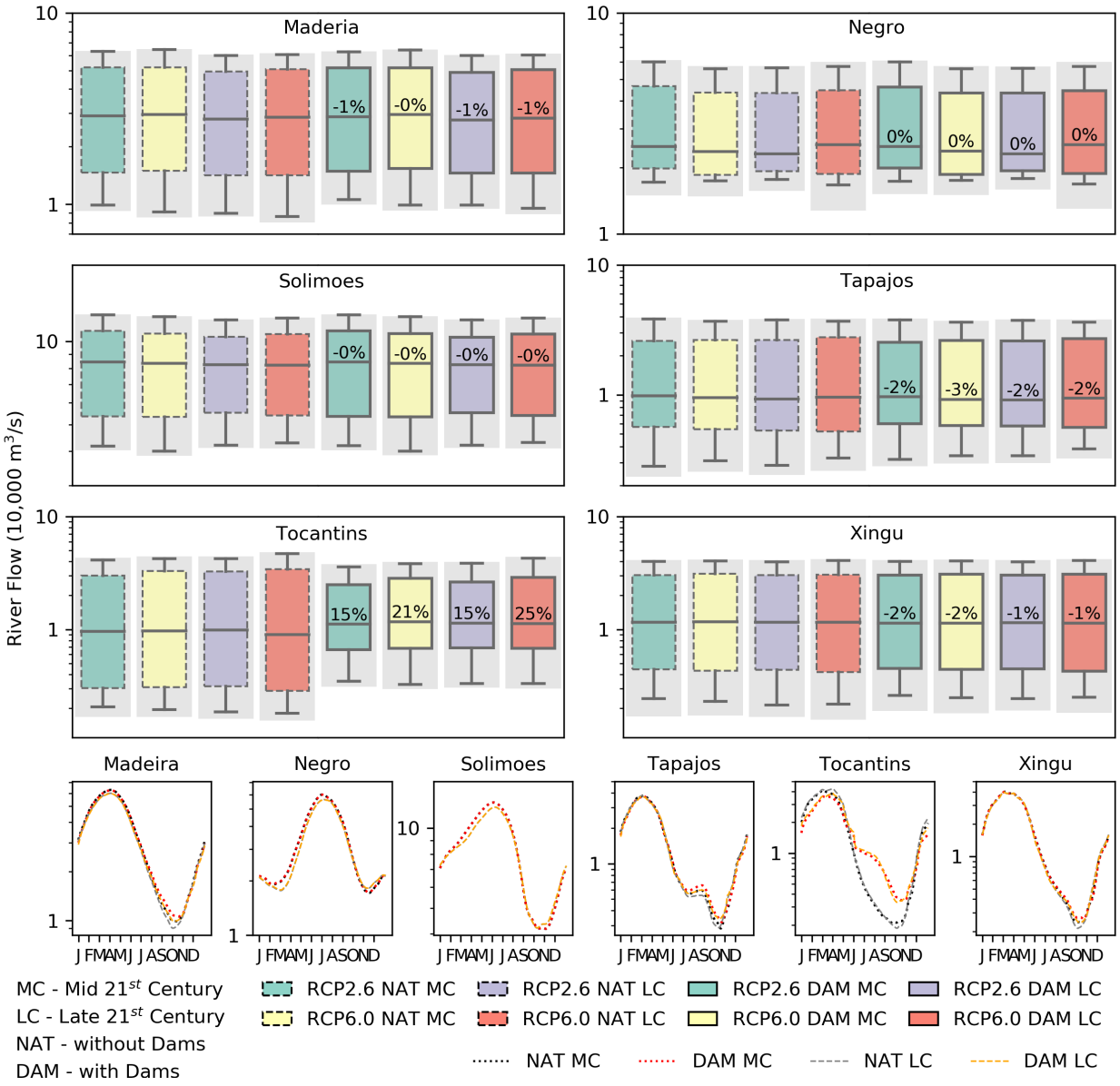


***Figure 4-7. Potential impact of dam operations on the river flow in the Amazon during the 21st century.*** *The box-and-whisker plots include the 95th and 5th range (whiskers), median (horizontal lines in each bar), and 1st and 3rd quartiles (box height) of the multi-model ensemble averaged daily climatological river flow for mid- and late-twenty-first century under RCP2.6 and RCP6.0. Percent values indicate the percent change in the median of the river flow between Nat and Dam simulations under respective RCP and period. Line plots indicate the climatological seasonal river flow at the mouth of the major Amazonian sub-basins obtained from RCP2.6-Nat and RCP2.6-Dam simulations.*

***Table 4-3. Alterations of the averaged river flow signatures from the RCP2.6-Dam simulation with respect to the RCP2.6-Nat simulation.***

| River Basin | Period | %Change in Median | %Change in Seasonal Amplitude | %Change in Peak flow | %Change in Low flow |
|---|---|---|---|---|---|
| Amazon | MC | 0.15 | -0.78 | -0.19 | 1.26 |
| | LC | 0.28 | -0.91 | -0.21 | 1.33 |
| Madeira | MC | -1.08 | -1.74 | -0.39 | 6.84 |
| | LC | -0.68 | -2.28 | -0.41 | 10.23 |
| Negro | MC | 0.32 | -0.69 | -0.27 | 0.78 |
| | LC | 0.38 | -0.83 | -0.32 | 0.79 |
| Solimoes | MC | -0.02 | -0.04 | 0.01 | 0.09 |
| | LC | -0.01 | -0.07 | -0.01 | 0.11 |
| Tapajos | MC | -2.21 | -2.24 | -1.13 | 12.84 |
| | LC | -1.71 | -2.84 | -1.26 | 18.02 |
| Tocantins | MC | 15.19 | -17.7 | -13.42 | 67.89 |
| | LC | 15.42 | -13.3 | -9.38 | 78.42 |
| Xingu | MC | -1.56 | -0.43 | 0.02 | 7.06 |
| | LC | -1.41 | -0.77 | 0.03 | 14.02 |

***Table 4-4. Alterations of the averaged river flow signatures from the RCP6.0-Dam simulation with respect to the RCP6.0-Nat simulation.***

| River Basin | Period | %Change in Median | %Change in Seasonal Amplitude | %Change in Peak flow | %Change in Low flow |
|---|---|---|---|---|---|
| Amazon | MC | 0.06 | -0.55 | -0.15 | 0.81 |
| | LC | -0.09 | -0.87 | -0.22 | 1.27 |
| Madeira | MC | -0.44 | -1.84 | -0.39 | 8.32 |
| | LC | -0.98 | -2.23 | -0.42 | 10.46 |
| Negro | MC | 0.35 | -0.69 | -0.31 | 0.54 |
| | LC | 0.33 | -0.75 | -0.33 | 0.67 |
| Solimoes | MC | -0.03 | -0.03 | 0.01 | 0.11 |
| | LC | -0.11 | -0.02 | 0.02 | 0.09 |
| Tapajos | MC | -3.40 | -2.26 | -1.26 | 9.21 |
| | LC | -1.66 | -3.24 | -1.39 | 17.49 |
| Tocantins | MC | 21.03 | -13.54 | -9.81 | 67.74 |
| | LC | 25.14 | -12.13 | -8.45 | 83.01 |
| Xingu | MC | -2.49 | -0.64 | -0.16 | 7.74 |
| | LC | -1.44 | -0.85 | -0.03 | 14.57 |

### 4.3.4. Implications of Dam Operations on the Amazon Mainstem

Figure 4-8 and Figure 4-9 presents the downscaled (~90m, 3 arcsec) 30-year flood occurrence along the main stem for both the mid- and late-21$^{st}$ century under RCP2.6 and RCP6.0, respectively. The change in flood occurrence due to dam operations is represented in terms of percent change with respect to the results from the natural simulation (RCP2.6- Nat and RCP6.0-Nat). Substantial alterations to the long-term flood occurrence along the Amazon mainstem due to the cumulative operation of existing and planned dams are expected in both the mid- and late-21$^{st}$ century. Several regions along the Amazon mainstem indicate >10% decrease in flood occurrence due to the direct influence from dam operations. As expected, downstream of a large

dam, Balbina (Box 1, Figure 4-8 and Figure 4-9), increased flood occurrence is found because of the dry season release from the reservoir. Moreover, results indicate that the shallow inundation extents along Amazon mainstem may greatly recede from mid- to late-21$^{st}$ century under the combined effect of climate change and dam operation (Box 2, Figure 4-8 and Figure 4-9).

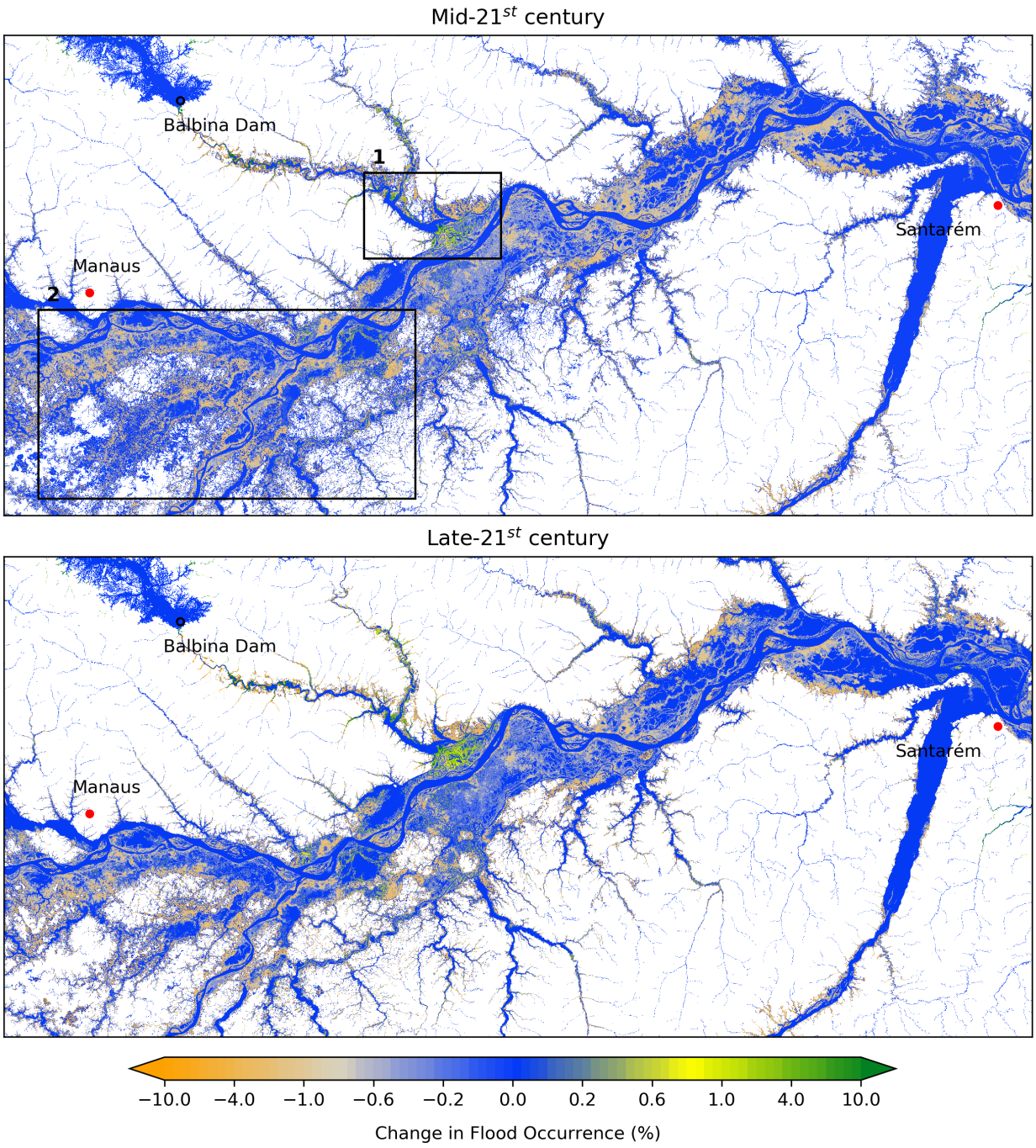


***Figure 4-8. Percent change in flood occurrence due to dam operations under RCP2.6.*** *Difference between the 30-year flood occurrence (%, 3 arcsec or ~90m spatial resolution) obtained from RCP2.6-Dam and RCP2.6-Nat simulations. Red markers indicate major city locations. Black markers indicate dam locations.*

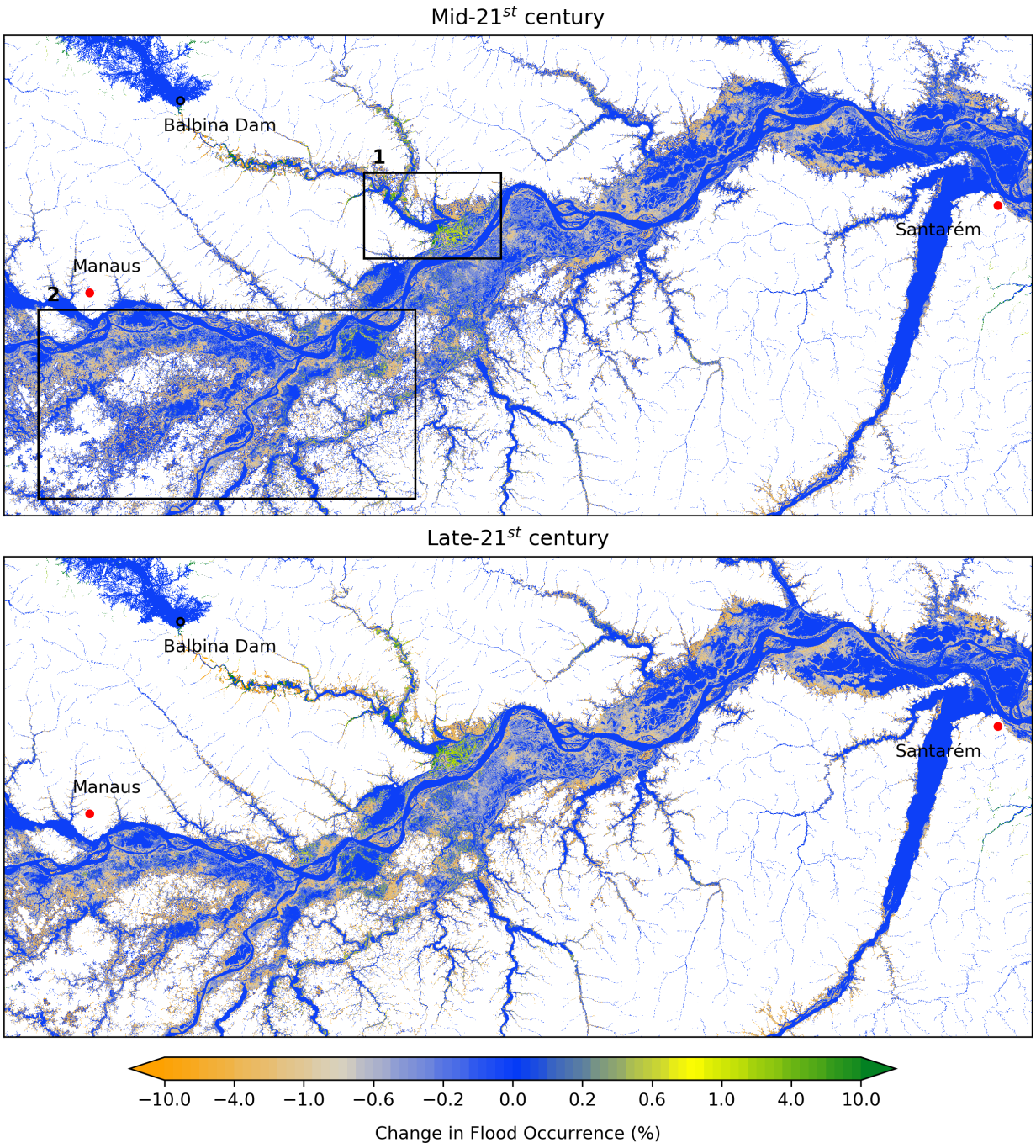


***Figure 4-9. Same as Figure 4-8 but for RCP6.0.***

## 4.4. Conclusion

In this chapter, the impacts of dam operations on the hydrological characteristics of the Amazon and its sub-basins are quantified by comparing a with- and without-Dam simulations conducted using a high-resolution hydrodynamic model, CaMa-Flood-Dam (CMFD). The CMFD is forced by multi-model ensemble data compiled from five global terrestrial hydrology models (i.e., CLM4.5, H08, LPJmL, PCR-GLOBWB, and WaterGAP2) with a climate forcing input from four GCMs (i.e., GFDL-ESM2, Had-GEM2-ES, IPSL-CM5-LR, and MIROC5) under three cases of radiative forcing: historical climate, the low (RCP2.6) and medium-high (RCP6.0) greenhouse gas concentration scenarios. Results under natural scenario (without dams) indicate a southwestern (dry)–northeastern (wet) contrast pattern in the mean river flow across the Amazon River basin. Further, the results indicate an intensification of extreme events in the Amazon, with the substantial drying of the entire basin suggesting a lengthening of the dry season and projected increase in the peak flow suggesting a strengthening of the monsoon seasonal cycle of the Amazon, during both the mid- and late-21$^{st}$ century. The cumulative impact from the operation of existing and planned dams, may bring forth a substantial dampening effect on the annual cycle of the river flow of the Amazon and its sub-basins. This dampening effect is found to have a substantial impact on the dry season flows with a pronounced alteration in the Tocantins, followed by Xingu, Madeira, and Tapajos River basin. Despite the inevitable uncertainties, this study is the first to simulate and mechanistically quantify the probable cumulative impacts of existing and planned dams on a basin-wide scale in the Amazon during the remaining 21$^{st}$ century under multiple climate change scenarios. As a greater number of large dams are being planned globally, the results from this study may prove beneficial for sustainable operation of the hydropower dams to reduce downstream dam impacts in the Amazon and globally.

# Chapter 5. In-stream turbines for rethinking hydropower development in the Amazon basin

*Based on*: **S. Chaudhari**, E. Brown, R. Quispe-Abad, E. F. Moran, N. Müller, Y. Pokhrel, 2021. In-stream turbines for rethinking hydropower development in the Amazon basin. ***Nature Sustainability***. DOI: https://doi.org/10.1038/s41893-021-00712-8

## 5.1. Introduction

Hydropower is by far the largest source of renewable energy and accounts for ~50% (International Renewable Energy Agency (IRENA), 2019b) and ~65% (International Renewable Energy Agency (IRENA), 2019a) of global renewable energy and electricity production, respectively. Given that hydropower is commonly considered as a benign source of energy and there is a predicted upsurge in the total hydropower contribution to the global energy mix (Gernaat et al., 2017; Moran et al., 2018), hydropower is expected to remain a promising source of energy for the foreseeable future (Moran et al., 2018; Pokhrel et al., 2018b, 2018a; Winemiller et al., 2016). However, there have been increasing concerns as to whether the energy benefits can outweigh the negative environmental impacts of storage reservoir-based hydropower projects (Moran et al., 2018). For far too long, hydropower has often been developed with a primary focus on energy generation, neglecting the social and environmental costs (Stone, 2016). Because the economic benefits are overestimated and the adverse effects are often overlooked or underestimated during the design and implementation processes, conventional hydropower technologies have been surrounded by controversies due to their adverse effects and long-term implications on environmental systems and social well-being (Fearnside and Pueyo, 2012; Stone, 2016; Winemiller et al., 2016). As the recognition of these adverse effects has grown, dam removal has been on the upward trend in recent years in the United States and Europe with aging

dams (O'Connor et al., 2015); concomitantly, hundreds of large and small dams are being built or planned in other global regions including the Amazon, Congo, and Mekong river basins (Winemiller et al., 2016).

Given these ongoing and planned hydropower development projects, appalling losses in biodiversity (Forsberg et al., 2017; Latrubesse et al., 2017; Moran et al., 2018; Timpe and Kaplan, 2017; Winemiller et al., 2016) and river connectivity (Anderson et al., 2018; Finer and Jenkins, 2012) are inevitable, when conventional hydropower technology is employed. Yet, dams continue to be built in exceptionally biodiverse sites (e.g., in the Amazon basin), setting records in biodiversity losses (Fearnside, 2014; Winemiller et al., 2016). Storage-based hydropower projects are known to dramatically alter basin hydrology with adverse, and often "characteristically irreversible" (Latrubesse et al., 2017) consequences on a range of ecological, environmental, agricultural, and socio-economic systems. Impediments to fish migration (Stone, 2016), alterations in freshwater discharge to oceans (Pokhrel et al., 2012b), reductions in sediment movement (Latrubesse et al., 2017) and nutrient transport (Eiriksdottir et al., 2017), river fragmentation (Anderson et al., 2018), disruption of flood pulse dynamics (Pokhrel et al., 2018b), and delta erosion (Yang et al., 2017), are some of the most palpable outcomes large dams have been associated with in many global river basins. Further, large-scale degradation of the environment by greenhouse gas emissions from reservoirs (Fearnside and Pueyo, 2012) has also become a growing concern, especially in tropical regions including the Amazon basin. There is evidence that even the run-of-the-river hydropower plants bring about profound changes in riverine habitat (Anderson et al., 2015) even though the impacts are less severe compared to that of large-reservoir dam projects.

Therefore, there is an urgent need to rethink hydropower technology to avoid the potentially catastrophic consequences of large dams. In storage-based hydropower generation systems, the flowing water is impounded to accumulate its potential energy and maximize power extraction in one location, which is then converted to kinetic energy; however, this approach has been found to be more environmentally disruptive than commonly reported (Anderson et al., 2018; Fearnside and Pueyo, 2012; Finer and Jenkins, 2012; Forsberg et al., 2017; Stone, 2016; Timpe and Kaplan, 2017; Winemiller et al., 2016). A more sustainable solution for generating power is the direct utilization of the kinetic nature of streams and river channels, avoiding water impoundment. Such kinetic energy can be harnessed by in-stream turbines that operate on fundamentally similar principles to that of wind turbines (VanZwieten et al., 2014) but under water. This leads to the question: is it feasible to use in-stream turbines to harness a significant portion of the power that is expected to be generated by building large dams? A large body of literature exists on the assessment of hydropower potential (Gernaat et al., 2017; Hoes et al., 2017; Pokhrel et al., 2008; Zhou et al., 2015), however, the aim of these studies has been to assess the potential that can be harnessed by using conventional technologies. In-stream turbine technology has been evolving in recent years (Bryden and Couch, 2006; Electrical Power Research Institute (EPRI), 2012; Karsten et al., 2013; Malki et al., 2014; Ortega-Achury et al., 2010; VanZwieten et al., 2014; Vennell et al., 2015); however, rather limited research has been conducted to assess the potential and feasibility of employing the technology over large regions such as the Amazon basin. The focus of the majority of the existing in-stream turbine related studies has been on the design of turbine arrays in tidal channels (Karsten et al., 2013; Malki et al., 2014; VanZwieten et al., 2014; Vennell et al., 2015); whereas studies with a focus on in-stream turbines in riverine environments are scarce, with some exceptions (Electrical Power

Research Institute (EPRI), 2012). Studies investigating kinetic energy extractions from tidal channels have shown that the safe extraction capacities for kinetic energy flux can be 10-20% of the total available energy without significantly altering the natural flow dynamics (Ortega-Achury et al., 2010; VanZwieten et al., 2014). Although, these studies represent tidal channels, it is reasonable to assume a similar principle for energy extraction in riverine environments with wide stream channels (Electrical Power Research Institute (EPRI), 2012) such as those in the Amazon.

Here, we estimate the Technical In-stream Potential (TIP) in the Amazon River basin which is a measure of the hydropower potential that can be extracted by employing in-stream turbines (see Methods). Our TIP assessment follows a novel approach that optimizes annual energy benefits by utilizing flow duration curves (Figure 5-2) derived from a high resolution (1 arc-minute; ~2km grid cell), physically-based continental-scale hydrological model, the LEAF-Hydro-Flood (LHF) (Chaudhari et al., 2019; Pokhrel et al., 2013). We consider multiple rows of in-stream turbines with constant spacing distinguished under two scenarios: 40D (where D is the turbine diameter), and 10D (see Methods). The 40D scenario is employed as a basin-wide sustainability criterion to analyze the in-stream potential in each grid cell, whereas the 10D scenario is employed for site-specific (e.g., planned dam locations) analysis. We also estimate the gross hydropower potential (GHP) using an approach similar to TIP referred to as the Integrated Gross Hydropower Potential at $Q_{30}$ ($IGHP_{30}$). We further evaluate the suitability for in-stream power generation within the Brazilian Amazon using a newly devised index referred here to as the In-stream Suitability Index (ISI) (see Methods). Finally, in-stream turbines are placed in an economical perspective with storage-based dams at the 11 largest planned dam sites in the

Amazonian lowlands (Figure 5-1) to show the additional merits of rethinking hydropower design for future development.

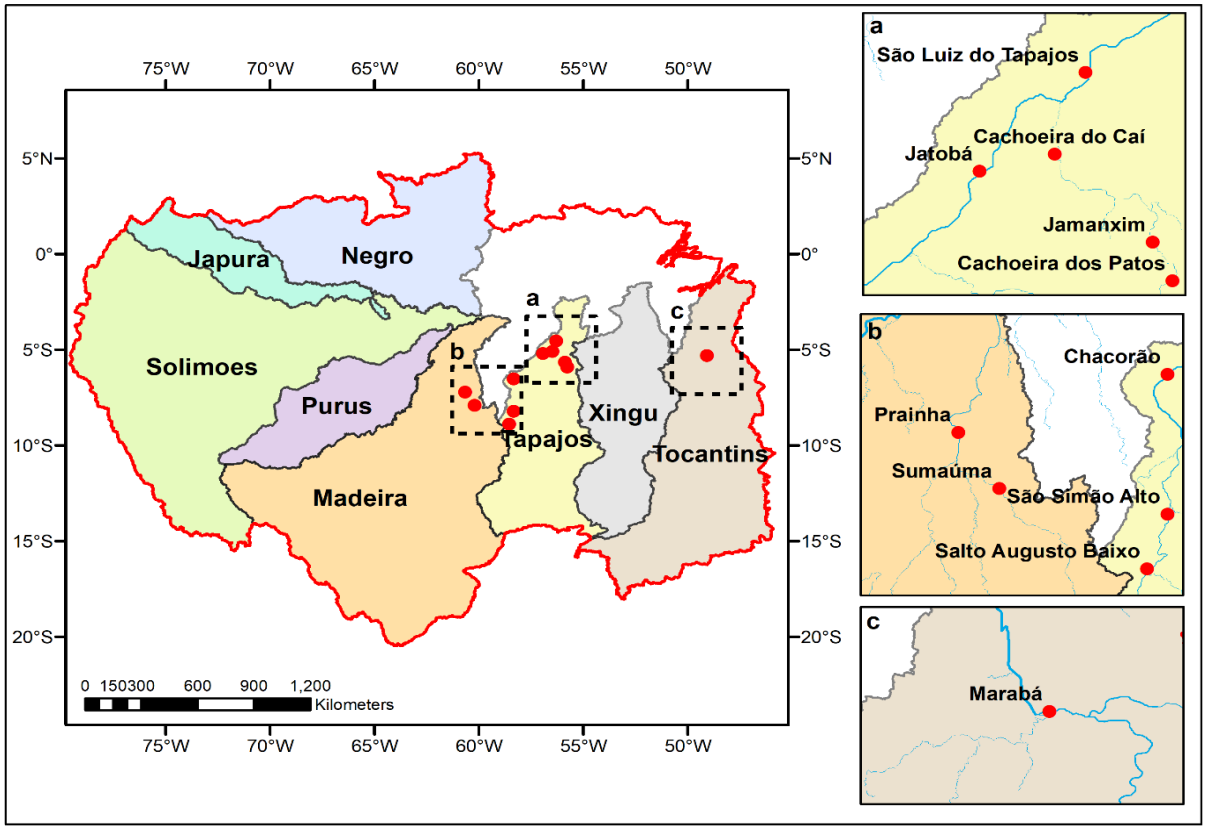


***Figure 5-1. Locations of 9 largest planned dams in the Brazilian Amazon.*** *Polygons indicate the extent of major sub-basins of the Amazon with identical color coding as in Figure 5-5 in the main text; note that the smaller sub-basins located in the northeast of the Amazon are excluded.*

## 5.2. Materials and Methods

### 5.2.1. Model and Data

High resolution (1 arc-minute; ~2km) climatological mean daily streamflow is simulated by the LEAF-Hydro-Flood model (Chaudhari et al., 2019; Miguez-Macho and Fan, 2012a), a physically-based continental-scale land hydrology model that resolves various land surface hydrologic and groundwater processes on a full physical basis. All simulation settings are identical to that used in our recent study (Chaudhari et al., 2019), Chapter 2). The annual flow duration curves (Figure 5-2) are generated from the 36-year (1980-2015) average streamflow simulated by LHF at 1 arcminute (~2km) grid cell. LHF model has been extensively used and validated over the Amazon in our previous studies (Chaudhari et al., 2019; Pokhrel et al., 2013) using a comprehensive set of ground- and satellite-based observations. For completeness, here we briefly revisit the validation of the simulated streamflow and terrestrial water storage (Figure 5-3). Streamflow estimates used in this study are without existing dam operations and could contain some uncertainties in the vicinity of existing dams because dams are known to alter the flow duration curve and the flow velocity in the channel. However, the impact of existing dams on streamflow in the majority of the Amazon is known to be minimal as the anthropogenic flow regulation is relatively small compared to the annual mean flow (Pokhrel et al., 2012a). Following our previous studies (Chaudhari et al., 2019; Pokhrel et al., 2014, 2013), river parameters (e.g., flow direction and river length within a grid cell) are obtained through up-scaling (Yamazaki et al., 2009) of the 15 arc-seconds flow direction data from HydroSHEDS (Lehner et al., 2008). The empirical relationship based on the drainage area is used to determine the channel width, following Coe et al. (Coe et al., 2008).

Information on the protected areas in the Amazon is obtained from the world database of protected area (WDPA; https://www.protectedplanet.net). Brazilian census data come from the Instituto Brasileiro de Geografia e Estatística (IBGE; https://www.ibge.gov.br), which are used to calculate the energy demand of municipalities by using the number of households without electricity available in the database.

Dam locations used in this study are compiled from four sources, (i) Global Georeferenced Database of Dams (GOOD) (Mulligan et al., 2009), (ii) Future Hydropower Reservoirs and Dams (FHReD) (Zarfl et al., 2015), (iii) Agência Nacional de Energia Elétrica (ANEEL; http://www.aneel.gov.br/) and (iv) State of World's Rivers dam database (International Rivers, n.d.). Detailed information about the dams such as dam height, reservoir capacity, power generation capacity is obtained from the ANEEL dam database.

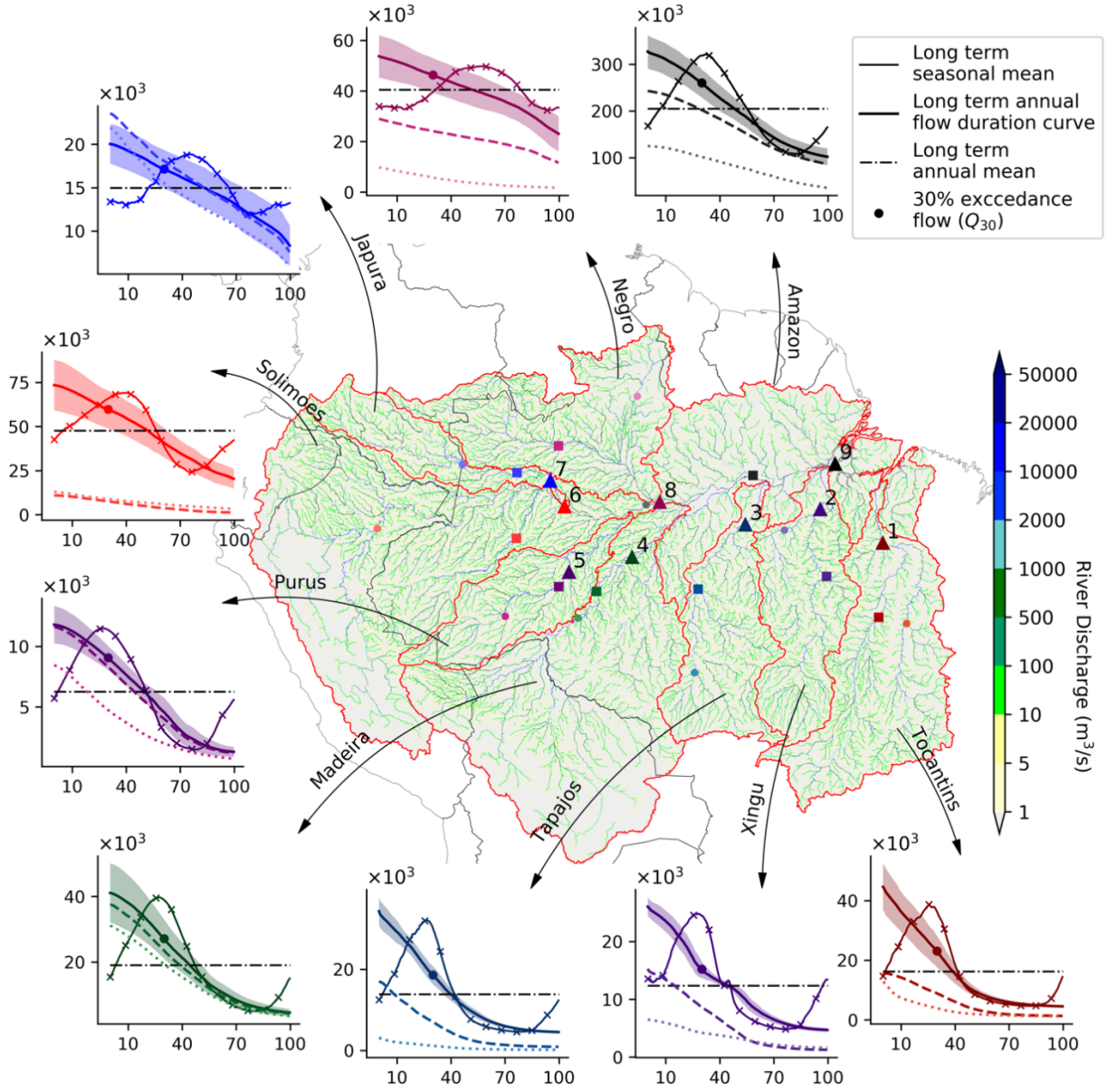


***Figure 5-2. Streamflow and flow duration curves for Amazonian sub-basins.*** *Spatial plot shows the $Q_{30}$ from long-term averaged streamflow obtained from LEAF-Hydro-Flood (LHF) model at the original model resolution of 1 arc-minute (~2km). Triangles indicate a downstream location of Amazon River and its tributaries, whereas squares and circles are random upstream locations. For the most downstream location in each sub-basin (triangles), annual flow duration curves obtained from LHF are displayed in respective subplots with the standard deviation (shaded area). Similarly, annual flow duration curve for the locations denoted by squares and circles are shown by dashed and dotted lines, respectively. Sub-plots also show the long-term seasonal mean (thin solid line) with scatter points indicating the months for the most downstream location (triangles) in each sub-basin.*

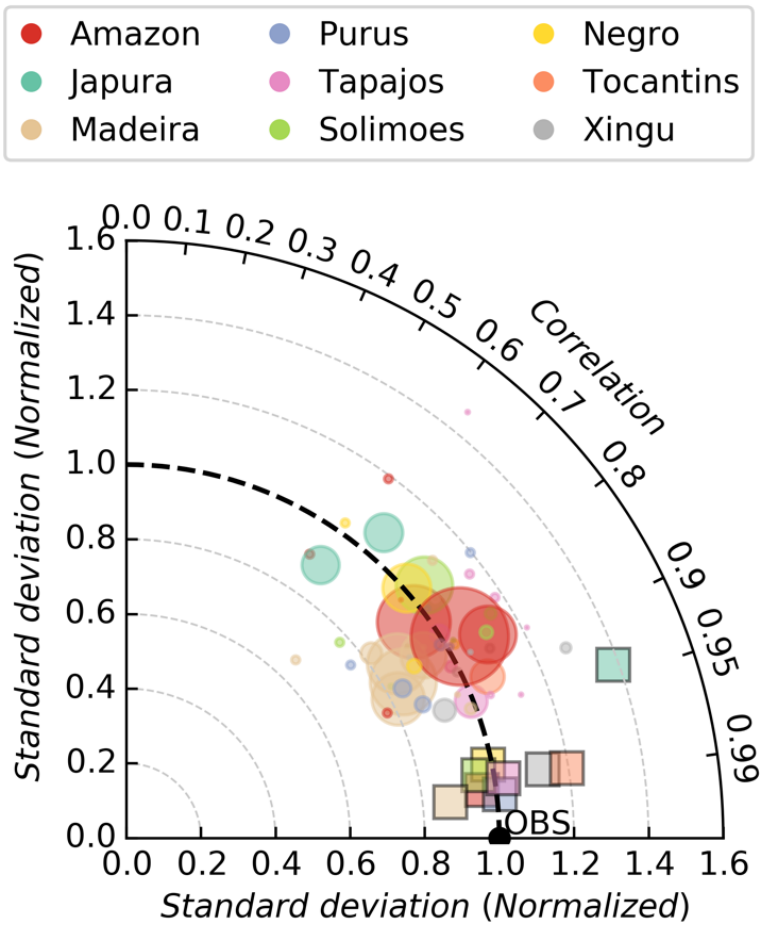


s

***Figure 5-3. Streamflow and TWS Validation of LEAF-Hydro-Flood (LHF) model.*** *Taylor Diagram showing the correlation and standard deviation ratio between simulated and observed streamflow at 55-gauge stations (circles) obtained from Agência Nacional de Águas (ANA) in Brazil (http:// hidroweb.ana.gov.br) and between simulated terrestrial water storage (TWS) from LHF and GRACE (mascon mean) for Amazon and its sub-basins (squares). Modified after Chaudhari et al. (2019).*

### 5.2.2. Integrated Gross Hydropower Potential

To calculate hydropower potential at every grid cell we employ the widely used potential energy-based formulation (Gernaat et al., 2017; Hoes et al., 2017; Pokhrel et al., 2008; Zhou et al., 2015):

$$E_{annual} = \sum_{i=1}^{365}(\rho \cdot g \cdot Q \cdot H) \cdot t \quad \begin{cases} Q = Q_D \; if \; Q_i > Q_D \\ Q = Q_i \quad if \; Q_i \leq Q_D \end{cases} \tag{5-1}$$

where Eannual is the annual potential energy in watt-hour [$M\ L^2\ T^{-3}$], ρ is the density of water [$M\ L^{-3}$], g is the gravitational acceleration [$L\ T^{-2}$], $Q_i$ [$L^3\ T^{-1}$] is the daily discharge in the grid cell, $Q_D$ is the design discharge, H [L] is the head difference, and t [T] is the operational hours per day. Head difference is estimated as the difference in riverbed elevation between the grid cell considered and its downstream grid cell. Riverbed elevation at every model grid cell is estimated by averaging the elevation of the river grid cells from a finer resolution (3 arc-second or ~90 meter) DEM from HydroSHEDS(Lehner et al., 2008). Such averaging provides a more realistic head gradient along the river compared to the head difference obtained as the difference of mean grid cell elevation between two consecutive grid cells. While there exists no common consensus regarding the streamflow threshold in the past literature, we use the flow with 30% exceedance probability ($Q_{30}$; which is the flow that is equaled or exceeded 30% of the time in a year) estimated from the flow duration curve for each grid cell, which is commonly used in hydropower design (Zhou et al., 2015). To maintain consistency with previous studies (Hoes et al., 2017; Pokhrel et al., 2008; Zhou et al., 2015), we also estimate annual potential energy using the annual mean flow, instead of the $Q_{30}$ (Figure 5-4). Furthermore, we employ a pragmatic approach—the annual integration approach—in view of the seasonal streamflow variations, by first calculating the daily hydropower potential with a $Q_{30}$ threshold and then integrating the potential to estimate Integrated Gross Hydropower Potential with $Q_{30}$ ($IGHP_{30}$), hence avoiding the overestimation of potential due to the use of mean annual streamflow (Figure 5-4).

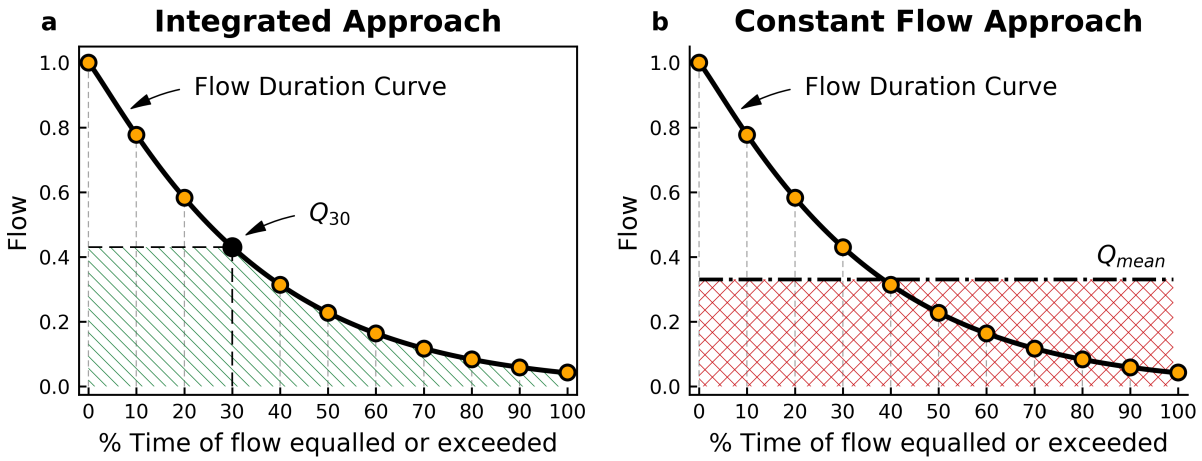


***Figure 5-4. Schematic representation of typical flow duration curves.*** *Subplots indicate the two methods used in this study to estimate hydropower potential. a, Integrated approach utilizes daily variations in the streamflow and estimates hydropower potential on a daily basis, which is then integrated to obtain the total hydropower potential. Black filled circle indicates an example of the discharge threshold (i.e., $Q_{30}$) used in the estimation of $IGHP_{30}$. Shaded green area indicates $IGHP_{30}$. b, the constant flow approach utilizes an annual mean flow to estimate hydropower potential. Shaded red area indicates the total hydropower potential included in $GHP_{Mean\ Annual\ Flow}$.*

### 5.2.3. Technical In-stream Production

Technical In-stream Potential is calculated at each grid cell using the kinetic energy formulation given as:

$$TIP_{annual} = \sum_{i=1}^{365} \eta \cdot C_p \cdot B \cdot \left(\frac{1}{2}\rho \cdot W \cdot H_{90} \cdot V_i^3\right) \cdot t \qquad (5\text{-}2)$$

where, η is turbine efficiency (90%; Gernaat et al., 2017), Cp is power coefficient, B is blockage ratio, ρ [M $L^{-3}$] is density of water, W [L] is river channel width, H90 [L] is flow depth which equals or exceeds 90% of the time, V [L $T^{-1}$] is flow velocity for each day of the year simulated by LHF (Chaudhari et al., 2019), and t [T] is operational hours per day. For blockage ratio, a constant value of 0.284 is assumed, following previous literature (Vennell et al., 2015). The power coefficient is assumed to be 0.35, which is an average value commonly used to estimate power conversion (Guney, 2011). Assumed blockage ratio and power coefficient together result

into an extraction of ~10% of the total available kinetic energy to minimize the impact on downstream flow characteristics, a limit commonly referred to as the "safe extraction limit" (Bryden and Couch, 2006; Ortega-Achury et al., 2010; VanZwieten et al., 2014). $H_{90}$ is estimated from the 36-year averaged daily flow depths simulated by LHF. To account for the high seasonality of flow in the Amazonian sub-basins (for example, Tocantins), in-stream turbines are considered only in a part of the river cross-section corresponding to the area with respect to H90. To remain conservative and for cost-effective power generation, river stretches with water depth <2 meter and velocity <0.5 meter/second, corresponding to $Q_{90}$ (the flow equaled or exceeded 90% of the time during a year) are excluded from the TIP analysis. Moreover, the river stretches within protected areas are entirely excluded.

In-stream power generation capacity at the planned dam sites is estimated as the sum of TIP in the river grid cells upstream of the dam site along the river, with an upper threshold of the river stretch that would be affected if the dam is constructed. River stretch affected by planned dams is estimated considering inundation areas, traced by upstream tracking of the reservoir on a high resolution (~90 meter) DEM using dam height (Shin et al., 2020). For planned dam sites with no dam height specified, we assume the affected river stretch to be equal to either the distance to an upstream dam or 50-kilometer, whichever is lower. The 50-kilometer threshold is selected to remain conservative in estimating the cost of planned dams. The length of reservoirs created by existing dams such as Jirau and Santo Antonio in the Madeira River basin is over 100 km even though both are considered run-of-the-river projects.

We adopt the physical properties of in-stream turbines, such as the diameter (1 meter) and the minimum flow depth required (2 meter), based on the specifications of Smart Hydro Power's Smart Mono Float turbine and Smart Free Stream turbine (https://www.smart-hydro.de/). The

Smart Hydro Power turbines are selected because these turbines are commercially available and have been successfully implemented and tested in river stretches around the world. Further, the structure of Smart Hydro Power turbines allows them to be installed on the riverbed, avoiding potential interferences with river navigation, prominent in the Amazonian rivers. Previous studies have shown that the flow recovery length following an upstream turbine array varies from 3-40 times the turbine diameter (D), depending on the array arrangement (straight and staggered) and turbulence model (Malki et al., 2014; Vennell et al., 2015). We take a conservative approach by considering a minimum inter-row spacing of arrays as 10 times the turbine diameter (10D; Electrical Power Research Institute (EPRI), 2012) at planned dam sites. For a basin-wide analysis, we employ an inter-row spacing of 40 times the turbine diameter (40D; Malki et al., 2014) as a sustainability criterion, which represents a case with high likelihood that the velocity becomes uniform before reaching the next turbine row. The 10D scenario, which still has a relatively high likelihood that the flow velocity becomes uniform before the next downstream array (Malki et al., 2014; Vennell et al., 2015), is considered strictly for site-specific analysis, such as the TIP comparison with planned dam capacities. Here, for the estimation of TIP, we assume complete velocity recovery to natural condition downstream of a turbine row. Note that our approach does not consider the influence of lateral turbine spacing on flow velocity, which has been known to benefit the total output of the turbine array from the "duct effect" caused by the lateral spacing between turbines (Vennell et al., 2015).

Suitable sites for in-stream power generation are identified by performing a site-specific multivariable analysis at the municipality level over the Brazilian Amazon, taking into account the (i) extent of protected areas, (ii) region's energy demand, and (iii) availability of TIP. Each of the criterion is expressed in terms of an index namely, the Protected Area Index (PAI) that

represents the extent of protected areas, Energy Demand Index (EDI) that quantifies the electricity demand not fulfilled by the country's power grid, and In-stream Potential Index (IPI) that represents the availability of in-stream potential, calculated for each municipality in the Brazilian Amazon.

The PAI is defined as the ratio of protected areas in a municipality to the total area of the municipality, which is normalized to a 0-1 scale by subtracting the minimum value from each value of the ratio and then dividing the difference by the range of percentage protected areas in the Brazilian Amazon. The PAI values are inverted by subtracting those from one, because the smaller the protected areas, the higher should be the development suitability.

The EDI is calculated as the mean of No Electricity Household Index (NEHI) and the Future Energy Demand Index (FEDI) for each municipality. NEHI is the ratio of number of households without electricity to the total number of households in a municipality normalized to a 0-1 scale. The future energy demand of a municipality is calculated using the total energy demand of Northern Brazil as reported by Operador Nacional do Sistema Elétrico (ONS), Brazil (http://www.ons.org.br/). The total energy demand of Brazil's northern sector for 2018 is distributed among the municipalities by weighing it by the distribution of population as per the 2010 Brazilian census data. Future energy demand for year 2030 is predicted by assuming a 4% increase per annum based on the linear trend of energy demand for the past years as reported by ONS. This future energy demand is then categorized into five classes: Micro (<1MW, EDI=0.2), Small (1-10 MW, EDI=0.4), Medium (10-30 MW, EDI=0.6), Large (30-1000 MW, EDI=0.8), and Mega (>1000 MW, EDI=1.0). We follow the classification of dams adopted by the Brazilian government to generate EDIs for each municipality with a slight modification. We note that for

better distribution of the EDI, we further sub-classify the small dam category (1-30 MW) as defined by the Brazilian government into small (1-10 MW) and medium dams (10-30 MW).

The IPI, an indicator of the available in-stream potential in a municipality, is calculated by aggregating the potential of all the model grid cells within each municipality and categorizing them following the same approach as for EDI. The available in-stream potential for the calculation of IPI is based on the 40D scenario.

Finally, the three indices (viz. PAI, EDI, IPI) are used to assess 644 municipalities in the Brazilian Amazon and determine the suitability of the region for in-stream hydropower development. This analysis is limited to the Brazilian Amazon because most of the in-stream potential is found in the Amazonian lowlands in Brazil. Further, detailed data, such as the number of households without electricity, is only available for Brazil.

### 5.2.4. Power Generation Cost Analysis

To assess the cost differences between storage-based hydropower and in-stream turbines, we individually estimate the cost of the nine selected planned dams in the Brazilian Amazon. Four of the selected nine dam are planned to be built in the coming decade (Ministry of mines and energy, 2019) and the others are the largest planned dams in the Brazilian Amazonian. In-stream turbine cost is adopted from market value as reported for Smart Hydro Power's Smart Mono Float turbine and Smart Free Stream turbine. Lifespan of the in-stream turbines is assumed to be 30 years following the information provided by the turbine manufacturers. Operation and maintenance (O&M) cost of in-stream turbines varies substantially among different case studies (Previsic, 2012; Previsic et al., 2008) based on the number of operational units. In this study, we assume the O&M cost of in-stream turbines to be $0.00047 /kWh, which is the extrapolated

O&M cost of 1,000 turbines from the trend of O&M cost against number of operational units compiled from previous case studies (Previsic, 2012; Previsic et al., 2008).

To estimate the overall cost of conventional hydropower, we employ the planning tools set by the United States and Norwegian hydropower industry, which are used in the recently published literature (for example, Gernaat et al., 2017). These cost formulations (Table 5-1) are functions of dam properties such as the power generation capacity, dam height, and design discharge. O&M cost for storage-based hydropower is assumed as $40/kW/year, following the global estimates provided by the International Renewable Energy Agency (IRENA)(International Renewable Energy Agency (IRENA), 2019c). Sub-basin-wise hydropower plant capacity factors are estimated using the power generation data of the existing dams in the Amazon basin as reported by ONS, Brazil (http://www.ons.org.br/). All investments are annualized with a discount factor of 10% (Gernaat et al., 2017). A lifespan of 50 years is assumed for storage-based hydropower, which is higher than the common trend of using 40 years (Gernaat et al., 2017; International Renewable Energy Agency (IRENA), 2019c). We use the dam information obtained from the ANEEL dam database as an input to these cost equations, whereas the discharge from the turbines was determined using LHF simulations. Dam heights are estimated as the difference between the upstream and downstream water levels obtained from the ANEEL database. Dam widths are derived using high resolution (3 arc-second, ~90 meter) DEM from HydroSHEDS (Lehner et al., 2008), as the shortest distance between the two contours representing the upstream water level in the vicinity of the dam location. Upstream inundation extent of planned dams is estimated by utilizing high resolution (3 arc-second or ~90 meter) DEM from HydroSHEDS (Lehner et al., 2008) and dam height. Gridded Population of the World ("Gridded Population of the World, Version 4 (GPWv4): Population Count Adjusted to Match

2015 Revision of UN WPP Country Totals," 2016) (GPWv4) dataset for 2020 generated by NASA's Socioeconomic Data and Applications Center (SEDAC) is employed to estimate the population affected by the planned dams.

***Table 5-1. Cost equations used to estimate the construction cost of planned dams.***

| No. | Cost Component | Equation | Units |
|---|---|---|---|
| 1 | Turbine (Gernaat et al., 2017) | $1.1943\ P^{0.7634}10^6$ | P (MW) |
| 2 | Power Station (Veileder, 2012) | $-0.0006\ Q_D^2 + 0.67Q_D\ - 6.95$ | Q ($m^3/s$) |
| 3 | Electric Equipment (Veileder, 2012) | $3.9142\ P^{0.6622}\ 10^6$ | P (MW) |
| 4 | Fish Passage (Hall et al., 2003) | $1.3 \times 10^6\ P^{0.56}$ | P (MW) |
| 5 | Miscellaneous (Veileder, 2012) | $[-38.795\ \log Q_D + 309.89]\ P$ | Q ($m^3/s$), P(kW) |
| 6 | Dam Construction (Veileder, 2012) | $0.72\ D_H^{0.78} D_L 10^3$ | D (m) |
| 7 | Population Displacement (Gernaat et al., 2017) | Number of people displaced times twice the GDP per capita of Brazil | |

## 5.3. Results

### 5.3.1. Integrated Gross Hydropower Potential

The total $IGHP_{30}$ for the entire Amazon basin is estimated at 3,793 TWh yr-1 (spatial distribution shown in Figure 5-5a). Characterized both by high flows and steep slopes, the Solimoes possesses the highest $IGHP_{30}$ (942 TWh yr-1) among the eight sub-basins (Figure 5-1), followed by the Madeira (433 TWh yr-1) and Negro (415 TWh yr-1) river basins (Table 5-2). About 23% of the gross potential is contained within the Andean Amazon due to the combined effect of high annual streamflow and rugged topography that provides high head drop. Our estimate of gross potential based on the annual mean flow totals 4,191 TWh yr-1 for the entire Amazon, which aligns closely with previous estimates (Table 5-2). However, differences are evident at the sub-

basin level (Table 5-2), which could be attributed to the differences in model input (e.g., the spatial distribution of precipitation within the basin) and model grid resolution. Previous studies used either low resolution (~100km) model grid cells (Pokhrel et al., 2008) or streamflow estimates derived by downscaling coarse resolution global hydrological model output (Hoes et al., 2017). Our approach, by comparison, directly utilizes high resolution streamflow that has been extensively validated across the entire basin (Chaudhari et al., 2019; Pokhrel et al., 2014, 2013), which adds confidence to our estimates (see Methods). Results differ strongly especially in the Madeira river basin where our estimate indicates ~61% and ~35% less potential compared to Hoes et al., (2017) and Pokhrel et al., (2008), respectively, which could be a result of the use of high-resolution streamflow and an improved treatment of head drop using a high-resolution digital elevation model (DEM) in this study (see Methods). A comparison of GHP estimates, calculated using the integrated and constant (i.e., annual mean) flow approach along with their sensitivity to different exceedance flows, is presented in Figure 5-5.

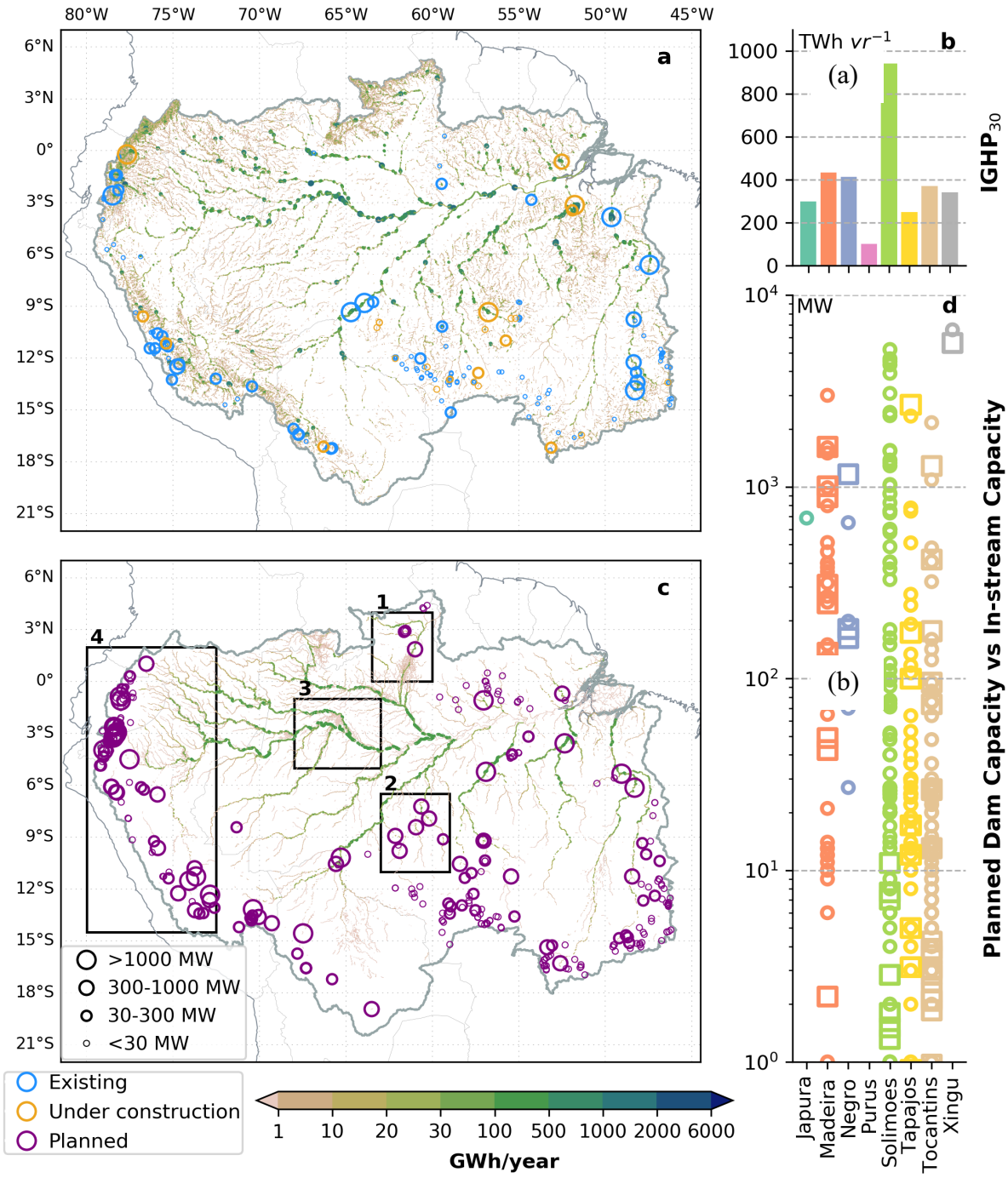


***Figure 5-5. Hydropower potential in the Amazon.*** ***a****, Gross hydropower potential (IGHP$_{30}$) in the Amazon River basin and its sub-basin level distribution in* ***b****.* ***c****, Technical instream potential (TIP) in the Amazon under the 40D scenario.* ***d****, Comparison of the power generation capacities and TIP under the 10D scenario at the planned dam sites in the Amazonian sub-basins. Squares and circles in* ***d*** *indicate in-stream capacities and planned dam capacities, respectively. The IGHP$_{30}$ for small sub-basins located in the northeast of the Amazon are not shown in* ***b****. Sub-basin boundaries are shown in Figure 5-1.*

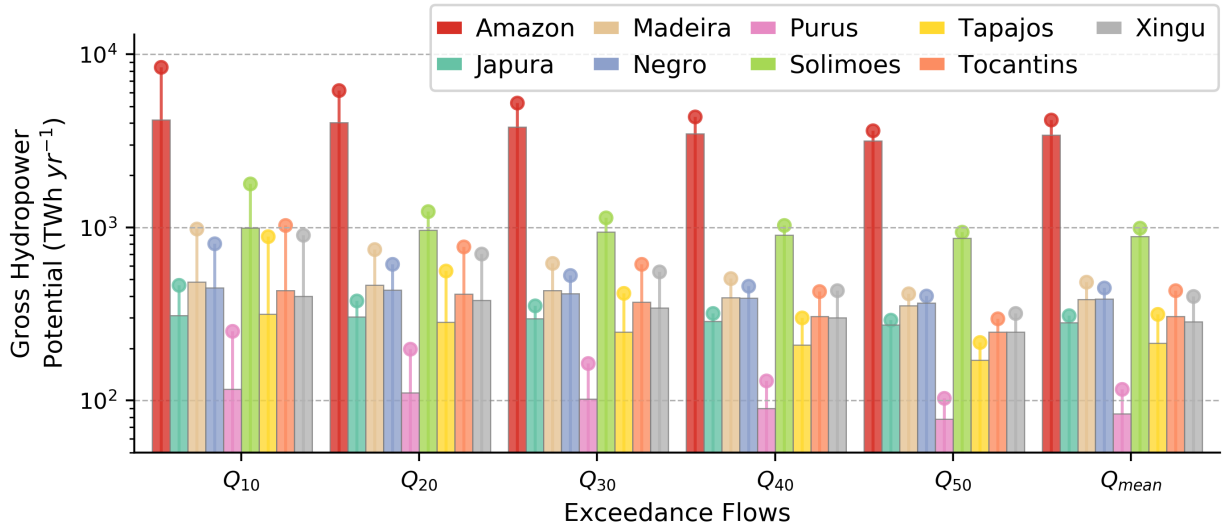


***Figure 5-6. Gross hydropower potential estimates for flows with different exceedance probability.*** *Bars show the potential estimated using the annual integration approach whereas the filled circles show that from the constant flow approach. Sub-basin-wise color coding is same as in Figure 5-5 and values for the entire Amazon basin are indicated in red.*

***Table 5-2. Comparison of our gross hydropower potential with previous estimates (TWh yr$^{-1}$).***

| River Basins | This Study | This Study | This Study (1980-2015) | This Study (1986-1995) | Pokhrel et al., (2008) (1986-1995) | Hoes et al. (2017)* |
|---|---|---|---|---|---|---|
| | $IGHP_{30}$ | $GHP_{30}$ | $GHP_{Mean\ Annual\ Flow}$ | | | |
| Amazon | 3,793 | 5,242 | 4,191 | 3,948 | 3,873 | 4,226 |
| Japura | 298 | 353 | 310 | 275 | 174 | 245 |
| Madeira | 433 | 622 | 484 | 452 | 748 | 1,236 |
| Negro | 415 | 530 | 447 | 428 | 294 | 445 |
| Purus | 102 | 164 | 116 | 109 | 101 | 109 |
| Solimoes | 942 | 1,138 | 992 | 878 | 1,023 | 964 |
| Tapajos | 249 | 417 | 315 | 309 | 343 | 308 |
| Tocantins | 370 | 612 | 432 | 425 | 617 | 328 |
| Xingu | 342 | 554 | 399 | 406 | 364 | 228 |

* GHP estimates from Hoes et al. are based on the discharge derived from different time periods.

### 5.3.2. Technical In-stream Potential

We find high potential for in-stream power generation across the Amazon basin (Figure 5-5c). As expected, high TIP is seen in the Amazonian lowlands, such as the Solimoes river floodplains (Figure 5-5c, Box 3) and the Amazon main stem, regions characterized by high flows and wide channels. Notwithstanding the high concentration of $IGHP_{30}$ in the Andes, TIP estimates suggest higher potential for using in-stream turbines in the Amazonian lowlands compared to the Andean River stretches (Figure 5-5c, Box 4). Narrow channels through rugged topography and shallow water depths are the primary reasons for low TIP in most of the Andean River stretches. Yet, for the Andean River stretches with sufficient water depths (>2 meter; see Methods), in-stream turbines may prove useful with site-specific optimization of the design factors, such as the inter-row turbine spacing and blockage ratio.

Evidently, most of the locations with high TIP in the Amazonian lowlands overlap with the planned dam sites with high generation capacity (Figure 5-5c, Boxes 1 & 2). At five of the nine planned dam sites considered in this study (Figure 5-1), in-stream turbines could be used to exploit the entirety of planned generation capacity while utilizing only a fraction of the river stretch under the 10D scenario. For example, high TIP (671 MW, Figure 5-5c, Box 1) is found in the ~15 kilometer river stretch in the vicinity of the Bem-Querer dam (650 MW), the largest dam planned to be built in the Amazon by 2029 (Ministry of mines and energy, 2019). Similarly, at other planned dam sites, such as Jatoba and Prainha (Figure 5-5c, Box 2), in-stream turbines could be used to harness the entire planned dam capacity from ~32 and ~47-kilometer river stretches, respectively. Overall, our estimate suggests that ~63% (~9,791 MW) of the total planned dam capacity in the Brazilian Amazon could be harnessed in the region of the planned dams (>30 MW) by employing in-stream turbines under the 10D scenario (Figure 5-5d and

Figure 5-7). This suggests that in-stream turbines are viable alternatives to conventional dam projects in many locations in the Amazon.

***Table 5-3. Planned dam capacities and the available in-stream potential at 9 selected dam sites in the Brazilian Amazon.*** *Available TIP is based on the 10D scenario (see Methods).*

| No. | Planned Dams | Planned Capacity (MW) | River Stretch Expected to be Affected (km) | Available TIP (MW) | Required River Length for TIP (km) | Planned Capacity (%) |
|---|---|---|---|---|---|---|
| 1 | Bem-Querer | 650 | 281 | 671 | 15 | 103% |
| 2 | Castaheira | 140 | 28 | 86 | 41 | 61% |
| 3 | Jatoba | 2338 | 232 | 2379 | 32 | 102% |
| 4 | Tabajara | 400 | 216 | 303 | 68 | 76% |
| 5 | Prainha | 796.34 | 212 | 798 | 47 | 100% |
| 6 | Sumaúma | 458.2 | 202 | 299 | 51 | 65% |
| 7 | Inferninho | 361.1 | 399 | 204 | 56 | 56% |
| 8 | Quebra Remo | 267.8 | 155 | 267 | 59 | 100% |
| 9 | Marabá | 2160 | 303 | 2358 | 36 | 109% |

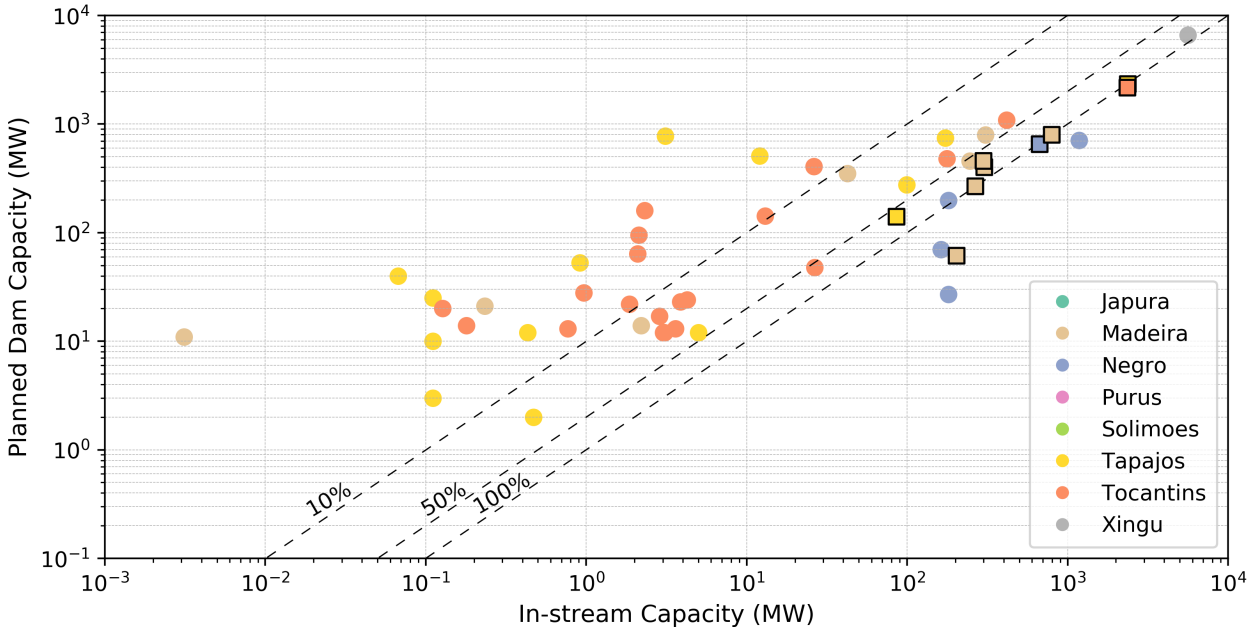


***Figure 5-7. Dam capacities versus in-stream power generation capacity.*** *Markers indicate planned dam sites in the Amazon, with square markers indicating the 9 dam sites selected for the cost comparison. Planned dam sites with in-stream potential less than 1 KW are removed from the figure.*

### 5.3.3. In-stream Suitability Index

Our results suggest that the Madeira and Tapajos—the sub-basins of the Amazon, likely to be threatened the most by a number of existing and planned hydropower dams (Latrubesse et al., 2017)—are the most suitable regions for deploying in-stream turbines instead of large dams. Regions with high in-stream suitability (for example, municipalities including Itaituba and Jacareacanga; Figure 5-8 and Figure 5-9), overlap with the locations of many of the planned dams such as Jatoba, which are included in Brazil's 10-year energy expansion plan (Ministry of mines and energy, 2019). These municipalities along with others in the middle reaches of the Tapajos and Madeira rivers are characterized by high suitability, making this region particularly suitable for in-stream turbines. Further, municipalities situated in the Negro river basin also indicate high suitability for in-stream turbines, especially around the Bem-Querer dam which is planned to be constructed in the coming decade (Ministry of mines and energy, 2019).

Further, high suitability can be seen in the Brazilian municipalities that house some of the major operational hydropower projects (Figure 5-8), which adds confidence to our finding about the possibility of using in-stream turbines as an alternative to large dams. For example, the high IPI is observed around Porto Velho—municipality where Santo Antonio (3,568 MW) and Jirau (3,750 MW) dams are located. Similarly, high suitability can be seen in the municipalities such as Baiao, Breu, Branco, Moju, Pacaja and Tailandia (Figure 5-8) that are in the vicinity of the largest dam in the Tocantins basin (Tucurui I and II; 8,370 MW).

Northern and southern stretches of the Brazilian Amazon also exhibit high suitability because of high PAI and IPI (see Methods); these areas include major cities such as Ji-Paraná and Sinop in the upstream reaches of the Madeira and Tapajos rivers, respectively (Figure 5-8 and Figure 5-9). In most of the central and eastern regions of the Brazilian Amazon, the suitability is dominated by IPI (Figure 5-8 and Figure 5-9) owing to the large areas under protection (low PAI) and sparse population (low EDI).

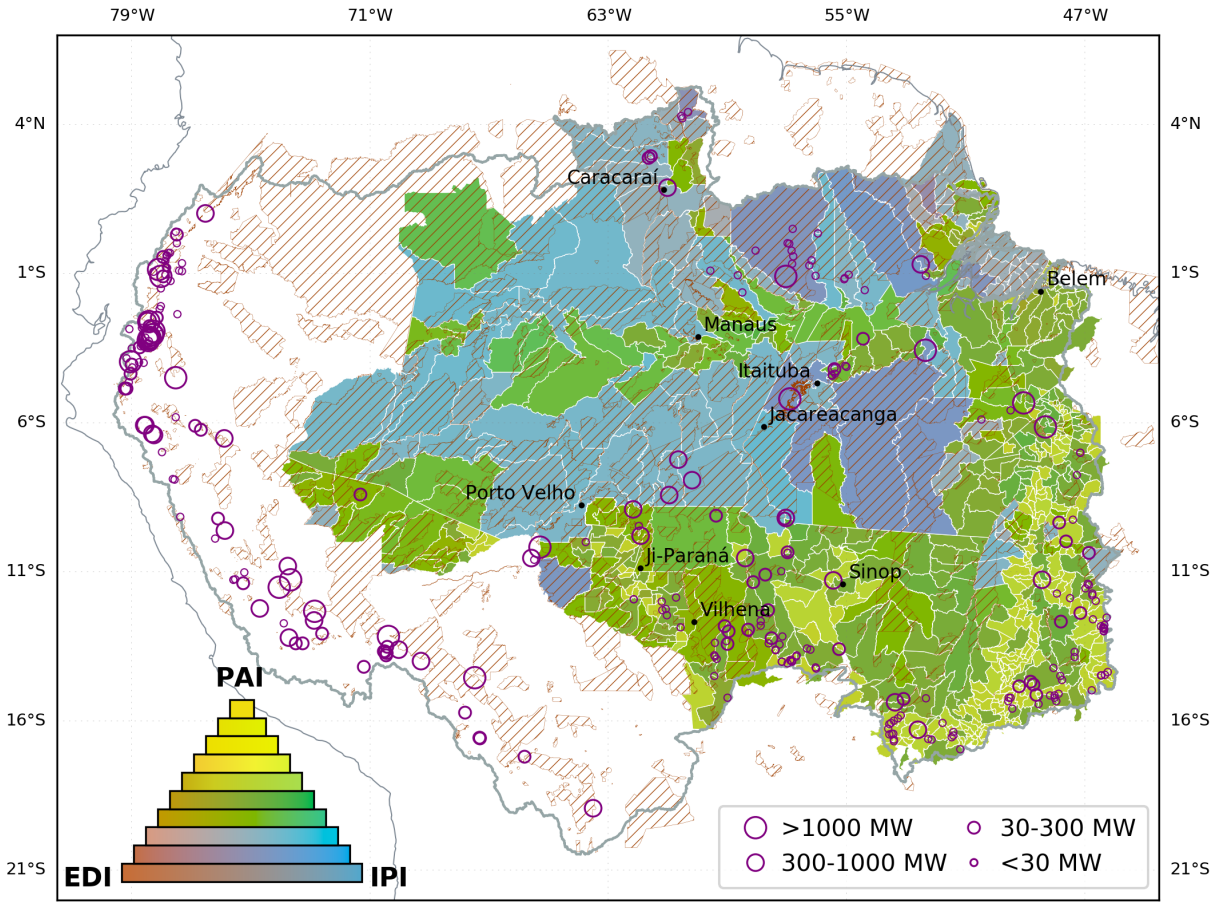


***Figure 5-8 Suitability indices for in-stream turbines in the Brazilian Amazon.*** *(i) Protected Area Index (PAI), (ii) In-stream Potential Index (IPI), and (iii) Energy Demand Index (EDI), at a municipality level in the Brazilian Amazon. Blue shade indicates domination of IPI, whereas yellow and red shades indicate domination of PAI and EDI, respectively. Brown hatches indicate the protected areas defined by the world database of protected area (WDPA). Purple circles mark the planned dam sites.*

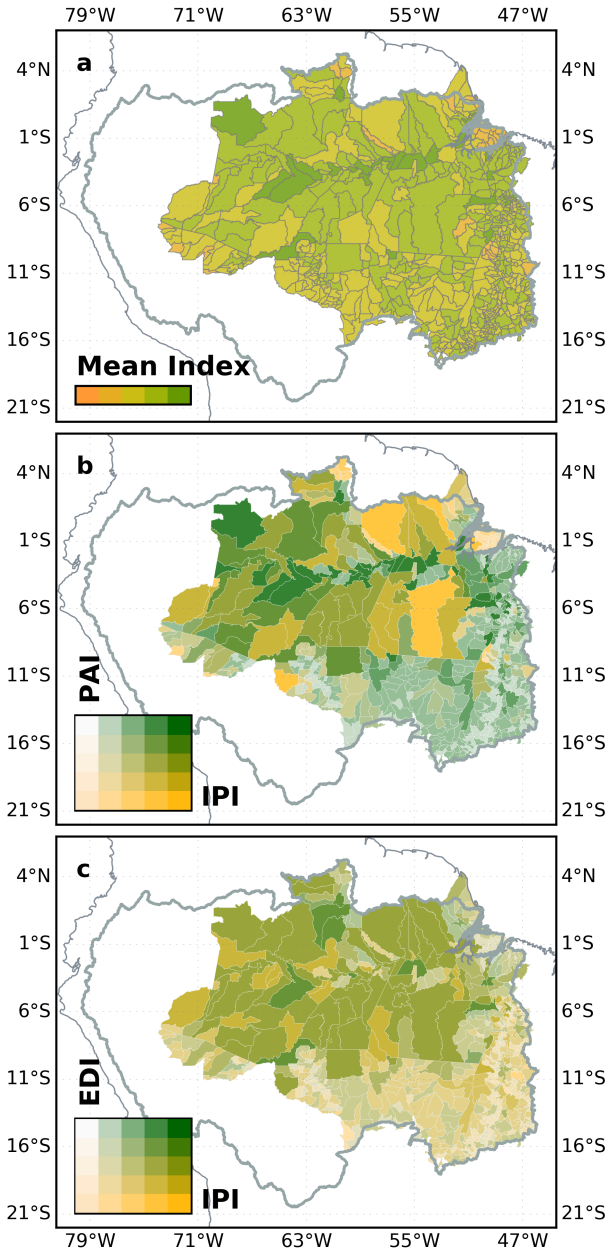


***Figure 5-9. Comparison of Individual Suitability Indices for In-stream Turbines in the Brazilian Amazon.*** *ISI (a), PAI versus IPI (b), and EDI versus IPI (c) at a municipality level in the Brazilian Amazon. Orange color indicates domination of IPI, whereas light green shades indicate domination of PAI and EDI in (b) and (c), respectively. Brown hatched regions in (b) indicate the protected areas as defined by the WDPA. Note that the color scales range from 0 to 1 with equal increment.*

### 5.3.4. Cost Comparison between Conventional and In-stream Hydropower

Levelized Cost of Electricity (LCOE) estimates for in-stream turbines (3.8-4.4 cents/kWh) is found to be 46-54% of the average reported cost of energy from existing hydropower dams (~8.2 cents/kWh) across Brazil (Figure 5-10) as reported in the Agência Nacional de Energia Elétrica (ANEEL) database (http://www.aneel.gov.br/). On a sub-basin level, the average reported cost for existing dams (>30MW) varies from 11.6 cents/kWh in the Madeira to 7.4 cents/kWh in the Tocantins. Although, the existing mega-dams (for example, Jirau and Santo Antonio) in the Madeira basin are run-of-the-river plants, their actual cost is high, with an average of 8.1 cents/kWh.

The estimated costs for the nine planned dams (Figure 5-10, brown polar bar) in the Brazilian Amazon are substantially lower than the reported cost of their predecessors (Figure 5-10, orange dots). This implies that for a proper interpretation of the costs for hydropower projects, it is essential to consider the actual costs of existing dams which may already account for the highly uncertain costs caused by social and environmental changes, construction difficulties, and management irregularities or, to certain extent, the delays in political decision making. Surprisingly, and as discussed above, the average estimated cost for planned dams in the Brazilian Amazon is found to be much lower (6.2 cents/kWh) than the average reported cost of existing dams (8.2 cents/kWh; Figure 5-10). Costs estimated for the existing dams account for only ~75% of their average reported costs in the ANEEL database, with some existing dam sites going as low as ~25%. Detailed cost breakdowns for hydropower dams are provided in Figure 5-11.

On the contrary, the cost of in-stream turbines (average 4.1 cents /kWh) is largely the same for all locations as the cost equation is only a function of generated power and is subject to less

uncertainties because the environmental and social costs, including those caused by water impoundment, sediment accumulation, resettlement of populations, reduced fish productivity, are bound to be minimal compared to storage-based hydropower projects.

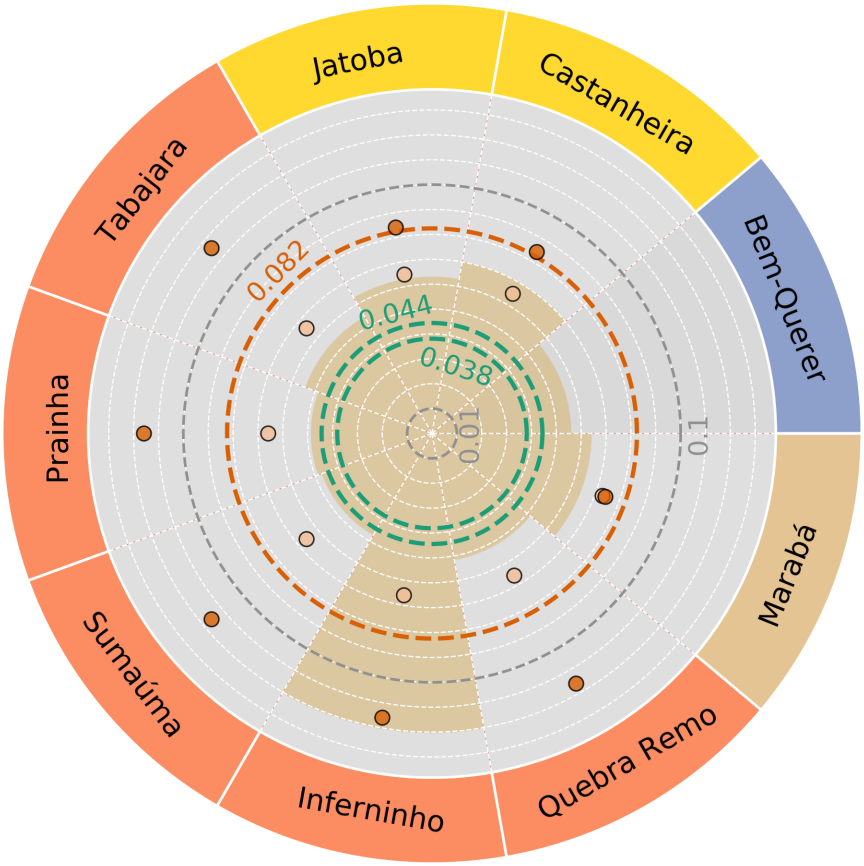


***Figure 5-10. Comparison of costs for conventional hydropower and in-stream turbines.*** *Results shown are for the nine planned dams in the Brazilian Amazon (Figure 5-1). Brown polar bar indicate the predicted storage-based hydropower dam cost. Green dashed lines indicate the range of estimated cost among three different types of in-stream turbines at the planned dam locations. Light and dark orange dots, respectively, show the average estimated cost and the average reported cost (obtained from ANEEL database) for existing dams (>30MW) in the corresponding sub-basin (color coding is same as in Figure 5-5; the sub-basins are shown in Figure 5-1). Orange dashed line shows the average cost of all existing dams (>30MW) in Brazil. All costs are expressed in terms of Levelized Cost of Energy (LCOE) in USD/kilowatt-hour ($/kWh). Note that no dams are currently operational in the Negro River basin.*

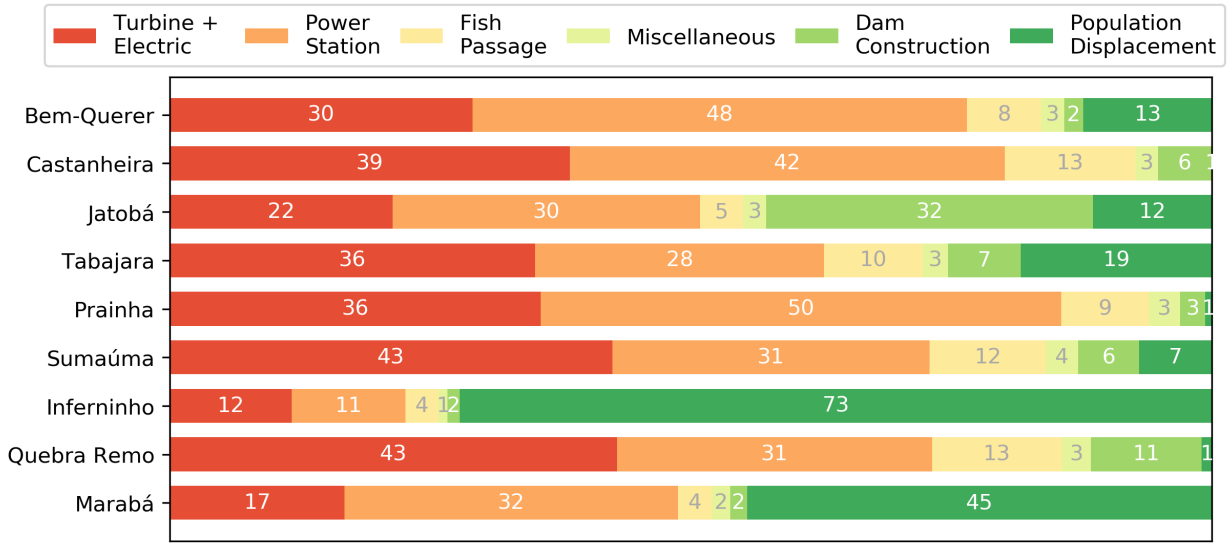


***Figure 5-11. Breakdown of costs for conventional hydropower.*** *Results shown are cost estimates for the 9 largest dams in the Brazilian Amazon. Costs for each component are calculated using the cost equations provided in Table 5-1.. Numbers indicate the percentage of the total cost. Owner's cost and Operation Maintenance cost are excluded from this analysis*

## 5.4. Discussion

Our findings suggest that there is high potential for using in-stream turbines in the Amazon as an alternative to the planned storage-based hydropower projects. Site-specific analysis indicates that at five of the nine planned dam sites in the Brazilian Amazon, in-stream turbines could be used to harness equivalent amounts of energy to be produced from storage-based dams, with substantial reduction in environmental and social impacts. High potential for using in-stream power generation is found also at the remaining four planned dam sites. These findings have important implications for sustainable hydropower development in the Amazon basin by reducing the environmental, social, and economical losses associated with large-scale, storage-based (Fearnside and Pueyo, 2012; Latrubesse et al., 2017; Moran et al., 2018; Stone, 2016; Winemiller et al., 2016) and even run-of-the-river (Cochrane et al., 2017) hydropower projects that are planned across the basin. With the assumed generic turbine array arrangement, we find that the potential for in-stream turbines is high in the Amazonian lowlands; site-specific

optimization of turbine array arrangement could lead to increased suitability of in-stream turbines at the Andean dam sites, which could help maintain the Andes-Amazon connectivity (Anderson et al., 2018; Finer and Jenkins, 2012).

Our power potential estimates are based on the best datasets currently available, combined with a state-of-the-art hydrological model. We expect that as specific projects in the Amazonian sub-basins are developed, enhanced site-specific analyses would enable optimization of in-stream turbine array design with respect to local site conditions. It is expected that the power potential would differ than that presented in this study because our approach leads to rather conservative estimates (see Methods). Combining our results with relevant regional information (for example, fishing hotspots, navigational routes, and areas of cultural importance) could help identify and prioritize locations for in-stream hydropower development and further examine their trade-offs with ecological factors including river bottom habitats and sediment transport.

Actual costs of conventional hydropower far exceeds the predicted costs, with as high as a four-fold increment in some dam sites (~96% higher globally; Ansar et al., 2014), which likely comes from the underestimation of environmental and social costs (Ansar et al., 2014) owing to inaccurate assessment of inundated areas and displaced population (Cochrane et al., 2017). Additional costs from construction difficulties due to geological complexities (Petheram and McMahon, 2019) and project delays (Ansar et al., 2014; Awojobi and Jenkins, 2015) also often occur in mega-dam projects. Furthermore, with ongoing deforestation (Moran et al., 2018) and potential reduction in power generation due to climate change and variability(Moran et al., 2018), the costs of conventional hydropower may increase in the future. For example, the Belo Monte dam in the Xingu River is expected to produce only 4.46 GW (Moran et al., 2018) of the 11.23 GW installed capacity in many months of each year due to low water levels. These

inevitable costs combined with the often neglected costs that incur from delays in juridical contestation and management irregularities (Moran et al., 2018) reduce the benefit-to-cost ratio of conventional hydropower well below one.

On the contrary, in-stream turbines can provide a relatively cost-efficient and benign energy production system compared to conventional hydropower. In-stream turbines have already been implemented globally, most of them being individual turbines in rural areas with the exception of the installations in the Alaskan rivers (Previsic et al., 2008). Since these installations are relatively new, many aspects of their operation, reliability and life span in varying geographic and hydrologic conditions are yet to be fully tested. However, the possible impacts of a large-scale implementation of in-stream turbines can be assessed based on the results of their marine counterparts—the tidal turbines. Deploying large turbine arrays in river channels may have undesirable consequences on the riverine environment. Reduced navigational capabilities during extreme droughts, alterations in fishing routine (Copping and Hemery, 2020) and increased water levels downstream could be some of the potential effects; however, the adverse socio-environmental impacts are expected to be relatively less than those of large dams. Further, the cost estimates provided in this study assume that each in-stream turbine in an array generates energy close to the rated power. Although this can be achieved by careful site-specific turbine array design and placement (Vennell et al., 2015), variations in the total power generation can be expected due to the fluctuations in river velocities, causing a deviation from the predicted costs of in-stream turbines. Further, in-stream turbine projects may also suffer from cost overruns—like large dam projects—owing to project delays, but the overruns caused by underestimated environmental and social costs, geological complexities, and decommissioning would be lower than those for large hydropower dams.

Nevertheless, in-stream turbine development in the Amazon aligns well with the needed efforts to preserve the Amazonian forests (Davidson et al., 2012; Lovejoy and Nobre, 2018) and their critical role on global terrestrial water balance and climate dynamics (Malhi et al., 2008), along with the preservation of unique Amazonian habitats (Latrubesse et al., 2017). Indeed, the benefits of developing in-stream turbines instead of large dams extend well beyond the reduction of environmental impacts caused by dams; other benefits include elimination of forced relocation of human populations along with economic, cultural, and social costs that dams impose. While, for the time being, conventional hydropower dam projects in the Amazon basin are on hold or being cancelled owing to injunctions requested by Indigenous peoples and local communities, the energy sector has not entirely renounced dam building in the region, making it increasingly important to examine alternatives to dams for continued use of renewable energy resources. However, replacing dams with in-stream turbines alone is not expected to entirely transform the hydropower sector. A transition from the single-minded focus on energy production, promoting integrated water management through incorporation of local community concerns, and a greater transparency in the decision process is essential. Strategic planning which follows a nexus approach that integrates food, energy, and water systems, and utilizes innovative analytical methods that account for larger implications which go beyond political boundaries should be considered to increase the overall credibility of hydropower.

In summary, this study provides a solid foundation to rethink hydropower dams and provides insights on new and important alternatives for sustainable hydropower development. Over the long run, this assessment could prove beneficial in investigating the future of hydropower in the Amazon and other regions worldwide (for example, the Mekong and Congo river basins) where a boom in construction of mega-scale hydropower dams is underway (Pokhrel et al., 2018a). The

flexibility of our framework also provides wide-ranging applications for future studies related to the development of hydrokinetic power generation globally.

# Chapter 6. Summary and Conclusion

Despite noteworthy progress that has been made in understanding the impact of human activities on the hydrology of the Amazon River, significant limitations and challenges remain in achieving a holistic understanding of the entire basin under the influence of climate change and intensive human activities, especially dam construction. With the increasing number of planned dams, it has become imperative to tackle this challenge and develop a framework to mechanistically simulate and understand the interactions between climate and human activities. This dissertation develops a holistic understanding of the basin-wide alterations and quantify the compounded impacts of existing and planned dams, and climate change toward developing strategies for the sustainability of hydropower development.

In Chapter 2, state-of-the-art model LEAF-Hydro-Flood (LHF), together with multiple GRACE products are used to investigate the interannual and interdecadal variability in TWS and drought events in the Amazon River basin over 1980–2015 period. The chapter also provides an in-depth understanding of the interrelation between different drought types and the response of the sub-surface storage to surface drought conditions. Overall, the LHF model is found to simulate the basin-averaged TWS variations and seasonal cycle remarkably well compared to GRACE data; however, some differences are observed in the spatial distribution of temporal trends for the post-2008 period. High negative long-term trends in TWS and increasing divergence between dry-season total water deficit (TWD) and corresponding TWS release (TWS- R) indicate that the Amazon is getting wetter (1.13mm $yr^{-1}$); however, its southern and southeastern portions are getting drier. Further, the sub-surface water storage of the Amazon River basin significantly modulates the drought propagation from meteorological droughts to hydrological droughts.

In Chapter 3, a new dam operation scheme is presented which is enhanced to realistically simulate hydropower dam operation considering maximized power production by building on the recently developed high-resolution (3-arcmin; ~5km) hydrodynamic model, the CaMa-Flood-Dam. The historical impacts of existing dams and the potential impacts from collective operation of existing and planned dams on a basin-wide scale in the Amazon for 1981-2019 period are mechanistically quantified. Flood simulations are further downscaled to 3-arcsec (~90m) to investigate the impact of dams on fine-scaled flood dynamics across the basin. Results indicate that existing dams have substantially altered downstream river flow and flooding patterns in the Amazon River basin. Specifically, large dams in the sub-basins of the Amazon, including the Xingu, Madeira, and Tocantins, have altered downstream river flow by up to three orders of magnitude. Further, collective operation of existing and planned dams could increasingly alter river flow patterns, causing ~10% decrease in flood duration in many parts of the Amazon mainstem

In Chapter 4, the impacts of existing and planned large-scale hydropower dams in the Amazon are investigated under multiple climate change scenarios. Five global terrestrial hydrology models (i.e., CLM4.5, H08, LPJmL, PCR-GLOBWB, and WaterGAP) with climate forcing data from four GCMs (i.e., GFDL-esm2, Had-GEM2-ES, IPSL-CM5-LR, and MIROC5) under three cases of radiative forcing: historical climate, the low (RCP2.6) and medium-high (RCP6.0) greenhouse gas concentration scenarios are employed for the analysis. As a result of climate change the Amazon River basin is projected to experience a southwestern (dry)–northeastern (wet) contrast pattern in the mean river flow. Further, projections suggest an intensification of extreme events in the Amazon, with the lengthening of the dry season and strengthening of the monsoon, during both the mid- and late-21$^{st}$ century. The cumulative impact from the operation

of existing and planned dams, may bring forth a substantial dampening effect on the annual cycle of the river flow of the Amazon and its sub-basins. This dampening effect is found to have a substantial impact on the dry season flows with a pronounced alteration in the Tocantins, followed by Xingu, Madeira, and Tapajos River basin.

Finally, in Chapter 5, ways for sustainable hydropower generation in the Amazon River basin are explored by estimating the hydropower potential that can be harnessed by employing in-stream turbines, which utilize the kinetic energy of water. We find that ~63% of the total hydropower energy planned to be generated by storage-based dams, can be harnessed using in-stream turbines, hence completely avoiding the detrimental impacts called upon by large-scale water impoundment. At five of the nine largest planned dam sites in the Brazilian Amazon, the entirety of energy from planned hydropower could be generated using in-stream turbines, by utilizing only a fraction of river stretch that would be affected otherwise. Further, the cost (US$ $kWh^{-1}$) for in-stream turbines is found to be ~50% of the conventional hydropower cost. Overall, the findings suggest that there is high potential for using in-stream turbines in the Amazon as a viable alternative to the planned storage-based hydropower projects.

# REFERENCES

## REFERENCES


Aires, F., Miolane, L., Prigent, C., Pham, B., Fluet-Chouinard, E., Lehner, B., Papa, F., 2017. A Global Dynamic Long-Term Inundation Extent Dataset at High Spatial Resolution Derived through Downscaling of Satellite Observations. J. Hydrometeorol. 18, 1305–1325. doi:10.1175/JHM-D-16-0155.1

Alho, C.J.R., Reis, R.E., Aquino, P.P.U., 2015. Amazonian freshwater habitats experiencing environmental and socioeconomic threats affecting subsistence fisheries. Ambio 44, 412–425. doi:10.1007/s13280-014-0610-z

Amigo, I., 2020. The Amazon's fragile future. Nature 578, 505–507. doi:10.1038/d41586-020-00508-4

Anderson, D., Moggridge, H., Warren, P., Shucksmith, J., 2015. The impacts of "run-of-river" hydropower on the physical and ecological condition of rivers. Water Environ. J. 29, 268–276. doi:10.1111/wej.12101

Anderson, E.P., Jenkins, C.N., Heilpern, S., Maldonado-Ocampo, J.A., Carvajal-Vallejos, F.M., Encalada, A.C., Rivadeneira, J.F., Hidalgo, M., Cañas, C.M., Ortega, H., Salcedo, N., Maldonado, M., Tedesco, P.A., 2018. Fragmentation of Andes-to-Amazon connectivity by hydropower dams. Sci. Adv. 4, eaao1642. doi:10.1126/sciadv.aao1642

Ansar, A., Flyvbjerg, B., Budzier, A., Lunn, D., 2014. Should we build more large dams? The actual costs of hydropower megaproject development. Energy Policy 69, 43–56. doi:10.1016/j.enpol.2013.10.069

Aragão, L.E.O.C., Anderson, L.O., Fonseca, M.G., Rosan, T.M., Vedovato, L.B., Wagner, F.H., Silva, C.V.J., Silva Junior, C.H.L., Arai, E., Aguiar, A.P., Barlow, J., Berenguer, E., Deeter, M.N., Domingues, L.G., Gatti, L., Gloor, M., Malhi, Y., Marengo, J.A., Miller, J.B., Phillips, O.L., Saatchi, S., 2018. 21st Century drought-related fires counteract the decline of Amazon deforestation carbon emissions. Nat. Commun. 9, 1–12. doi:10.1038/s41467-017-02771-y

Aragão, L.E.O.C., Malhi, Y., Roman-Cuesta, R.M., Saatchi, S., Anderson, L.O., Shimabukuro, Y.E., 2007. Spatial patterns and fire response of recent Amazonian droughts. Geophys. Res. Lett. 34, L07701. doi:10.1029/2006GL028946

Arantes, A.E., Ferreira, L.G., Coe, M.T., 2016. The seasonal carbon and water balances of the Cerrado environment of Brazil: Past, present, and future influences of land cover and land use. ISPRS J. Photogramm. Remote Sens. 117, 66–78. doi:10.1016/j.isprsjprs.2016.02.008

Arantes, C.C., Fitzgerald, D.B., Hoeinghaus, D.J., Winemiller, K.O., 2019. Impacts of hydroelectric dams on fishes and fisheries in tropical rivers through the lens of functional traits. Curr. Opin. Environ. Sustain. 37, 28–40. doi:https://doi.org/10.1016/j.cosust.2019.04.009

Arias, M.E., Farinosi, F., Lee, E., Livino, A., Briscoe, J., Moorcroft, P.R., 2020. Impacts of climate change and deforestation on hydropower planning in the Brazilian Amazon. Nat. Sustain. doi:10.1038/s41893-020-0492-y

Asner, G.P., Scurlock, J.M.O., A. Hicke, J., 2003. Global synthesis of leaf area index observations: implications for ecological and remote sensing studies. Glob. Ecol. Biogeogr. 12, 191–205. doi:10.1046/j.1466-822X.2003.00026.x

Awojobi, O., Jenkins, G.P., 2015. Were the hydro dams financed by the World Bank from 1976 to 2005 worthwhile? Energy Policy 86, 222–232. doi:https://doi.org/10.1016/j.enpol.2015.06.040

Barbarossa, V., Schmitt, R.J.P., Huijbregts, M.A.J., Zarfl, C., King, H., Schipper, A.M., 2020. Impacts of current and future large dams on the geographic range connectivity of freshwater fish worldwide. Proc. Natl. Acad. Sci. 117, 201912776. doi:10.1073/pnas.1912776117

Barletta, M., Jaureguizar, A.J., Baigun, C., Fontoura, N.F., Agostinho, A.A., Almeida-Val, V.M.F., Val, A.L., Torres, R.A., Jimenes-Segura, L.F., Giarrizzo, T., Fabré, N.N., Batista, V.S., Lasso, C., Taphorn, D.C., Costa, M.F., Chaves, P.T., Vieira, J.P., Corrêa, M.F.M., 2010. Fish and aquatic habitat conservation in South America: a continental overview with emphasis on neotropical systems. J. Fish Biol. 76, 2118–2176. doi:10.1111/j.1095-8649.2010.02684.x

Barthem, R.B., Goulding, M., Leite, R.G., Cañas, C., Forsberg, B., Venticinque, E., Petry, P., Ribeiro, M.L. de B., Chuctaya, J., Mercado, A., 2017. Goliath catfish spawning in the far western Amazon confirmed by the distribution of mature adults, drifting larvae and migrating juveniles. Sci. Rep. 7, 41784. doi:10.1038/srep41784

Bates, P.D., Horritt, M.S., Fewtrell, T.J., 2010. A simple inertial formulation of the shallow water equations for efficient two-dimensional flood inundation modelling. J. Hydrol. 387, 33–45. doi:10.1016/j.jhydrol.2010.03.027

Beck, H.E., van Dijk, A.I.J.M., de Roo, A., Dutra, E., Fink, G., Orth, R., Schellekens, J., 2016. Global evaluation of runoff from ten state-of-the-art hydrological models. Hydrol. Earth Syst. Sci. Discuss. 1–33. doi:10.5194/hess-2016-124

Berga, L., 2016. The Role of Hydropower in Climate Change Mitigation and Adaptation: A Review. Engineering 2, 313–318. doi:https://doi.org/10.1016/J.ENG.2016.03.004

Berkun, M., 2010. Hydroelectric potential and environmental effects of multidam hydropower projects in Turkey. Energy Sustain. Dev. 14, 320–329. doi:10.1016/j.esd.2010.09.003

Best, J., 2019. Anthropogenic stresses on the world's big rivers. Nat. Geosci. 12, 7–21. doi:10.1038/s41561-018-0262-x

Betts, A.K., Ball, J.H., Viterbo, P., Dai, A., Marengo, J., 2005. Hydrometeorology of the Amazon in ERA-40. J. Hydrometeorol. 6, 764–774. doi:10.1175/JHM441.1

Boisier, J.P., Ciais, P., Ducharne, A., Guimberteau, M., 2015. Projected strengthening of Amazonian dry season by constrained climate model simulations. Nat. Clim. Chang. 5, 656–660. doi:10.1038/nclimate2658

Bonnet, M.P., Barroux, G., Martinez, J.M., Seyler, F., Moreira-Turcq, P., Cochonneau, G., Melack, J.M., Boaventura, G., Maurice-Bourgoin, L., León, J.G., Roux, E., Calmant, S., Kosuth, P., Guyot, J.L., Seyler, P., 2008. Floodplain hydrology in an Amazon floodplain lake (Lago Grande de Curuaí). J. Hydrol. 349, 18–30. doi:10.1016/j.jhydrol.2007.10.055

Boulange, J., Hanasaki, N., Yamazaki, D., Pokhrel, Y., 2021. Role of dams in reducing global flood exposure under climate change. Nat. Commun. 12, 417. doi:10.1038/s41467-020-20704-0

Brando, P.M., Balch, J.K., Nepstad, D.C., Morton, D.C., Putz, F.E., Coe, M.T., Silverio, D., Macedo, M.N., Davidson, E.A., Nobrega, C.C., Alencar, A., Soares-Filho, B.S., 2014. Abrupt increases in Amazonian tree mortality due to drought-fire interactions. Proc. Natl. Acad. Sci. 111, 6347–6352. doi:10.1073/pnas.1305499111

Brondizio, E.S., Moran, E.F., 2008. Human dimensions of climate change: The vulnerability of small farmers in the Amazon. Philos. Trans. R. Soc. B Biol. Sci. 363, 1803–1809. doi:10.1098/rstb.2007.0025

Bryden, I.G., Couch, S.J., 2006. ME1—marine energy extraction: tidal resource analysis. Renew. Energy 31, 133–139. doi:https://doi.org/10.1016/j.renene.2005.08.012

Cardinale, B.J., Duffy, J.E., Gonzalez, A., Hooper, D.U., Perrings, C., Venail, P., Narwani, A., Mace, G.M., Tilman, D., Wardle, D.A., Kinzig, A.P., Daily, G.C., Loreau, M., Grace, J.B., Larigauderie, A., Srivastava, D.S., Naeem, S., 2012. Biodiversity loss and its impact on humanity. Nature 486, 59–67. doi:10.1038/nature11148

Castello, L., Isaac, V.J., Thapa, R., 2015. Flood pulse effects on multispecies fishery yields in the Lower Amazon. R. Soc. Open Sci. 2, 150299. doi:10.1098/rsos.150299

Castello, L., Macedo, M.N., 2016. Large-scale degradation of Amazonian freshwater ecosystems. Glob. Chang. Biol. 22, 990–1007. doi:10.1111/gcb.13173

Castello, L., Mcgrath, D.G., Hess, L.L., Coe, M.T., Lefebvre, P.A., Petry, P., Macedo, M.N., Renó, V.F., Arantes, C.C., 2013. The vulnerability of Amazon freshwater ecosystems. Conserv. Lett. 6, 217–229. doi:10.1111/conl.12008

Chaudhari, S., Brown, E., Quispe-Abad, R., Moran, E., Müller, N., Pokhrel, Y., 2021. In-stream turbines for rethinking hydropower development in the Amazon basin. Nat. Sustain. doi:10.1038/s41893-021-00712-8

Chaudhari, S., Felfelani, F., Shin, S., Pokhrel, Y., 2018. Climate and Anthropogenic Contributions to the Desiccation of the Second Largest Saline Lake in the Twentieth Century. J. Hydrol. 560, 342–353. doi:https://doi.org/10.1016/j.jhydrol.2018.03.034

Chaudhari, S., Pokhrel, Y., Moran, E.F., Miguez-Macho, G., 2019. Multi-decadal Hydrologic Change and Variability in the Amazon River Basin: Understanding Terrestrial Water Storage Variations and Drought Characteristics. Hydrol. Earth Syst. Sci. 23, 2841–2862. doi:10.5194/hess-23-2841-2019

Chen, G., Powers, R.P., de Carvalho, L.M.T., Mora, B., 2015. Spatiotemporal patterns of tropical deforestation and forest degradation in response to the operation of the Tucuruí hydroelectric dam in the Amazon basin. Appl. Geogr. 63, 1–8. doi:10.1016/j.apgeog.2015.06.001

Chen, J.L., Wilson, C.R., Tapley, B.D., 2010. The 2009 exceptional Amazon flood and interannual terrestrial water storage change observed by GRACE. Water Resour. Res. 46, 1–10. doi:10.1029/2010WR009383

Chen, J.L., Wilson, C.R., Tapley, B.D., Yang, Z.L., Niu, G.Y., 2009. 2005 drought event in the Amazon River basin as measured by GRACE and estimated by climate models. J. Geophys. Res. Solid Earth 114, 1–9. doi:10.1029/2008JB006056

Christensen, N.S., Christensen, N.S., Wood, A.W., Wood, A.W., Voisin, N., Voisin, N., Lettenmaier, D.P., Lettenmaier, D.P., Palmer, R.N., Palmer, R.N., 2004. The Effects of Climate Change on the Hydrology and Water Resources of the Colorado River Basin. Clim. Change 62, 337–363. doi:10.1023/B:CLIM.0000013684.13621.1f

Clapp, R.B., Hornberger, G.M., 1978. Empirical equations for some soil hydraulic properties. Water Resour. Res. 14, 601–604. doi:10.1029/WR014i004p00601

Clark, E.A., Sheffield, J., van Vliet, M.T.H., Nijssen, B., Lettenmaier, D.P., 2015. Continental Runoff into the Oceans (1950–2008). J. Hydrometeorol. 16, 1502–1520. doi:10.1175/JHM-D-14-0183.1

Cochrane, S.M.V., Matricardi, E.A.T., Numata, I., Lefebvre, P.A., 2017. Landsat-based analysis of mega dam flooding impacts in the Amazon compared to associated environmental impact assessments: Upper Madeira River example 2006–2015. Remote Sens. Appl. Soc. Environ. 7, 1–8. doi:10.1016/j.rsase.2017.04.005

Cochrane, T.A., Arias, M.E., Piman, T., 2014. Historical impact of water infrastructure on water levels of the Mekong River and the Tonle Sap system. Hydrol. Earth Syst. Sci. 18, 4529–4541. doi:10.5194/hess-18-4529-2014

Coe, M.T., Costa, M.H., Botta, A., Birkett, C., 2002. Long-term simulations of discharge and floods in the Amazon Basin. J. Geophys. Res. Atmos. 107, 1–17. doi:10.1029/2001JD000740

Coe, M.T., Costa, M.H., Howard, E.A., 2008. Simulating the surface waters of the Amazon River basin: impacts of new river geomorphic and flow parameterizations. Hydrol. Process. 22, 2542–2553. doi:10.1002/hyp.6850

Coe, M.T., Costa, M.H., Soares-Filho, B.S., 2009. The influence of historical and potential future

deforestation on the stream flow of the Amazon River - Land surface processes and atmospheric feedbacks. J. Hydrol. 369, 165–174. doi:10.1016/j.jhydrol.2009.02.043

Cook, B., Zeng, N., Yoon, J.H., 2012. Will Amazonia dry out? Magnitude and causes of change from IPCC climate model projections. Earth Interact. 16. doi:10.1175/2011EI398.1

Cook, K.H., Vizy, E.K., 2008. Effects of twenty-first-century climate change on the Amazon rain forest. J. Clim. 21, 542–560. doi:10.1175/2007JCLI1838.1

Copping, A.E.., Hemery, L.G., 2020. OES-Environmental 2020 State of the Science Report: Environmental Effects of Marine Renewable Energy Development Around the World. doi:10.2172/1632878

Costa, M.H., Botta, A., Cardille, J.A., 2003. Effects of large-scale changes in land cover on the discharge of the Tocantins River, Southeastern Amazonia. J. Hydrol. 283, 206–217. doi:10.1016/S0022-1694(03)00267-1

Costa, M.H., Foley, J.A., 1999. Trends in the hydrologic cycle of the Amazon Basin. J. Geophys. Res. Atmos. 104, 14189–14198. doi:10.1029/1998JD200126

Cox, P.M., Betts, R.A., Collins, M., Harris, P.P., Huntingford, C., Jones, C.D., 2004. Amazonian forest dieback under climate-carbon cycle projections for the 21st century. Theor. Appl. Climatol. 78, 137–156. doi:10.1007/s00704-004-0049-4

da Costa, C.L., Galbraith, D., Almeida, S., Tanaka Portela, B.T., da Costa, M., de Athaydes Silva Junior, J., Braga, A.P., de Gonçalves, P.H.L., de Oliveira, A.A., Fisher, R., Phillips, O., Metcalfe, D.B., Levy, P., Meir, P., 2010. Effect of seven years of experimental drought on the aboveground biomass storage of an eastern Amazonian rainforest. New Phytol. 187, 579–591. doi:10.1111/j.1469-8137.2010.03309.x

Davidson, E.A., de Araújo, A.C., Artaxo, P., Balch, J.K., Brown, I.F., C. Bustamante, M.M., Coe, M.T., DeFries, R.S., Keller, M., Longo, M., Munger, J.W., Schroeder, W., Soares-Filho, B.S., Souza, C.M., Wofsy, S.C., 2012. The Amazon basin in transition. Nature 481, 321–328. doi:10.1038/nature10717

Dias, L.C.P., Macedo, M.N., Costa, M.H., Coe, M.T., Neill, C., 2015. Effects of land cover change on evapotranspiration and streamflow of small catchments in the Upper Xingu River Basin, Central Brazil. J. Hydrol. Reg. Stud. 4, 108–122. doi:10.1016/j.ejrh.2015.05.010

Dórea, J.G., Barbosa, A.C., 2007. Anthropogenic impact of mercury accumulation in fish from the Rio Madeira and Rio Negro Rivers (Amazonia). Biol. Trace Elem. Res. 115, 243–254. doi:10.1007/BF02685999

Eiriksdottir, E.S., Oelkers, E.H., Hardardottir, J., Gislason, S.R., 2017. The impact of damming on riverine fluxes to the ocean: A case study from Eastern Iceland. Water Res. 113, 124–138. doi:https://doi.org/10.1016/j.watres.2016.12.029

Electrical Power Research Institute (EPRI), 2012. Assessment and Mapping of the Riverine

Hydrokinetic Energy Resource in the Continental United States, Rep. No. 1026880, Palo Alto, CA.

Eltahir, E.A.B., Bras, R.L., 1994. Precipitation recycling in the Amazon basin. Q. J. R. Meteorol. Soc. 120, 861–880. doi:10.1002/qj.49712051806

Espinoza, J.C., Chavez, S., Ronchail, J., Junquas, C., Takahashi, K., Lavado, W., 2015. Rainfall hotspots over the southern tropical Andes: Spatial distribution, rainfall intensity, and relations with large-scale atmospheric circulation. Water Resour. Res. 51, 3459–3475. doi:10.1002/2014WR016273

Espinoza, J.C., Guyot, J.L., Ronchail, J., Cochonneau, G., Filizola, N., Fraizy, P., Labat, D., de Oliveira, E., Ordoñez, J.J., Vauchel, P., 2009. Contrasting regional discharge evolutions in the Amazon basin (1974-2004). J. Hydrol. 375, 297–311. doi:10.1016/j.jhydrol.2009.03.004

Espinoza, J.C., Ronchail, J., Guyot, J.L., Junquas, C., Vauchel, P., Lavado, W., Drapeau, G., Pombosa, R., 2011. Climate variability and extreme drought in the upper Solimões River (western Amazon Basin): Understanding the exceptional 2010 drought. Geophys. Res. Lett. 38, 1–6. doi:10.1029/2011GL047862

Espinoza, J.C., Segura, H., Ronchail, J., Drapeau, G., Gutierrez-Cori, O., 2016. Evolution of wet-day and dry-day frequency in the western Amazon basin: Relationship with atmospheric circulation and impacts on vegetation. Water Resour. Res. 52, 8546–8560. doi:10.1002/2016WR019305

Espinoza Villar, J.C., Ronchail, J., Guyot, J.L., Cochonneau, G., Naziano, F., Lavado, W., De Oliveira, E., Pombosa, R., Vauchel, P., 2009. Spatio-temporal rainfall variability in the Amazon basin countries (Brazil, Peru, Bolivia, Colombia, and Ecuador). Int. J. Climatol. 29, 1574–1594. doi:10.1002/joc.1791

Fan, Y., Clark, M., Lawrence, D.M., Swenson, S., Band, L.E., Brantley, S.L., Brooks, P.D., Dietrich, W.E., Flores, A., Grant, G., Kirchner, J.W., Mackay, D.S., McDonnell, J.J., Milly, P.C.D., Sullivan, P.L., Tague, C., Ajami, H., Chaney, N., Hartmann, A., Hazenberg, P., McNamara, J., Pelletier, J., Perket, J., Rouholahnejad-Freund, E., Wagener, T., Zeng, X., Beighley, E., Buzan, J., Huang, M., Livneh, B., Mohanty, B.P., Nijssen, B., Safeeq, M., Shen, C., van Verseveld, W., Volk, J., Yamazaki, D., 2019. Hillslope Hydrology in Global Change Research and Earth System Modeling. Water Resour. Res. 55, 1737–1772. doi:10.1029/2018WR023903

Fan, Y., Li, H., Miguez-Macho, G., 2013. Global Patterns of Groundwater Table Depth. Science (80-. ). 339, 940–943. doi:10.1126/science.1229881

Fan, Y., Miguez-Macho, G., 2010. Potential groundwater contribution to Amazon evapotranspiration. Hydrol. Earth Syst. Sci. 14, 2039–2056. doi:10.5194/hess-14-2039-2010

Fearnside, P.M., 2015. Amazon dams and waterways: Brazil's Tapajós Basin plans. Ambio 44, 426–439. doi:10.1007/s13280-015-0642-z

Fearnside, P.M., 2014. Impacts of Brazil's Madeira River dams: Unlearned lessons for hydroelectric development in Amazonia. Environ. Sci. Policy 38, 164–172. doi:10.1016/j.envsci.2013.11.004

Fearnside, P.M., 2006. Dams in the Amazon: Belo Monte and Brazil's hydroelectric development of the Xingu River Basin. Environ. Manage. 38, 16–27. doi:10.1007/s00267-005-0113-6

Fearnside, P.M., Pueyo, S., 2012. Greenhouse-gas emissions from tropical dams. Nat. Clim. Chang. 2, 382.

Felfelani, F., Wada, Y., Longuevergne, L., Pokhrel, Y.N., 2017. Natural and human-induced terrestrial water storage change: A global analysis using hydrological models and GRACE. J. Hydrol. 553, 105–118. doi:10.1016/j.jhydrol.2017.07.048

Fernandes, K., Baethgen, W., Bernardes, S., Defries, R., Dewitt, D.G., Goddard, L., Lavado, W., Lee, D.E., Padoch, C., Pinedo-Vasquez, M., Uriarte, M., 2011. North Tropical Atlantic influence on western Amazon fire season variability. Geophys. Res. Lett. 38, 1–5. doi:10.1029/2011GL047392

Fernandes, K., Fu, R., Betts, A.K., 2008. How well does the ERA40 surface water budget compare to observations in the Amazon River basin? J. Geophys. Res. Atmos. 113, 1–9. doi:10.1029/2007JD009220

Field, C.B., Behrenfeld, M.J., Randerson, J.T., Falkowski, P., 1998. Primary Production of the Biosphere: Integrating Terrestrial and Oceanic Components. Science (80-. ). 281, 237–240. doi:10.1126/science.281.5374.237

Filizola, N., Latrubesse, E.M., Fraizy, P., Souza, R., Guimarães, V., Guyot, J.L., 2014. Was the 2009 flood the most hazardous or the largest ever recorded in the Amazon? Geomorphology 215, 99–105. doi:10.1016/j.geomorph.2013.05.028

Finer, M., Jenkins, C.N., 2012. Proliferation of hydroelectric dams in the andean amazon and implications for andes-amazon connectivity. PLoS One 7, 1–9. doi:10.1371/journal.pone.0035126

Forsberg, B.R., Melack, J.M., Dunne, T., Barthem, R.B., Goulding, M., Paiva, R.C.D., Sorribas, M. V., Silva, U.L., Weisser, S., 2017. The potential impact of new Andean dams on Amazon fluvial ecosystems. PLoS One 12, 1–35. doi:10.1371/journal.pone.0182254

Frappart, F., Papa, F., Güntner, A., Werth, S., Santos da Silva, J., Tomasella, J., Seyler, F., Prigent, C., Rossow, W.B., Calmant, S., Bonnet, M.P., 2011. Satellite-based estimates of groundwater storage variations in large drainage basins with extensive floodplains. Remote Sens. Environ. 115, 1588–1594. doi:10.1016/j.rse.2011.02.003

Frappart, F., Ramillien, G., Ronchail, J., 2013. Changes in terrestrial water storage versus rainfall and discharges in the Amazon basin. Int. J. Climatol. 33, 3029–3046. doi:10.1002/joc.3647

Freitas, F.L.M., Sparovek, G., Berndes, G., Persson, U.M., Englund, O., Barretto, A., Mörtberg, U., 2018. Potential increase of legal deforestation in Brazilian Amazon after Forest Act revision. Nat. Sustain. 1, 665–670. doi:10.1038/s41893-018-0171-4

Frieler, K., Lange, S., Piontek, F., Reyer, C.P.O., Schewe, J., Warszawski, L., Zhao, F., Chini, L., Denvil, S., Emanuel, K., Geiger, T., Halladay, K., Hurtt, G., Mengel, M., Murakami, D., Ostberg, S., Popp, A., Riva, R., Stevanovic, M., Suzuki, T., Volkholz, J., Burke, E., Ciais, P., Ebi, K., Eddy, T.D., Elliott, J., Galbraith, E., Gosling, S.N., Hattermann, F., Hickler, T., Hinkel, J., Hof, C., Huber, V., Jägermeyr, J., Krysanova, V., Marcé, R., Müller Schmied, H., Mouratiadou, I., Pierson, D., Tittensor, D.P., Vautard, R., van Vliet, M., Biber, M.F., Betts, R.A., Bodirsky, B.L., Deryng, D., Frolking, S., Jones, C.D., Lotze, H.K., Lotze-Campen, H., Sahajpal, R., Thonicke, K., Tian, H., Yamagata, Y., 2017. Assessing the impacts of 1.5°C global warming – simulation protocol of the Inter-Sectoral Impact Model Intercomparison Project (ISIMIP2b). Geosci. Model Dev. 10, 4321–4345. doi:10.5194/gmd-10-4321-2017

Gernaat, D.E.H.J., Bogaart, P.W., Vuuren, D.P.V., Biemans, H., Niessink, R., 2017. High-resolution assessment of global technical and economic hydropower potential. Nat. Energy 2, 821–828. doi:10.1038/s41560-017-0006-y

Gernaat, D.E.H.J., de Boer, H.S., Daioglou, V., Yalew, S.G., Müller, C., van Vuuren, D.P., 2021. Climate change impacts on renewable energy supply. Nat. Clim. Chang. 11, 119–125. doi:10.1038/s41558-020-00949-9

Getirana, A.C. V., Bonnet, M.-P., Rotunno Filho, O.C., Collischonn, W., Guyot, J.-L., Seyler, F., Mansur, W.J., 2010. Hydrological modelling and water balance of the Negro River basin: evaluation based on in situ and spatial altimetry data. Hydrol. Process. 24, 3219–3236. doi:10.1002/hyp.7747

Getirana, A.C. V., Boone, A., Yamazaki, D., Decharme, B., Papa, F., Mognard, N., 2012. The Hydrological Modeling and Analysis Platform (HyMAP): Evaluation in the Amazon Basin. J. Hydrometeorol. 13, 1641–1665. doi:10.1175/JHM-D-12-021.1

Gloor, M., Brienen, R.J.W., Galbraith, D., Feldpausch, T.R., Schöngart, J., Guyot, J.L., Espinoza, J.C., Lloyd, J., Phillips, O.L., 2013. Intensification of the Amazon hydrological cycle over the last two decades. Geophys. Res. Lett. 40, 1729–1733. doi:10.1002/grl.50377

Gridded Population of the World, Version 4 (GPWv4): Population Count Adjusted to Match 2015 Revision of UN WPP Country Totals, 2016. . Cent. Int. Earth Sci. Inf. Netw. doi:http://dx.doi.org/10.7927/H4SF2T42

Grill, G., Lehner, B., Thieme, M., Geenen, B., Tickner, D., Antonelli, F., Babu, S., Borrelli, P., Cheng, L., Crochetiere, H., Ehalt Macedo, H., Filgueiras, R., Goichot, M., Higgins, J., Hogan, Z., Lip, B., McClain, M.E., Meng, J., Mulligan, M., Nilsson, C., Olden, J.D., Opperman, J.J., Petry, P., Reidy Liermann, C., Sáenz, L., Salinas-Rodríguez, S., Schelle, P., Schmitt, R.J.P., Snider, J., Tan, F., Tockner, K., Valdujo, P.H., van Soesbergen, A., Zarfl, C., 2019. Mapping the world's free-flowing rivers. Nature 569, 215–221. doi:10.1038/s41586-019-1111-9

Guan, K., Pan, M., Li, H., Wolf, A., Wu, J., Medvigy, D., Caylor, K.K., Sheffield, J., Wood, E.F., Malhi, Y., Liang, M., Kimball, J.S., Saleska, S.R., Berry, J., Joiner, J., Lyapustin, A.I., 2015. Photosynthetic seasonality of global tropical forests constrained by hydroclimate. Nat. Geosci. 8, 284–289. doi:10.1038/ngeo2382

Gudmundsson, L., Boulange, J., Do, H.X., Gosling, S.N., Grillakis, M.G., Koutroulis, A.G., Leonard, M., Liu, J., Müller Schmied, H., Papadimitriou, L., Pokhrel, Y., Seneviratne, S.I., Satoh, Y., Thiery, W., Westra, S., Zhang, X., Zhao, F., 2021. Globally observed trends in mean and extreme river flow attributed to climate change. Science (80-. ). 371, 1159 LP – 1162. doi:10.1126/science.aba3996

Guimberteau, M., Ciais, P., Pablo Boisier, J., Paula Dutra Aguiar, A., Biemans, H., De Deurwaerder, H., Galbraith, D., Kruijt, B., Langerwisch, F., Poveda, G., Rammig, A., Andres Rodriguez, D., Tejada, G., Thonicke, K., Von Randow, C., Randow, R., Zhang, K., Verbeeck, H., 2017. Impacts of future deforestation and climate change on the hydrology of the Amazon Basin: A multi-model analysis with a new set of land-cover change scenarios. Hydrol. Earth Syst. Sci. 21, 1455–1475. doi:10.5194/hess-21-1455-2017

Guney, M.S., 2011. Evaluation and measures to increase performance coefficient of hydrokinetic turbines. Renew. Sustain. Energy Rev. 15, 3669–3675. doi:https://doi.org/10.1016/j.rser.2011.07.009

Haddeland, I., Heinke, J., Biemans, H., Eisner, S., Flörke, M., Hanasaki, N., Konzmann, M., Ludwig, F., Masaki, Y., Schewe, J., Stacke, T., Tessler, Z.D., Wada, Y., Wisser, D., 2014. Global water resources affected by human interventions and climate change. Proc. Natl. Acad. Sci. U. S. A. 111, 3251–6. doi:10.1073/pnas.1222475110

Haddeland, I., Skaugen, T., Lettenmaier, D.P., 2006. Anthropogenic impacts on continental surface water fluxes. Geophys. Res. Lett. 33.

Hall, D.G., Hunt, R.T., Reeves, K.S., Carroll, G.R., 2003. Estimation of Economic Parameters of U.S. Hydropower Resources.

Hanasaki, N., Yoshikawa, S., Pokhrel, Y., Kanae, S., 2018. A global hydrological simulation to specify the sources of water used by humans. Hydrol. Earth Syst. Sci. Discuss. 08, 1–53. doi:10.5194/hess-2017-280

Hansen, M.C., Potapov, P. V, Moore, R., Hancher, M., Turubanova, S.A., Tyukavina, A., Thau, D., Stehman, S. V, Goetz, S.J., Loveland, T.R., Kommareddy, A., Egorov, A., Chini, L., Justice, C.O., Townshend, J.R.G., 2013. High-Resolution Global Maps of 21st-Century Forest Cover Change. Science (80-. ). 342, 850 LP – 853. doi:10.1126/science.1244693

Hirabayashi, Y., Mahendran, R., Koirala, S., Konoshima, L., Yamazaki, D., Watanabe, S., Kim, H., Kanae, S., 2013. Global flood risk under climate change. Nat. Clim. Chang. 3, 816–821. doi:10.1038/nclimate1911

Hoes, O.A.C., Meijer, L.J.J., Van Der Ent, R.J., Van De Giesen, N.C., 2017. Systematic high-resolution assessment of global hydropower potential. PLoS One 12, 1–10.

doi:10.1371/journal.pone.0171844

IEA, 2021. Global Energy Review 2021, IEA, Paris. doi:10.1787/a60abbf2-en

International Renewable Energy Agency (IRENA), 2019a. Renewable energy highlights.

International Renewable Energy Agency (IRENA), 2019b. Renewable capacity highlights.

International Renewable Energy Agency (IRENA), 2019c. Renewable Power Generation Costs in 2019.

International Rivers, n.d. The State of the World's Rivers [WWW Document]. www.internationalrivers.org/worldsrivers.

Jiménez-Muñoz, J.C., Mattar, C., Barichivich, J., Santamaría-Artigas, A., Takahashi, K., Malhi, Y., Sobrino, J.A., Schrier, G. Van Der, 2016. Record-breaking warming and extreme drought in the Amazon rainforest during the course of El Niño 2015-2016. Sci. Rep. 6, 1–7. doi:10.1038/srep33130

Joetzjer, E., Douville, H., Delire, C., Ciais, P., Decharme, B., Tyteca, S., 2013. Hydrologic benchmarking of meteorological drought indices at interannual to climate change timescales: A case study over the Amazon and Mississippi river basins. Hydrol. Earth Syst. Sci. 17, 4885–4895. doi:10.5194/hess-17-4885-2013

Kahn, J.R., Freitas, C.E., Petrere, M., 2014. False shades of green: The case of Brazilian Amazonian hydropower. Energies 7, 6063–6082. doi:10.3390/en7096063

Kalamandeen, M., Gloor, E., Mitchard, E., Quincey, D., Ziv, G., Spracklen, D., Spracklen, B., Adami, M., Aragão, L.E.O.C., Galbraith, D., 2018. Pervasive Rise of Small-scale Deforestation in Amazonia. Nature 8, 1600. doi:10.1038/s41598-018-19358-2

Karsten, R., Swan, A., Culina, J., 2013. Assessment of arrays of in-stream tidal turbines in the Bay of Fundy. Philos. Trans. R. Soc. A Math. Phys. Eng. Sci. 371, 20120189. doi:10.1098/rsta.2012.0189

Kemenes, A., Forsberg, B.R., Melack, J.M., 2011. CO2 emissions from a tropical hydroelectric reservoir (Balbina, Brazil). J. Geophys. Res. Biogeosciences 116, 1–11. doi:10.1029/2010JG001465

Kemenes, A., Forsberg, B.R., Melack, J.M., 2007. Methane release below a tropical hydroelectric dam. Geophys. Res. Lett. 34, 1–5. doi:10.1029/2007GL029479

Kleinschroth, F., Laporte, N., Laurance, W.F., Goetz, S.J., Ghazoul, J., 2019. Road expansion and persistence in forests of the Congo Basin. Nat. Sustain. 2, 628–634. doi:10.1038/s41893-019-0310-6

Landerer, F.W., Swenson, S.C., 2012. Accuracy of scaled GRACE terrestrial water storage estimates. Water Resour. Res. 48, 1–11. doi:10.1029/2011WR011453

Latrubesse, E.M., Arima, E.Y., Dunne, T., Park, E., Baker, V.R., d'Horta, F.M., Wight, C., Wittmann, F., Zuanon, J., Baker, P.A., Ribas, C.C., Norgaard, R.B., Filizola, N., Ansar, A., Flyvbjerg, B., Stevaux, J.C., 2017. Damming the rivers of the Amazon basin. Nature 546, 363–369. doi:10.1038/nature22333

Lee, J.-E., Lintner, B.R., Boyce, C.K., Lawrence, P.J., 2011. Land use change exacerbates tropical South American drought by sea surface temperature variability. Geophys. Res. Lett. 38. doi:10.1029/2011GL049066

Lehner, B., Grill, G., 2013. Global river hydrography and network routing: baseline data and new approaches to study the world's large river systems. Hydrol. Process. 27, 2171–2186. doi:10.1002/hyp.9740

Lehner, B., Liermann, C.R., Revenga, C., Vörösmarty, C., Fekete, B., Crouzet, P., Döll, P., Endejan, M., Frenken, K., Magome, J., Nilsson, C., Robertson, J.C., Rödel, R., Sindorf, N., Wisser, D., 2011. High-resolution mapping of the world's reservoirs and dams for sustainable river-flow management. Front. Ecol. Environ. 9, 494–502. doi:10.1890/100125

Lehner, B., Verdin, K., Jarvis, A., 2008. New global hydrography derived from spaceborne elevation data. Eos, Trans. Am. Geophys. Union 89, 93–94. doi:10.1029/2008EO100001

Lenton, T.M., Held, H., Kriegler, E., Hall, J.W., Lucht, W., Rahmstorf, S., Schellnhuber, H.J., 2009. Tipping elements in the Earth System. Proc. Natl. Acad. Sci. 106, 20561–20563. doi:10.1073/pnas.0911106106

Lesack, L.F.W., 1993. Water Balance and Hydrologic Characteristics of a Rain Forest Catchment in the Central Amazon Basin. Water Resour. Res. 29, 759–773.

Lewis, S.L., Brando, P.M., Phillips, O.L., van der Heijden, G.M.F., Nepstad, D., 2011. The 2010 Amazon Drought. Science (80-. ). 331, 554 LP – 554. doi:10.1126/science.1200807

Liang, S., Xiao, Z., 2012. Global land surface products: Leaf area index product data collection (1985–2010). Beijing Norm. Univ.

Lima, Letícia S., Coe, M.T., Soares Filho, B.S., Cuadra, S. V., Dias, L.C.P., Costa, M.H., Lima, Leandro S., Rodrigues, H.O., 2014. Feedbacks between deforestation, climate, and hydrology in the Southwestern Amazon: Implications for the provision of ecosystem services. Landsc. Ecol. 29, 261–274. doi:10.1007/s10980-013-9962-1

Longuevergne, L., Scanlon, B.R., Wilson, C.R., 2010. GRACE hydrological estimates for small basins: Evaluating processing approaches on the High Plains aquifer, USA. Water Resour. Res. 46, 1–15. doi:10.1029/2009WR008564

Lovejoy, T.E., Nobre, C., 2018. Amazon Tipping Point. Sci. Adv. 4, eaat2340. doi:10.1126/sciadv.aat2340

Malhi, Y., Aragão, L.E.O.C., Galbraith, D., Huntingford, C., Fisher, R., Zelazowski, P., Sitch, S., McSweeney, C., Meir, P., 2009. Exploring the likelihood and mechanism of a climate-

change-induced dieback of the Amazon rainforest. Proc. Natl. Acad. Sci. 106, 20610–20615. doi:10.1073/pnas.0804619106

Malhi, Y., Roberts, J.T., Betts, R. a, Killeen, T.J., Li, W., Nobre, C. a, 2008. Climate Change, Deforestation, and the Fate of the Amazon. Science (80-. ). 319, 169–172. doi:10.1126/science.1146961

Malki, R., Masters, I., Williams, A.J., Nick Croft, T., 2014. Planning tidal stream turbine array layouts using a coupled blade element momentum – computational fluid dynamics model. Renew. Energy 63, 46–54. doi:https://doi.org/10.1016/j.renene.2013.08.039

Marengo, J.A., 2006. On the Hydrological Cycle of the Amazon Basin: A Historical Review and Current State-of-the-art. Rev. Bras. Meteorol. 21, 1–19.

Marengo, J.A., 2005. Characteristics and spatio-temporal variability of the Amazon river basin water budget. Clim. Dyn. 24, 11–22. doi:10.1007/s00382-004-0461-6

Marengo, J.A., 2004. Interdecadal variability and trends of rainfall across the Amazon basin. Theor. Appl. Climatol. 78, 79–96. doi:10.1007/s00704-004-0045-8

Marengo, J.A., 1995. Variations and change in south American streamflow. Clim. Change 31, 99–117. doi:10.1007/BF01092983

Marengo, J.A., 1992. Interannual variability of surface climate in the Amazon basin. Int. J. Climatol. 12, 853–863.

Marengo, J.A., Espinoza, J.C., 2016. Extreme seasonal droughts and floods in Amazonia: Causes, trends and impacts. Int. J. Climatol. 36, 1033–1050. doi:10.1002/joc.4420

Marengo, J.A., Nobre, C.A., Tomasella, J., Oyama, M.D., Sampaio de Oliveira, G., de Oliveira, R., Camargo, H., Alves, L.M., Brown, I.F., 2008. The Drought of Amazonia in 2005. J. Clim. 21, 495–516. doi:10.1175/2007JCLI1600.1

Marengo, J.A., Tomasella, J., Alves, L.M., Soares, W.R., Rodriguez, D.A., 2011. The drought of 2010 in the context of historical droughts in the Amazon region. Geophys. Res. Lett. 38, 1–5. doi:10.1029/2011GL047436

Marengo, J.A., Tomasella, J., Uvo, C.R., 1998. Trends in streamflow and rainfall in tropical South America: Amazonia, eastern Brazil, and northwestern Peru. J. Geophys. Res. Atmos. 103, 1775–1783. doi:10.1029/97JD02551

Matsuyama, H., 1992. The Water Budget in the Amazon River Basin during the FGGE Period. Meteorol. Soc. Japan 1071–1084.

Mckee, T.B., Doesken, N.J., Kleist, J., 1993. The relationship of drought frequency and duration to time scales. AMS 8th Conf. Appl. Climatol. 179–184. doi:citeulike-article-id:10490403

Miguez-Macho, G., Fan, Y., 2012a. The role of groundwater in the Amazon water cycle: 1.

Influence on seasonal streamflow, flooding and wetlands. J. Geophys. Res. Atmos. 117, 1–30. doi:10.1029/2012JD017539

Miguez-Macho, G., Fan, Y., 2012b. The role of groundwater in the Amazon water cycle: 2. Influence on seasonal soil moisture and evapotranspiration. J. Geophys. Res. Atmos. 117. doi:10.1029/2012JD017540

Miguez-Macho, G., Li, H., Fan, Y., 2008. Simulated water table and soil moisture climatology over North America. Bull. Am. Meteorol. Soc. 89, 663–672. doi:10.1175/BAMS-89-5-663

Ministry of mines and energy, B., 2019. 10-year energy expansion plan 2029, Brazil.

Monteiro, J.A.F., Strauch, M., Srinivasan, R., Abbaspour, K., Gücker, B., 2016. Accuracy of grid precipitation data for Brazil: Application in river discharge modelling of the Tocantins catchment. Hydrol. Process. 30, 1419–1430. doi:10.1002/hyp.10708

Monteith, J.L., 1965. Evaporation and environment. The state and movement of water in living organisms. Symposium of the society of experimental biology, Vol. 19 (pp. 205-234).

Moran, E.F., Lopez, M.C., Moore, N., Müller, N., Hyndman, D.W., 2018. Sustainable hydropower in the 21st century. Proc. Natl. Acad. Sci. 115, 201809426. doi:10.1073/pnas.1809426115

Muller-Karger, F.E., McClain, C.R., Richardson, P.L., 1988. The dispersal of the Amazon's water. Nature 333, 56–59. doi:10.1038/332141a0

Mulligan, M.., Saenz-Cruz, L.., van Soesbergen, A.., Smith, V.T.., Zurita, L., 2009. Global dams database and geowiki. Version 1 [WWW Document]. http://geodata.policysupport.org/dams. URL http://geodata.policysupport.org/dams

Myneni, R.B., Yang, W., Nemani, R.R., Huete, A.R., Dickinson, R.E., Knyazikhin, Y., Didan, K., Fu, R., Negron Juarez, R.I., Saatchi, S.S., Hashimoto, H., Ichii, K., Shabanov, N. V., Tan, B., Ratana, P., Privette, J.L., Morisette, J.T., Vermote, E.F., Roy, D.P., Wolfe, R.E., Friedl, M.A., Running, S.W., Votava, P., El-Saleous, N., Devadiga, S., Su, Y., Salomonson, V. V., 2007. Large seasonal swings in leaf area of Amazon rainforests. Proc. Natl. Acad. Sci. 104, 4820–4823. doi:10.1073/pnas.0611338104

Nepstad, D.C., Stickler, C.M., Filho, B.S., Merry, F., 2008. Interactions among Amazon land use, forests and climate: prospects for a near-term forest tipping point. Philos. Trans. R. Soc. B Biol. Sci. 363, 1737–1746. doi:10.1098/rstb.2007.0036

Newbold, T., Hudson, L.N., Arnell, A.P., Contu, S., De Palma, A., Ferrier, S., Hill, S.L.L., Hoskins, A.J., Lysenko, I., Phillips, H.R.P., Burton, V.J., Chng, C.W.T., Emerson, S., Gao, D., Pask-Hale, G., Hutton, J., Jung, M., Sanchez-Ortiz, K., Simmons, B.I., Whitmee, S., Zhang, H., Scharlemann, J.P.W., Purvis, A., 2016. Has land use pushed terrestrial biodiversity beyond the planetary boundary? A global assessment. Science (80-. ). 353, 288 LP – 291. doi:10.1126/science.aaf2201

Nilsson, C., Reidy, C.A., Dynesius, M., Revenga, C., 2005. Fragmentation and Flow Regulation of the World ' s Large River Systems. Science (80-. ). 308, 405–408. doi:10.1126/science.1107887

Nobre, C.A., Sampaio, G., Borma, L.S., Castilla-Rubio, J.C., Silva, J.S., Cardoso, M., 2016. Land-use and climate change risks in the Amazon and the need of a novel sustainable development paradigm. Proc. Natl. Acad. Sci. 113, 10759 LP – 10768. doi:10.1073/pnas.1605516113

Nobre, C.A., Sellers, P.J., Shukla, J., 1991. Amazonian Deforestation and Regional Climate Change. J. Clim. 4, 957–988. doi:10.1175/1520-0442(1991)004<0957:ADARCC>2.0.CO;2

O'Connor, J.E., Duda, J.J., Grant, G.E., 2015. 1000 dams down and counting. Science (80-. ). 348, 496 LP – 497. doi:10.1126/science.aaa9204

Ortega-Achury, S., McAnally, W., Davis, T., Martin, J., 2010. Hydrokinetic power review, Mississippi State University.

Paiva, Rodrigo Cauduro Dias, Buarque, D.C., Collischonn, W., Bonnet, M.P., Frappart, F., Calmant, S., Bulhões Mendes, C.A., 2013. Large-scale hydrologic and hydrodynamic modeling of the Amazon River basin. Water Resour. Res. 49, 1226–1243. doi:10.1002/wrcr.20067

Paiva, Rodrigo C D, Collischonn, W., Bonnet, M.P., De Gonçalves, L.G.G., Calmant, S., Getirana, A., Santos Da Silva, J., 2013. Assimilating in situ and radar altimetry data into a large-scale hydrologic-hydrodynamic model for streamflow forecast in the Amazon. Hydrol. Earth Syst. Sci. 17, 2929–2946. doi:10.5194/hess-17-2929-2013

Panday, P.K., Coe, M.T., Macedo, M.N., Lefebvre, P., Castanho, A.D. de A., 2015. Deforestation offsets water balance changes due to climate variability in the Xingu River in eastern Amazonia. J. Hydrol. 523, 822–829. doi:10.1016/j.jhydrol.2015.02.018

Pekel, J.-F., Cottam, A., Gorelick, N., Belward, A.S., 2016. High-resolution mapping of global surface water and its long-term changes. Nature 540, 1–19. doi:10.1038/nature20584

Petheram, C., McMahon, T.A., 2019. Dams, dam costs and damnable cost overruns. J. Hydrol. X 3, 100026. doi:https://doi.org/10.1016/j.hydroa.2019.100026

Phillips, O.L., Aragão, L.E.O.C., Lewis, S.L., Fisher, J.B., Lloyd, J., López-González, G., Malhi, Y., Monteagudo, A., Peacock, J., Quesada, C. a, van der Heijden, G., Almeida, S., Amaral, I., Arroyo, L., Aymard, G., Baker, T.R., Bánki, O., Blanc, L., Bonal, D., Brando, P., Chave, J., de Oliveira, A.C.A., Cardozo, N.D., Czimczik, C.I., Feldpausch, T.R., Freitas, M.A., Gloor, E., Higuchi, N., Jiménez, E., Lloyd, G., Meir, P., Mendoza, C., Morel, A., Neill, D. a, Nepstad, D., Patiño, S., Peñuela, M.C., Prieto, A., Ramírez, F., Schwarz, M., Silva, J., Silveira, M., Thomas, A.S., Steege, H. Ter, Stropp, J., Vásquez, R., Zelazowski, P., Alvarez Dávila, E., Andelman, S., Andrade, A., Chao, K., Erwin, T., Di Fiore, A., Honorio C, E., Keeling, H., Killeen, T.J., Laurance, W.F., Peña Cruz, A., Pitman, N.C. a, Núñez Vargas, P., Ramírez-Angulo, H., Rudas, A., Salamão, R., Silva, N., Terborgh, J., Torres-Lezama,

A., Heijden, G. Van Der, Cristina, Á., Oliveira, A. De, Dávila, E.A., Fiore, A. Di, C, E.H., Cruz, A.P., Vargas, P.N., 2009. Drought sensitivity of the Amazon rainforest. Science (80-. ). 323, 1344–1347. doi:10.1126/science.1164033

Phipps, S.J., Mcgregor, H. V., Gergis, J., Gallant, A.J.E., Neukom, R., Stevenson, S., Ackerley, D., Brown, J.R., Fischer, M.J., Van Ommen, T.D., 2013. Paleoclimate data-model comparison and the role of climate forcings over the past 1500 years. J. Clim. 26, 6915–6936. doi:10.1175/JCLI-D-12-00108.1

Pielke, R.A., Cotton, W.R., Walko, R.L., Tremback, C.J., Lyons, W.A., Grasso, L.D., Nicholls, M.E., Moran, M.D., Wesley, D.A., Lee, T.J., Copeland, J.H., 1992. A comprehensive meteorological modeling system-RAMS. Meteorol. Atmos. Phys. 49, 69–91. doi:10.1007/BF01025401

Pokhrel, Y., Burbano, M., Roush, J., Kang, H., Sridhar, V., Hyndman, D., 2018a. A Review of the Integrated Effects of Changing Climate, Land Use, and Dams on Mekong River Hydrology. Water 10, 266. doi:10.3390/w10030266

Pokhrel, Y., Felfelani, F., Satoh, Y., Boulange, J., Burek, P., Gädeke, A., Gerten, D., Gosling, S.N., Grillakis, M., Gudmundsson, L., Hanasaki, N., Kim, H., Koutroulis, A., Liu, J., Papadimitriou, L., Schewe, J., Müller Schmied, H., Stacke, T., Telteu, C.-E., Thiery, W., Veldkamp, T., Zhao, F., Wada, Y., 2021. Global terrestrial water storage and drought severity under climate change. Nat. Clim. Chang. doi:10.1038/s41558-020-00972-w

Pokhrel, Y., Felfelani, F., Shin, S., Yamada, T.J., Satoh, Y., 2017. Modeling large-scale human alteration of land surface hydrology and climate. Geosci. Lett. 4, 10. doi:10.1186/s40562-017-0076-5

Pokhrel, Y., Hanasaki, N., Koirala, S., Cho, J., Yeh, P.J.-F., Kim, H., Kanae, S., Oki, T., 2012a. Incorporating Anthropogenic Water Regulation Modules into a Land Surface Model. J. Hydrometeorol. 13, 255–269. doi:10.1175/JHM-D-11-013.1

Pokhrel, Y., Hanasaki, N., Yeh, P.J.-F., Yamada, T.J., Kanae, S., Oki, T., 2012b. Model estimates of sea-level change due to anthropogenic impacts on terrestrial water storage. Nat. Geosci. 5, 389–392.

Pokhrel, Y., Shin, S., Lin, Z., Yamazaki, D., Qi, J., 2018b. Potential Disruption of Flood Dynamics in the Lower Mekong River Basin Due to Upstream Flow Regulation. Sci. Rep. 8, 17767. doi:10.1038/s41598-018-35823-4

Pokhrel, Y.N., Fan, Y., Miguez-Macho, G., 2014. Potential hydrologic changes in the Amazon by the end of the 21st century and the groundwater buffer. Environ. Res. Lett. 9, 084004. doi:10.1088/1748-9326/9/8/084004

Pokhrel, Y.N., Fan, Y., Miguez-Macho, G., Yeh, P.J.F., Han, S.C., 2013. The role of groundwater in the Amazon water cycle: 3. Influence on terrestrial water storage computations and comparison with GRACE. J. Geophys. Res. Atmos. 118, 3233–3244. doi:10.1002/jgrd.50335

Pokhrel, Y.N., Oki, T., Kanae, S., 2008. A Grid Based Assessment of Global Theoretical Hydropower Potential. Annu. J. Hydraul. Eng. 52, 7–12.

Previsic, M., 2012. Cost Breakdown Structure for River Current Device.

Previsic, M., Bedard, R., Polagye, B., 2008. System level design, performance, cost and economic assessment–Alaska river in-stream power plants, EPRI.

Prudhomme, C., Giuntoli, I., Robinson, E.L., Clark, D.B., Arnell, N.W., Dankers, R., Fekete, B.M., Franssen, W., Gerten, D., Gosling, S.N., Hagemann, S., Hannah, D.M., Kim, H., Masaki, Y., Satoh, Y., Stacke, T., Wada, Y., Wisser, D., 2014. Hydrological droughts in the 21st century, hotspots and uncertainties from a global multimodel ensemble experiment. Proc. Natl. Acad. Sci. 111, 3262–3267. doi:10.1073/pnas.1222473110

Rammig, A., Jupp, T., Thonicke, K., Tietjen, B., Heinke, J., Lucht, W., Cramer, W., Cox, P., Jupp, T., 2010. Estimating the risk of Amazonian forest dieback Estimating. New Phytol. 187, 694–706. doi:10.1111/j.1469-8137.2010.03318.x

Räsänen, T.A., Someth, P., Lauri, H., Koponen, J., Sarkkula, J., Kummu, M., 2017. Observed river discharge changes due to hydropower operations in the Upper Mekong Basin. J. Hydrol. 545, 28–41. doi:10.1016/j.jhydrol.2016.12.023

Resende, A.F. de, Schöngart, J., Streher, A.S., Ferreira-Ferreira, J., Piedade, M.T.F., Silva, T.S.F., 2019. Massive tree mortality from flood pulse disturbances in Amazonian floodplain forests: The collateral effects of hydropower production. Sci. Total Environ. 659, 587–598. doi:https://doi.org/10.1016/j.scitotenv.2018.12.208

Ritter, C.D., McCrate, G., Nilsson, R.H., Fearnside, P.M., Palme, U., Antonelli, A., 2017. Environmental impact assessment in Brazilian Amazonia: Challenges and prospects to assess biodiversity. Biol. Conserv. 206, 161–168. doi:10.1016/j.biocon.2016.12.031

Rockström, J., Steffen, W., Noone, K., Persson, Å., Chapin, F.S., Lambin, E., Lenton, T.M., Scheffer, M., Folke, C., Schellnhuber, H.J., Nykvist, B., de Wit, C.A., Hughes, T., van der Leeuw, S., Rodhe, H., Sörlin, S., Snyder, P.K., Costanza, R., Svedin, U., Falkenmark, M., Karlberg, L., Corell, R.W., Fabry, V.J., Hansen, J., Walker, B., Liverman, D., Richardson, K., Crutzen, P., Foley, J., 2009. Planetary boundaries: Exploring the safe operating space for humanity. Ecol. Soc. 14. doi:10.5751/ES-03180-140232

Rodell, M., Famiglietti, J.S., Wiese, D.N., Reager, J.T., Beaudoing, H.K., Landerer, F.W., Lo, M.-H., 2018. Emerging trends in global freshwater availability. Nature 557, 651–659. doi:10.1038/s41586-018-0123-1

Sahoo, A.K., Pan, M., Troy, T.J., Vinukollu, R.K., Sheffield, J., Wood, E.F., 2011. Reconciling the global terrestrial water budget using satellite remote sensing. Remote Sens. Environ. 115, 1850–1865. doi:10.1016/j.rse.2011.03.009

Salati, E., Vose, P.B., 1984. Amazon Basin : A System in Equilibrium. Science (80-. ). 225, 129–138.

Saleska, S.R., Didan, K., Huete, A.R., Da Rocha, H.R., 2007. Amazon forests green-up during 2005 drought. Science (80-. ). 318, 612. doi:10.1126/science.1146663

Saleska, S.R., Wu, J., Guan, K., Araujo, A.C., Huete, A., Nobre, A.D., Restrepo-Coupe, N., 2016. Dry-season greening of Amazon forests. Nature 531, E4–E5. doi:10.1038/nature16457

Santos, M.J., Ferreira, P., Araújo, M., Portugal-Pereira, J., Lucena, A.F.P., Schaeffer, R., 2017. Scenarios for the future Brazilian power sector based on a multi-criteria assessment. J. Clean. Prod. 167, 938–950. doi:https://doi.org/10.1016/j.jclepro.2017.03.145

Satyamurty, P., Da Costa, C.P.W., Manzi, A.O., Candido, L.A., 2013. A quick look at the 2012 record flood in the Amazon Basin. Geophys. Res. Lett. 40, 1396–1401. doi:10.1002/grl.50245

Scanlon, B.R., Zhang, Z., Rateb, A., Sun, A., Wiese, D., Save, H., Beaudoing, H., Lo, M.H., Müller-Schmied, H., Döll, P., van Beek, R., Swenson, S., Lawrence, D., Croteau, M., Reedy, R.C., 2019. Tracking Seasonal Fluctuations in Land Water Storage Using Global Models and GRACE Satellites. Geophys. Res. Lett. 0. doi:10.1029/2018GL081836

Scanlon, B.R., Zhang, Z., Save, H., Sun, A.Y., Müller Schmied, H., van Beek, L.P.H., Wiese, D.N., Wada, Y., Long, D., Reedy, R.C., Longuevergne, L., Döll, P., Bierkens, M.F.P., 2018. Global models underestimate large decadal declining and rising water storage trends relative to GRACE satellite data. Proc. Natl. Acad. Sci. 201704665. doi:10.1073/pnas.1704665115

Scanlon, B.R., Zhang, Z., Save, H., Wiese, D.N., Landerer, F.W., Long, D., Laurent, L., Chen, J., 2016. Global evaluation of new GRACEmascon products for hydrologic applications. Water Resour. Res. 9412–9429. doi:10.1002/2016WR019494

Schmidt, C., 2015. Alarm over a sinking delta. Science (80-. ). 348, 845 LP – 846. doi:10.1126/science.348.6237.845

Schmidt, J., Cancella, R., Pereira, A.O., 2016. An optimal mix of solar PV, wind and hydro power for a low-carbon electricity supply in Brazil. Renew. Energy 85, 137–147. doi:10.1016/j.renene.2015.06.010

Schmied, H.M., Eisner, S., Franz, D., Wattenbach, M., Portmann, F.T., Flörke, M., Döll, P., 2014. Sensitivity of simulated global-scale freshwater fluxes and storages to input data, hydrological model structure, human water use and calibration. Hydrol. Earth Syst. Sci. 18, 3511–3538. doi:10.5194/hess-18-3511-2014

Schöngart, J., Junk, W.J., 2007. Forecasting the flood-pulse in Central Amazonia by ENSO-indices. J. Hydrol. 335, 124–132. doi:10.1016/j.jhydrol.2006.11.005

Sena, J.A., de Deus, L.A.B., Freitas, M.A. V., Costa, L., 2012. Extreme Events of Droughts and Floods in Amazonia: 2005 and 2009. Water Resour. Manag. 26, 1665–1676. doi:10.1007/s11269-012-9978-3

Shin, S., Pokhrel, Y., Miguez-Macho, G., 2019. High Resolution Modeling of Reservoir Release and Storage Dynamics at the Continental Scale. Water Resour. Res. 55, 787– 810. doi:10.1029/2018WR023025

Shin, S., Pokhrel, Y., Yamazaki, D., Huang, X., Torbick, N., Qi, J., Pattanakiat, S., Ngo-Duc, T., Nguyen, T.D., 2020. High Resolution Modeling of River-Floodplain-Reservoir Inundation Dynamics in the Mekong River Basin. Water Resour. Res. 56, e2019WR026449. doi:10.1029/2019WR026449

Shukla, J., Nobre, C., Sellers, P., 1990. Amazon Deforestation and Climate Change. Science (80-. ). 247, 1322 LP – 1325. doi:10.1126/science.247.4948.1322

Siqueira, V.A., Paiva, R.C.D., Fleischmann, A.S., Fan, F.M., Ruhoff, A.L., Pontes, P.R.M., Paris, A., Calmant, S., Collischonn, W., 2018. Toward continental hydrologic–hydrodynamic modeling in South America. Hydrol. Earth Syst. Sci. 1–50. doi:10.5194/hess-2018-225

Smith, L.T., Aragão, L.E.O.C., Sabel, C.E., Nakaya, T., 2014. Drought impacts on children's respiratory health in the Brazilian Amazon. Sci. Rep. 4, 1–8. doi:10.1038/srep03726

Soares-Filho, B., Moutinho, P., Nepstad, D., Anderson, A., Rodrigues, H., Garcia, R., Dietzsch, L., Merry, F., Bowman, M., Hissa, L., Silvestrini, R., Maretti, C., 2010. Role of Brazilian Amazon protected areas in climate change mitigation. Proc. Natl. Acad. Sci. 107, 10821–10826. doi:10.1073/pnas.0913048107

Soito, J.L.D.S., Freitas, M.A.V., 2011. Amazon and the expansion of hydropower in Brazil: Vulnerability, impacts and possibilities for adaptation to global climate change. Renew. Sustain. Energy Rev. 15, 3165–3177. doi:10.1016/j.rser.2011.04.006

Steffen, W., Rockström, J., Richardson, K., Lenton, T.M., Folke, C., Liverman, D., Summerhayes, C.P., Barnosky, A.D., Cornell, S.E., Crucifix, M., Donges, J.F., Fetzer, I., Lade, S.J., Scheffer, M., Winkelmann, R., Schellnhuber, H.J., 2018. Trajectories of the Earth System in the Anthropocene. Proc. Natl. Acad. Sci. 115, 8252 LP – 8259. doi:10.1073/pnas.1810141115

Stehman, S., 1996. Estimating the kappa coefficient and its variance under stratified random sampling. Photogramm. Eng. Remote Sensing 62, 401–407.

Stone, R., 2016. Dam-building threatens Mekong fisheries. Science (80-. ). 354, 1084 LP – 1085. doi:10.1126/science.354.6316.1084

Stone, R., 2011. Mayhem on the Mekong. Science (80-. ). 333, 814 LP – 818. doi:10.1126/science.333.6044.814

Strand, J., Soares-Filho, B., Costa, M.H., Oliveira, U., Ribeiro, S.C., Pires, G.F., Oliveira, A., Rajão, R., May, P., van der Hoff, R., Siikamäki, J., da Motta, R.S., Toman, M., 2018. Spatially explicit valuation of the Brazilian Amazon Forest's Ecosystem Services. Nat. Sustain. 1, 657–664. doi:10.1038/s41893-018-0175-0

Sun, A.Y., Scanlon, B.R., Zhang, Z., Walling, D., Bhanja, S.N., Mukherjee, A., Zhong, Z., 2019. Combining Physically Based Modeling and Deep Learning for Fusing GRACE Satellite Data: Can We Learn From Mismatch? Water Resour. Res. 55, 1179–1195. doi:10.1029/2018WR023333

Syvitski, J.P.M., Kettner, A.J., Overeem, I., Hutton, E.W.H., Hannon, M.T., Brakenridge, G.R., Day, J., Vörösmarty, C., Saito, Y., Giosan, L., Nicholls, R.J., 2009. Sinking deltas due to human activities. Nat. Geosci. 2, 681–686. doi:10.1038/ngeo629

Taylor, K.E., 2001. Summarizing multiple aspects of model performance in a single diagram. J. Geophys. Res. Atmos. 106, 7183–7192. doi:10.1029/2000JD900719

Timpe, K., Kaplan, D., 2017. The changing hydrology of a dammed Amazon. Sci. Adv. 3, 1–14. doi:10.1126/sciadv.1700611

Tófoli, R.M., Dias, R.M., Zaia Alves, G.H., Hoeinghaus, D.J., Gomes, L.C., Baumgartner, M.T., Agostinho, A.A., 2017. Gold at what cost? Another megaproject threatens biodiversity in the Amazon. Perspect. Ecol. Conserv. 15, 129–131. doi:10.1016/j.pecon.2017.06.003

Tollefson, J., 2016. Deforestation rates spike in Brazil. Nature 540, 182–183. doi:10.1038/nature.2016.21083

Toomey, M., Roberts, D.A., Still, C., Goulden, M.L., McFadden, J.P., 2011. Remotely sensed heat anomalies linked with Amazonian forest biomass declines. Geophys. Res. Lett. 38. doi:10.1029/2011GL049041

Towner, J., Cloke, H.L., Zsoter, E., Flamig, Z., Hoch, J.M., Bazo, J., Coughlan de Perez, E., Stephens, E.M., 2019. Assessing the performance of global hydrological models for capturing peak river flows in the Amazon Basin. Hydrol. Earth Syst. Sci. Discuss. 1–37. doi:10.5194/hess-2019-44

Van Loon, A.F., Laaha, G., 2015. Hydrological drought severity explained by climate and catchment characteristics. J. Hydrol. 526, 3–14. doi:10.1016/j.jhydrol.2014.10.059

Van Loon, A.F., Van Huijgevoort, M.H.J., Van Lanen, H.A.J., 2012. Evaluation of drought propagation in an ensemble mean of large-scale hydrological models. Hydrol. Earth Syst. Sci. 16, 4057–4078. doi:10.5194/hess-16-4057-2012

VanZwieten, J., McAnally, W., Ahmad, J., Davis, T., Martin, J., Bevelhimer, M., Cribbs, A., Lippert, R., Hudon, T., Trudeau, M., 2014. In-Stream Hydrokinetic Power: Review and Appraisal. J. Energy Eng. 141, 04014024. doi:10.1061/(asce)ey.1943-7897.0000197

Veers, P., Dykes, K., Lantz, E., Barth, S., Bottasso, C.L., Carlson, O., Clifton, A., Green, J., Green, P., Holttinen, H., Laird, D., Lehtomäki, V., Lundquist, J.K., Manwell, J., Marquis, M., Meneveau, C., Moriarty, P., Munduate, X., Muskulus, M., Naughton, J., Pao, L., Paquette, J., Peinke, J., Robertson, A., Sanz Rodrigo, J., Sempreviva, A.M., Smith, J.C., Tuohy, A., Wiser, R., 2019. Grand challenges in the science of wind energy. Science (80-. ). 366, eaau2027. doi:10.1126/science.aau2027

Veileder, 2012. Cost base for hydropower plants. Oslo.

Vennell, R., Funke, S.W., Draper, S., Stevens, C., Divett, T., 2015. Designing large arrays of tidal turbines: A synthesis and review. Renew. Sustain. Energy Rev. 41, 454–472. doi:https://doi.org/10.1016/j.rser.2014.08.022

Vorosmarty, C.J., Willmott, C.J., Choudhury, B.J., Schloss, A.L., Stearns, T.K., Robeson, S.M., Dorman, T.J., 1996. Analyzing the discharge regime of a large tropical river through remote sensing , ground-based climatic data , and modeling differences ( HVPTD ) from the 37-GHz scanning multichannel microwave radiometer model ( WBM / WTM ). Monthly. Water Resour. Res. 32, 3137–3150. doi:10.1029/96WR01333

Waldman, J., Sharma, S., Afshari, S., Fekete, B., 2019. Solar-power replacement as a solution for hydropower foregone in US dam removals. Nat. Sustain. 2, 872–878. doi:10.1038/s41893-019-0362-7

Walko, R.L., Band, L.E., Baron, J., Kittel, T.G.F., Lammers, R., Lee, T.J., Ojima, D., Pielke, R. a, Taylor, C., Tague, C., Tremback, C.J., Vidale, P.L., 2000. Coupled atmosphere, biophysics and hydrology models for environmental modeling. J. Appl. Meteorol. 39, 931–944. doi:10.1175/1520-0450(2000)039<0931:CABHMF>2.0.CO;2

Wanders, N., Van Lanen, H.A.J., 2015. Future discharge drought across climate regions around the world modelled with a synthetic hydrological modelling approach forced by three general circulation models. Nat. Hazards Earth Syst. Sci. 15, 487–504. doi:10.5194/nhess-15-487-2015

Wanders, N., Wada, Y., 2015. Human and climate impacts on the 21st century hydrological drought. J. Hydrol. 526, 208–220. doi:10.1016/j.jhydrol.2014.10.047

Wanders, N., Wada, Y., Van Lanen, H.A.J., 2015. Global hydrological droughts in the 21st century under a changing hydrological regime. Earth Syst. Dyn. 6, 1–15. doi:10.5194/esd-6-1-2015

Wang, K., Shi, H., Chen, J., Li, T., 2019. An improved operation-based reservoir scheme integrated with Variable Infiltration Capacity model for multiyear and multipurpose reservoirs. J. Hydrol. doi:10.1016/j.jhydrol.2019.02.006

Warszawski, L., Frieler, K., Huber, V., Piontek, F., Serdeczny, O., Schewe, J., 2014. The Inter-Sectoral Impact Model Intercomparison Project (ISI–MIP): Project framework. Proc. Natl. Acad. Sci. 111, 3228 LP – 3232. doi:10.1073/pnas.1312330110

Weedon, G.P., Balsamo, G., Bellouin, N., Gomes, S., Best, M.J., Viterbo, P., 2014. Data methodology applied to ERA-Interim reanalysis data. Water Resour. Res. 50, 7505–7514. doi:10.1002/2014WR015638

Wei, J., Dirmeyer, P.A., 2019. Sensitivity of land precipitation to surface evapotranspiration: a nonlocal perspective based on water vapor transport. Geophys. Res. Lett. 46, 12588–12597. doi:10.1029/2019GL085613

Winemiller, K.O., McIntyre, P.B., Castello, L., Fluet-Chouinard, E., Giarrizzo, T., Nam, S., Baird, I.G., Darwall, W., Lujan, N.K., Harrison, I., Stiassny, M.L.J.J., Silvano, R.A.M.M., Fitzgerald, D.B., Pelicice, F.M., Agostinho, A.A., Gomes, L.C., Albert, J.S., Baran, E., Petrere, M., Zarfl, C., Mulligan, M., Sullivan, J.P., Arantes, C.C., Sousa, L.M., Koning, A.A., Hoeinghaus, D.J., Sabaj, M., Lundberg, J.G., Armbruster, J., Thieme, M.L., Petry, P., Zuanon, J., Vilara, G.T., Snoeks, J., Ou, C., Rainboth, W., Pavanelli, C.S., Akama, A., Soesbergen, A. v., Saenz, L., Torrente Vilara, G., Snoeks, J., Ou, C., Rainboth, W., Pavanelli, C.S., Akama, A., Van Soesbergen, A., Sáenz, L., 2016. Balancing hydropower and biodiversity in the Amazon, Congo, and Mekong. Science (80-. ). 351, 128–129. doi:10.1126/science.aac7082

Wongchuig Correa, S., Paiva, R.C.D. de, Espinoza, J.C., Collischonn, W., 2017. Multi-decadal Hydrological Retrospective: Case study of Amazon floods and droughts. J. Hydrol. 549, 667–684. doi:10.1016/j.jhydrol.2017.04.019

Woodroffe, J.F., 1914. The upper reaches of the Amazon. Methuen & Company, Limited.

Xavier, L., Becker, M., Cazenave, A., Longuevergne, L., Llovel, W., Filho, O.C.R., 2010. Interannual variability in water storage over 2003-2008 in the Amazon Basin from GRACE space gravimetry, in situ river level and precipitation data. Remote Sens. Environ. 114, 1629–1637. doi:10.1016/j.rse.2010.02.005

Xiao, Z., Liang, S., Wang, J., Chen, P., Yin, X., Zhang, L., Song, J., 2014. Use of general regression neural networks for generating the GLASS leaf area index product from time-series MODIS surface reflectance. IEEE Trans. Geosci. Remote Sens. 52, 209–223. doi:10.1109/TGRS.2013.2237780

Xu, B., Park, T., Yan, K., Chen, C., Zeng, Y., Song, W., Yin, G., Li, J., Liu, Q., Knyazikhin, Y., Myneni, R.B., 2018. Analysis of Global LAI/FPAR Products from VIIRS and MODIS Sensors for Spatio-Temporal Consistency and Uncertainty from 2012–2016. Forests 9. doi:10.3390/f9020073

Xu, L., Samanta, A., Costa, M.H., Ganguly, S., Nemani, R.R., Myneni, R.B., 2011. Widespread decline in greenness of Amazonian vegetation due to the 2010 drought. Geophys. Res. Lett. 38, 2–5. doi:10.1029/2011GL046824

Yamazaki, D., Baugh, C.A., Bates, P.D., Kanae, S., Alsdorf, D.E., Oki, T., 2012a. Adjustment of a spaceborne DEM for use in floodplain hydrodynamic modeling. J. Hydrol. 436–437, 81–91. doi:10.1016/j.jhydrol.2012.02.045

Yamazaki, D., De Almeida, G.A.M., Bates, P.D., 2013. Improving computational efficiency in global river models by implementing the local inertial flow equation and a vector-based river network map. Water Resour. Res. 49, 7221–7235. doi:10.1002/wrcr.20552

Yamazaki, D., Ikeshima, D., Tawatari, R., Yamaguchi, T., O'Loughlin, F., Neal, J.C., Sampson, C.C., Kanae, S., Bates, P.D., 2017. A high-accuracy map of global terrain elevations. Geophys. Res. Lett. 44, 5844–5853. doi:https://doi.org/10.1002/2017GL072874

Yamazaki, D., Kanae, S., Kim, H., Oki, T., 2011. A physically based description of floodplain inundation dynamics in a global river routing model. Water Resour. Res. 47, 1–21. doi:10.1029/2010WR009726

Yamazaki, D., Lee, H., Alsdorf, D.E., Dutra, E., Kim, H., Kanae, S., Oki, T., 2012b. Analysis of the water level dynamics simulated by a global river model: A case study in the Amazon River. Water Resour. Res. 48. doi:10.1029/2012WR011869

Yamazaki, D., Oki, T., Kanae, S., 2009. Deriving a global river network map and its sub-grid topographic characteristics from a fine-resolution flow direction map. Hydrol. Earth Syst. Sci. 13, 2241–2251. doi:10.5194/hess-13-2241-2009

Yang, H.F., Yang, S.L., Xu, K.H., Wu, H., Shi, B.W., Zhu, Q., Zhang, W.X., Yang, Z., 2017. Erosion potential of the Yangtze Delta under sediment starvation and climate change. Sci. Rep. 7, 10535. doi:10.1038/s41598-017-10958-y

Zarfl, C., Berlekamp, J., He, F., Jähnig, S.C., Darwall, W., Tockner, K., 2019. Future large hydropower dams impact global freshwater megafauna. Sci. Rep. 9, 18531. doi:10.1038/s41598-019-54980-8

Zarfl, C., Lumsdon, A.E., Berlekamp, J., Tydecks, L., Tockner, K., 2015. A global boom in hydropower dam construction. Aquat. Sci. 77, 161–170. doi:10.1007/s00027-014-0377-0

Zemp, D.C., Schleussner, C.F., Barbosa, H.M.J., Rammig, A., 2017. Deforestation effects on Amazon forest resilience. Geophys. Res. Lett. 44, 6182–6190. doi:10.1002/2017GL072955

Zeng, N., 1999. Seasonal cycle and interannual variability in the Amazon hydrologic cycle. J. Geophys. Res. Atmos. 104, 9097–9106. doi:10.1029/1998JD200088

Zeng, N., Yoon, J.-H.H., Marengo, J.A., Subramaniam, A., Nobre, C.A., Mariotti, A., Neelin, J.D., 2008. Causes and impacts of the 2005 Amazon drought. Environ. Res. Lett. 3, 14002. doi:10.1088/1748-9326/3/1/014002

Zhao, F., Veldkamp, T.I.E., Frieler, K., Schewe, J., Ostberg, S., Willner, S., Schauberger, B., Gosling, S.N., Schmied, H.M., Portmann, F.T., Leng, G., Huang, M., Liu, X., Tang, Q., Hanasaki, N., Biemans, H., Gerten, D., Satoh, Y., Pokhrel, Y., Stacke, T., Ciais, P., Chang, J., Ducharne, A., Guimberteau, M., Wada, Y., Kim, H., Yamazaki, D., 2017. The critical role of the routing scheme in simulating peak river discharge in global hydrological models. Environ. Res. Lett. 12. doi:10.1088/1748-9326/aa7250

Zhao, M., A, G., Velicogna, I., Kimball, J.S., 2017a. A Global Gridded Dataset of GRACE Drought Severity Index for 2002–14: Comparison with PDSI and SPEI and a Case Study of the Australia Millennium Drought. J. Hydrometeorol. 18, 2117–2129. doi:10.1175/JHM-D-16-0182.1

Zhao, M., Geruo, A., Velicogna, I., Kimball, J.S., 2017b. Satellite observations of regional drought severity in the continental United States using GRACE-based terrestrial water storage changes. J. Clim. 30, 6297–6308. doi:10.1175/JCLI-D-16-0458.1

Zhou, Y., Hejazi, M., Smith, S., Edmonds, J., Li, H., Clarke, L., Calvin, K., Thomson, A., 2015. A comprehensive view of global potential for hydro-generated electricity. Energy Environ. Sci. 8, 2622–2633. doi:10.1039/C5EE00888C

Zulkafli, Z., Buytaert, W., Manz, B., Rosas, C.V., Willems, P., Lavado-Casimiro, W., Guyot, J.-L.L., Santini, W., 2016. Projected increases in the annual flood pulse of the Western Amazon. Environ. Res. Lett. 11, 14013. doi:10.1088/1748-9326/11/1/014013